Strathclyde Institute of Pharmacy and Biomedical Sciences

NOVEL METHODS TO DELIVER PLATINUM(II) CHEMOTHERAPEUTICS TO THE NOSE

By

Shonagh Walker

A thesis submitted to the University of Strathclyde in fulfilment of the requirements for the degree of Doctor of Philosophy

2013

Declaration

‘This thesis is the result of the author’s original research. It has been composed by the author and has not been previously submitted for examination which has led to the award of a degree.’

Signed:

Date:

Dedication

I would like to dedicate this thesis to my parents, George and Irene Walker, for their unwavering support and countless sacrifices towards my brother and I's success and happiness.

And to our friend, Joanne Monaghan, who lost her battle with cancer in August 2011.

Together, they taught me it is impossible to open a jar with your elbows.

Acknowledgements

I would like to thank the following people for their assistance in the completion of this thesis. Firstly I would like to express my heartfelt gratitude to Professor Clive Wilson, for taking me under his wing in the eleventh hour, and integrating me into his wonderful research group. I would also like to express my sincere appreciation to Fiona McInnes for her continued support after leaving the Institute. I also acknowledge my original supervisor, Nial Wheate, for giving me the opportunity to carry out this research project.

I would like to thank Katie Trotter for her assistance with X-ray diffraction of K6, and Denise Gilmour from the Department of Pure and Applied Chemistry for carrying out ICP-MS analysis. I am also grateful to Wojciech Chrzanowski at the University of Sydney for carrying out SEM. For their assistance with microrheology, I would like to thank Nial McAlinden from the Department of Photonics and Alexander Hope from the Department of Chemical Engineering. For assistance in tissue harvesting, I would like to thank Michelle Mathie.

On a more personal level, thanks must go to The Robertson Scholarship Trust, who sponsored me through my undergraduate degree. To my brother (and hero) Stephen, who I never see enough of, but always look up to. To Martin, for believing in me when I didn't believe in myself, and for providing me the support and encouragement I could not have done without. And for always doing the dishes. To the founding members of Shomma and Jenelle, we might not have cured cancer together, but you light up my world like nobody else. To Gemma Craig, for being Gemma Craig - my friend and inspiration. To Mainsy, Lisa, Kelly, Gracie, Ruairidh, Joe, Katie and Gordy for making me laugh through the hard times. And to Sarah and Scott for their expertise in furniture removals. For being patient with me throughout my 23 years of education, I would like to thank Gemmanoid, my oldest friend in the world. Finally, I would like to thank the members of the Mugen Taiko Dojo, for their support and friendship over the last ten years, and with whom the next part of my journey lies.

Contents

ABSTRACT

Efforts to reduce side effects and improve efficacy of platinum-based drugs have seen the focus shift away from developing new drugs, towards improving the delivery of existing ones. This thesis presents an investigation into improving the delivery of platinum(II) drugs using lyophilised hydroxypropyl methylcellulose (HPMC) nasal insert formulations, designed to resist rapid mucociliary clearance *in vivo* and extend drug absorption.

Cisplatin was conjugated to carbon nanotubes (CNTs), which was expected to improve tumour targeting through the enhanced permeability and retention effect; however this project was halted due to safety concerns.

Cucurbiturils (CB[*n*]s) were investigated as an alternative drug delivery vehicle, as they have been shown to improve platinum(II) drug stability. The high cost of the most soluble homologue, CB[7] prompted an investigation into whether or not more readily available CB[6] could be used as reliable a model for CB[7] in nasal insert formulations. A series of investigations revealed that CB[6] had a similar effect on HPMC nasal inserts as CB[7]. A theory for the observed behaviour has been proposed, whereby the CB[*n*]s act as points of pseudo-cross-linking in the HPMC matrix by forming hydrogen bonds with adjacent polymer chains.

CB[6] and CB[7] have been shown to increase the thermal stability of the di-nuclear platinum(II) drug di-Pt, and the fluorescent dye, K6. Additionally, the encapsulated forms have shown improved distribution throughout a lyophilised nasal insert. This work may represent the formulation of a pH-responsive supramolecular delivery system for di-Pt. Cucurbit[*n*]urils have, therefore, been shown to warrant further investigation as pharmaceutical excipients for controlled release.

Finally, cisplatin protected in CB[7] was included in lyophilised nasal inserts. The encapsulation was shown to improve the thermal stability of cisplatin, but not significantly affect the hardness, spreadability or mucoadhesion of the nasal insert formulation. Additionally, the release of cisplatin@CB[7] was more repeatable than its cisplatin counterpart.

1. INTRODUCTION

1.1 PLATINUM(II) CHEMOTHERAPEUTICS

1.1.1 Cancer

Data from Cancer Research UK suggests that more than one in three people in the UK will develop cancer.[1] In 2007, there were 155,000 deaths from the disease in the UK alone, rising to 157,275 during 2010.[1,2] The global incidence is increasing and the World Health Organization (WHO) has estimated that in 2030 there will be around 12 million deaths from cancer worldwide.[3] Over 200 different types of cancer are known,[1] all of which can arise from a mutation of a single cell.[3] Breast, lung, colorectal and prostate cancer account for over half (54%) of new cases diagnosed in the UK.[1]

Despite advances in oncology, long-term survival rates for some cancers continue to fall. Ten-year survival rates for brain tumour patients, for example, fell steadily over the 1990s. This highlights a need for new developments and continuing improvements to treatments for the disease.

1.1.2 Growth and spread of cancer

Cancer occurs when there are specific failures in gene expression, resulting in uncontrolled cell division. The resultant abnormal cells are non-differentiated[4] and form tumours of excess tissue.[5] Benign (non-cancerous) tumours exist when this non-differentiated mass is contained from adjacent tissues.[4] Malignant (cancerous)[5] growths occur when the tumour spreads, invading and destroying neighbouring tissue as it competes for space and nutrients.[4] As they grow, tumours become more hypoxic, stimulating the release of tumour angiogenesis factors (TAFs). These cause local blood vessels to intervasate into the tumour, supplying it with oxygen and nutrients for continued growth[4] and allowing metastasis to occur (Figure 1.1).

During this process, some malignant cells break off, invading body cavities or entering the blood or lymphatic circulation system.[5] The abnormal cells can then proliferate, generating secondary tumours elsewhere in the body.[4] With each of these progressive stages, the patient's prognosis worsens.[4]

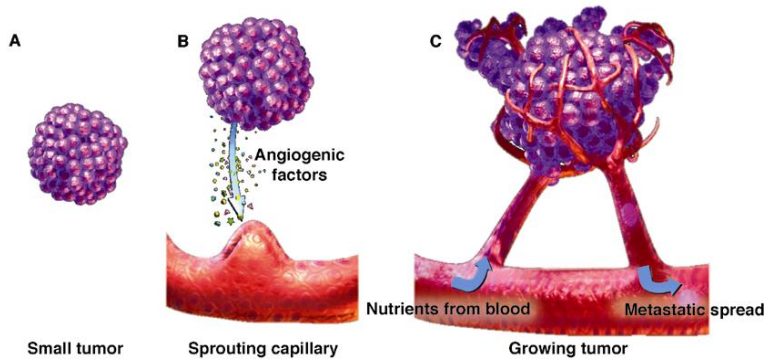

Figure 1.1. The progress of angiogenesis and metastasis in solid tumours.[6]

The smallest clinically detectable tumour lump will already contain around one billion cancerous cells, and so the potential for metastasis and secondary tumour formation, before diagnosis, is high.[7] Surgery and radiotherapy are useful treatments for localised cancers, but most deaths result from metastatic disease. It is therefore vital that cancer treatments which can exert a systemic effect are available, and to this end, cytotoxic drugs are employed.[7] Of the wide range of chemotherapeutics on the market, one of the best-selling and most potent is the platinum-based drug, cisplatin.[8-10]

1.1.3 Cisplatin

Cisplatin (*cis*-diamminedichloridoplatinum(II), Figure 1.2) is a neutral, square planar platinum anticancer chemotherapeutic which binds to deoxyribonucleic acid (DNA).[9] It was the first metal-based drug to receive worldwide approval for the treatment of cancer.[8,11] First synthesised in 1844,[12] its usefulness as an anticancer agent was not realised until an accidental discovery by Prof. Barnett Rosenberg in 1960s.[13-15]

Cisplatin was approved by the US Food and Drug Administration (FDA) in 1978 and remains an important agent in the treatment of cancer.

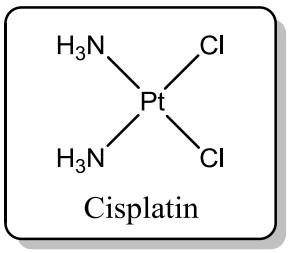

Figure 1.2. The chemical structure of cisplatin.

***"…it is now appropriate for inorganic chemists to join their organic brothers in submitting their syntheses …for screening for antitumor activities."* – Rosenberg, 1971[13]**

1.1.4 Clinical use and action of cisplatin

Cisplatin is not a typical "drug-like" molecule and so is associated with specific formulation and administration requirements. It is formulated as a sterile aqueous saline solution, NaCl (0.9%)[16,17] and the resulting high concentration of choride ions in the solution means the platinum atom remains coordinated by two chlorido ligands. Administered intravenously, it enters the bloodstream where the chloride concentration is high (~100 mM). When the drug finally enters the intracellular cytoplasm, the lower chloride concentration (~4 mM) allows the spontaneous and sequential replacement of the *cis*-chlorido ligands with water molecules. This process is known as aquation (Figure 1.3).[8]

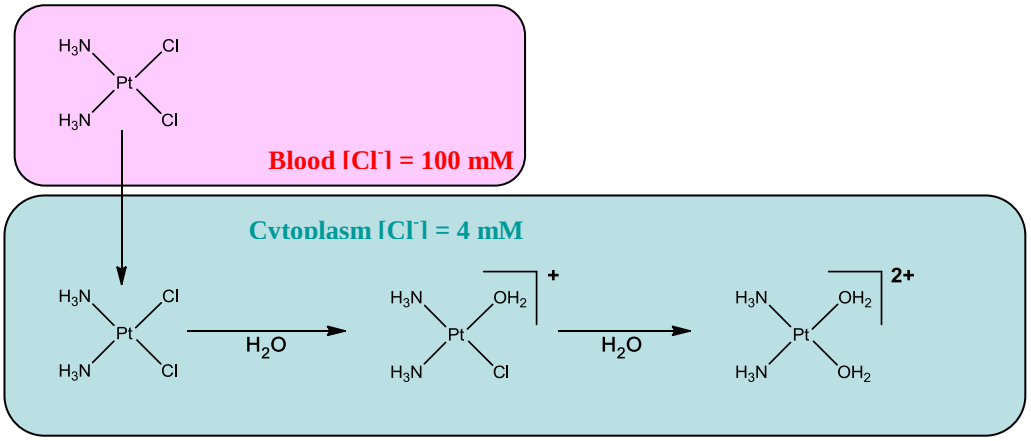

Figure 1.3. Reaction scheme for the aquation of cisplatin *in vivo*. *Adapted from Kartalou.*[18]

The newly formed *bis*-aquated species is positively charged and can coordinate with the nucleophilic N7 positions of guanine and adenine bases, forming inter- and intra-strand crosslinks[11,18] (Figure 1.4). Crosslinking DNA in this manner causes inhibition of replication[19,20] and transcription,[21] arrest at the G2 phase of the cell cycle, and/or apoptosis.[13,18,22]

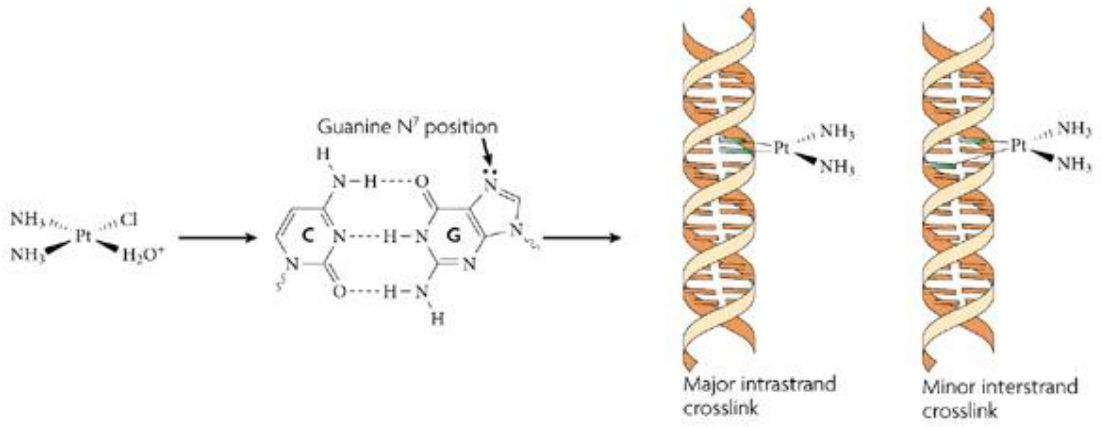

Figure 1.4. Once the aquated cisplatin has entered the nucleus, preferential covalent binding at the N7 position of guanine occurs. The major covalent *bis*-adduct that is formed involves adjacent guanines on the same strand of DNA (intra-strand cross-linking). The minor adduct involves binding to guanosines on opposite strands (inter-strand cross-linking).[8]

Current opinion is that cisplatin is taken up by cells *via* a combination of passive diffusion and active transport mechanisms.[23] For example, Binks and colleagues have reported that absorption is linear with time, could not be achieved against a concentration gradient, is not saturable, and could not be reduced by metabolic

deactivation. These observations suggest a passive mechanism.[24] Additionally, increasing fluidity of the cell membrane through hyperthermia increases cellular accumulation[25] and uptake is not inhibited by a structural analogue.[23]

Contrary to this, a growing body of evidence now supports the involvement of some kind of protein-mediated active transport mechanism.[18,23] Inhibition of membrane proteins with benzaldehyde has been shown to reduce uptake by up to 50% in some cases. It may, therefore, be the case that the transport of cisplatin does indeed occur *via* a combination of active and passive mechanisms, which vary in proliferation between tissue types.

When used to treat metastatic testicular cancer, cisplatin-based combination therapies result in complete clinical response in 95% of patients.[18] Cisplatin is also used to treat ovarian, genitourinary, lung, head and neck cancers, although efficacy in these applications is reduced due to dose-limiting toxicities, along with intrinsic and/or acquired resistance.[9,18]

1.1.5 Side effects of cisplatin therapy

Cisplatin has a narrow therapeutic window and is associated with a number of dose-limiting side effects.[11] It is highly emetogenic (causes severe nausea and vomiting, perceived by many patients as one of the most troublesome side effects of chemotherapy),[16,26] causes dose-dependent nephrotoxicity (requiring aggressive prehydration to ameliorate, and worsening with continued treatment),[8,27] ototoxicity, hypomagnesaemia, myelosuppression, allergic reactions, peripheral neuropathy, tinnitus and anemia.[7,9,16] There are also difficulties associated with the actual administration, which must be intravenous (IV) in order to maintain platinum coordination by the *cis*-chlorides.[11] Administration is typically IV infusion over a number of hours,[11] alongside intensive IV hydration and is generally an in-patient procedure.[16] Inflammation and nerve damage at the injection site can cause pain and the open wound created is susceptible to infection. Patients may also present an aversion to needles.[28]

1.1.6 Resistance to cisplatin

The efficacy of cisplatin is limited by drug resistance, which may be acquired through prolonged treatment (as seen in, for example, ovarian cancer) or may be an intrinsic property of the tumour (as seen in: for example, colorectal, lung and breast cancer).[8,18,22]

Mechanisms of resistance can be broadly categorised into resistance through insufficient intracellular accumulation, resistance through insufficient DNA binding and resistance mediated after DNA binding. Decreased accumulation can result from cisplatin-induced under-expression of transport proteins, such as the copper transporter-1 (CTR-1),[29,30] or, to a lesser extent, increased efflux due to over-expression of transport proteins.[31]

Insufficient DNA binding in cisplatin resistant cell lines has also been associated with elevated levels of intracellular thiol-containing species and associated enzymes, such as glutathione (GSH) and metallothioneins.[32,33] These species are rich in cysteine and methionine and will bind platinum species readily. One day after cisplatin administration, up to 98% of platinum in the blood is protein bound. As well as causing early deactivation of the drug, protein binding has been blamed for some severe side effects of cisplatin therapy, including nephrotoxicity and ototoxicity.[34] Secondary metabolic conjugation to GSH can occur *via* nucleophilic attack by the glutathione thiolate ion. This conjugation inhibits cross-linking and the GS-drug conjugate is transported out of the cell by an adenosine triphosphate (ATP)-dependant pump[35] before it is able to elicit a therapeutic effect (Figure 1.5).

Many cisplatin-resistant cell lines have been shown to have increased DNA-repair capacity. This has been rationalised by Ferry *et al.* to result from an increase in the proteins that catalyse nucleotide-excision repair.[36] Additionally, increased tolerance to DNA damage can occur through a loss of cell-signalling pathways in resistant cells.[8,37]

Drug resistance is therefore a major limiting factor in cisplatin treatment. To put this into clinical relevance, cisplatin-based therapy for ovarian cancer has an initial response rate of 70% but this is not sustained; the 5-year survival rate is as low as 15-20%.[38] With small cell lung cancer, the recurrence rate is as high as 95%.[39] Finding ways to overcome tumour resistance to cisplatin is, therefore, a major and on-going initiative.[8]

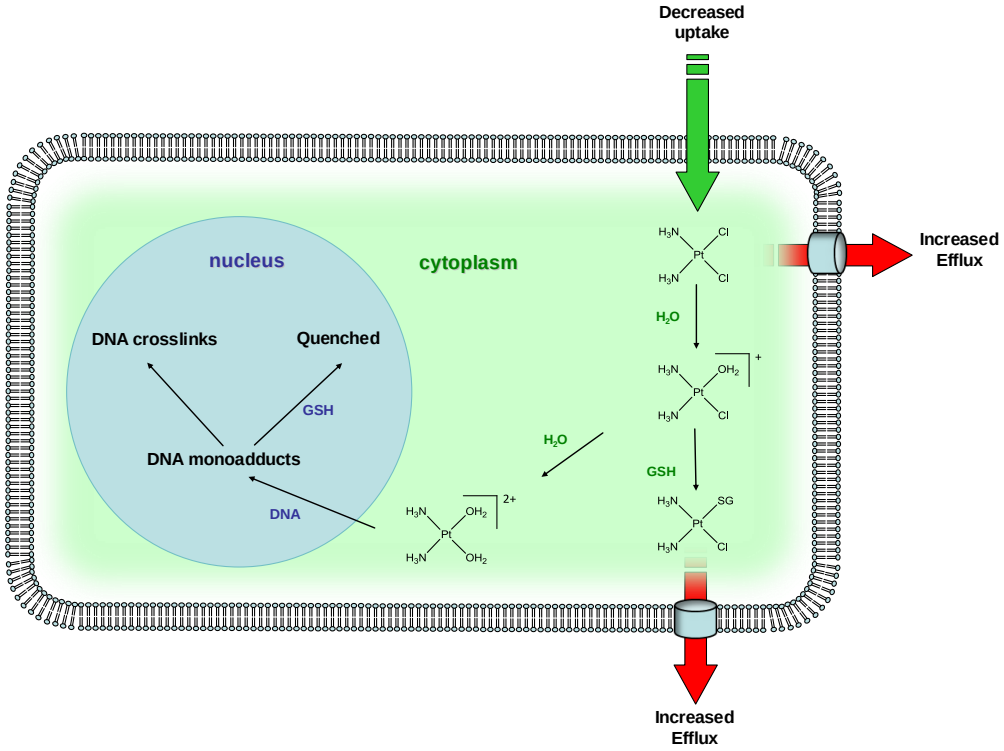

Figure 1.5. Intracellular reactions of cisplatin with DNA and GSH as well as the efflux of the GS-Pt complex. GSH in the nucleus can quench Pt-DNA monoadducts before crosslinking can occur. The membrane-bound GS-X pump eliminates the GS-Pt complex from the cell, and is ATP-reliant. *Adapted from Ishikawa*[35] *and Kartalou*.[18]

1.1.7 Second and third generation platinum(II) chemotherapeutics

New platinum anticancer agents were developed in attempts to overcome the problems with cisplatin toxicity and resistance. Second generation drugs include carboplatin and oxaliplatin (Figure 1.6) which display very significant reductions in nephro- and ototoxicity *c.f.* cisplatin, allowing administration of higher, more effective doses.[10,40] Carboplatin, [Pt(cyclobutane-1,1-dicarboxylate-*O,O'*)$(NH_3)_2$],

was first approved by the FDA in 1989 for the treatment of ovarian cancer.[8] It possesses a six-membered dicarboxylate ring, imparting greater stability through a chelate effect.[10] It is currently in clinical use, although it is associated with increased thrombocytopenia,[9] and is a myelosuppressant, leaving patients prone to infection.[11] Oxaliplatin, [Pt(ox-*O,O'*)((1*R*,2*R*)-1,2-diaminocyclohexane-*N,N'*)], is less myelosuppressive and, unlike carboplatin, can be used to treat cisplatin-resistant tumours. Oxaliplatin causes peripheral neuropathy, which is irreversible after prolonged administration; this is a source of dose limitation.[40]

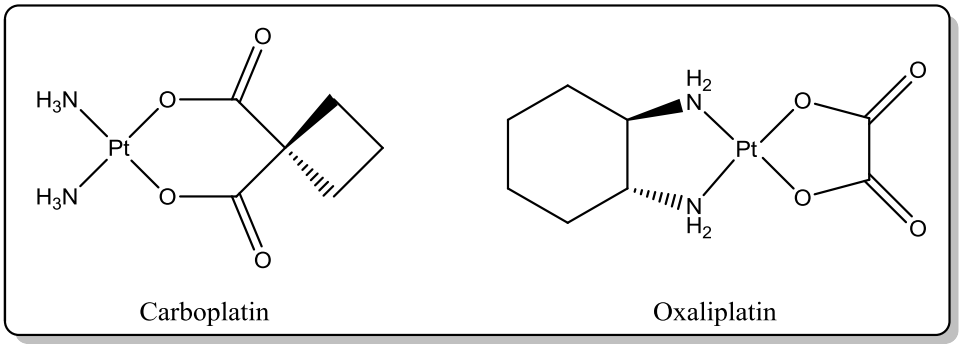

Figure 1.6. Structures of carboplatin and oxaliplatin.[11]

Newer, third generation, platinum anticancer drugs have received regional approval (Figure 1.7). Nedaplatin is in clinical use in Japan; its dosage is limited by myelosuppression. Lobaplatin (*R,R*/*S,S*) is in use in China; its dosage is limited by thrombocytopenia. Heptaplatin is approved in South Korea; it is known to cause dose-limiting nephrotoxicity.[41] Of the second and third generation of platinum anticancer drugs, only carboplatin and oxaliplatin are in use worldwide.[11]

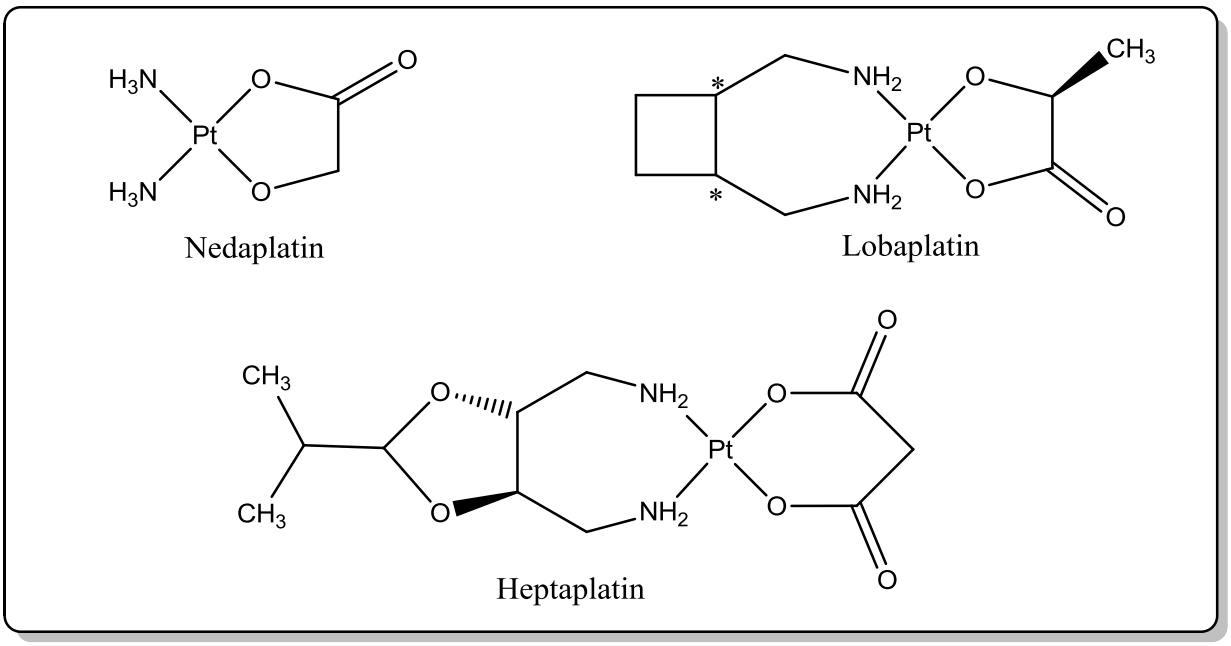

Figure 1.7. Structures of some Pt(II) anticancer drugs which have received regional approval.

1.1.8 Improving the delivery of cisplatin

No new small molecule platinum anticancer drugs have entered clinical trials since 1999.[42] Instead, the field has seen investment in developing drug delivery technology to improve the toxicity and pharmacodynamic/pharmacokinetic profiles achievable with platinum anticancer drugs.[8]

There are a number of approaches being explored (often concurrently) in order to achieve this, including new formulations of cisplatin-based agents. Currently undergoing clinical trial, Lipoplatin™ is a liposomally encapsulated IV formulation of cisplatin developed to improve targeting tumours and reduce side-effects.[42]

Alternative delivery routes have also been explored. There are examples of pulmonary delivery of cisplatin for the local treatment of lung cancer.[43] An oral formulation of cisplatin has undergone a Phase I trial,[44] but no advance to Phase II and no comparison to IV cisplatin efficacy has since been reported.

Nasal drug delivery (NDD) offers an alternative administration route which can be exploited for both systemic and local drug delivery.

1.2 NASAL DRUG DELIVERY

1.2.1 Local and systemic drug delivery *via* the nose

Nasal drug delivery is traditionally associated with topical administration of drugs which act locally, *e.g.* decongestant nasal sprays, corticosteroids, histamine H_1-antagonists and steroidal anti-inflammatories.[45] The nose is now receiving major attention as a route for systemic administration, as it is highly vascularised and highly permeable, allowing suitable drugs to be rapidly absorbed into the systemic circulation.[46-49]

The growing popularity of NDD for systemic effect may be in part due to the growing research into protein and peptide-based treatments, and the accompanying need to explore alternatives to oral and parenteral delivery.[50] Already, a number of drugs including peptides (*e.g.* oxytocin, insulin, growth hormone and adrenocorticotropic hormone), steroids (*e.g.* corticosteroids, estradiol, progesterone, testosterone), antihypertensives (*e.g.* nifedipine, propranolol), analgesics (*e.g.* buprenorphine), antibiotics and antivirals have been administered successfully *via* the nasal cavity, producing systemic effect.[51] Products already on the market include anti-migraine drugs (sumatriptan by GlaxoSmithKline, zolmitriptan by AstraZeneca, ergotamine by Novartis and butorphanol by BristolMyersSquibb) and peptide products (calcitonin by Novartis, desmopressin by Ferring and buserelin by Aventis).[49]

As well as showing usefulness for systemic drug delivery, the intranasal (IN) route is being investigated as a potential path to deliver drugs to the central nervous system (CNS), including the brain.[49]

1.2.2 Direct nose-to-brain delivery

In vivo efficacy of drugs designed to treat depression, schizophrenia, epilepsy, encephalitis, multiple sclerosis and neurodegenerative diseases is limited by poor permeation across the blood brain barrier (BBB).[52] The neuroepithelium of the

olfactory region represents the only area in the human body where an extension of the central nervous system comes into direct contact with the external environment.[53,54] This olfactory epithelium presents a drug absorption route, which by the absence of the BBB, allows direct nose-to-brain absorption. Exploiting this route may offer a non-invasive approach for improved delivery of drugs to the central nervous system (CNS). Drugs such as levodopa,[55] cephalexin[56] and insulin-like growth factor-1[57] delivered *via* the nasal cavity have shown significant improvement in neurological activity of the brain, supporting the argument that drugs may be administered through the nose to the CNS.[49,58-64]

Chen and colleagues found that a significant amount of recombinant human nerve growth factor (NGF) could be delivered to the brain *via* the olfactory pathway, compared to little or no delivery to the brain following IV administration.[65] Accumulation of NGF in the olfactory bulb of the brain has been found to a be linear function of the IN dose and concentration at the olfactory epithelium, supporting the evidence for a nose-to-brain pathway *via* the olfactory mucosa.[54] Colombo and colleagues have observed rapid uptake of ribavirin into the CNS following IN administration, with drug found in deep regions such as the hippocampus and basal ganglia.[66] Other substances which have been successfully delivered to the brain in animal models include the hexapeptide hexarelin[61] and ergoloid mesylate.[67]

It should be noted that other studies have found limited delivery from the mucosa to pharmacologically relevant targets in the CNS.[68] Bagger and Bechgaard have reported that brain targeting of sodium fluorescein to the brain *via* the olfactory epithelium was limited.[68] Limited absorption across the olfactory mucosa may be the case for many small, hydrophilic as permeability coefficient increases with increasing water/octanol partition coefficient. However, good aqueous solubility is required for nasal drug delivery and so the correct balance must be sought.[45,66,68] The potential for nose to brain delivery may therefore be drug specific.

Whilst direct delivery to the CNS may not be the aim of this work, it should be noted that this route offers a potential source of drug toxicity which would not have been a

consideration where IV delivery prevented CNS absorption due to the BBB. This is a potential disadvantage for NDD.

1.2.3 Advantages of nasal drug delivery

Intravenous infusion is the current route of cisplatin administration and is associated with pain, inflammation, infection risk and patient acceptability issues.

Nasal administration is convenient; the nasal epithelium presents a large porous surface area for absorbing drugs and a good systemic blood supply, ensuring rapid drug absorption which by-passes hepatic first pass metabolism.[46,48,69] Additionally, nasal administration supports convenient self-medication, improving patient compliance compared to parenteral routes for non-orally available drugs.[45,50] For example, IN calcitonin is now used more often than its subcutaneous predecessor due to improved patient acceptability.[70]

Absorption of drugs delivered nasally is generally very much higher than oral delivery of the same compound. Additionally, the molecular weight (MW) cut off for absorption of peroral drugs is around 200 Da. This cut-off reportedly rises to 1,000 - 20,000 Da for nasal delivery, making it a useful route for large MW compounds.[46,59,71]

From an intellectual property perspective, reformulation of existing drugs as NDD products may extend the patent lifetime of a pharmaceutical product.[59] Nasal drug delivery is also useful when multiple dosing is required,[45] for example, during cancer chemotherapy.

1.3 STRUCTURE AND FUNCTION OF THE NOSE

It is important to bear in mind that the nose has been fashioned by evolution to be suited its function. An insight into the anatomy and physiology used to achieve this function will allow an understanding of the advantages which can be exploited, and the barriers which must be overcome for successful NDD.

1.3.1 The nose

The nose has two main functions: olfaction (the sensory perception of smell) and conditioning inspired air before it reaches the lungs.[47] The outermost region of the nose, the nasal vestibule, runs for about 15 mm between the nostrils and the nasal valve (Figure 1.8). Behind this valve the nasal cavity extends posteriorly for about 60 mm before passing into the nasopharynx.[46] The nasal cavity between consists of the atrium, turbinates, and the olfactory region (Figure 1.8).

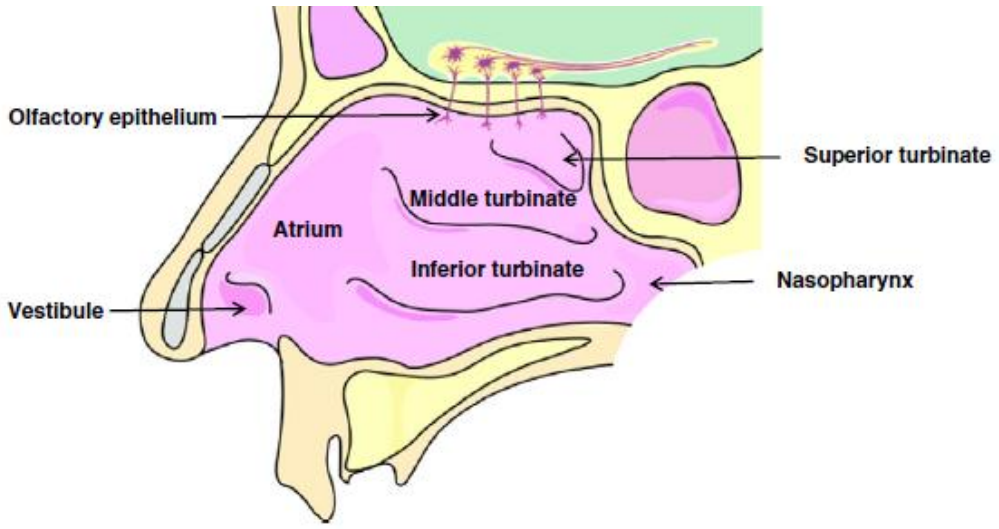

Figure 1.8. Diagram showing the different regions of the human nasal cavity: the vestibule; atrium; inferior, middle and superior turbinate; olfactory region and the nasopharynx.[72]

1.3.2 The turbinates

The nasal cavity is divided into two by the median septum. The wall opposite each side of the septum is convoluted into three folds, or turbinates (Figure 1.8), which provide resistance to air flow and present a relatively large mucosal surface area.[47,69,73] The epithelium in this region contains pseudostratified ciliated columnar cells, each with around 300 microvilli.[51] Despite a small total volume of 20 mL, the folded turbinates and ciliated epithelial cells provide an overall surface area of around 160 cm^2.[51] The high density of underlying vasculature combined with this large surface area allow for efficient transfer of heat and moisture from the mucosa to the inspired air, thus conditioning it before it reaches the lungs.[73] These characteristics also make the respiratory region a good site for drug absorption.[46]

The dense network of blood capillaries drain into the sphenopalatine, facial and ophthalmic veins, followed by the internal jugular vein and then into the heart.[72] Ultimately, this means that a drug absorbed *via* the nasal respiratory region can avoid hepatic first pass metabolism.

1.3.3 The olfactory region

Whilst the anterior regions of the nasal cavity from the vestibule to the turbinates is lined with squamous epithelium, the upper area of the cavity is lined with olfactory membrane.[46] This olfactory region accounts for up to 5%[74] (around 5 cm^2, although up to 10%, or 10 cm^2 has been reported in the literature)[47] of the total surface area and contains the sensory olfactory cells as well as serous and mucosal cells.[46] The olfactory region has several million sensory neurones, allowing the human nose to detect more than 100,000 different odours and discriminate between 5,000.[75] The nose can also sense chemical burning when stimulated by, for example, ammonia or chilli pepper. This type of sensation stimulates nasal secretions and sneezing, acting as a protective mechanism.[75] Drug absorption *via* the olfactory region provides a direct route to the cerebrospinal fluid whilst bypassing hepatic first pass metabolism.[51,76]

The structural features and permeability of the nasal cavity regions are summarised in Table 1.1.

Table 1.1. Structural features of the nasal cavity and their impact on permeability.[51]

Region	Structural features	Permeability
Nasal vestibule	Nasal hairs (vibrissae). Epithelial cells are stratified, squamous and keratinised. Sebaceous glands present.	Least, due to keratinisation.
Atrium	Transepithelial region. Stratified squamous cells present anteriorly. Pseudostratified cells with microvilli present posteriorly. Narrowest region of the nasal cavity.	Less permeable due to small surface area and stratified cells posteriorly.
Respiratory region (turbinates)	Pseudostratified ciliated columnar cells with microvilli (300 per cell), large surface area. Receives maximum nasal secretions due to the seromucus glands, nasolacrimal duct and goblet cells. Richly supplied with blood for conditioning inspired air.	Most permeable region due to large surface area and rich vasculature.
Olfactory region	Specialised ciliated olfactory nerve cells for smell perception. Received ophthalmic and maxillary divisions of trigeminal nerve. Direct access to cerebrospinal fluid.	Direct access to cerebrospinal fluid.
Nasopharynx	Upper part contains ciliated cells and lower part contains squamous epithelium.	Receives nasal cavity drainage.

1.3.4 Defence

Another vital function of the nose is to prevent noxious substances (allergens, bacteria, viruses, toxins *etc.*) from entering the lungs.[59] The nasal secretions contain a number of enzymes, lymphocytes and immunoglobins which perform an immunological role.[75] Particles over 30 μm are filtered out of the inspired air by the vibrissae. Others are trapped in the mucus and cleared from the nasal cavity by the beating of the cilia.[75] Whilst the structure and physiology of the nose is suited to its function, the protective mechanisms in operation often raise barriers to drug absorption.

1.4 BARRIERS TO DRUG ABSORPTION

A nasally delivered drug will have to permeate the nasal mucosal layer in order to access the underlying capillaries. This permeation is governed by structural, biochemical and physiological properties of the nasal mucosa, as well as the characteristics of the drug itself.

1.4.1 Nasal metabolism degrades drugs

Whilst the nasal route avoids hepatic first pass metabolism, it must be noted that the nasal mucosa retains a degree of metabolic capacity, particularly in the olfactory region.[46] Cytrochrome P450 monooxygenases, which facilitate primary oxidative metabolism of many drug compounds, are present in the nose at concentrations second only to the liver.[45,77,78] Other metabolic enzymes include dehydrogenases, hydroxylases, carboxylesterases, carbonic anhydrase and various phase II enzymes.[46] Additionally, nasal secretions contain albumin, to which a labile drug may be sequestered.[51]

In order for a nasally delivered drug to reach therapeutic concentrations at the site of action, it must be able to withstand this nasal metabolism.

1.4.2 Nasal mucus forms a physical barrier

About 1.5–2 L of nasal secretions are produced each day, forming a double-layer mucus blanket. These secretions consist of up to 90% water, 2% mucin, 1% salts, 1% proteins (including albumin, immunoglobulins and lysosome) and some lipids. The drug must be soluble in this complex mixture in order to be absorbed.[51]

Mucins are produced in the goblet cells and seromucinous glands and released by exocytosis.[79] They are high MW glycoproteins up to 4 μm in length, consisting of random coils of carbohydrate chains attached to a protein core by *O*-glycoside linkages. Large amounts of sugar residues, consisting of a sugar side chain

covalently linked to a polypeptide chain, are polymerised by disulfide bridges, influencing the rheology of the mucus. There are also a high number of hydroxylated amino acid residues.[79] Mucins can therefore link through covalent bonds and non-covalent bonds, forming a three-dimensional network (Figure 1.9). The network is hygroscopic and forms a gel on interaction with water and ions.[79]

A drug to be administered nasally must be able to pass through the mucus layer in order to reach the underlying mucosa. Since mucins are negatively charged, a positively charged drug moiety would bind to the mucus, slowing or preventing the effect of the drug.[80]

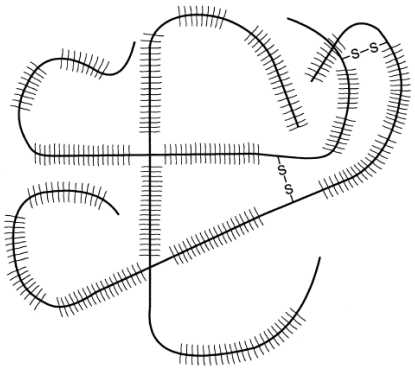

Figure 1.9. Diagram representing the structure of a mucin network. Each mucin is made up of a peptide backbone with glycosylated regions. In this representation, three mucin molecules form a lattice and are linked by weak non-covalent bonds and strong disulfide covalent bonds.[79]

The mucus protects the nasal mucosa physically and enzymatically, it maintains a high moisture level, exhibits surface electrical properties and allows for efficient heat exchange. Importantly, the mucus also acts as an adhesive which catches foreign particles. The mucus, containing xenobiotics and foreign bodies, is then eliminated from the nose *via* mucociliary clearance.

1.4.3 Mucociliary clearance reduces contact time

Nasal mucus is cleared by the beating of the cilia from the nasal cavity to the nasopharynx and then gastrointestinal (GI) tract from where it will ultimately be eliminated or destroyed.[46] The mucus clearance half-life is approximately 15 min in humans.[47,73] This mucociliary clearance (MCC) is a non-specific defence

mechanism which helps protect the respiratory system from viruses, bacteria, toxins and allergens.[59,81]

The clearance is possible because the mucus exists in two layers: the lower viscosity sol layer on the surface of the mucosa, and the more viscous gel layer on top of that. The cilia protrude through the sol layer and into the gel layer. Rapid beating of the cilia moves the gel layer forward, and then a slower recovery stroke pulls the cilia back through the low viscosity sol layer, enabling successive beating (Figure 1.10). The cilia are each between 5-10 μm long, 0.1-0.3 μm wide, and beat with a frequency of 20 Hz. The rate of MCC has been estimated at 6 mm/min.[59]

A nasal formulation must be able to overcome the physical barrier of mucus but also evade MCC for long enough to facilitate drug dissolution and absorption, without long-term interruption of the normal physiological performance.[46]

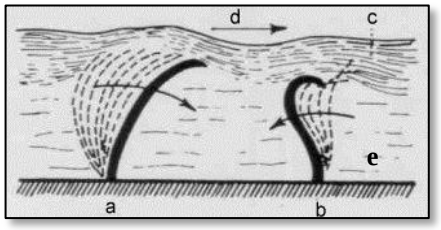

Figure 1.10. The ciliary motion and double mucus layer that contribute to MCC, showing a) an effective stroke, b) a recovery stroke, c) the gel layer, d) the direction of gel layer movement, and e) the sol layer.[82]

1.4.4 Influence of drug characteristics

Once a drug penetrates the mucus layer, it must be able to permeate the mucosa in order to reach the capillaries below. Low MW lipophilic drugs may penetrate the nasal mucosa transcellularly, as they are able to partition across the phospholipid bilayer.[45] For drugs which are more hydrophilic, or if tight junctions between cells are opened, paracellular routes dominate.[45] Transport through tight junctions is limited for molecules larger than 3 Å, and negligible above 15 Å.[83] The largest flux

of drugs is seen when they are in their unionised state; however, significant absorption has also been observed with some ionised drugs.[45]

In order to overcome some of the barriers to drug absorption, a number of strategies have been developed including the use of enzyme inhibitors and absorption promoters.

1.4.5 Strategies for optimising absorption

Due to the constant movement and replacement of the mucus layer in the nasal cavity, there will only be a short window for drug absorption to occur.[73,84] Absorption promoters such as bile salts, surfactants and cyclodextrins, are commonly used to improve nasal drug bioavailability by increasing the rate at which a drug is absorbed. Cyclodextrins are a class of macrocycle which can form inclusion complexes with a drug, improving solubility and improving bioavailability. Other enhancers act by opening tight junctions (*e.g.* chitosan) or increasing membrane fluidity (*e.g.* sodium dodecyl sulfate) by creating disorders in the phospholipid layer or by facilitating the leaching of proteins and lipids from the membrane.[85] This can cause membrane damage and cessation of mucociliary clearance. In fact, some authors have suggested that increased absorption may be due to damage caused to the mucosa. [86]

An ideal drug formulation would not interfere with the natural function of the nose.[87] An alternative to using absorption enhancers is to increase the residence time of the formulation in the nasal cavity, allowing more time for the drug to be absorbed. This can be achieved using a mucoadhesive formulation designed to resist MCC.[88]

1.5 MUCOADHESIVE DOSAGE FORMS

1.5.1 Mucoadhesion

Bioadhesion is the state in which two materials, one of which being biological in nature, are held together by interfacial forces for an extended period of time. Specifically, mucoadhesion operates when the biological material is mucus or a mucous membrane.[89]

The first stages of bioadhesion involve intimate contact between the bioadhesive and the biological tissue due to wetting and swelling of the polymer. During hydration, the polymer-water interaction becomes greater than the polymer-polymer interactions and the solid will wick up moisture and swell, freeing the polymer chains.[59] The polymer then penetrates into the tissue crevices and/or infiltrates the chain aggregates of the mucus.[90] In addition, it has been proposed that water uptake by a swelling polymer causes transient osmotic opening of tight junctions, aiding drug absorption.[91,92] The total work of bioadhesion includes both interaction of the polymer chains with glycoproteins on the cell surface[93] and interaction with mucus.

Mucoadhesion is generally considered to be the result of both chemical interaction (van der Waals, hydrogen, hydrophobic and electrostatic interactions) and physical interpenetration of the polymer and mucin chains, although a number of models have been proposed.[94]

1.5.2 The theories of mucoadhesion

A number of theories are used to describe and quantify mucoadhesion. The **wettability theory** considers the physical contact of the polymer with the surface. Mainly applicable to liquids and low viscosity polymers, this theory postulates that the mucoadhesive agent spreads across the surface, penetrating irregularities, hardening, and anchoring itself.[95]

The **electronic theory** considers the transfer of electrons in the system, postulating that transfer between mucoadhesive and the mucus establishes an electronic double layer and subsequent attractive forces.[96]

The **fracture theory** quantifies the strength of a mucoadhesive bond as the force required to separate the two surfaces.[97] This model assumes that the point of failure of a mucoadhesive bond is the interface between the two media.[95]

The **adsorption theory** defines the strength of adhesion as the sum of ionic, covalent, metallic, van der Waals bonds, hydrophobic interactions and hydrogen bonding between the mucoadhesive surface and the mucus.[95] It has been proposed that these forces are mainly responsible for the adhesion.[95]

The **diffusion-interlocking theory** (interpenetration) considers the diffusion of mucoadhesive polymer chains into the mucus layer (and the diffusion of the mucin chains into the mucoadhesive chains) in a time-dependent manner. The rate of this inter-diffusion is influenced by concentration gradients, MW, cross-linking density, chain flexibility/mobility, temperature and the expansion capacity of both networks.[95,98,99]

These theories should be considered, not as alternatives to each other, but as supplementary and complimentary processes which may occur at different stages in the interaction, although the main contributions are thought to come from interpenetration and non-covalent bonding.[95]

1.5.3 Polymer effects on mucoadhesion

Various polymer properties are understood to affect mucoadhesion, including pH, charge, polymer concentration, MW, chain length, degree of cross-linking, conformation, degree of hydration and functional groups. Given the contribution that non-covalent bonding makes to mucoadhesion, the presence of hydrophilic functional groups such as carboxyl (-COOH), hydroxyl (-OH), amide ($-NH_2$) and

sulfate (-SO_4H) allows the mucoadhesive polymer to interact more strongly with the mucus glycoproteins.[99]

The degree to which the polymer is hydrated can influence mucoadhesion. For example, in conditions where the amount of water is limited (*e.g.* dry polymer), the polymer may exhibit mucoadhesion through a combination of capillary action and osmotic forces, acting to dehydrate the mucus layer. Where a swollen ("wet") mucoadhesive is adhering to a mucosal surface, the hydration of the polymer is essential for relaxation and interpenetration of the polymer chains. If the polymer is too hydrated however, a reduction in mucoadhesion can occur due to the formation of a slippery mucilage. Cross-linked polymers that only allow a certain degree of hydration may be useful for providing prolonged mucoadhesion.[95]

Molecular weight and chain length influence the degree of mucoadhesion. In general, the longer the chain, the more entanglement is possible and the greater the mucoadhesion achieved. Excessively long polymers however lose their ability to interpenetrate mucus.

A polymer with a higher degree of cross-linking will retain its structure upon swelling, whereas a linear polymer will be more readily swellable and dispersible. More cross linking also results in less chain mobility, meaning that interpenetration and entanglement is hampered.[95]

The pH of the physiological environment will affect the ionisation of any ionisable functional groups on the polymer. Undissociated anionic pendant functional groups provide the greatest potential for hydrogen bonding between the mucoadhesive and the mucin. This means that lower pH may be favoured to retain a high degree of association.[95]

The concentration of the mucoadhesive polymer is also important. For semisolids, an optimal concentration exists for each polymer, above which reduced adhesion

occurs. For solid formulations, increased mucoadhesion can be observed upon increasing concentration.[59,95]

1.5.4 Mucoadhesive delivery of drugs to the nose

A number of studies are reviewed in the literature, showing that mucoadhesion is the predominant factor responsible for improving drug absorption in mucoadhesive nasal drug delivery systems. For example, the pharmacokinetic profiles of apomorphine after nasal administration have been improved using mucoadhesive polymers, such as polyacrylic acid, carbopol and carboxymethylcellulose, with bioavailability equal to subcutaneous injection.[100,101] Antibiotics have been delivered *via* mucoadhesive nasal delivery systems, but questions have been raised regarding the prolonged residence in the nasal cavity upsetting normal microbial flora.[59] The technology is also being explored for use in vaccination, DNA delivery and protein delivery without the need for needles.[59]

Mucoadhesive polymeric gel formulations are often viscous and difficult to apply intranasally. Currently, suitable delivery devices are not readily available, and require great energy output in order to disperse the formulation. The energy and shear required may cause degradation of a number of drugs and biopharmaceuticals.[59] This has led to the investigation of a dry dosage form, which hydrates *in situ*, yielding a mucoadhesive polymer gel.

1.6 LYOPHILISED NASAL INSERTS

1.6.1 The lyophilised nasal insert

With the route of administration established, consideration must be given to the type of formulation. Solid form powders and microparticles require sophisticated delivery apparatus for accurate dosing and deposition.[102] Solutions have been shown to experience rapid clearance, not allowing for extended drug release.[103] Additionally, solutions or gels can present drug stability issues.

Increasing the viscosity of a formulation acts to increase the contact time with the nasal mucosa, increasing drug absorption. Additionally, highly viscous materials are detrimental to ciliary beating, mucociliary clearance, and postnasal drip, thus extending residence time.[51]

A nasal insert formulation can provide an easy-to-handle solid formulation that hydrates rapidly *in situ* to produce a mucoadhesive gel, with extended residence time inside the nasal cavity and minimal cognition of a foreign body.[50] The self-contained unit presented by a lyophilised nasal insert also allows for accurate dosing.

Bertram[50], McInnes[84,88] and Luppi[104] have previously reported the lyophilisation of polymer gel-based formulations to produce dose-unit bioadhesive nasal inserts providing extended drug delivery.[50]

1.6.2 Delivery of therapeutics using lyophilised nasal inserts

McInnes and colleagues have shown that a 2% (w/w) hydroxypropyl methylcellulose (HPMC) nasal insert can evade mucociliary clearance for 4-5 h.[88] Gamma scintigraphy was used to show that a lyophilised nasal insert, placed in the anterior nasal cavity will spread posteriorly before being cleared eventually *via* the nasopharynx.[88] They have also shown that delivery of nicotine using these nasal inserts can sustain a significant plasma level for around 2 h, followed by a gradual decrease in plasma levels, at a lower rate than those seen for an equivalent nasal powder and spray.[84]

Bertram and Bodmeier have reported that release of a drug from a nasal insert is influenced by the solubility of the drug, the physical state of the drug and the electrostatic interactions between the drug and polymer.[105] Lyophilised chitosan/pectin inserts for the delivery of antipsychotics have been demonstrated by Luppi and colleages.[106] They reported that the water uptake and subsequent drug release from the inserts could be tuned by varying the chitosan/pectin ratio.[104]

1.6.3 Hydroxypropyl methylcellulose

Hydroxypropyl methylcellulose HPMC is a partly *O*-methylated and *O*-(2-hydroxypropylated) cellulose (Figure 1.11). It is available in a number of grades which vary in viscosity and degree of substitution.

HPMC is generally regarded as safe (GRAS) and commonly used as an excipient in ophthalmic, nasal, oral and topical formulations, finding use as a bioadhesive, coating agent, controlled release agent, mucoadhesive, stabilising agent and tablet binder. Additionally, it is accepted for use as a food additive in Europe, has been included in the FDA Inactive Ingredients Database and has been included in non-parenteral medicines licensed in the United Kingdom.[107]

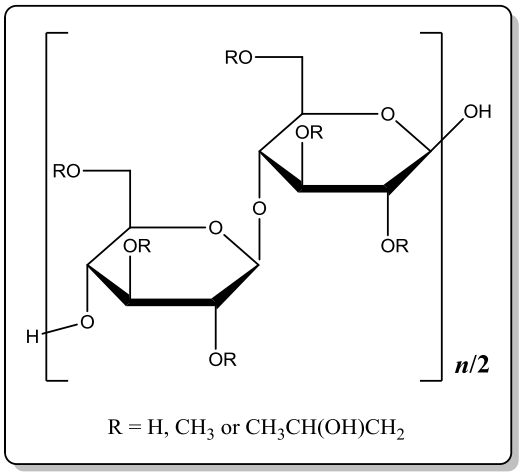

Figure 1.11. The general formula of hydroxypropyl methylcellulose.

HPMC gel remains amorphous after freeze-drying, producing a network-like lyophilisate which is porous and sponge-like. Crystalline materials do not behave in this way, producing a powder, rather than a sponge, upon freeze-drying.[50] Some other amorphous polymers, such as sodium carboxymethylcellulose, form long, stratified layers instead of fine pores and so are unsuitable for controlled release formulation.[50] HPMC is neutral, and so its mucoadhesive nature is thought to be linked to entanglement by virtue of its high MW.[50] McInnes and colleagues have previously used HPMC for the production of lyophilised nasal insert formulations

containing nicotine and insulin.[84,88] These are designed to hydrate rapidly *in situ*, producing a mucoadhesive gel.

1.6.4 Lyophilisation

Freeze drying, or lyophilisation, is the process by which frozen solvent is sublimed from a sample, without passing into the liquid phase. The technique is used commonly in the pharmaceutical industry, often as a tool for preserving a substance which is labile in solution or must remain free from microbial activity (*e.g.* parenteral formulations).[108] The use of preservatives in "wet" nasal formulations has been shown to affect cilliary beat frequency in *vivo*,[87] in addition to triggering allergic responses.[109] A lyophilised formulation offers substance-free preservation. Freeze dried materials are often easily reconstituted because the process leaves pores in the material where the frozen solvent molecules previously resided.

The process consists of three main stages: freezing, primary drying and secondary drying.[108] In the freezing stage, the sample must be cooled to below the temperature at which solid, liquid and gaseous phases can coexist (the material's triple point[110]). This ensures that the solvent is sublimed, rather than melted and evaporated. The triple point of water is 273.16 K at 0.0060373 atm (Figure 1.12).

Primary drying sees the pressure of the chamber lowered and enough heat applied to sublime the frozen solvent.[108] The application of a partial vacuum encourages sublimation. The sublimed water vapor is then refrozen at a condenser, preventing it from entering the vacuum pump or returning to the sample. About 95% of water is removed during this primary drying step.[108]

During secondary drying, the temperature is raised to overcome any interactions which may exist between any remaining, unfrozen, solvent and the sample being dried.[108] Additionally, the chamber pressure is often lowered further to promote desorption.

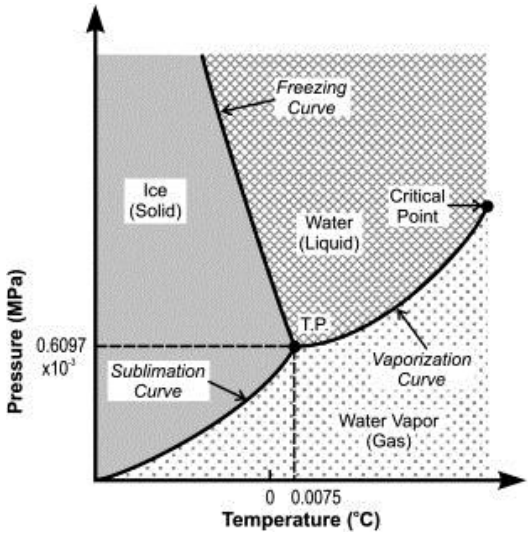

Figure 1.12. A typical phase diagram showing the triple point (indicated as TP), the unique temperature and pressure at which all three phases can coexist in equilibrium.[111]

1.7 SUMMARY

The use of cisplatin-based chemotherapy against cancer is hampered by resistance and dose limiting toxicities. The development of new platinum-based drugs to overcome these problems is now being overshadowed by investment in improved delivery of existing ones. This includes the use of drug delivery vehicles and exploration of new delivery routes.

A route *via* the nasal cavity is attractive as it offers a large area for drug absorption, improved patient compliance, avoidance of first-pass metabolism and no need for parenteral administration; however, nasal drug delivery is complicated by rapid clearance and nasal metabolism.

A mucoadhesive delivery system can be used to extend residence time in the nasal cavity, allowing for optimised drug absorption. Lyophilised nasal inserts would provide the means of administering this formulation as a robust, dry, single unit which hydrates *in situ*, forming a mucoadhesive gel.

The chapters that follow describe two drug delivery vehicles, cucurbiturils and carbon nanotubes, which have been shown to improve metabolic and physical stability of a guest drug molecule. These were investigated as potential vectors to reduce metabolism and enhance the nasal delivery of platinum(II) chemotherapeutics, for eventual inclusion in a lyophilised nasal insert formulation.

1.8 REFERENCES

(1) http://info.cancerresearchuk.org/cancerstats/index.htm, *accessed 25th November 2009.*

(2) http://info.cancerresearchuk.org/cancerstats/, *accessed 24th August 2012.*

(3) Fact Sheet No. 297 Cancer, http://www.who.int/mediacentre/factsheets/fs297/en/index.html, *accessed 13th January 2010.*

(4) Mader, S.S., *Biology*, 5th ed., Wm. C. Brown Publishers, Dubuque, 1996.

(5) Tortora, G.J. and Grabowski, S.R., *Principles of Anatomy and Physiology*, 8th ed., Harper Collins, New York, 1996.

(6) http://www.angioworld.com/images/DominiqueGarrel/fig1.png, *accessed 14th January 2010.*

(7) Watson, M., Barrat, A., Spence, R. and Twelves, C., *Oncology*, 2nd ed., Oxford University Press, Oxford, 2006.

(8) Kelland, L., *Nat. Rev. Cancer*, 2007, **7**, 573-584.

(9) Cassidy, J., Bissett, D., Spence, R.A.J. and Payne, M. (Ed), *Oxford Handbook of Oncology*, 2nd ed., Oxford University Press, Oxford, 2007.

(10) Boulikas, T. and Vougiouka, M., *Oncol. Rep.*, 2003, **10**, 1663-1682.

(11) Dabrowiak, J.C., *Metals in Medicine*, 1st ed., John Wiley & Sons, Chichester, 2009.

(12) Peyrone, M., *Liebigs Ann. Chem.*, 1844, **51**, 1-29.

(13) Rosenberg, B., *Platinum Met. Rev.*, 1979, **15**, 42-51.

(14) Rosenberg, B., Van Camp, L., Trosko, J.E. and Mansour, V.H., *Nature*, 1969, **222**, 385-386.

(15) Rosenberg, B., Vancamp, L. and Krigas, T., *Nature*, 1965, **205**, 698-699.

(16) *British National Formulary*, 53rd ed., BMJ Publishing Group Ltd & RPS Publishing, London, 2007.

(17) *The British Pharmacopoeia*, Vol. 2, The Stationary Office, London, 2001.

(18) Kartalou, M. and Essigmann, J.M., *Mutat. Res.-Fund. Mol. M.*, 2001, **478**, 23-43.

(19) Salles, B., Butour, J.L., Lesca, C. and Macquet, J.P., *Biochem. Biophys. Res. Comm.*, 1983, **112**, 555-563.

(20) Uchida, K., Tanaka, Y., Nishimura, T., Hashimoto, Y., Watanabe, T. and Harada, I., *Biochem. Biophys. Res. Comm.*, 1986, **138**, 631-637.

(21) Mello, J.A., Lippard, S.J. and Essigmann, J.M., *Biochemistry*, 1995, **34**, 14783–14791.

(22) Siddik, Z.H., *Oncogene*, 2003, **22**, 7265-7279.

(23) Gately, D.P. and Howell, S.B., *Br. J. Cancer*, 1993, **67**, 1171-1176.

(24) Binks, S.P. and Dobrota, M., *Biochem. Pharmacol.*, 1990, **40**, 1329-1336.

(25) Toffoli, G., Bevilacqua, C., Franceschin, A. and Boiocchi, M., *Int. J. Hyperther.*, 1989, **5**, 163-172.

(26) Griffin, A.M., Butow, P.N., Coates, A.S., Childs, A.M., Ellis, P.M., Dunn, S.M. and Tattersall, M.H.N., *Ann. Oncol.*, 1996, **7**, 189-195.

(27) Yao, X., Panichpisal, K., Kurtzman, N. and Nugent, K., *Am. J. Med. Sci.*, 2007, **334**, 115-124.

(28) Lewis, J.G., *Pharmaceutics*, 4th ed., Hodder and Stoughton, London, 1980.

(29) Holzer, A.K. and Howell, S.B., *Cancer Res.*, 2006, **66**, 10944-10952.

(30) Howell, S.B., Safaei, R., Larson, C.A. and Sailor, M.J., *Mol. Pharmacol.*, 2010, **77**, 887-894.

(31) Fujii, R.-I., Mutoh, M., Niwa, K., Yamada, K., Aikou, T., Nakagawa, M., Kuwano, M. and Akiyama, S.-I., *Cancer Sci.*, 1994, **85**, 426-433.

(32) Holford, J., Beale, P.J., Boxall, F.E., Sharp, S.Y. and Kelland, L.R., *Eur. J. Cancer*, 2000, **36**, 1984-1990.

(33) Meijer, C., Mulder, N.H., Timmer-Bosscha, H., Sluiter, W.J., Meersma, G.J. and de Vries, E.G.E., *Cancer Res.*, 1992, **52**, 6885-6889.

(34) Hall, M.D., Alderden, R.A., Zhang, M., Beale, P.J., Cai, Z., Lai, B., Stampfl, A.P.J. and Hambley, T.W., *J. Struct. Biol.*, 2006, **155**, 38-44.

(35) Ishikawa, T. and Ali-Osman, F., *J. Biol. Chem.*, 1993, **268**, 20116-20125.

(36) Ferry, K.V., Hamilton, T.C. and Johnson, S.W., *Biochem. Pharmacol.*, 2000, **60**, 1305-1313.

(37) Gadducci, A., Cosio, S., Muraca, S. and Genazzani, A.R., *Eur. J. Gynaecol. Oncol.*, 2002, **23**, 390-396.

(38) Ozols, R.F., *Cancer Treat. Rev.*, 1991, **18**, 77-83.

(39) Giaccone, G., *Drugs*, 2000, **59**, 9-17.

(40) Cersosimo, R.J., *Ann. Pharmacother.*, 2005, **39**, 128-135.

(41) Galanski, M., Jakupec, M.A. and Keppler, B.K., *Curr. Med. Chem.*, 2005, **12**, 2075.

(42) Wheate, N.J., Walker, S., Craig, G.E. and Oun, R., *Dalton T.*, 2010, **39**, 8113-8127.

(43) Xie, Y., Aillon, K.L., Cai, S., Christian, J.M., Davies, N.M., Berkland, C.J. and Forrest, M.L., *Int. J. Pharm.*, 2010, **392**, 156-163.

(44) Tao, Y., Rezaï, K., Brain, E., Etessami, A., Lusinchi, A., Temam, S., Urien, S., Van, M.-L.V., Vauzelle-Kervroedan, F., Lokiec, F., Daly-Schveitzer, N. and Bourhis, J., *Radiother. and Oncol.*, 2011, **98**, 42-47.

(45) Costantino, H.R., Illum, L., Brandt, G., Johnson, P.H. and Quay, S.C., *Int. J. Pharm.*, 2007, **337**, 1-24.

(46) Taylor, K.M.G. in *Aulton's Pharmaceutics*, 3rd ed., Aulton, M.E. (Ed). Churchill Livingstone Elsevier, Oxford, 2007, p 539-554.

(47) Gizurarson, S., *Adv. Drug Deliver. Rev.*, 1993, **11**, 329-347.

(48) Rathbone, M.J., Drummond, B.K. and Tucker, I.G., *Adv. Drug Deliver. Rev.*, **13**, 1-22.

(49) Illum, L., *J. Control. Rel.*, 2003, **87**, 187-198.

(50) Bertram, U. and Bodmeier, R., *Eur. J . Pharm. Biopharm.*, 2006, **27**, 62-71.

(51) Arora, P., Sharma, S. and Garg, S., *Drug Discov. Today*, 2002, **7**, 967-975.

(52) Brasnjevic, I., Steinbusch, H.W.M., Schmitz, C. and Martinez-Martinez, P., *Progress in Neurobiology*, 2009, **87**, 212-251.

(53) Stockhorst, U. and Pietrowsky, R., *Physiol. Behav.*, 2004, **83**, 3-11.

(54) Frey, W.H., Liu, J., Chen, X., Thorne, R.G., Fawcett, J.R., Ala, T.A. and Rahman, Y.-E., *Drug Deliv.*, 1997, **4**, 87-92.

(55) Kao, H.D., Traboulsi, A., Itoh, S., Dittert, L. and Hussain, A., *Pharm. Res.*, 2000, **17**, 978-984.

(56) Sakane, T., Akizuki, M., Yoshida, M., Yamashita, S., Nadai, T., Hashida, M. and Sezaki, H., *J. Pharm. Pharmacol.*, 1991, **43**, 449-451.

(57) Liu, X.-F., Fawcett, J.R., Thorne, R.G., DeFor, T.A. and Frey, W.H., *J. Neurol. Sci.*, 2001, **187**, 91-97.

(58) von Hoegen, P., *Adv. Drug Deliver. Rev.*, 2001, **51**, 113-125.

(59) Ugwoke, M.I., Agu, R.U., Verbeke, N. and Kinget, R., *Adv. Drug Deliver. Rev.*, 2005, **57**, 1640-1665.

(60) Mistry, A., Stolnik, S. and Illum, L., *Int. J. Pharm.*, 2009, **379**, 146-157.

(61) Yu, H. and Kim, K., *Int. J. Pharm.*, 2009, **378**, 73-79.

(62) Kandimalla, K.K. and Donovan, M.D., *Int. J. Pharm.*, 2005, **302**, 133-144.

(63) Henkin, R.I., *Nutrition*, 2010, **26**, 624-633.

(64) Shipley, M.T., *Brain Res. Bull.*, 1985, **15**, 129-142.

(65) Chen, X.Q., Fawcett, J.R., Rahman, Y.E., Ala, T.A. and Frey, I.W., *J Alzheimers Dis*, 1998, **1**, 35-44.

(66) Colombo, G., Lorenzini, L., Zironi, E., Galligioni, V., Sonvico, F., Balducci, A.G., Pagliuca, G., Giuliani, A., Calzà, L. and Scagliarini, A., *Antivir. Res.*, 2011, **92**, 408-414.

(67) Chen, J., Wang, X., Wang, J., Liu, G. and Tang, X., *Eur. J . Pharm. Biopharm.*, 2008, **68**, 694-700.

(68) Bagger, M.A. and Bechgaard, E., *Eur. J. Pharm. Sci.*, 2004, **21**, 235-242.

(69) Fransén, N., Björk, E. and Nyström, C., *Eur. J. Pharm. Biopharm.*, 2007, **67**, 370-376.

(70) Mu, N., oz-Torres, M., Alonso, G. and Pedro Mezquita, R., *Treat. Endocrinol.*, 2004, **3**, 117-132.

(71) Ugwoke, M.I., Verbeke, N. and Kinget, R., *J. Pharm. Pharmacol.*, 2001, **53**, 3-22.

(72) Grassin-Delyle, S., Buenestado, A., Naline, E., Faisy, C., Blouquit-Laye, S., Couderc, L.-J., Le Guen, M., Fischler, M. and Devillier, P., *Pharmacol. Therapeut.*, 2012, **134**, 366-379.

(73) Mygind, N. and Dahl, R., *Adv. Drug Deliver. Rev.*, 1998, **29**, 3-12.

(74) Morrison, E.E. and Costanzo, R.M., *Microsc. Res. Techniq.*, 1992, **23**, 49-61.

(75) Jones, N., *Adv. Drug Deliv. Rev.*, 2001, **51**, 5-19.

(76) Char, H., Kumar, S., Patel, S., Piemontese, D., Iqbal, K., Malick, A.W., Salvador, R.A. and Behl, C.R., *J. Pharm. Sci.*, 1992, **81**, 750-752.

(77) Gibson, G.G. and Skett, P., *Introduction to Drug Metabolism*, 2nd ed., Stanley Thornes (Publishers) Ltd, Cheltenham, 1994.

(78) Minn, A., Leclerc, S., Heydel, J.-M., Minn, A.-L., Denizot, C., Cattarelli, M., Netter, P. and Gradinaru, D., *J. Drug Target.*, 2002, **10**, 285-296.

(79) Quraishi, M.S., Jones, N.S. and Mason, J., *Clin. Otolaryngolog.*, 1998, **23**, 403-413.

(80) Widdicombe, J., *Eur. Respir. J.*, 1997, **10**, 2194-2197.

(81) Marttin, E., Schipper, N.G.M., Verhoef, J.C. and Merkus, F.W.H.M., *Adv. Drug Deliver. Rev.*, 1998, **29**, 13-38.

(82) Proetz, A., *The Applied Physiology of the Nose*, 1st ed., Annals Publishing Company, St Louis, 1953.

(83) Madara, J.L., *Adv. Drug Deliver. Rev.*, 2000, **41**, 2521-3253.

(84) McInnes, F.J., Thapa, P., Baillie, A.J., Welling, P.G., Watson, D.G., Gibson, I., Nolan, A. and Stevens, H.N.E., *Int. J. Pharm.*, 2005, **304**, 72-82.

(85) Merkus, F.W.H.M., Schipper, N.G.M., Hermens, W.A.J.J., Romeijn, S.G. and Verhoef, J.C., *J. Control. Rel.*, 1993, **24**, 201-208.

(86) Shao, Z. and Mitra, A.K., *Pharm. Res.*, 1992, **9**, 1184-1189.

(87) Romeijn, S.G., Verhoef, J.C., Marttin, E. and Merkus, F.W.H.M., *Int. J. Pharm.*, 1996, **135**, 137-145.

(88) McInnes, F.J., O'Mahony, B., Lindsay, B., Band, J., Wilson, C.G., Hodges, L.A. and Stevens, H.N.E., *Eur. J. Pharm. Sci.*, 2007, **31**, 25-31.

(89) Gu, J.M., Robinson, J.R. and Leung, S.H., *Crit. Rev. Ther. Drug Carrier Syst.*, 1988, **5**, 21-67.

(90) Ducheňe, D., Touchard, F. and Peppas, N.A., *Drug Dev. Ind. Pharm.*, 1988, **14**, 283-318.

(91) Edman, P., Björk, E. and Rydén, L., *J. Control. Rel.*, 1992, **21**, 165-172.

(92) Charlton, S.T., Davis, S.S. and Illum, L., *J. Control. Rel.*, 2007, **118**, 225-234.

(93) Nakamura, K., Maitani, Y., Lowman, A.M., Takayama, K., Peppas, N.A. and Nagai, T., *J. Control. Rel.*, 1999, **61**, 329-335.

(94) Ponchel, G., Touchard, F., Duchêne, D. and Peppas, N.A., *J. Control. Rel.*, 1987, **5**, 129-141.

(95) Andrews, G.P., Laverty, T.P. and Jones, D.S., *Eur. J . Pharm. Biopharm.*, 2009, **71**, 505-518.

(96) Dodou, D., Breedveld, P. and Wieringa, P.A., *Eur. J. Pharm. Biopharm.*, 2005, **60**, 1-16.

(97) Ahagon, A. and Gent, A.N., *J. Polym. Sci. Pol. Phys.*, 1975, **13**, 1285-1300.

(98) Lee, J.W., Park, J.H. and Robinson, J.R., *J. Pharm. Sci.*, 2000, **89**, 850-866.

(99) Madsen, F., Eberth, K. and Smart, J.D., *Biomaterials*, 1998, **19**, 1083-1092.

(100) Ugwoke, M.I., Exaud, S., Van Den Mooter, G., Verbeke, N. and Kinget, R., *Eur. J. Pharm. Sci.*, 1999, **9**, 213-219.

(101) Ugwoke, M.I., Kaufmann, G., Verbeke, N. and Kinget, R., *Int. J. Pharm.*, 2000, **202**, 125-131.

(102) Kublik, H. and Vidgren, M.T., *Adv. Drug Deliver. Rev.*, 1998, **29**, 157-177.

(103) Soane, R.J., Hinchcliffe, M., Davis, S.S. and Illum, L., *Int. J. Pharm.*, 2001, **217**, 183-191.

(104) Luppi, B., Bigucci, F., Abruzzo, A., Corace, G., Cerchiara, T. and Zecchi, V., *Eur. J . Pharm. Biopharm.*, 2010, **75**, 381-387.

(105) Bertram, U. and Bodmeier, R., *Eur. J . Pharm. Biopharm.*, 2006, **63**, 310-319.

(106) Luppi, B., Bigucci, F., Abruzzo, A., Corace, G., Cerchiara, T. and Zecchi, V., *Eur. J. Pharm. Biopharm.*, 2010, **75**, 381-387.

(107) Rowe, R.C., Sheskey, P.J. and Quinn, M.E. (Ed), *Handbook of Pharmaceutical Excipients*, 6th ed., Pharmaceutical Press, London, 2009.

(108) Cameron, P. (Ed), *Good Pharmaceutical Freeze-Drying Practice*, 1st ed., Interpharm Press, Inc., Buffalo Grove, 1997.

(109) Graf, P., *Clin. Ther.*, 1999, **21**, 1749-1755.

(110) McNaught, A.D. and Wilkinson, A.; 2nd ed.; Blackwell Scientific Publications: Oxford, 1997.

(111) Ettema, R., Kirkil, G. and Daly, S., *Cold Reg. Sci. Technol.*, 2009, **55**, 202-211.

2. CARBON NANOTUBES

2.1 NANOMEDICINE

The term "*chemotherapy*" was coined in 1904 by Nobel Laureate Paul Ehrlich. He envisaged "*magic bullets*" - compounds designed to combat specific diseases whilst leaving all else alone.[1] According to this concept, pathogens and toxins in the body could be treated with a chemical agent possessing high enough affinity for the causative entity to be efficacious at concentrations which would be harmless to the patient.[2] One of the most significant steps to realising such disease-specific drugs was the discovery of the *β*-lactam antibiotic, penicillin. Penicillin inhibits a transpeptidase necessary for the synthesis of cell walls in invading bacteria, but as animal cells do not possess cell walls, the patient remains unaffected by disruption of this pathway.[3] Discovery of anti-viral agents saw the targeted chemotherapy model advance further, with development of drugs designed to bind specifically to viral proteins.

The ability of the drug to "seek" the target is dependent on a high affinity for the target and a low affinity for normal body tissues and functions. In the early days of cancer chemotherapy however, drugs simply targeted over-proliferating cells. This means that there was not a large difference between the affinity of the drug for cancerous cells and healthy cells, particularly rapidly dividing ones, resulting in extensive toxicity. Since the late 20th century, the drive to improve the therapeutic index of cancer chemotherapeutics has seen the development of drugs which target a specific gene or protein responsible for cancer proliferation.[4]

These approaches have all involved manipulating the chemical structures of the drug molecule to actively improve drug targeting. Newer approaches involve using nano-sized drug delivery vehicles to carry the drug to the target site. Over 100 years after Ehrlich's magic bullets were hypothesised, the concept of selective chemotherapeutics is now being realised on the nanoscale.

2.1.1 Nanostructures for drug delivery

The Royal Society defines "nanoscale" particles to have dimensions in the magnitude of 100 nm down to the size of atoms (approximately 0.2 nm). At this level, materials can display properties that differ significantly from those at a larger scale.[5] Nanometre size can confer the ability to cross biological membranes or to target certain tissues, passively.[6]

The stability and surface functionalization potential of nanoparticles also provide targeting opportunities.[7] Acting as vehicles for drug delivery, nanoparticles have the potential to target tumours selectively, delivering cytotoxic anticancer agents directly to diseased cells, whilst leaving healthy tissue alone.[7]

2.1.2 The enhanced permeability and retention effect

Once in the systemic circulation, a nanoparticle larger than 1-2 nm is prevented from exiting *via* normal vasculature by its size. Tumorous vasculature, however, is more permeable due to: intrinsic structural defects, such as the lack of smooth muscle layer; angiogenesis, resulting in high vascular density; and the generation of a number of permeability-enhancing factors including: prostaglandins, proteases, collagenases, vascular endothelial growth factor (VEGF) and vascular permeability factor (VPF).[7-13] As a result, nanoparticulate delivery systems (> 2 nm) with long plasma half-lives passively accumulate in tumours at higher concentrations than other tissues and plasma.

Whilst healthy tissues are able to rapidly remove macromolecules from the interstitial space, compromised lymphatic drainage in tumours means that the nanoparticles will be retained in the tumour for extended periods. This phenomenon is referred to as the enhanced permeability and retention (EPR) effect (Figure 2.1).[7-13]

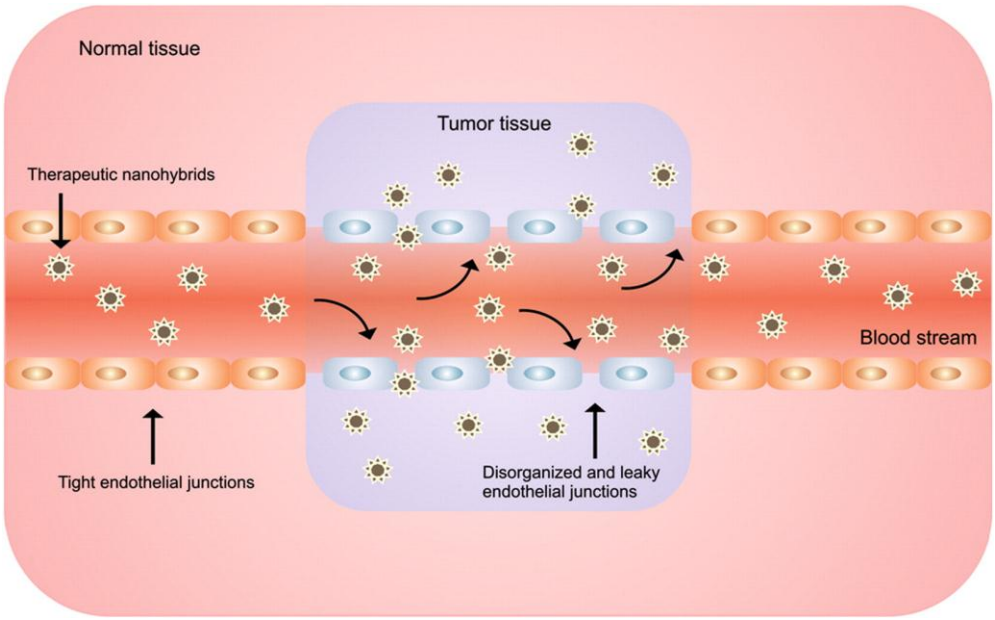

Figure 2.1. The enhanced permeability and retention effect.[14]

2.1.3 Nanoparticulate drug delivery vehicles

A variety of nanoparticulate drug delivery vehicles which exploit the EPR effect are currently under investigation and/or in clinical use, and include but are not limited to: liposomes, dendrimers, metallic nanoparticles and fullerenes. Liposomes are small vesicles which are self-assembled from phospholipids and cholesterol, with an aqueous compartment inside the phospholipid lamellae (Figure 2.2).[7] They are currently used in Janssen's anticancer drug Caelyx® (a liposomal formulation of doxorubicin).[15] Liposomes have been investigated for the delivery of cisplatin, with mixed success. Whilst one formulation is currently in Phase III clinical trials, others have shown promising results *in vitro*, but have been shown to have extremely slow drug release kinetics which resulted in a lack of clinical activity.[16-20]

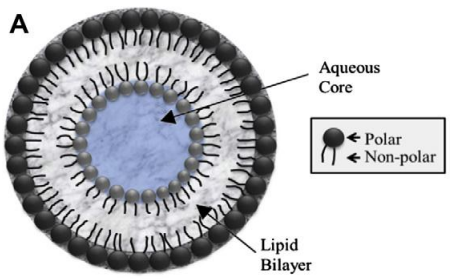

Figure 2.2. The general structure of a phospholipid liposome for drug delivery.[7]

Dendrimers are polymeric carriers based on a highly branched structure (from the Greek "δένδρον" or "tree") generally produced from carbohydrates or amino acids *via* step growth polymerisation. They form roughly spherical macromolecules around a central core (Figure 2.3).[21-24] Drugs can be incorporated in to the cavities between branches, as part of a dendrimer/drug network, or through covalent or non-covalent binding (producing a macromolecular prodrug). Another class of drug delivery vector currently under investigation is the carbon nanotube (CNT), a class of fullerene.

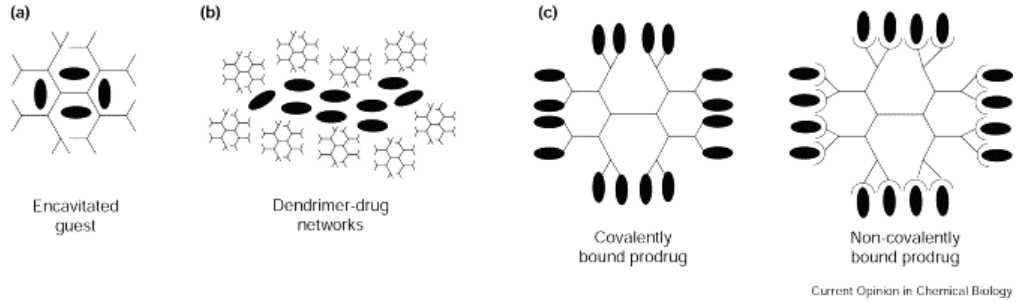

Figure 2.3. Some dendrimer drug delivery systems (drug substances represented as dark ovals). Drug molecules can be incorporated into the cavities (a) between branches (b) as part of a dendrimer-drug network or (c) bonded covalently or non-covalently to the dendrimer.[21]

2.2 CARBON NANOTUBES

***"…it is rare to come across a material that has such a range of remarkable properties"* – Ajayan *et al.*, 1999.[25]**

In 1985, Harry Kroto and Richard Smalley reported the synthesis of the first discrete molecule which was purely carbonaceous, Buckminsterfullerene (C_{60}), paving the way for a myriad of research into fullerene-type carbon molecules.[26] Six years later Japanese microscopist, Sumio Iijima, was examining cathodic residues from C_{60} synthesis by transmission electron microscopy (TEM) when he stumbled upon "*microtubules of graphitic carbon*", now known as carbon nanotubes.[27]

2.2.1 Carbon nanotubes - structure and properties

These so-called carbon nanotubes (CNTs) ranged in length from a few tens of nanometres to several micrometres and about 2.5-30 nm in diameter.[27] Carbon nanotubes consist of three co-ordinate carbon atoms arranged to form a lattice of hexagonal rings (graphene sheets) rolled into seamless cylinders.[28] The orbital hybridisation present is predominantly sp^2, although the high curvature of the tubes results in a degree of sp^3 character.[29] The graphene sheets can be rolled along one of the symmetry axes to produce either a zigzag or armchair configuration. Alternatively, the sheet can be rolled in a non-symmetrical fashion, producing a chiral nanotube[30,31] (Figure 2.4).

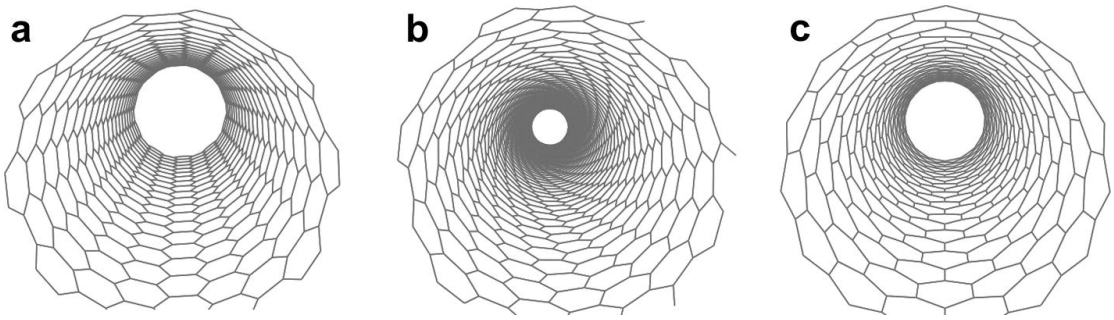

Figure 2.4. A schematic diagram showing: (a) armchair (b) chiral and (c) zig-zag CNTs.[32]

Carbon nanotubes can be open-ended or capped with half a C_{60} molecule[30] (consisting of five and six-membered rings).[29] They have a tendency to aggregate into rope-like structures held together by van der Waals forces.[30] Both single-walled (SWNTs) and multi-walled (MWNTs) types are known, the latter consisting of 2-50 concentric tubes (Figure 2.5).[28]

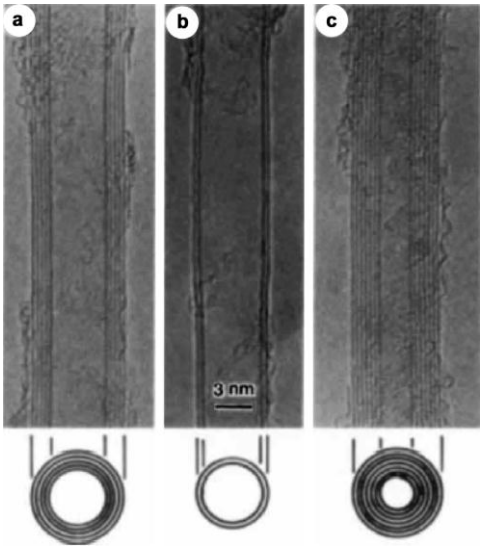

Figure 2.5. The first TEM images of MWNTs produced by Ijima: (a) 6.7 nm (b) 5.5 nm and (c) 6.5 nm diameter.[27]

Carbon nanotubes display a unique and fascinating set of chemical, physical and mechanical properties including a high aspect ratio (ratio of length over diameter *i.e.*, they are very long and thin),[28] ultra-light-weight, high mechanical strength (C-C bond lengths of 0.14 nm, making them shorter than those of diamond),[33] high thermal conductivity, semi-metallic or metallic behaviour and high surface-to-volume area.[34]

These properties give CNTs applications in sporting goods, batteries, sensors, probes and hydrogen storage technologies.[34,35] Potential applications in biomedical fields are eclectic, with proposed uses as components in DNA and protein biosensors,[36] ion channel blockers[37] and biocatalysts,[38] as well as structural applications in implantable orthopaedic,[39] vascular[40] and neural[41] prostheses. In addition, there is growing interest in the use of CNTs in drug delivery applications.[42]

2.2.2 Analytical techniques

Transmission electron microscopy, Scanning electron microscopy (SEM) and atomic force microscopy (AFM) have been used to elucidate the structure of CNTs (Figure 2.6).[28,43,44]

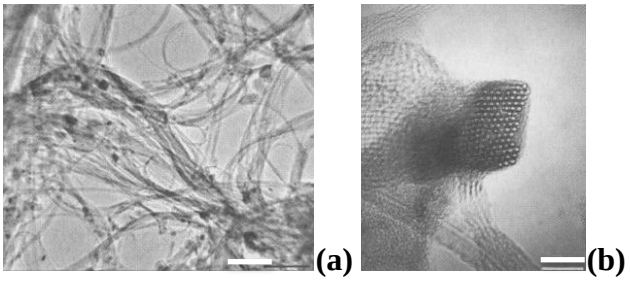

Figure 2.6. SEM images showing: (a) ropes of SWNTs with small quantities of metal catalyst coated with amorphous carbon (scale bar 100 nm); and (b) a rope of ~100 SWNTs. As it bends through the image plane a cross-section of the regular triangular packing can be seen (scale bar 10 nm).[45]

Thermogravimetric analysis has been used to determine the amount of carbon and non-carbon material in CNT samples.[43] Nuclear magnetic resonance,[46] infrared and Raman[43] spectroscopy have been used for quantitative analysis of attached functional groups. The conjugated nature of CNTs also means that they are UV-active when in dispersion,[47] and so UV-visible spectroscopy has been utilised to evaluate efficiency of dispersing agents.[48] Whilst in bundles however, the effective particle size approaches the wavelength of light resulting in decreased apparent absorption coefficients.[48]

2.2.3 SWNTs as nanoscale platinum drug delivery vectors

The unique properties of CNTs also make them applicable as nano-vehicular drug delivery systems.[49,50] Once solubilised, CNTs can easily cross biological membranes by clathrin-dependant endocytosis to enter cancerous cells (Figure 2.7),[50,51] or by utilising their high aspect ratios to pierce through membranes like needles,[52] internalising attached drug moieties.[53] Well-functionalised CNTs can circulate in the blood with half-lives in the order of hours, allowing them to exploit the EPR effect

and accumulate in tumours, with the remainder being slowly excreted into the faeces *via* biliary pathways.[54,55] Non-biodegradable CNTs could potentially accumulate in various tissues and organs, however myeloperoxidase, an enzyme produced at sites of inflammation, has been found to catalyse the degradation of *f*-CNTS.[56]

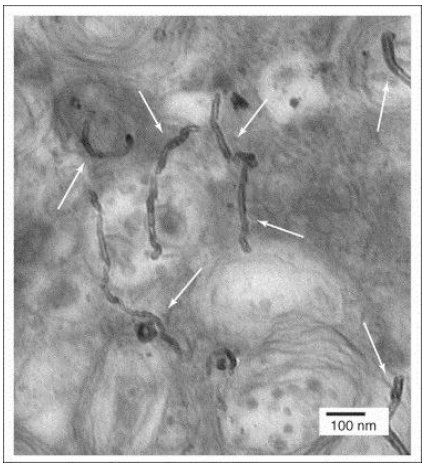

Figure 2.7. A TEM micrograph showing MWNTs in the cytoplasm of HeLa cells.[57]

Lippard[54,58] and colleagues have shown that the addition of targeting moieties such as folic acid derivatives can be used to aid tumour targeting. The use of a folate targeting group has been shown to increase intracellular accumulation of CNT-bound doxorubicin. This suggests that the ability of CNTs to cross the cell membrane can be improved by exploiting the folate receptor, which is known to be upregulated in cancerous cells.[59]

Acting as scaffolds for nano-assemblies, these functionalised CNTs (*f*-CNTs) can be exploited for the improved delivery of small drug molecules.[60] Carbon nanotubes have already been used for the delivery of amphotericin B with increased antifungal activity and reduced toxicity to mammalian cells.[61] Doxorubicin has been loaded onto CNTs by π-π stacking to the sidewalls. *In vivo* evaluation of this system in mice showed enhanced efficacy and a reduction in toxicity compared to native doxorubicin.[62] Paclitaxel conjugated to SWNTs has been found to inhibit tumour growth more effectively than native paclitaxel in tumour bearing mice. This improvement in efficacy was attributed to longer circulation time and increased

tumour uptake *via* the EPR effect.[63] Research has also been carried out on the use of *f*-CNTs for DNA,[64] RNA[65] and protein delivery.[66,67]

A number of papers have demonstrated the usefulness of carbon nanotubes as delivery vehicles for platinum-based anticancer drugs. Iijima's research group have explored the use of nanohorns (nanotubes that adopt a cone shape) as a cisplatin delivery vector; physically encapsulating the drug within their structure.[68,69] It has been demonstrated that platinum(IV) prodrugs delivered as CNT conjugates achieve greater intracellular concentrations than those delivered traditionally.[54] Feazell[58] and colleagues have reported the preparation of a cisplatin prodrug: SWNT coated with lipid-polyethyleneglycol-platinum(IV), which is reduced to active Pt(II) in the intracellular environment (Figure 2.8). Use of a more stable platinum(IV) complex avoids early deactivation, and reduction in the intracellular environment yields active cisplatin.

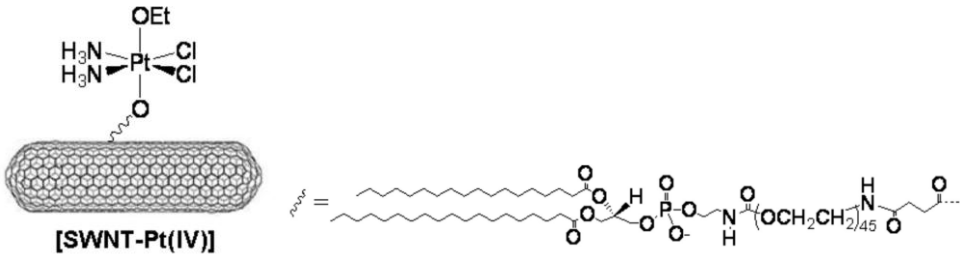

Figure 2.8. The structure of Feazell's SWNT lipid-PEG-Pt(IV) drug.[58]

Bhirde and colleagues have shown that the use of epidermal growth factor as a targeting group on a cisplatin-CNT conjugate improves the uptake of the complex into squamous cancer cells.[70] This resulted in a rapid decrease of tumour size in mice, compared to a non-targeted control.

As-supplied, *f*-CNTs are highly aggregated in bundles, with minimal exposed surface area for drug conjugation. In order to disperse them effectively in solution, exposing the functional groups for conjugation, sonication can be used.

2.2.4 Sonication prior to conjugation

The first observation of sonication was reported as far back as 1895.[71] Since then the phenomenon has been utilised in the laboratory and the use of sonication baths and probes is now commonplace.[72] With both baths and probes, sonic waves are generated by applying an alternative tunable voltage across a piezoelectric ceramic material.[73] This results in the rapid formation, growth and implosion of gas bubbles, a process known as cavitation.[72] In a heterogeneous solid-liquid system the collapse of these cavitational bubbles is accompanied by shock waves of up to 10^4 bar, causing a liquid jet to erode the solid surface[73,74] (Figure 2.9).

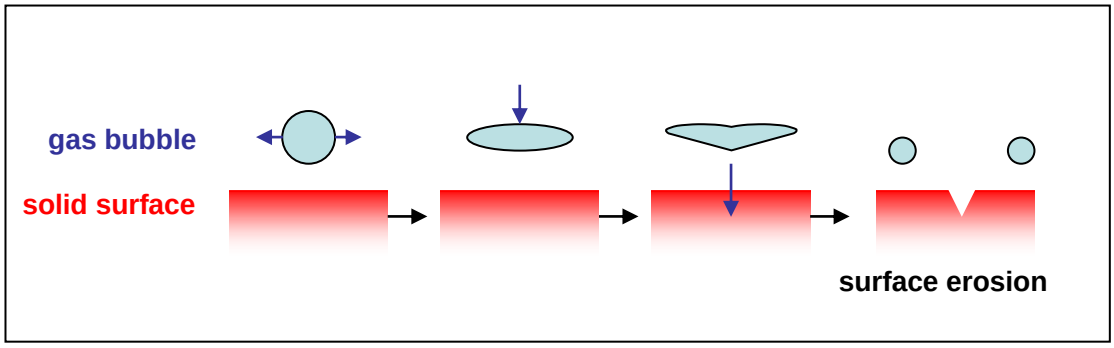

Figure 2.9. During sonication, cavitation bubbles form, change shape and collapse. This collapse causes a liquid jet to strike the solid surface at speeds exceeding 100 m/s[74], resulting in surface erosion. *Adapted from Einhorn.*[73]

Sonication in these circumstances acts to reduce particle size and mix the phases, creating a pseudo liquid-liquid phase system.[73] Additionally, the process of cavitation produces "reactive hotspots" with nanosecond lifetimes, with elevated temperatures and pressures (~3,000 K and ~300 bar).[72,75]

In a bath sonicator the energy is transmitted to the sample container through a liquid medium, usually water.[73] With a probe device, the energy is emitted directly into the sample with no loss to any transmitting medium.[73]

2.3 AIMS

The ultimate goal of this project was to make cisplatin treatment more effective with reduced side-effects. It is proposed that this can be achieved through improving drug targeting to tumours by exploiting the EPR effect, using CNTs as both drug delivery vehicles and as molecular scaffolds for functionalisation. Cisplatin conjugated to CNTs in this manner would be expected to display improved distribution/retention profiles *in vivo*. Additionally, this modification may provide increased drug stability under the metabolic conditions of the nasal cavity, allowing formulation into a nasal dosage form. In view of this goal the primary aims of this work are to:

- synthesise and characterise cisplatin conjugated CNTs (Pt-CNTs),
- examine the ability of the Pt-CNTs to release cisplatin and to monitor the drug's binding to DNA,
- determine the efficacy of the Pt-CNT drugs in a panel of human cancer cell lines,
- determine the cellular uptake and accumulation profiles of the Pt-CNT drugs in a panel of human cancer cell lines, and
- formulate the Pt-CNT drugs into dosage forms for nasal delivery.

2.4 MATERIALS & METHODS

2.4.1 Materials

Carbon nanotubes, single-walled, carboxylic acid functionalised (4-5 nm x 500-1500 nm bundles, 80-90% carbonaceous purity), *cis*-diamminedichloridoplatinum(II) (99.9%+, cisplatin), *N*,*N*-diisopropyethylamine, (biotech grade), Pluronic F-127, sodium chloride, nitric acid, guanosine 5'-monophosphate disodium salt hydrate, silver chloride, deuterium oxide and Vivaspin20™ centrifugal concentrators were purchased from Sigma-Aldrich. All water was obtained from a MilliQ water purification system.

2.4.2 Instrumentation

UV-visible (UV-vis) spectroscopy: UV-vis spectroscopy was carried out on a Varian Carey 50 Bio UV-visible spectrometer, operating with Carey WinUV software. All samples were analysed in multiple (minimum n=3). Data were exported as ASCII files and processed with Microsoft Excel 2010.

^{1}H Nuclear magnetic resonance (NMR): NMR spectra were obtained on a JOEL JNM-LA400 spectrometer using a Varian Oxford AS400 magnet operating at 400 MHz. Spectra were obtained using at least 64 scans, a relaxation delay of 4 s and presaturation at 4.78 ppm.

Scanning electron microscopy (SEM): SEM micrographs were recorded using a FEI Sirion 200 ultrahigh-resolution Schottky field-emission scanning electron microscope running FEI software. An accelerating voltage of 5 kV was applied to each sample, and a spot size of 3 was used. One µL of each sample was dropped onto the silicon substrate and allowed to dry under vacuum before analysis. Sample preparation and image collection was carried out by a trained technician.

Differential Centrifugal Sedimentation (DCS): DCS was carried out on a CPS Disc Centrifuge DC24000 operating at 24,000 rpm with an 8-24% sucrose gradient, and monitored at 405 nm.

Elemental analysis: Elemental analysis was performed on a Perkin Elmer 2400 CHN Analyser.

2.4.3 Dispersion of CNTs by sonication

Direct contact sonication was carried out with a Vibracell™ model VC50 probe sonicator, manufactured by Sonics & Materials Inc., Danbury, CT, USA. The following samples were prepared (any sonication was carried out for 20 min unless otherwise stated): single-walled carboxylic acid functionalised CNTs (*f*-CNTs) in water with no sonication; *f*-CNTs in water with bath sonication in a glass vial; *f*-CNTs in water with direct sonication in a glass vial; *f*-CNTs in water with direct sonication in 15 mL centrifuge tubes; *f*-CNTs in 0.1% sodium dodecyl sulfate (SDS) solution with bath sonication and *f*-CNTs in 0.1% SDS solution with direct contact sonication. Scanning electron microscope images were obtained for each sample.

2.4.4 Aquation of cisplatin

Cisplatin was dissolved in 10 mM NaCl to form a 1 mM stock solution. Silver nitrate solution (0.95 equivalents of a 12 mM aqueous solution) was added, and the reaction was stirred at 50 ºC for one hour, as per a method reported by Hostetter and colleagues (Figure 2.10).[76] Both starting solutions were stored in the dark at 4 ºC when not in use. The AgCl by-product, which precipitated during the reaction, was removed by filtering the solution through a 0.2 µm syringe-driven filter. The aquated cisplatin solution was then rotary evaporated to reduce the sample volume before being freeze-dried. For *bis*-aquated cisplatin (used in a UV-vis calibration) 1.9 equivalents of $AgNO_3$ were used, with all other parameters remaining the same.

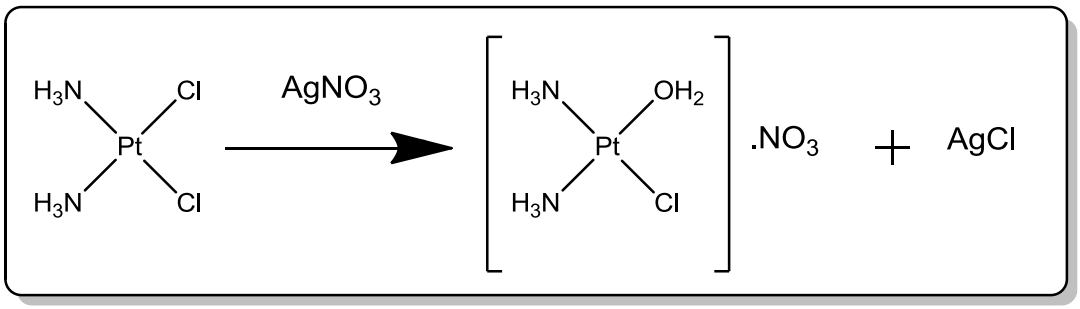

Figure 2.10. Reaction scheme for the *mono*-aquation of cisplatin.

2.4.5 Conjugation of cisplatin to *f*-CNTS

Carboxylic acid functionalised CNTs (*f*-CNTs, 20 mg) were dispersed in water (up to 900 mL) using bath or direct contact sonication and *N*,*N*-Diisopropylethylamine (DIPEA, 45-910 µL) was added. Subsequently, or after 12 h stirring at 45 ºC, *mono*-aquated cisplatin (22 mg) was added in powder form to the suspension with stirring, or sonicated in water (~ 2 mg/mL) before being added. The reaction was then wrapped in foil to exclude light and stirred for up to two days at ~ 65 ºC, before further stirring for up to two days at RT.

The reaction mixture was then centrifuged in 5,000 molecular weight cut-off (MWCO) Vivaspin™ 20 tubes (Figure 2.11). The cisplatin-CNT conjugates (Pt-CNTs) were then rinsed with water and re-centrifuged before being collected and freeze-dried. The filtrate from this process contains any un-conjugated platinum drug. This filtrate was concentrated by rotary evaporation before being analysed for platinum content, by UV-vis spectroscopy and/or flame atomic absorption spectroscopy (F-AAS), to allow calculation of the quantity of cisplatin conjugated to the CNTs.

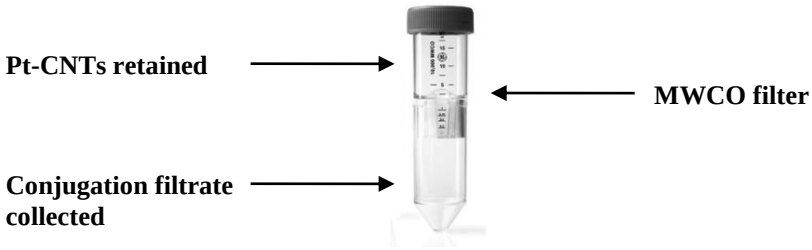

Figure 2.11. A Vivaspin™ 20 centrifuge tube, with a 5,000 MWCO filter.

The first batch of conjugated Pt-CNTs were soaked in HCl:H_2O (3:1) to detach any conjugated cisplatin. After suspension in acid for three days, the mixture was centrifuged through a Vivaspin™ tube. The acid filtrate was then analysed for platinum content by either UV-vis spectroscopy or F-AAS. A sample of dispersed CNT was analysed by DCS before, and after, conjugation to cisplatin to characterise the size of the particles at each stage.

2.4.6 Establishing a UV-vis method for quantifying cisplatin content

Concentration calibration data were obtained for the following stock solutions: cisplatin in 100 µM HCl; cisplatin in 100 mM NaCl; *mono*-aquated cisplatin in 100 mM NaCl, and *bis*-aquated cisplatin in 100 mM NaCl. UV analysis (200-600 nm) of solutions between 0.1–1.0 mg/mL were obtained. Calibration curves were then plotted. Conjugation filtrates were diluted to 100 mL in volumetric flasks. These solutions were then analysed by UV-vis spectroscopy and compared with calibration data.

2.4.7 F-AAS for quantifying conjugation of platinum to CNTs

Some conjugation filtrates were analysed for platinum content by F-AAS. Samples and standards were prepared in 1% HCl and analysed on a PerkinElmer AAnalyst 200 Atomic Absorption Spectrometer. Nebulisation flow rate of 6.2 mL/min with acetylene flow optimised to 2 L/min was used. Platinum lamp was operated with a 12 mA current. Integration time of 3 s, 3 replicates, and a read delay of 2 s were used. Platinum content was measured in mg/mL and these figures were used to ascertain the extent of conjugation.

2.4.8 Monitoring drug release through guanosine binding

Proton NMR spectra of the following samples in D_2O were obtained with presaturation to reduce the intensity of the HDO peak: 50 mM guanosine 5'-monophosphate (at day 0 and after incubation for three days at 60 ºC); Pt-CNT; Pt-CNT conjugate + 50 mM guanosine monophosphate (at day 0, after three days incubation at 37 ºC and subsequently after three days at 60 ºC), and *f*-CNT + 50 mM guanosine monophosphate (at day 0, after three days incubation at 37 ºC and after three days at 60 ºC).

Samples containing CNTs were bath sonicated briefly (< 2 min) to redisperse before analysis. In all cases CNTs were visibly aggregated after analysis and/or after incubation. The sample containing *f*-CNT + 50 mM guanosine monophosphate was then centrifuged through a Vivaspin™ tube and the filtrate collected. Remaining CNTs were washed with water and centrifuged repeatedly. The filtrates were combined, freeze-dried and a ^{1}H NMR spectrum of the recovered guanosine was obtained to examine the degree of binding.

2.4.9 Evaluating dispersants for improved bioavailability of Pt-CNTs

Cisplatin-CNT conjugates (Pt-CNTs, ~1.2 mg) were sonicated directly in various media within 15 mL plastic centrifuge tubes. Direct contact sonication was carried out for three 20 min intervals in an ice bath to prevent sample overheating. Sonication intensity was increased to a maximum intermittently to create a standing wave and disperse any material that became attached to the probe. The samples were then sonicated for 1 min each before being transferred to 30 mL centrifuge tubes, diluted with the appropriate surfactant solution and centrifuged at 40,000 rpm for 40 min. Supernatant was removed by pipette as no well-aggregated pellet was formed, making decanting difficult and inaccurate. UV-vis spectra were then obtained for each of the Pt-CNT solutions. The following solutions were investigated: water; 0.1% SDS; 1% SDS; phosphate buffered saline (PBS); 0.1% Danagel, and 1% Pluronic F-127.

2.5 RESULTS AND DISCUSSION

2.5.1 Sonication of carboxylic acid functionalised CNTs

The hydrophobic nature of the CNT sidewalls, along with π-π stacking, means that as supplied *f*-CNTs aggregate into bundles. Before cisplatin could be conjugated to the *f*-CNTs, the *f*-CNTs first had to be dispersed in water to obtain a uniform and stable dispersion with the carboxylic acid functional groups exposed.[77]

The term "swollen" has been used to describe the partial dispersion of CNTs with aggregation, precipitation and phase separation evident within days of sonication.[78] The carboxylic acid functionalised CNTs (*f*-CNTs) became swollen after direct contact sonication in water for 20 min (Figure 2.12). However, as full dispersion was not achieved (*i.e.* it was not clear liquid with a black hue, no visible sign of aggregation), the *f*-CNTs settled out of suspension within a few days.

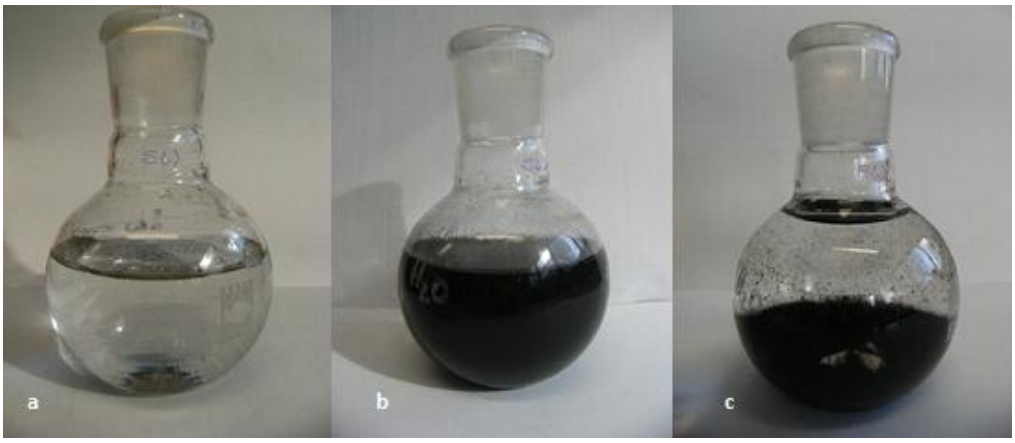

Figure 2.12. Images of ~ 20 mg *f*-CNT in a 100 mL round-bottom flask after: (a) no sonication, (b) direct contact sonication for 20 min, and (c) being further diluted with water and left to stand for a number of days. Note that in image (b) the *f*-CNTs were swollen, not fully dispersed, after 20 min, apparent from the opaqueness of the solution. After being left to stand for a number of days the *f*-CNTs have settled but remain swollen *c.f.* the starting image.

It was important to optimise the sonication conditions so that stable dispersions of well-exfoliated *f*-CNTs could be obtained for subsequent conjugation reactions.

Further investigation of pre- and post-sonication *f*-CNTs was carried out by SEM. The as-supplied *f*-CNTs were visible as large aggregated bundles (Figure 2.13a). After 20 min bath sonication in a 100 mL round bottomed flask, bundles became less aggregated and strand-like shapes became more visible in the SEM image (Figure 2.13b). More effective exfoliation was observed after 20 min direct contact sonication in a plastic 15 mL centrifuge tube (Figure 2.13c). This difference may have been due to the volume of liquid held around the probe by the vessel or perhaps the way in which the ultrasonic waves are reflected off the vessel walls back into the sample. As the effects of cavitation reduce axially and radially, minimising the distance from the probe to the wall maintains the particles in the area under cavitation.[79] Santos suggests using a vessel with "as small a diameter as possible so as to raise the liquid level for a given volume".[79] This suggests that, in this case, the shape of the vessel was important and explains why greater exfoliation was obtained in the centrifuge tubes.

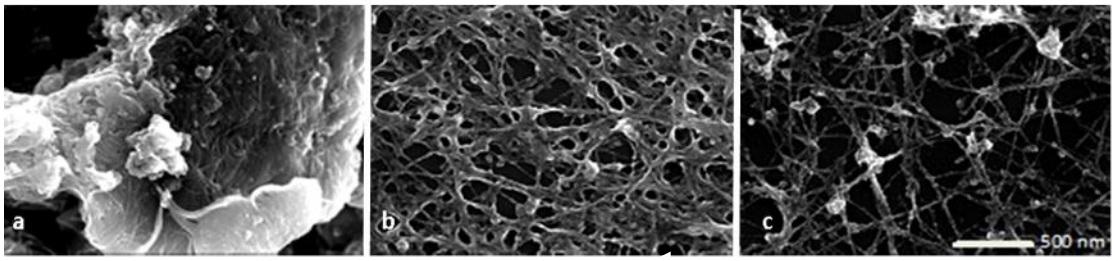

Figure 2.13. SEM images (50,000× magnification) of: (a) as-supplied *f*-CNTs. Highly bundled *f*-CNTs have formed a large aggregate; (b) *f*-CNTs after bath sonication in water for 20 min. The bundles have become exfoliated from their original state; and (c) *f*-CNTs after direct contact sonication in water in a centrifuge tube for 20 min, tubes appear to be further dispersed. White clumps may be amorphous carbon and/or catalytic impurities.

2.5.2 Dispersing *f*-CNTs prior to conjugation

In accordance with the results of the sonication investigation, *f*-CNTs were sonicated in water with a direct contact probe in 15 mL centrifuge tubes. After 20 min sonication, the liquid containing fully suspended *f*-CNTs was decanted off then centrifuged for a further 10 min at 40,000 rpm to concentrate any undispersed

nanotubes into the bottom of the tube (it should be noted that this was not a solid pellet, but a region of partially dispersed and undispersed *f*-CNTs). The fully dispersed *f*-CNTs were decanted and collected. The remaining undispersed *f*-CNTs were diluted, re-sonicated and the clear black dispersion obtained was decanted off and centrifuged once more. This process was repeated until all of the material was fully dispersed system was obtained.

For a starting mass of ~20 mg *f*-CNT the final volume of aqueous dispersion was ~900 mL. The remaining undispersed material was collected, freeze dried and weighed and the actual mass of *f*-CNT in the starting solution was calculated. Although this method was labour intensive, subsequent conjugation reactions with cisplatin using these solutions were more successful than earlier experiments where only one session of direct contact sonication was applied to each sample.

Once the *f*-CNTs were adequately dispersed, they were ready to be conjugated with cisplatin. In order to make the cisplatin reactive, it had to be aquated to the *mono*-aqua form by replacing an ammine ligand with water.

2.5.3 Aquation of cisplatin

Aquated cisplatin was produced by stirring cisplatin in NaCl solution with 0.95 equivalents of $AgNO_3$ at ~ 50 ºC for 1 h (Figure 2.14).

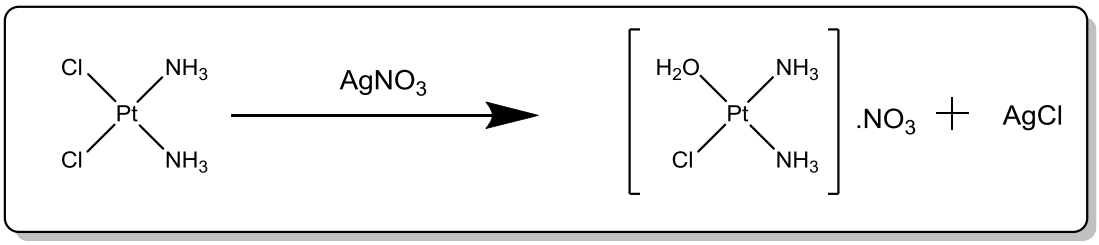

Figure 2.14. Reaction of cisplatin with $AgNO_3$ to form *mono*-aquated cisplatin and AgCl.

The expected product from this reaction was the *mono*-aqua species: *cis*-$[PtCl(H_2O)(NH_3)_2](NO_3)$ (H=2.25%, N=15.62% and Cl=9.89%). Average

elemental analysis results for the batches produced were: H=1.67%, N=12.87% and Cl=11.49%. This may mean that instead of forming the *mono*-aqua species, the reaction had produced the *bis*-aqua species: *cis*-$[Pt(H_2O)_2(NH_3)_2](NO_3)_2$ (H=2.59%, N=14.40% and Cl=0%) along with unreacted starting material $[PtCl_2(NH_3)_2]$ (H=2.02%, N=9.34% and Cl=23.63%), or a combination.

2.5.4 Conjugation of aquated cisplatin to *f*-CNTs

Conjugation of aquated cisplatin to *f*-CNTs was carried out by replacement of the OH_2 ligand on the platinum drug with deprotonated carboxylic acid group of the *f*-CNTs (Figure 2.15). The extent of this conjugation was characterised by UV-vis spectroscopy, DCS and F-AAS.

It should be noted that the potential formation of *bis*-aquated cisplatin may have allowed the "cross-linking" two *f*-CNTs, resulting in the formation of aggregated networks.

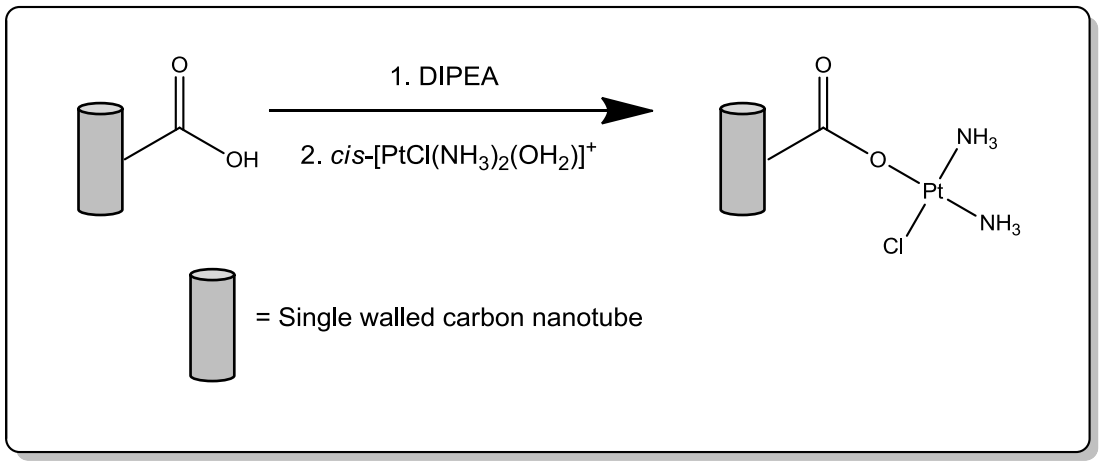

Figure 2.15. Reaction scheme for the conjugation of aquated cisplatin to *f*-CNTs.

2.5.5 Differential centrifugal sedimentation

Differential centrifugal sedimentation analysis was carried out to examine particle size and determine if this increased during the conjugation, which would indicate a layer of cisplatin around the nanotubes.

The disc centrifuge instrument examines differential sedimentation in order to obtain particle size. The differential sedimentation is described by Stoke's Law which predicts the settling velocity of the particles exposed to acceleration in a fluid as a function of their diameter. The sample is injected into the centre of a rotating hollow disc which contains a gradient of sucrose and water. The sample is spread over the surface of this fluid and subjected to centrifugal acceleration. The particles will then sediment towards the outside edge of the rotating disc. At a specific distance from the centre, extinction is measured as a function of time. From these measurements the particle diameter can be ascertained.[80]

First, a sample of *f*-CNTs starting material which had been sonicated directly in water, was examined. The fully exfoliated and dispersed fraction of *f*-CNTs was represented by a sharp peak with narrow particle size distribution (Figure 2.16a). A shoulder representing a smaller number of particles with a wide particle size distribution pertained to the fraction which remained aggregated. This suggests that direct contact sonication has successfully produced exfoliated CNTs at a ratio of around 10:1 to agglomerated CNTs. Following the reaction of dispersed *f*-CNTs with aquated cisplatin, a larger peak particle size was measured (0.0311 µm compared with 0.0233 µm), as would be expected upon conjugation to another moiety (Figure 2.16b). In order to quantify the extent of this conjugation, UV-vis spectroscopy was employed.

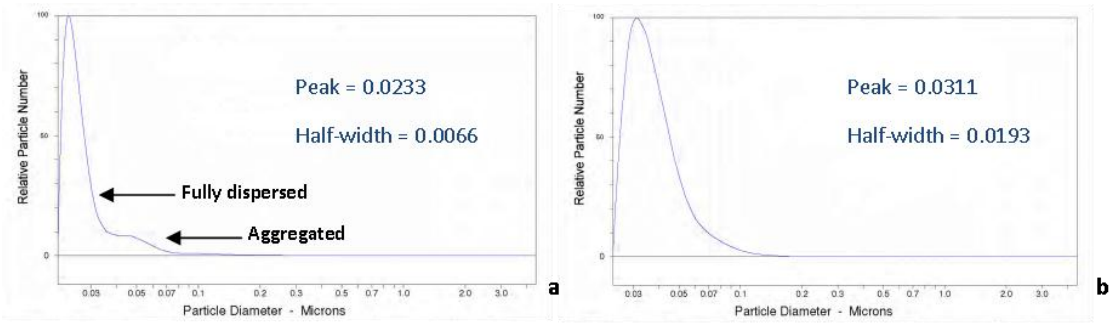

Figure 2.16. Particle size distribution determined by DCS showing: (a) sample of *f*-CNTs treated with direct contact sonication. The sharp peak on the left represents the fully exfoliated CNTs which have a smaller overall particle size. The shoulder on the right represents the CNTs which remain agglomerated;[80] and (b) after conjugation, there is a greater number of particles with a larger size.

2.5.6 Establishing a UV-vis method for quantifying Pt conjugation to CNTs

Direct analysis of cisplatin which is conjugated to CNTs is difficult as many techniques (*e.g.* F-AAS) require the sample to be fully solubilised and samples containing high concentrations of carbon cannot be analysed. Instead of measuring the attached platinum directly, it was decided to quantify the amount of drug which had not become conjugated to the CNTs during the reaction.

The British Pharmacopoeia (BP) reports that UV-vis analysis between 230-350 nm of cisplatin gives one maximum at 300 nm.[81] As such, UV-vis spectroscopy of the conjugation filtrate (the washed-off reaction medium containing any unconjugated cisplatin) was explored as a possible method for quantifying conjugation.

The first conjugation reaction was deliberately reversed by the action of conc. HCl on the Pt-CNTs. The reaction was then centrifuged through Vivaspin™ columns and the filtrate rotary evaporated to obtain a yellow oil. UV-vis analysis of this yellow substance between 200–400 nm produced a spectrum with an apparent maximum at ~273 nm. This was presumed to be an aquated form of cisplatin.

In order to quantify this aquated form removed directly from the final product, and also the unconjugated platinum washed off of subsequent products, calibration data were obtained for *mono*-aquated, *bis*-aquated and native cisplatin.

2.5.7 Speciation of cisplatin in aqueous media

The *mono*-aquated, *bis*-aquated forms of cisplatin can be produced spontaneously in aqueous solution, where *cis*-$[PtCl_2(NH_3)_2]$ (**1**) sequentially loses its two chlorido ligands (Figure 2.17). The first step involves the attack of a water molecule on the Pt^{2+} centre, forming the *mono*-aquated species *cis*-$Pt[Cl(NH_3)_2(OH_2)]^+$ (**2**). Loss of a proton leads to the *mono*-hydroxo form, (**4**). Further aquation of (**2**) leads to the *bis*-aquated species, and loss of one and two protons yields the *mono*- and *bis*-hydroxo

species respectively (**5** and **6**).[82] This creates a system of equilibria where the fraction of each species is determined by pH and ion concentration in the solution.

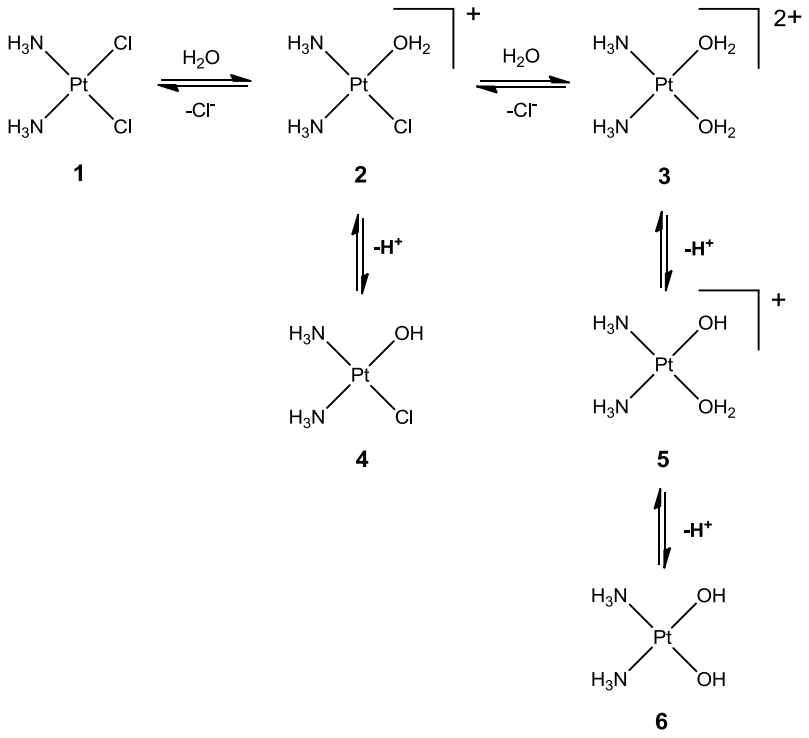

Figure 2.17. The speciation of cisplatin in aqueous solution. Adapted from Berners-Price *et al.*[82]

2.5.8 UV-vis calibration for *mono*-aquated cisplatin

As the species used in the conjugation reactions, *mono*-aquated cisplatin was hypothesised to be the species present in the reaction filtrate. In order to quantify it, UV-vis spectra were obtained for standards prepared from this platinum species in 100 mM NaCl (Figure 2.18) and calibration graphs calculated for peaks at both 273 and 300 nm, assumed to be *mono*-aquated and native cisplatin respectively (Figure 2.19). Calibration equations were calculated from these data.

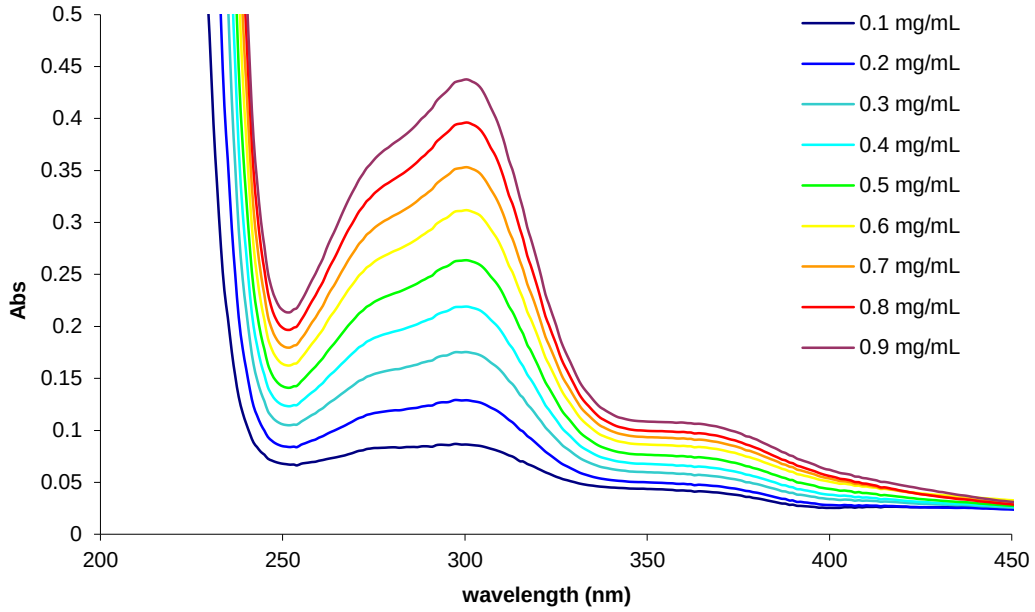

Figure 2.18. Average UV absorption spectra (*n*=3) for *mono*-aquated cisplatin in 100 mM NaCl solution. Peaks at both 273 and 300 nm are assumed to be *mono*-aquated and native cisplatin, respectively.

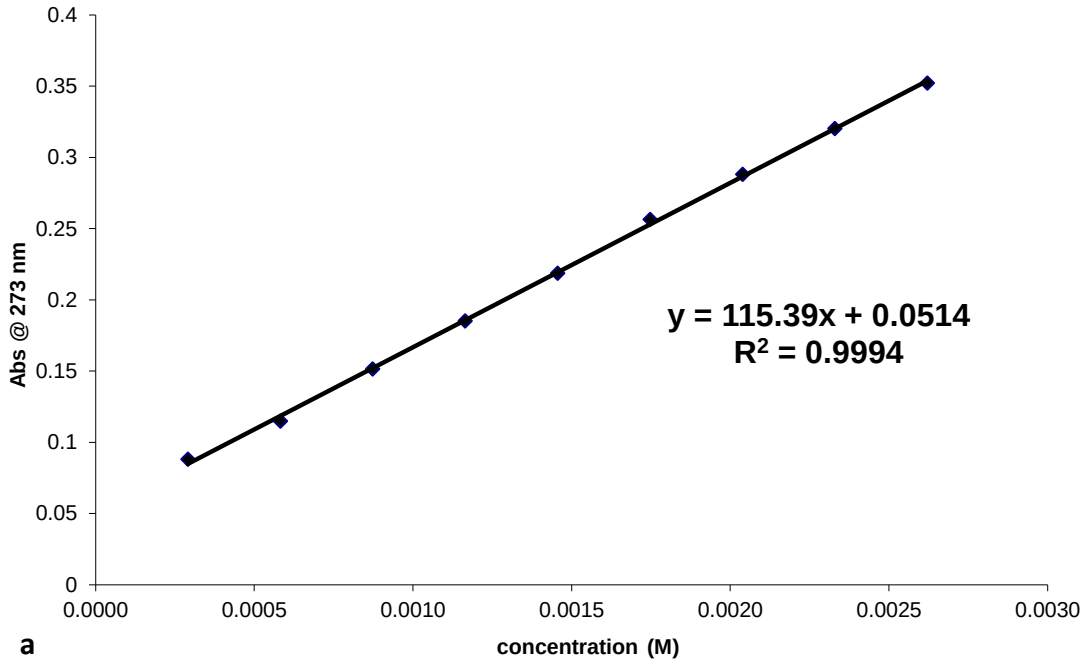

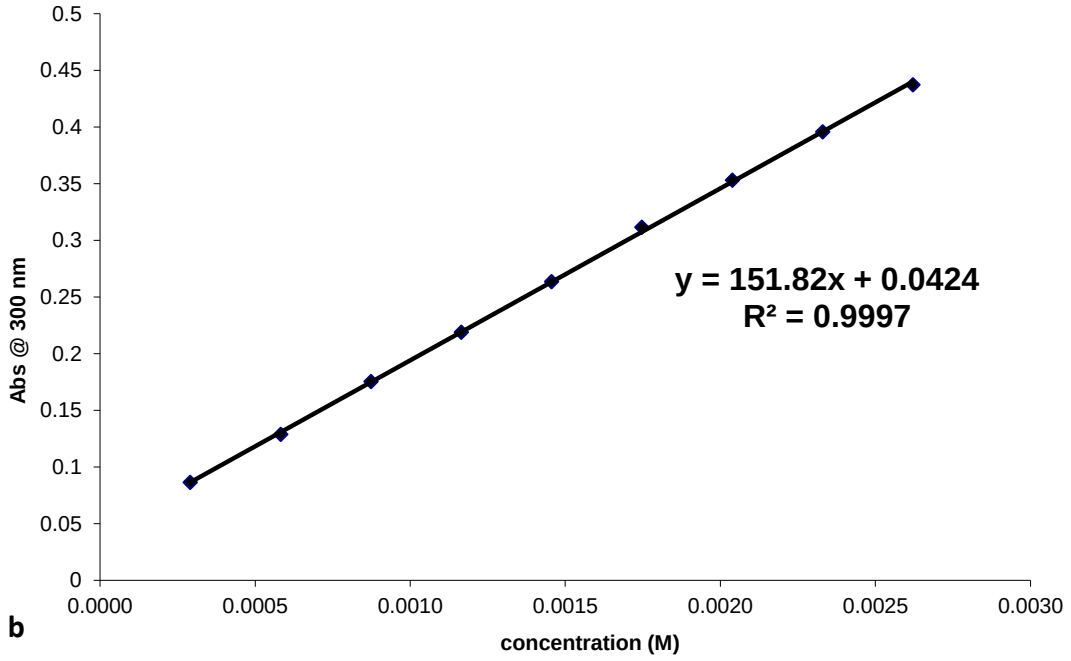

Figure 2.19. UV Calibration graph for *mono*-aquated cisplatin in 100 mM NaCl, as measured at (a) 273 nm and (b) 300 nm; where *y* = absorption (arbitrary units) and *x* = concentration (M).

It was decided that these calibrations were still not representative of the spectra obtained for some of the conjugation filtrates, as they also showed unidentified maxima at 260 nm, in addition to the peaks at 273 nm and 300 nm. It was hypothesised that the concentration of chloride ions was not high enough to prevent further aquation to *bis*-aquated cisplatin (see Figure 2.17), and so calibration data was also obtained for this species.

2.5.9 UV calibration for *bis*-aquated cisplatin

UV spectra were obtained for standards prepared from *bis*-aquated cisplatin and calibration graphs calculated for the shoulder at 260 nm, consistent with a local maximum seen in analysis of the filtrates (Figure 2.20).

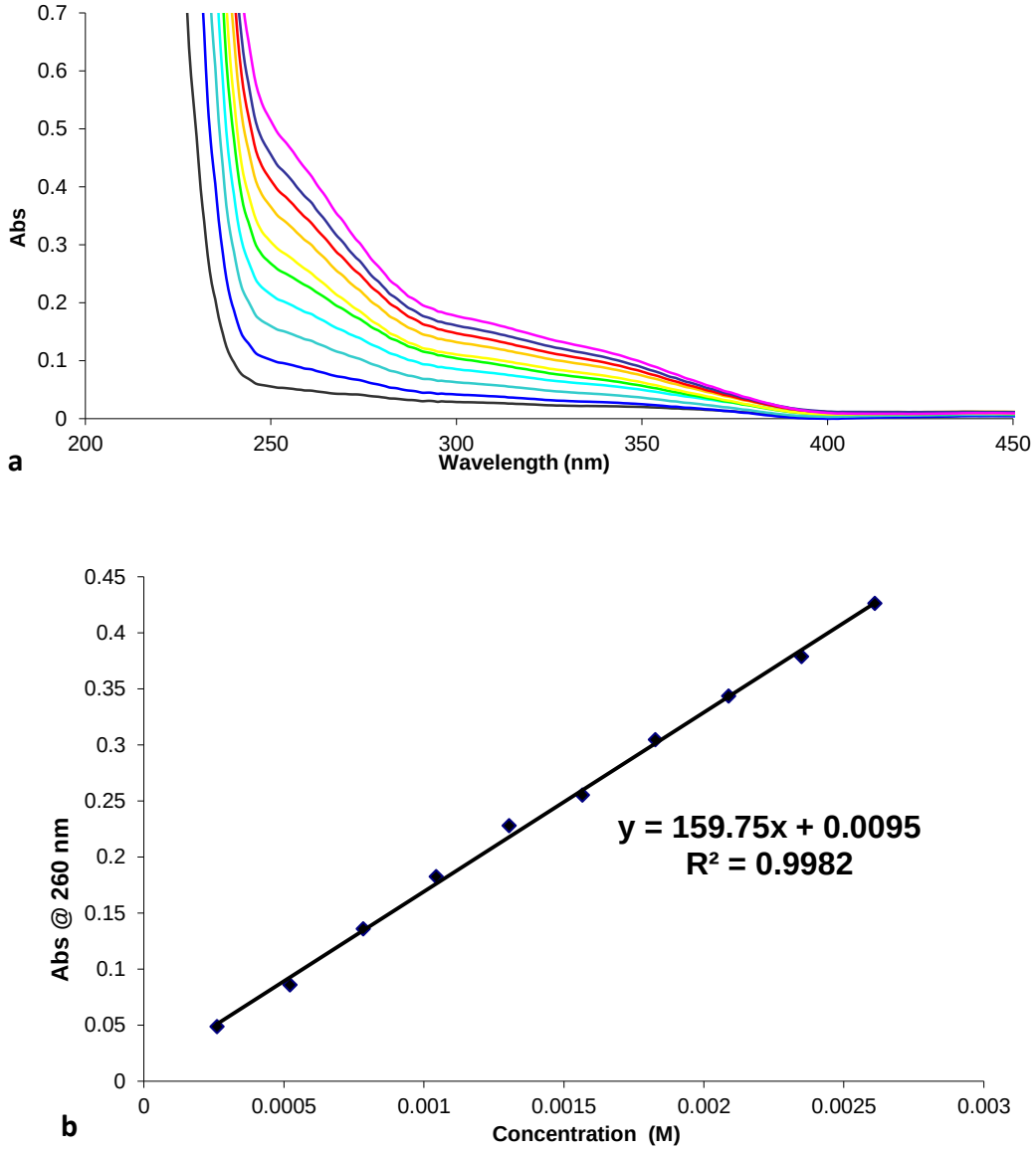

Figure 2.20. Graphs showing: (a) UV-vis spectra of the *bis*-aquated cisplatin standards, and (b) the calibration chart for *bis*-aquated cisplatin, measured at 260 nm.

2.5.10 UV calibration for cisplatin in 100 mM NaCl

As well as the *mono*- and *bis*-aquated species, calibration data were also obtained for native cisplatin in 100 mM NaCl solution (Figure 2.21). It was expected that the NaCl content would provide Cl^- concentration enough to retain coordination to the chlorido ligands through a common-ion effect. An aqueous solution of NaCl was chosen because cisplatin is generally prepared for administration in saline. In this case the UV maximum occurred at 301 nm, consistent with the BP value of 300 nm.

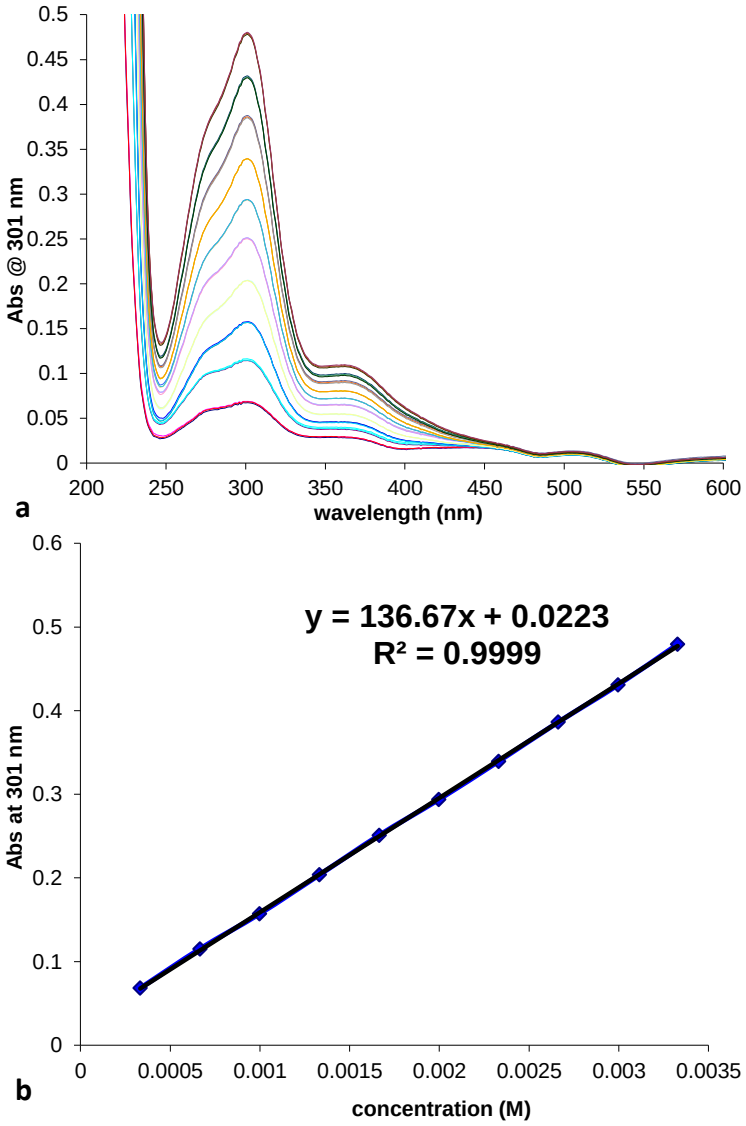

Figure 2.21. Graphs showing: (a) UV-vis spectra of the cisplatin standards, prepared in 100 mM NaCl with a maximum absorbance at 301 nm; and (b) the calibration chart for cisplatin standards in 100 mM NaCl.

Unfortunately, conjugation filtrate samples did not show consistent UV-vis profiles upon analysis. Whilst some showed a maximum at ~273 nm (consistent with *mono*-aquated cisplatin, others showed overlapping peaks with maxima around 300 nm and 260 nm (consistent with cisplatin and *bis*-aquated cisplatin). It became evident that mixtures of the different forms were present, consistent with a system of equilibria between species (Figure 2.17). This made quantification of cisplatin attachment by UV-vis spectroscopy difficult, as even the amount of each species in the standards could not be accurately known. As a result of this issue, examination of various reaction filtrates by UV-vis spectroscopy indicated that cisplatin was conjugated to CNTs at between 8.53×10^{-7} and 7.53×10^{-6} moles of cisplatin per mg *f*-CNT starting material - representing between 2.7% and 113.1% attachment. As well as showing substantial variance, the higher results suggested that there was more platinum moiety conjugated to the CNTs than was initially added.

In an effort to avoid the problems with various aquation states, it was decided to try to push the equilibrium towards the parent cisplatin species by increasing the chloride ion concentration in the samples. The cisplatin in 100 mM NaCl calibration data could then be used to quantify the amount of cisplatin in the filtrate.

2.5.11 Manipulating speciation with increased chloride concentration

Taking an aqueous solution of *bis*-aquated cisplatin and adding NaCl to 100 mM shifted the maximum from a shoulder at 260 nm to a plateau between 273-300 nm, similar to the profile observed with native cisplatin (Figure 2.22).

In light of this result, NaCl was then added to a sample of conjugation filtrate. If successful, this would have pushed the equilibrium towards cisplatin, providing a simplified solution for UV-vis analysis. A sample of filtrate was examined in 100 mM, 200 mM and 300 mM NaCl. A similar shift in absorption was not observed, suggesting that the equilibrium was not being shifted towards the chlorinated form (Figure 2.22).

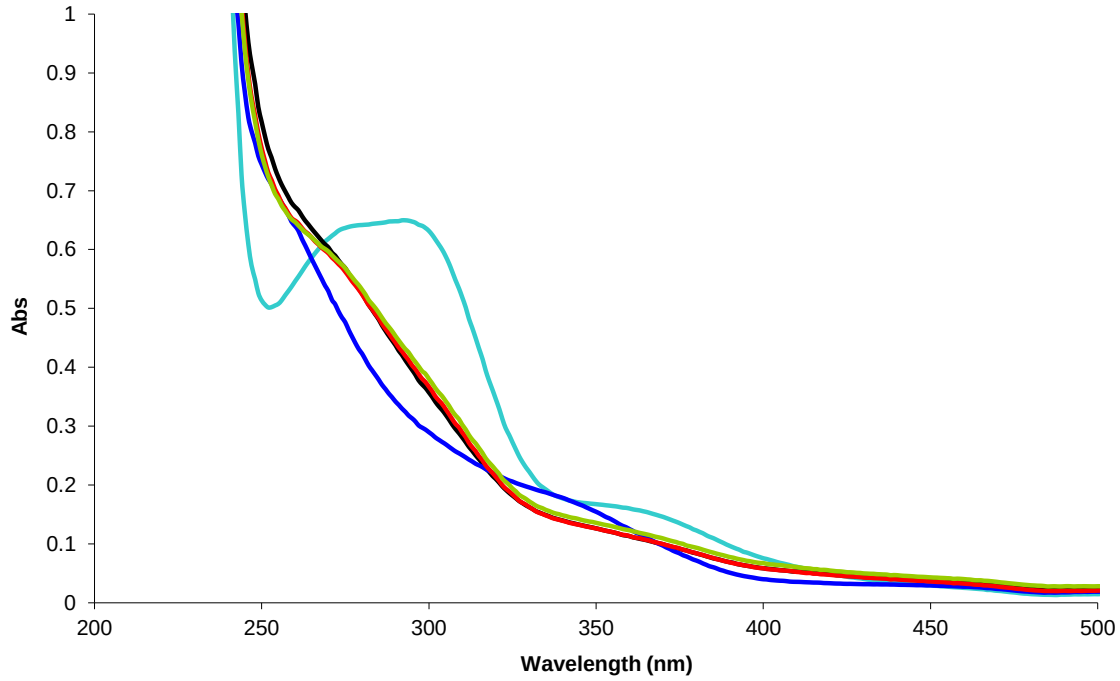

Figure 2.22. UV absorption spectra of: (i) *bis*-aquated cisplatin with no NaCl (dark blue) (ii) *bis*-aquated cisplatin with 100 mM NaCl (light blue); and (iii) a filtrate sample with 100 mM, 200 mM and 300 mM NaCl (black, red and green, respectfully). Addition of NaCl to the filtrate did not alter the UV profile, suggesting the species was not becoming more chlorinated.

Given the complexity of aqueous solutions of cisplatin and its associated species, an alternative analysis method was sought which was capable of quantifying the platinum drug, regardless of the aquation state. Flame atomic absorption spectroscopy was therefore chosen as the next technique to investigate.

2.5.12 Quantifying conjugation by F-AAS

Flame atomic absorption spectroscopy measures the concentration of a specific atom, in this case platinum. This means that it can be used to quantify the amount of cisplatin present, regardless of the degree of aquation.

The instrument uses an air/acetylene flame to evaporate solvent and dissociate the molecules their constituent atoms. Light from a hollow cathode lamp is absorbed by the atom of interest and the remaining light is measured by a detector. The element

of interest can then be quantified by comparing the absorption with a calibration curve (Figure 2.23).[83]

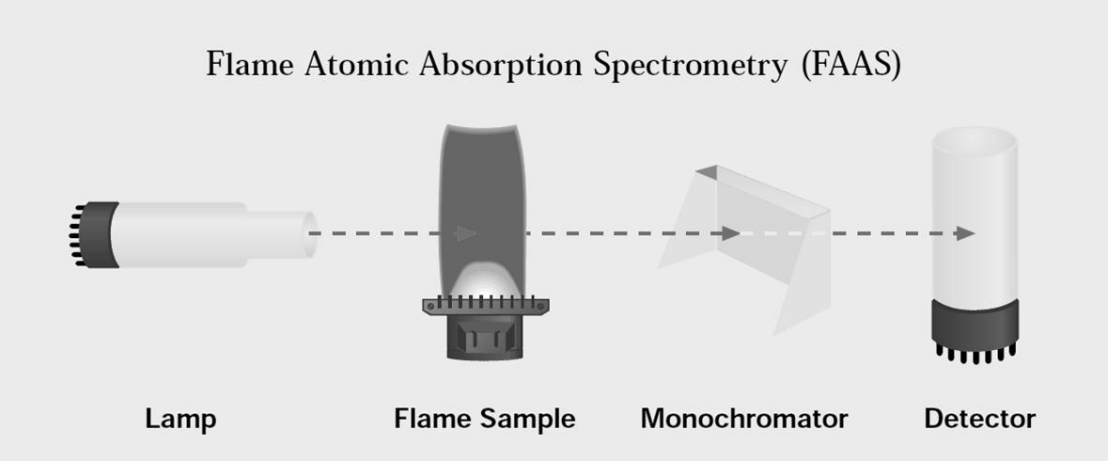

Figure 2.23. Schematic diagram of a flame atomic absorption spectrometer.[83]

From analysis of unconjugated platinum in reaction filtrates by F-AAS, cisplatin attachment to CNTs was found to be between 2.83×10^{-6} and 1.07×10^{-5} moles cisplatin per mg CNT starting material. This represents 71.2% - 91.6% attachment of the *mono*-aquated cisplatin starting material.

Elemental analysis of the as-supplied *f*-CNT starting material showed that there was up to 30.235% oxygen (although the true figure would be lower than this due to heavy metal impurities which were not quantified). This means that there was a maximum of 5.69×10^{24} –COOH functional groups per gram of starting material. The level of attachment of cisplatin is therefore around 1 cisplatin moiety per 2702 –COOH functional groups. Feazell has previously reported attachment of 65 platinum moieties per 50-100 amine functional groups on 200 nm SWNTs, a significantly higher loading.[58] Whilst the differing reactivity of the carboxylic acid and amino groups mean that a direct comparison of these results cannot be made, Feazell's work represents higher loading and therefore this work has not improved on that. It should also be noted that the potential for *bis*-aquated cisplatin to cross link adjacent CNTs is a source of uncertainty in this quantification.

Once the attachment of cisplatin to the nanotubes was completed and evaluated, the next step was to check that the drug was released in an active form, capable of binding to its target, DNA. A binding study with guanosine was therefore undertaken.

2.5.13 Drug binding study with guanosine residues

Cisplatin is known to bind to DNA at the nucleophilic N7 position (Figure 2.24) of guanine and adenine forming inter- and intra-strand crosslinks.[84,85] An NMR binding experiment was undertaken in order to evaluate the potential for DNA binding by the Pt-CNT conjugate or detached platinum moiety. If DNA binding occurs upon incubation with the Pt-CNT conjugate, there will be a shift in the position of the signal for the H8 proton.

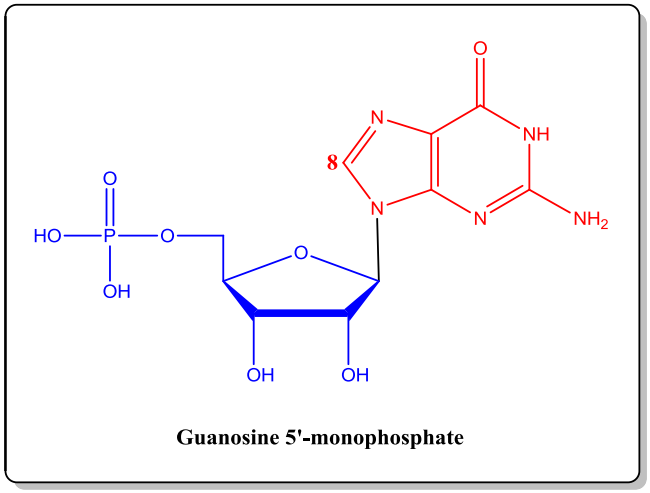

Figure 2.24. The structure of guanosine 5'-monophosphate, composed of one guanine residue (red) and a ribose sugar unit and phosphate group (blue). The H8 position is indicated.

A 50 mM guanosine 5'-monophosphate solution was prepared in D_2O and a NMR spectrum obtained (Figure 2.25). This represented the unbound form of the nucleotide and the experimental control.

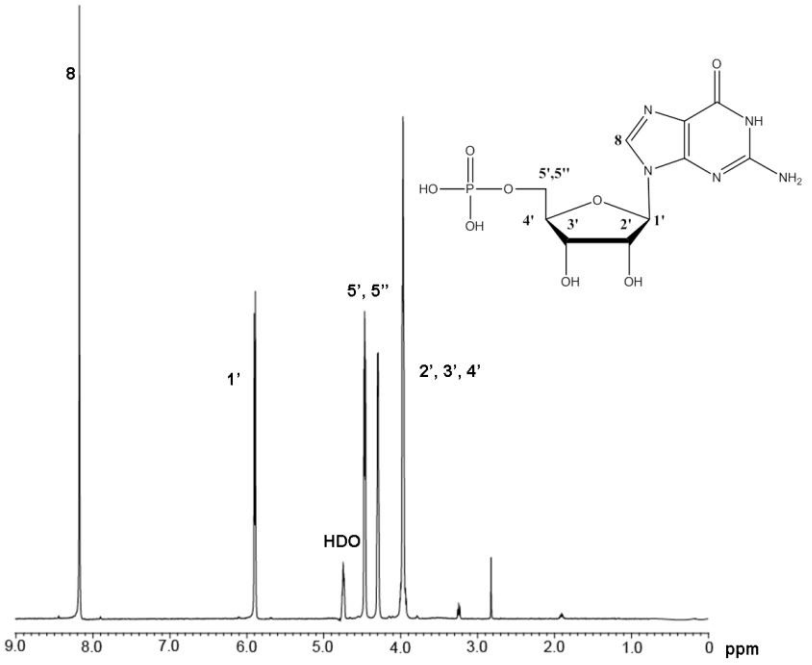

Figure 2.25. ^{1}H NMR spectrum of guanosine 5'-monophosphate. Note the strong signal at ~8.2 ppm for the H8 proton.

A ^{1}H NMR was obtained of Pt-CNT with guanosine 5'-monophosphate in D_2O immediately after mixing, at which point the guanosine NMR resonances were consistent with free guanosine (Figure 2.26a). After incubation with Pt-CNT at 37 ºC for three days, there were no significant changes in chemical shifts, indicating that no guanosine binding had taken place (Figure 2.26b). The sample was then incubated for three days at 60 ºC. It was hoped that if an interaction with the guanosine was possible then heating the system above physiological temperature may force it to occur more rapidly. The NMR spectrum obtained for this sample showed no significant chemical shift differences, but a considerable reduction in intensity of the H8 peak (Figure 2.26).

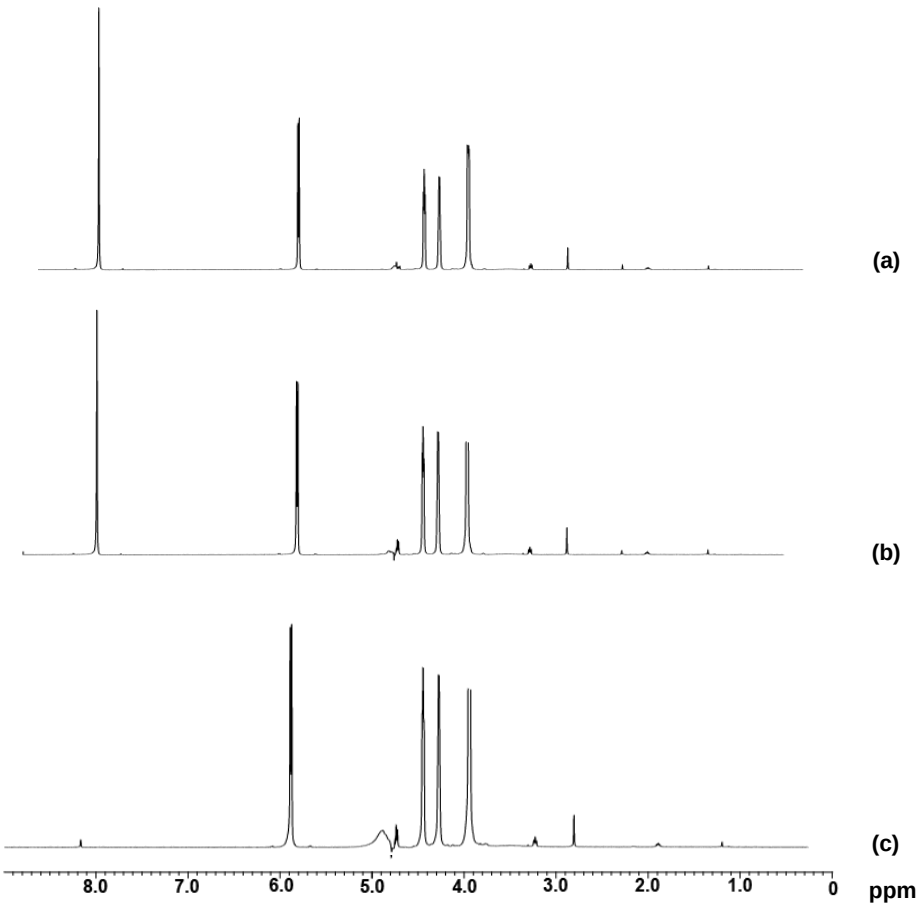

Figure 2.26. ^{1}H NMR spectra of Pt-CNT with guanosine monophosphate solution (a) at day 0, (b) after three days at 37 ºC and (c) after three days at 60 ºC, at which point the signal at ~8.2 ppm is visibly reduced.

It was interesting to note that the majority (if not all) of the CNTs in the sample were visibly not dispersed on completion of the NMR acquisition (Figure 2.27). This suggested that the Pt-CNTs re-aggregated during the experiment.

Figure 2.27. An NMR tube after the experiment, showing visibly aggregated CNTs.

Four hypotheses were considered for the disappearance of the peak at 8.2 ppm and the aggregation of the Pt-CNTs: 1) there was some Pt-CNT and/or cisplatin interaction with the guanosine of an unknown nature, 2) the guanosine itself was unstable at 60 ºC, 3) the pyrimidine ring system was π-π stacking with the CNT (which may have contributed to aggregation in the system), or 4) the CNT was forming some kind of inclusion complex with the guanosine.

The experiment was repeated with *f*-CNT and guanosine monophosphate in the absence of any platinum moiety in order to determine if this phenomenon was drug-dependant or involved only the CNT moiety. After three days at 37 ºC there were no significant chemical shift difference, but after incubation at 60 ºC the H8 peak intensity dropped once more (Figure 2.28). This suggested either some interaction between *f*-CNT and guanosine, or that the elevated temperature was responsible.

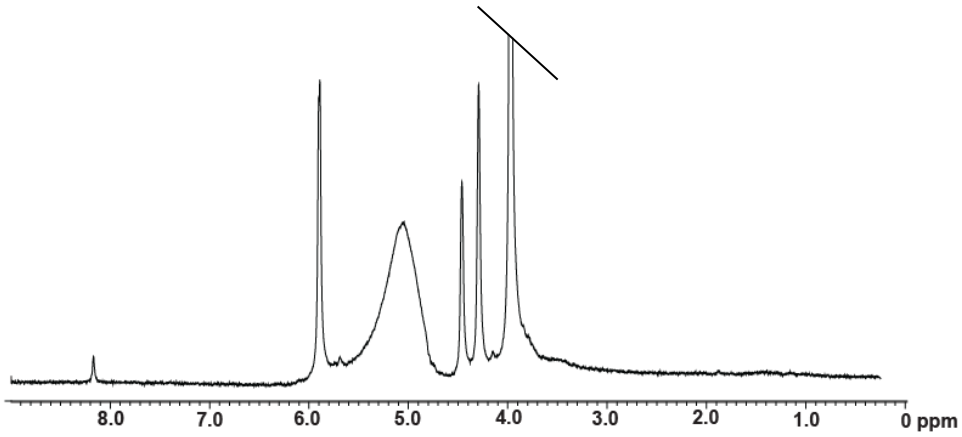

Figure 2.28. ^{1}H NMR spectrum of guanosine monophosphate in D_2O after incubation with *f*-CNT for three days at 60 ºC. The peak at ~8.2 ppm is significantly reduced in intensity.

To determine whether or not the elevated temperature was contributing to the peak reduction, a sample of 50 mM guanosine 5'-monophosphate in D_2O was analysed after incubation at 60 ºC for three days (Figure 2.29). Again, the peak at 8.2 ppm was significantly reduced in intensity.

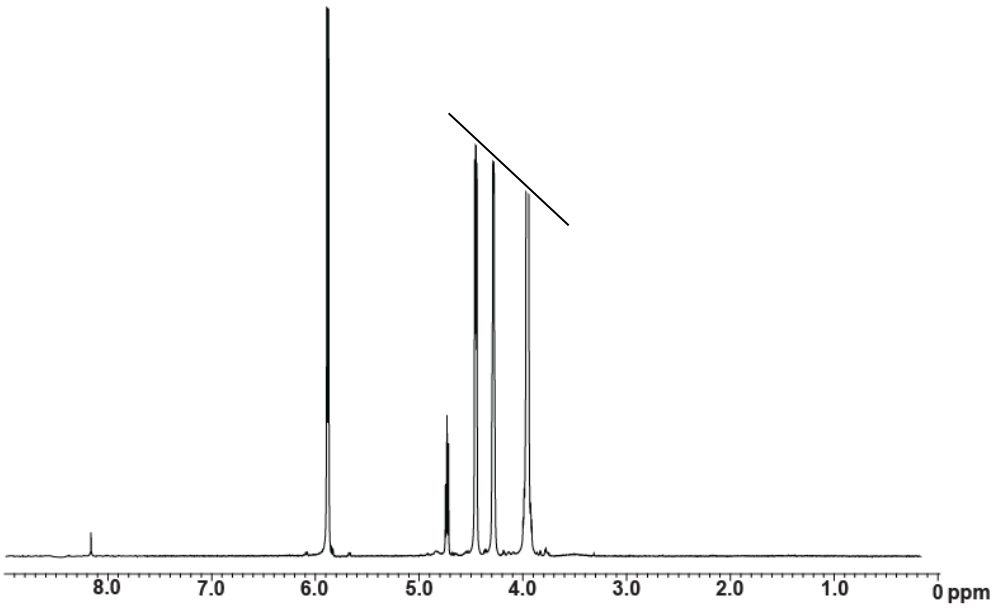

Figure 2.29. ^{1}H NMR spectrum of 5'-guanosine monophasphate after incubation at 60 ºC for three days. The peak at ~8.2 ppm is once more reduced in intensity.

Although the use of this assay to evaluate DNA binding potential has been reported in the literature,[23] this experiment showed that the assay at 60 ºC was unsuitable for evaluating Pt-CNT binding as there would be an inherent reduction in the H8 peak, regardless of drug or CNT presence. Either longer incubation at 37 ºC or an alternative *in vitro* assay would be required.

2.5.14 Evaluation of Pt-CNT dispersants

The biological applications of CNTs are greatly limited by their insolubility in biologically compatible solvents. This must be overcome if CNTs are to be successfully utilised as drug delivery vehicles.[28] Whilst the *f*-CNTs had been successfully dispersed prior to conjugation, the Pt-CNTs quickly became aggregated (as shown in Figure 2.27). In order to ensure the Pt-CNTs remained soluble and therefore bioavailable *in vivo*, a number of pharmaceutical surfactants were investigated. These were expected to adsorb onto the surface of the CNT, preventing them from re-aggregating. Each sample was assessed by eye following sonication

and agitation (Figure 2.30). All solutions produced, at least, swollen Pt-CNT (evident from visible increase in the amount of material in the bottom of the tube).

Sonication in water produced visibly swollen Pt-CNT with some dispersion, evident from clear supernatant with a black hue. Settled, undispersed Pt-CNT remained visible at the bottom of the tube. Sonication in phosphate buffered saline (pH 7.4) also produced swollen Pt-CNT which remained at the bottom of the tube and rapidly settled after brief agitation. Sonication in 0.1% Danagel produced minimal dispersion, by eye.

More successfully, sonication in 0.1% SDS solution produced visibly better dispersion with a clear supernatant but some settled Pt-CNT remained visible. Increasing this to a 1% SDS solution produced a more opaque dispersion which may have been a result of the concentration of SDS in solution (visible as a pearlescent liquid), although minimnal settled Pt-CNT were evident. Sonication in 1% Pluronic F-127 produced a slightly opaque solution with minimal visible settling.

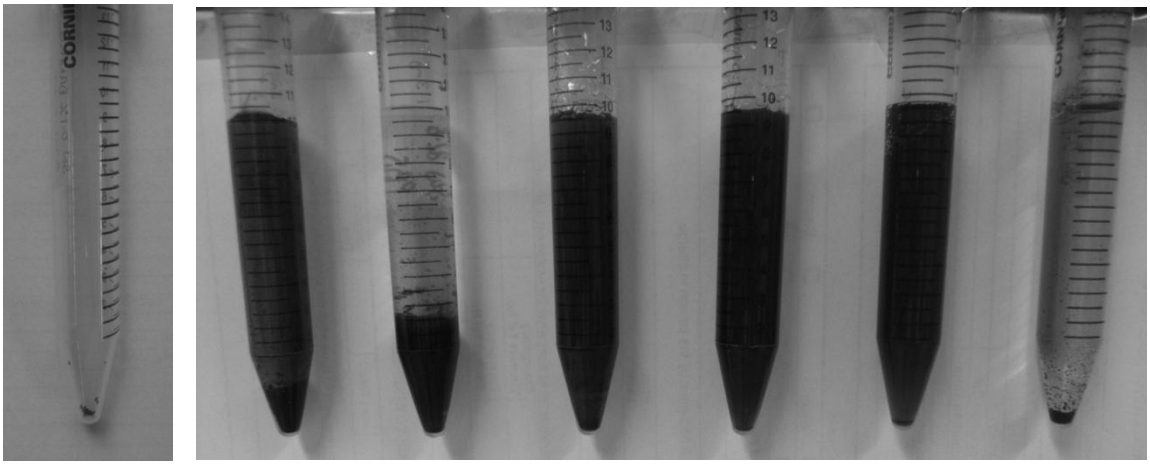

Figure 2.30. Left, a typical amount of Pt-CNT before sonication in any solution. Right, each Pt-CNT/dispersant sample after 60 min sonication. Left to right: water; PBS; 0.1% SDS; 1% SDS; 1% Pluronic F-127; and 0.1% Danagel.

After centrigugation, supernatant from the solutions was then removed and placed in 50 mL centrifuge tubes before UV-vis analysis (Figure 2.31). Phosphate buffered saline and Danagel produced the poorest dispersion (second and sixth from left). One per cent SDS appeared to produce the best dispersion (fourth from left), although the opacity of the dispersant made this difficult to assess.

Ham and colleagues have found that the success of dispersing single-walled carbon nanotubes in water is dependent on using a surfactant possessing a lipophilic chain of dodecyl size (12 carbons) or longer. This explains why the SDS and Pluronic F-127 (a co-block polymer) were successful at dispersing the nanotubes.[78]

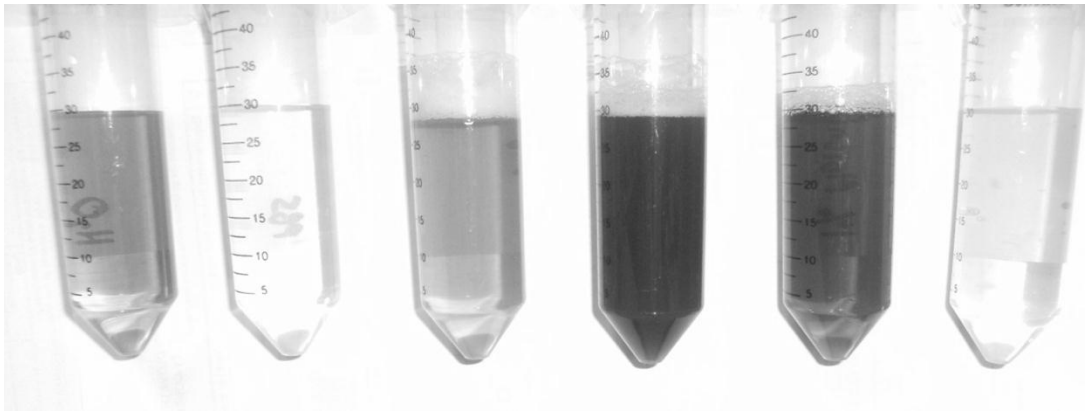

Figure 2.31. The supernatant from each sample. Left to right: water; PBS; 0.1% SDS; 1% SDS; 1% Pluronic F-127; and 0.1% Danagel.

2.5.15 UV-vis spectroscopy of dispersions

As previously discussed, fully exfoliated CNTs absorb in the UV region.[48,86] This can be exploited to evaluate the concentration of dispersed of CNTs in solution, and thus evaluate how effective each dispersant is.

A baseline spectrum was obtained for each solution, except 1% SDS which exceeded the detection limit of the instrument. UV-vis spectra were obtained for each saturated dispersion and baseline corrections performed (Figure 2.32). From these data it was apparent that 0.1% SDS solution, PBS and 1% Danagel solution were less efficient at dispersing Pt-CNT than both water and 1% Pluronic solution.

The 1% SDS solution was too highly absorbing in this region to obtain a spectrum for comparison.

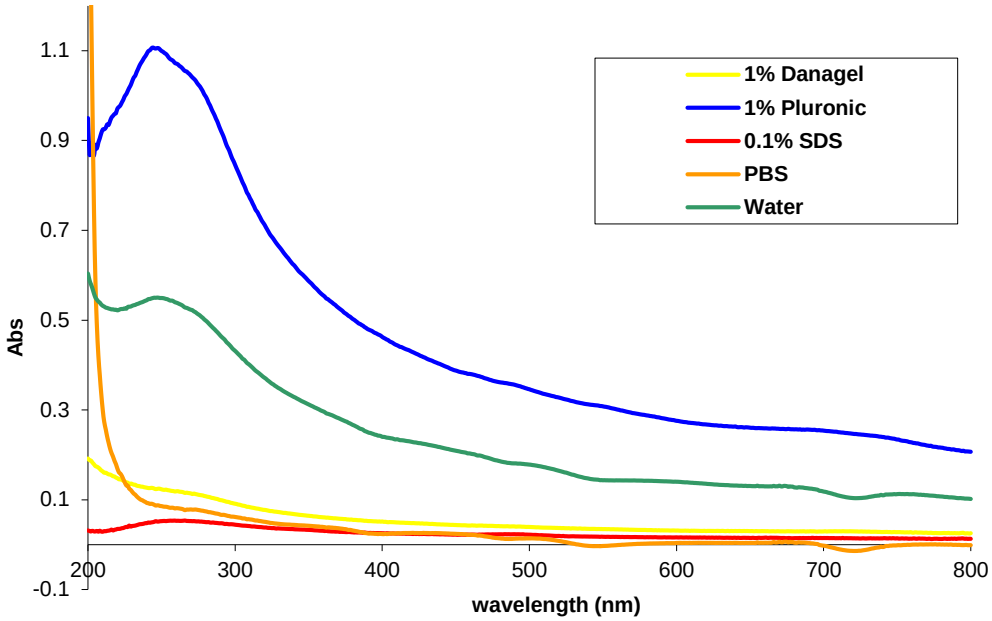

Figure 2.32. UV-vis spectra for saturated dispersions of Pt-CNT in various surfactants.

From these data, a 1% Pluronic F-127 solution was most effective when attempting to exfoliate and disperse bundled Pt-CNTs, although it could not be compared to 1% SDS. A sample of the Pluronic F-127 dispersion was freeze-dried and simulated intestinal fluid at 37 ºC added. The solution became clear, indicating that the Pluronic had the potential to resuspend the Pt-CNTs *in vivo*, after oral administration. This should be repeated in simulated nasal electrolyte solution (SNES) to determine if similar solubility (and therefore bioavailability) can be achieved in the nose.

Strano and colleagues have postulated the mechanism of dispersion of SWNTs in ionic surfactants with ultrasonication.[87] They suggest that gaps are formed at the ends of SWNT bundles as a result of the high shear environment created by sonication. The surfactant moleules diffuse into these spaces, adsorbing onto the surface and propagating the space between SWNTs in an "unzipping" manner. The experimental results suggest that Pluronic F-127 is more efficient at infiltrating these spaces and assisting the unzipping process.

This experiment should be repeated with a new concentration of SDS between 0.1-1% (w/v) in an attempt to optimise this surfactant, as evaluation of its usefulness was hampered by its own absorption at this concentration. However, Strano and colleagues have also reported that dispersion of SWNTs in SDS is limited when an equilibrium is established between aggregates and fully exfoliated SWNTs, and that the position of this equilibrium is a function of SDS concentration.[87] This suggests that the concentration of SDS used (1%) may have been too high, not only for UV-vis analysis, but also for efficient dispersion, pushing the equilibrium back towards the aggregated state.

Other surfactants including polyethylene glycol (PEG)[88,89] and an Fmoc derivative could also be investigated. Ulijn's group have previously investigated the use of Fmoc-tyrosine, phenylalanine, histidine, tryptophan and glycine as a methods of non-covalent functionalisation for increasing dispersability of SWNTs.[90] Lysine has been covalently attached to MWNTs by Hu *et al*.[91] to aid dispersion. It is proposed that an Fmoc-lysine compound be investigated as it could provide the dispersion efficiency of lysine whilst requiring no covalent functionalisation.

2.6 SAFETY CONCERNS

Although CNT delivery vehicles can reduce systemic toxicity by passively targeting drugs to tumours, there is evidence that they may be associated with their own inherent toxicity. Pulmonary exposure to SWNTs has been found to cause dose-dependent and persistent alterations in pulmonary activity, along with a reduced rate of bacterial clearance, oxidative stress, granulomas and lowered glutathione levels in the lungs.[92,93] Much research has focussed on assessment of pulmonary toxicity, as their high aspect-ratios are similar to those of asbestos.[93] As well as exhibiting pulmonary toxicity, SWNTs have been found to inhibit the growth of HEK293 cells (human embryo kidney cells) by initiating apoptosis and reducing cellular adhesion.[94] It has also been suggested that the metal catalysts[95] (including Ni[96] and

Fe[44]) and/or graphite[97] present as impurities in industrial batches of CNT could be responsible for toxicity. In view of this evidence, there has been call for extensive *in vivo* screening of CNTs and other nanoparticles to allow full correlation between physiochemical properties of nanomaterials and their biodistribution and toxicity profiles.[98]

Toxicity data however, remain contradictory, with some studies highlighting toxicity and others a complete lack of. This may simply be due to the experimental variables in operation. For example, intraperitoneal delivery of SWNTs (regardless of size) has resulted in formation of aggregates in Swiss strain mice. These aggregates persisted in the cells for up to five months and formation of granulomas occurred where aggregates reached 10 μm.[99] However, the same study showed that highly purified SWNTs and ultra-short (US) nanotubes were well tolerated in high doses after oral delivery.[99] These findings suggest that the safety profile of CNT-based delivery systems can be improved by engineering the delivery vehicles as ultrapure discrete "molecule-like" entities, and giving consideration to the delivery route.[99] It has now been recognised that toxicity can vary with structure (MWNT *vs* SWNT), length and aspect ratio, surface area, type and degree of functionalisation, impurities, concentration and dose.[100]

Further difficulties arise when toxicity data is cited at face value, with insufficient consideration of the test specifications and their influence. Some *in vitro* studies which have reportedly shown cytotoxicity may be giving "false positives". For example, the traditional 2-(4,5-dimethyl-2-thiazolyl)-3,5-diphenyl-2H-tetrazolium bromide (MTT) assay, used to assess cytotoxicity, has been shown to be unsuitable for accessing CNT cytotoxicity.[101] During this assay, the MTT dye is reduced in viable cells to MTT-formazan, which is then measured spectrophotometrically. When CNTs are present however, they interact with MTT-formazan, sequestering them from the solution, resulting in false readings of cytotoxicity.[102] Additionally, it has been shown that CNTs can adsorb the nutrients, cytokines and growth factors out of cell culture medium, indirectly resulting in a reduction in cell viability in any *in vitro* assay.[103]

It is apparent that when carrying out toxicity studies, assessment of all contributing factors is required, along with a sound understanding the mechanisms of *in vitro* (and *in vivo*) assays and their limitations. This is also true of cytotoxicity assays for investigational drug delivery vehicles.

Since uncertainty prevails, the Health and Safety Executive in the United Kingdom has issued guidelines pertaining to the use of all CNTs in the workplace, recommending a precautionary approach. These guidelines include preventing the material from becoming airborne, and keeping it enclosed during all processes. CNTs should also be handled in a ducted fume cupboard fitted with a high-efficiency particulate air (HEPA) filter. These conditions could not be met by the group at present, leading to the suspension of this work.

.

2.7 CONCLUSIONS AND FURTHER WORK

Prior to platinum conjugation reactions, *f*-CNTs have been successfully dispersed in water using a direct contact sonication probe followed by centrifugation and further rounds of sonication on the undispersed material. Cisplatin has been aquated at high yields and conjugated to *f*-CNTs. Analyses by F-AAS were carried out after it became apparent that UV-vis spectroscopy of the conjugation filtrates was unsuitable due to uncontrollable speciation of cisplatin in aqueous media. Conjugation of up to 5.84×10^{-5} moles cisplatin per mg CNT has been achieved, although this represents lower attachment per functional groups than has been achieved by others. Although this represents around 1 platinum moiety per 2,702 functional groups, it is also up to 91.6% of the aquated cisplatin added. This suggests that there is further potential for attachment which could be exploited by repeating the conjugations with higher concentrations of aquated cisplatin. Additionally, careful analysis of the *f*-CNT starting material is required to ensure a more accurate value for functionalisation, and consequently the degree of functionalisation is known. The potential for any *bis*-aquated cisplatin which may have been formed to cross-link adjacent CNTs remains a source of uncertainty in quantifying functionalisation in this manner, as does the potential for cisplatin to form an inclusion complex with the nanotubes.

Guanosine binding studies using ^{1}H NMR have had limited value to date, due to the disappearance of the H8 resonance at ~ 8.2 ppm. This has been shown to occur after heating a guanosine sample to 60 ºC for three days and may not occur if the reaction is allowed to progress at 37 ºC.

A number of surfactants were under investigation for their ability to disperse Pt-CNT in aqueous media. Pluronic F-127 and direct contact sonication in water has proven to be the most useful, and the resulting product was able to be redispersed in simulated intestinal fluid at 37 ºC, showing promise for bioavailability following oral administration. A similar investigation in simulated nasal electrolyte solution will be required to provide evidence for nasal bioavailability. It should however be noted

that the use of surfactants in a nasal formulation may be harmful to the nasal mucosa.[104]

Before this study could be taken to *in vitro* testing in cancer cell lines, an assay must be carefully designed, modified or controlled to properly access cytotoxicity of the Pt-CNT conjugate without interference resulting from the nature of the CNT material. This may involve comparing a combination of assays and controls.

Since the initiation of this work the field has progressed, and new methods of anticancer drug delivery with nanotubes have emerged. Recently, cisplatin has been encapsulated within MWNTs and capped in place using gold nanoparticles.[105] Physically encapsulating the drug maintains the integrity of the CNT structure and avoids chemical modification of the drug. Although internalisation of cisplatin in CNTs has been achieved previously,[106] the novel use of gold "caps" allows the cisplatin to remain protected within the CNT nano-environment before being released in a controlled manner, prevents dose dumping.[105] Further developments in this technology may include a removable cap which releases the contents upon reaching a specific pH or temperature.[105] Other emerging techniques include the use of ultra-short CNTs (US-CNTs), supported by research by Guven and colleagues which has shown that encapsulation of cisplatin within US-CNTs can increase uptake of the drug in cisplatin-resistant cell lines.[107] Should this work recommence, these are technologies which could also be investigated to further enhance the delivery of cisplatin using CNTs. Additionally, the further functionalisation of Pt-CNTs with a targeting group such as folic acid could improve tumour targeting.

Whilst contradictory evidence on the toxicity of CNTs remains, the field is beginning to recognise that delivery route/manner and CNT specifications can affect toxicity greatly. More conclusive data on this subject is required before CNTs can be effectively applied as drug delivery vehicles. As work with CNT was halted, a new delivery vehicle was sought. The following chapters discuss the use of cucurbiturils, a relatively young family of macrocycles, which is finding application in a wide range of fields.

2.8 REFERENCES

(1) Patrick, G.L., *An Introduction to Medicinal Chemistry*, 2nd ed., Oxford University Press, Oxford, 2001.

(2) Winau, F., Westphal, O. and Winau, R., *Microbes and Infection*, 2004, **6**, 786-789.

(3) Patrick, G.L., *An Introduction to Medicinal Chemistry*, 2nd ed., Oxford University Press, Oxford, 2001.

(4) Cancer Drugs: Long Odds and Magic Bullets, http://www.cancer.org/cancer/news/expertvoices/post/2012/08/13/cancer-drugs-long-odds-and-magic-bullets.aspx, *accessed 9th February 2013.*

(5) *Nanoscience and Nanotechnologies: Opportunities and Uncertainties - Summary and Recommendations*, The Royal Society, 2004, pp 11.

(6) Wagner, V., Dullaart, A., Bock, A-K., and Zweck, A., *Nature Biotechnol.*, 2006, **24**, 1211-1217.

(7) Steichen, S.D., Caldorera-Moore, M. and Peppas, N.A., *Eur. J. Pharm. Sci.*, 2013, **48**, 416-427.

(8) Matsumura, Y. and Maeda, H., *Cancer Res.*, 1986, **46**, 6387-6392.

(9) Maeda, H., *Adv. Enzyme Regul.*, 2001, **41**, 189-207.

(10) Iyer, A.K., Khaled, G., Fang, J. and Maeda, H., *Drug Discov. Today*, 2006, **11**, 812-818.

(11) Maeda, H., Wu, J., Sawa, T., Matsumura, Y. and Hori, K., *J. Control. Release*, 2000, **65**, 271-284.

(12) Tanaka, T., Shiramoto, S., Miyashita, M., Fujishima, Y. and Kaneo, Y., *Int. J. Pharm.*, 2004, **277**, 39-61.

(13) Peer, D., Karp, J.M., Hong, S., Farokhzad, O.C., Margalit, R. and Langer, R., *Nature Nanotech.*, 2007, **2**, 751-760.

(14) Prakash, S., Malhotra, M., Shao, W., Tomaro-Duchesneau, C. and Abbasi, S., *Adv. Drug Deliver. Rev.*, 2011, **63**, 1340-1351.

(15) Caelyx Patient Information Leaflet, http://www.janssen.co.uk/product/detail.jhtml?itemname=caleyx_info, *4th May 2012.*

(16) Koukourakis, M.I., Giatromanolaki, A., Pitiakoudis, M., Kouklakis, G., Tsoutsou, P., Abatzoglou, I., Panteliadou, M., Sismanidou, K., Sivridis, E. and Boulikas, T., *Int. J. Radiat. Oncol.*, 2010, **78**, 150-155.

(17) Lv, Q., Li, L.-M., Han, M., Tang, X.-J., Yao, J.-N., Ying, X.-Y., Li, F.-Z. and Gao, J.-Q., *Int. J. Pharm.*, 2013, **444**, 1-9.

(18) Bandak, S., Goren, D., Horowitz, A., Tzemach, D. and Gabizon, A., *Anti-Cancer Drug.*, 1999, **10**, 911-922.

(19) Harrington, K.J., Lewanski, C.R., Nothcote, A.D., Whittaker, J., Wellbank, H., Vile, R.G., Peters, A.M. and Stewart, J.S.W., *Ann. Oncol.*, 2001, **12**, 493.

(20) Kim, E.S., Lu, C., Khuri, F.R., Tonda, M., Glisson, B.S., Liu, D., Jung, M., Hong, W.K. and Herbst, R.S., *Lung Cancer*, 2001, **34**, 427-432.

(21) Cloninger, M.J., *Curr. Opin. Chem. Bio.*, 2002, **6**, 742-748.

(22) Rawat, M., Singh, D., Saraf, S. & Saraf, S., *Biol. Pharm. Bull.*, 2006, **29**, 1790-1798.

(23) Kirkpatrick, G.J., Plumb, J.A., Sutcliffe, O.B., Flint, D.J. and Wheate, N.J., *J. Inorg. Biochem.*, 2011, **105**, 1115-1122.

(24) Mignani, S., El Kazzouli, S., Bousmina, M. and Majoral, J.-P., *Adv. Drug Deliver. Rev.*,

(25) Ajayan, P.M., Charlier, J-C., and Rinzler, A.G., *Proc. Natl. Acad. Sci.*, 1999, **96**, 14199-14200.

(26) Kroto, H.W., Heath, J.R., O'Brien, S.C., Curl, R.F. and Smalley, R.E., *Nature*, 1985, **318**, 162-163.

(27) Iijima, S., *Nature*, 1991, **354**, 56-58.

(28) Bianco, A., Kostarelos, K., Partidos, C.D. and Prato, M., *Chem. Commun.*, 2005, **5**, 571-577.

(29) Kuchibhatla, S.V.N.T., Karakoti, A.S., Bera, D. and Seal, S., *Prog. Mater. Sci.*, 2007, **52**, 699-913.

(30) Mamalis, A.G., Vogtländer, L.O.G. & Markopoulos, A., *Precis. Eng.*, 2002, **28**, 16-30.

(31) Mir, M., Hosseini, A. and Majzoobi, G.H., *Comp. Mater. Sci.*, 2008, **43**, 540-548.

(32) Meng, L., Zhang, X., Lu, Q., Fei, Z. and Dyson, P.J., *Biomaterials*, 2012, **33**, 1689-1698.

(33) Bonard, J.-M., Kind, H., Stöckli, T. and Nilsson, L.-O., *Solid-State Electron.*, 2001, **45**, 893-914.

(34) Harris, P.J., *Carbon Nanotube Science: Synthesis, Properties and Applications*, 1st ed., Cambridge University Press, Cambridge, UK., 2009.

(35) Baughman, R.H., Zakhidov, A.A. and de Heer, W.A., *Science*, 2002, **297**, 787-792.

(36) Cai, H., Cao, X., Jiang, Y., He, P. and Fang, Y., *Anal. Bioanal. Chem*, 2003, **375**, 287.

(37) Park, K.H., Chhowalla, M., Iqbal, Z. and Sesti, F., *J. Biol. Chem*, 2003, **278**, 50212.

(38) Mitchell, D.T., Lee, S.B., Trofin, L., Li, N., Nevanen, T.K., Soderlund, H. and Martin, C.R., *J. Am. Chem. Soc.*, 2002, **124**, 11864.

(39) Nien, Y.-H. and Huang, C.-l., *Mat. Sci. Eng. B*, 2010, **169**, 134-137.

(40) Meng, J., Song, L., Xu, H., Kong, H., Wang, C., Guo, X. and Xie, S., *Nanomedicine: N.B.M*, 2005, **1**, 136– 142.

(41) McKenzie J.L, W.M.C., Shib R and Webster T.J, *Biomaterials*, 2004, **25**, 1309–1317.

(42) Pastorin, G., *Pharmaceut. Res.*, 2009, **26**, 746-769.

(43) Itkis, M.E., Perea, D.E., Jung, R., Niyogi, S. and Haddon, R.C., *J. Am. Chem. Soc.*, 2005, **127**, 3439-3448.

(44) Klumpp, C., Kostarelos, K., Prato, M. and Bianco, A., *B.B.A.-Biomembranes*, 2006, **1758**, 404-412.

(45) Thess, A., Lee, R., Nikolaev, P., Dai, H., Petit, P., Robert, J., Xu, C., Lee, Y.H., Kim, S.G., Rinzler, A.G., Colbert, D.T., Scuseria, G.E., Tomanek, D., Fischer, J.E. and Smalley, R.E., *Science*, 1996, **273**, 483-487.

(46) Pantarotto, D., Partidos, C.D., Graff, R., Hoebeke, J., Briand, J.-P. and Prato, M., *J. Am. Chem. Soc.*, 2003, **125**, 6160-6164.

(47) Foldarvi, M. and Bagonlure, M., *Nanomedicine: N.B.M*, 2008, **4**, 173-182.

(48) Riggs, J.E., Walker, D.B., Carroll, D.L. and Sun, Y.-P., *J. Phys. Chem. B*, 2000, **104**, 7071-7076.

(49) Venkatesan, N., Yoshimitsu, J., Ito, Y., Shibata, N. and Takada, K., *Biomaterials*, 2005, **26**, 7154 - 7163.

(50) Kam, N.W.S., Jessop, T.C., Wender, P.A. and Dai, H., *J. Am. Chem. Soc.*, 2004, **126**, 6850-6851.

(51) Kam, N.W.S., Liu, Z. and Dai, H., *Angew. Chem. Int. Ed.*, 2006, **45**, 577 –581.

(52) Serag, M.F., Kaji, N., Gaillard, C., Okamoto, Y., Terasaka, K., Jabasini, M., Tokeshi, M., Mizukami, H., Bianco, A. and Baba, Y., *ACS Nano*, 2010, **5**, 493-499.

(53) Kam, N.W.S., Jessop, T.C., Wender, P.A. & Dai, H., *J. Am. Chem. Soc.*, 2004, **126**, 6850-6851.

(54) Dhar, S., Liu, Z., Thomale, J., Dai, H. and Lippard, S.J., *J. Am. Chem. Soc.*, 2008, **130**, 11467-11476.

(55) Deng, X., Jia, G., Wang, H., Sun, H., Wang, X., Yang, S., Wang, T. and Liu, Y., *Carbon*, 2007, **45**, 1419–1424.

(56) Kagan, V.E., Konduru, N.V., Feng, W., Allen, B.L., Conroy, J., Volkov, Y., Vlasova, I.I., Belikova, N.A., Yanamala, N., Kapralov, A., Tyurina, Y.Y., Shi, J., Kisin, E.R., Murray, A.R., Franks, J., Stolz, D., Gou, P., Klein-Seetharaman, J., Fadeel, B., Star, A. and Shvedova, A.A., *Nat. Nano*, 2010, **5**, 354-359.

(57) Bianco, A., Kostarelos, K. and Prato, M., *Curr. Opin. Chem. Biol.*, 2005, **9**, 674-679.

(58) Feazell, R.P., Nakayama-Ratchford, N., Dai, H. and Lippard, S.J., *J. Am. Chem. Soc.*, 2007, **129**, 8438-8439.

(59) Zhang, X., Meng, L., Lu, Q., Fei, Z. and Dyson, P.J., *Biomaterials*, 2009, **30**, 6041-6047.

(60) Thrall, J.H., *Radiology*, 2004, **230**, 315-318.

(61) Wu, W., Wieckowski, S., Pastorin, G., Benincasa, M., Klumpp, C., Briand, J.-P., Gennaro, R., Prato, M. and Bianco, A., *Angew. Chem. Int. Ed.*, 2005, **44**, 6358-6362.

(62) Ji, Z., Lin, G., Lu, Q., Meng, L., Shen, X., Dong, L., Fu, C. and Zhang, X., *J. Colloid Interf. Sci.*, 2012, **365**, 143-149.

(63) Liu, Z., Chen, K., Davis, C., Sherlock, S., Cao, Q., Chen, X. and Dai, H., *Cancer Res.*, 2008, **68**, 6652-6660.

(64) Pantarotto, D., Singh, R., McCarthy, D., Erhardt, M., Braind, J.-P., Prato, M., Kostarelos, K. and Bianco, A., *Angew. Chem. Int. Ed.*, 2004, **43**, 5242-5246.

(65) Lu, Q., Moore, J.M., Huang, G., Mount, A.S., Rao, A.M., Larcom, L.L. and Ke, P.C., *Nano Lett.*, 2004, **4**, 2473-2477.

(66) Lee, H.K., Park, K.M., Jeon, Y.J., Kim, D., Oh, D.H., Kim, H.S., Park, C.K. and Kim, K., *J. Am. Chem. Soc*, 2005, **127**, 5006-5007.

(67) Kam, N.W.S. and Dai, H.J., *J. Am. Chem. Soc.*, 2005, **127**, 6021-6026.

(68) Ajima, K., Maigne, A., Yudasaka, M. and Iijima, S., *J. Phys. Chem. B*, 2006, **110**, 19097-19099.

(69) Ajima, K., Yudasaka, M., Murakami, T., Maigné, A., Shiba, K. and Iijima, S., *Mol. Pharmaceut.*, 2005, **2**, 475-480.

(70) Bhirde, A.A., Patel, V., Gavard, J., Zhang, G., Sousa, A.A., Masedunskas, A., Leapman, R.D., Weigert, R., Gutkind, J.S. and Rusling, J.F., *ACS Nano*, 2009, **3**, 307-316.

(71) Thornycroft, J. and Barnaby, S.W., *Inst. C. E.*, 1895, **122**, 51-102.

(72) Suslick, K.S., Goodale, J.W., Schubert, P.F. and Wang, H.H., *J. Am. Chem. Soc.*, 1983, **105**, 5781-5785.

(73) Einhorn, C., Einhorn, J. and Luche, J.-L., *Synthesis*, 1989, **1989**, 787-813.

(74) Lauterborn, W. and Hentschel, W., *Ultrasonics*, 1985, **23**, 260-268.

(75) Sehgal, C., Steer, R.P., Sutherland, R.G. and Verralla, R.E., *J. Chern. Phys.*, 1978, **70**, 2242-2248.

(76) Hostetter, A.A., Chapman, E.G. and DeRose, V.J., *J. Am. Chem. Soc.*, 2009, **131**, 9250-9257.

(77) Foldvari, M. and Bagonluri, M., *Nanomed. Nanotechnol.*, 2008, **4**, 173-182.

(78) Ham, H.T., Choi, Y.S. and Chung, I.J., *J. Colloid Interf. Sci.*, 2005, **286**, 216-223.

(79) Santos, H.M., Lodeiro, C. and Capelo-Martinez, J. in *Ultrasound in Chemistry*, 1st ed., Capelo-Martinez, J.-L. (Ed). Wiley-VCH, Darmstadt, 2008, p 171

(80) Nadler, M., Mahrholz, T., Riedel, U., Schilde, C. and Kwade, A., *Carbon*, 2008, **46**, 1384-1392.

(81) *The British Pharmacopoeia*, Vol. 2, The Stationary Office, London, 2001.

(82) Berners-Price, S.J., Ronconi, L. and Sadler, P.J., *Prog. Nuc. Mag. Res. Spec.*, 2006, **49**, 65-98.

(83) http://www.thermo.com/eThermo/CMA/PDFs/Articles/articlesFile_18407.pdf, *accessed 5th May 2012.*

(84) Dabrowiak, J.C., *Metals in Medicine*, 1st ed., John Wiley & Sons, Chichester, 2009.

(85) Kartalou, M. and Essigmann, J.M., *Mutat. Res.-Fund. Mol. M.*, 2001, **478**, 23-43.

(86) Kam, N.W.S., O'Connell, M., Wisdom, J.A. and Dai, H., *P. Natl. Acad. Sci. USA*, 2005, **102**, 11600-11605.

(87) Strano, M.S., Moore, V.C., Miller, M.K., Allen, M.J., Haroz, E.H., Kittrell, C., Hauge, R.H. and Smalley, R.E., *J. Nanosc. Nanotechnol.*, 2003, **3**, 81-86.

(88) Yan, A., Von Dem Bussche, A., Kane, A.B. and Hurt, R.H., *Carbon*, 2007, **45**, 2463-2470.

(89) Zhang, T., Tang, M., Kong, L., Li, H., Zhang, T., Zhang, S., Xue, Y. and Pu, Y., *J. Hazard. Mater.*, 2012, **219–220**, 203-212.

(90) Li, Y., Cousins, B.G., Ulijn, R.V. and Kinloch, I.A., *Langmuir*, 2009, **25**, 11760-11767.

(91) Hu, N., Dang, G., Zhou, H., Jing, J. and Chen, C., *Mater. Lett.*, 2007, **61**, 5285-5287.

(92) Shvedova A.A, K.E.R., Mercer R, Murray A.R. et al. , *Am. J. Physiol. Lung Cell Mol. Physiol.*, 2005, **289**, 698-708.

(93) Donaldson, K., Aitken, R., Tran, L., Stone, V., Duffin, R., Forrest, G. and Alexander, A., *Toxicol. Sci.*, 2006, **92**, 5-22.

(94) Cui, D., Tian, F., Ozkan, C.S., Wang, M. and Gao, H., *Toxicol. Lett.*, 2005, **155**, 73-85.

(95) Pulskamp, K., Diabate, S. and Krug, H.F. , *Toxicol. Lett.*, 2007, **168**, 58-74.

(96) Ryman-Rasmussenm, J.P., Cesta, M.F., Brody, A.R., Shipley-Phillips et al., *Nature Nanotech.*, 2009, **4**, 747-751.

(97) Lam, C.-W., James, J.T, McCluskey, R. and Hunter, R.L., *Toxicol. Sci.*, 2004, **77**, 126-134.

(98) Fischer, H.C.C., W.C.W., *Curr. Opin. Biotechnol.*, 2007, **18**, 565–571.

(99) Kolosnjaj-Tabi, J., Hartman, K.B., Boudjemaa, S., Ananta, J.S., Morgant, G., Szwarc, H., Wilson, L.J. and Moussa, F., *ACS Nano*, 2010, **4**, 1481-1492.

(100) Kayat, J., Gajbhiye, V., Tekade, R.K. and Jain, N.K., *Nanomed. Nanotechnol.*, 2011, **7**, 40-49.

(101) Wörle-Knirsch, J.M., Pulskamp, K. and Krug, H.F., *Nano Letters*, 2006, **6**, 1261-1268.

(102) Belyanskaya, L., Manser, P., Spohn, P., Bruinink, A. and Wick, P., *Carbon*, 2007, **45**, 2643-2648.

(103) Casey, A., Herzog, E., Lyng, F.M., Byrne, H.J., Chambers, G. and Davoren, M., *Toxicol. Lett.*, 2008, **179**, 78-84.

(104) Jabbal Gill, I., Fisher, A.N., Hinchcliffe, M., Whetstone, J., Farraj, N., De Ponti, R. and Illum, L., *European Journal of Pharmaceutical Sciences*, 1994, **1**, 237-248.

(105) Li, J., Yap, S.Q., Yoong, S.L., Nayak, T.R., Chandra, G.W., Ang, W.H., Panczyk, T., Ramaprabhu, S., Vashist, S.K., Sheu, F.-S., Tan, A. and Pastorin, G., *Carbon*, 2012, **50**, 1625-1634.

(106) Hilder, T.A. and Hill, J.M., *Curr. Appl. Phys.*, 2008, **8**, 258-261.

(107) Guven, A., Rusakova, I.A., Lewis, M.T. and Wilson, L.J., *Biomaterials*, 2012, **33**, 1455-1461.

3. CUCURBIT[*n*]URILS and the USE OF CB[6] AS A MODEL FOR CB[7]

3.1 CUCURBIT[*n*]URILS

Cucurbiturils (CB[*n*]s) are a family of barrel-shaped macrocycles which have received an increasing amount of attention in the literature as drug delivery vehicles, as they are able to alter solubility and/or increase stability of an encapsulated drug.[1-6] The potential applications of CB[*n*]s have led to comparisons with the cyclodextrin family.

3.1.1 Discovery and development

In 1905 Behrend and colleagues reported a product isolated from the acid catalysed condensation of glycoluril and excess formaldehyde.[7] The product could not be dissolved in any common laboratory solvents, with the exception of hot concentrated sulfuric acid. When the solution was diluted with cold water, filtered and subsequently boiled, they obtained a crystalline hydrate which was characterised as $C_{10}H_{11}N_7O_4.2H_2O$. Behrend's group offered no structure for this new compound, but noted its stability towards many potent reagents and its ability to form complexes with a wide range of metal salts and dyes including $KMnO_4$, $AgNO_3$, H_2PtCl_6, $NaAuCl_4$, Congo red and methylene blue.[7]

The research into this enigmatic compound was picked up over 70 years later by Freeman *et al.*[8] who carried out experiments to characterise the molecule's structure. Examining infrared absorption spectra, a peak at 1720 cm^{-1} suggested that the glycoluril carbonyl was retained in the product. ^1H NMR analysis produced a spectrum consisting of only three peaks, all aliphatic in nature. This was indicative of a highly-symmetrical non-aromatic structure.

The material was not volatile enough for mass spectroscopy to be carried out, and so MW could not be confirmed by this method. Also, X-ray crystallography could not be carried out on the compound, as suitable crystals could not be obtained. Instead, crystals of a calcium bisulfate complex, $(C_6H_6N_4O_2)_3.CaSO_4.H_2SO_4.(H_2O)_{6.5}$ were produced and the structure determined from these crystals. The compound of interest proved to be a cyclic hexamer of dimethanoglycoluril, consisting of nineteen rings held together with aminoacetal linkages (Figure 3.1).

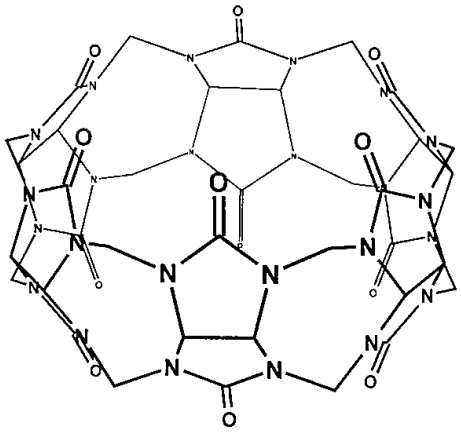

Figure 3.1. The structure of cucurbit[6]uril.[9]

Notably, at the centre of the structure lay a cavity with a diameter of 5.5 Å. This cavity could be accessed *via* two 4 Å diameter portals bordered by carbonyl groups. The trivial name **Cucurbituril** was chosen to reflect the similarity in shape to that of a pumpkin (family *Cucurbitaceae* order *cucurbitales*).[8]

Homologues of this molecule, containing fewer or greater dimethanoglycoluril monomers were not available until Kim *et al.*[10-12] and Day *et al.*[13,14] began their work on cucurbituril in the 1990s. Both teams discovered separately that by reducing the temperature at which the condensation was carried out (from >100 °C to 75-90 °C) they could obtain not just the original hexamer, cucurbit[6]uril (CB[6]), but also significant quantities of CB[5], CB[7], CB[8] and CB[10] (Figure 3.2).[15]

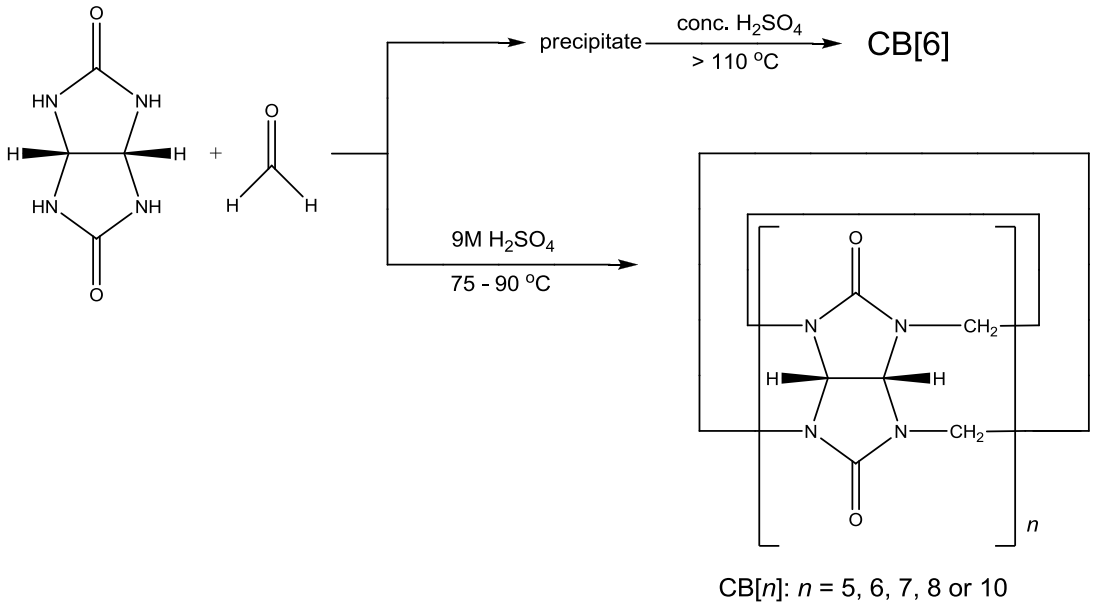

Figure 3.2. The synthesis of the CB[*n*]s, adapted from Kim *et al*.[15]

3.1.2 Structure and properties

The CB[*n*] homologues have the general formula $[C_6H_6N_4O_2]_n$ where n = 5, 6, 7, 8 or 10 (the structures of the 5, 6, 7 and 8 homologues are shown in Figure 3.3). They possess a hydrophobic cavity within which they are able to fully or partially encapsulate a drug molecule, driven by hydrophobic effect between the cavity and a hydrophobic moiety on the drug. The encapsulation can be further stabilised by electrostatic interactions between the carbonyl-lined portals and nearby hydrophilic groups on the drug.[1]

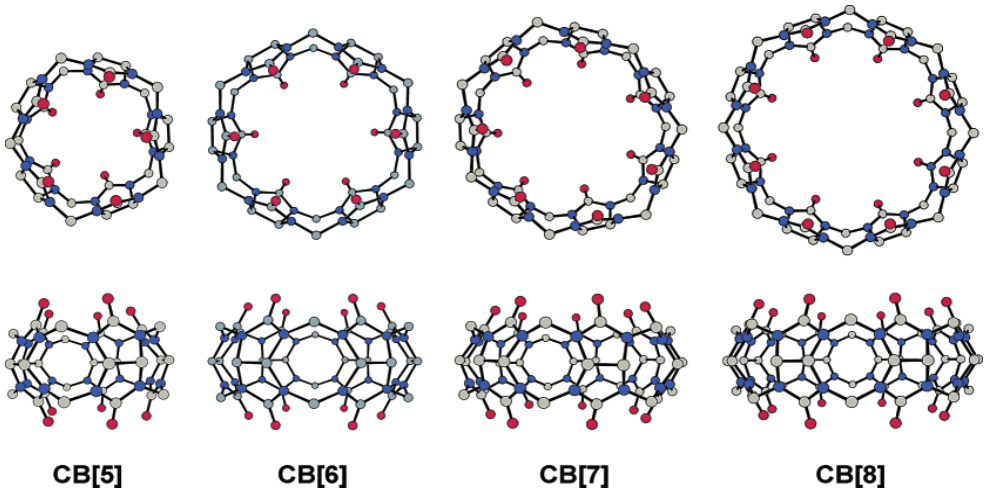

Figure 3.3. The structures of CB[5], CB[6], CB[7] and CB[8].[12]

All of the CB[*n*] homologues have the same height and a difference of ~2 Å between the cavity and portal diameters. This narrowing at the portals presents a significant steric obstacle to guest association and dissociation.[16] The size of the portals and the cavity increases with increasing homologue number (Figure 3.4 and Table 3.1).

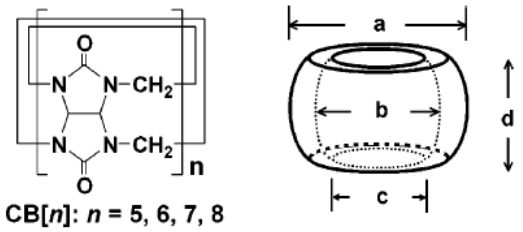

Figure 3.4. The general structure and shape of the CB[*n*] family.[12]

Table 3.1. The dimensions of the CB[*n*] family from Kim *et al.* and Day *et al.*[8,12,14,17]

		CB[5]	CB[6]	CB[7]	CB[8]	CB[10]
Outer diameter (Å)	a	13.1	14.4	16.0	17.5	-
Cavity diameter (Å)	b	4.4	5.8	7.3	8.5	10.7-12.6
Portal diameter (Å)	c	2.4	3.9	5.4	6.9	9.0-11.0
Height (Å)	d	9.1	9.1	9.1	9.1	9.1

The CB[*n*] family is associated with a high degree of stability, with CB[5]-[8] able to withstand temperatures exceeding 370 °C.[15,18] However, a major drawback of the CB[*n*] family is their relatively poor solubility in aqueous and organic solvents. CB[6] and CB[8] are only sparingly soluble in water. CB[5] and [7] are more

soluble, with aqueous solubilities of 20-30 mM. The carbonyl groups are essentially weak bases, with pK_a=3.02 (of the conjugate acid). As such, the solubility of CB[*n*] increases dramatically in concentrated aqueous acid.[19,20]

Since the discovery of the 5, 7, 8 and 10 homologues, interest in CB[*n*]s has increased. The ability to bind a guest molecule has led to the parent macrocycles, and their derivatives, receiving attention in a broad spectrum of applications as components of: molecular switches,[21] catalysts,[22,23] supramolecular assemblies,[24] biochips,[25] polymers,[26-28] water treatment systems,[29] and recently, as drug delivery vehicles.[1,4,30]

This range of applications has led to comparisons with another class of cavitand: the cyclodextrins.

3.1.3 Cucurbit[*n*]urils – the successors to cyclodextrins?

Cyclodextrins (CDs) are a class of macrocycle which have established commercial use as delivery vehicles for a number of organic drugs,[31-33] as well as application in the food and agricultural industries. The CDs are cyclic oligosaccharides composed of D-(+)-glucopyranose units linked by α-(1,4)-glucosidic bonds and form cone shaped macrocycles. The natural homologues: *α*-CD, *β*-CD and *γ*-CD consist of 6, 7 and 8 repeat units respectively (Figure 3.5).[32] Many of the pharmaceutical applications involve modified CDs, such as hydroxypropylated, methylated and branched modifications.[33]

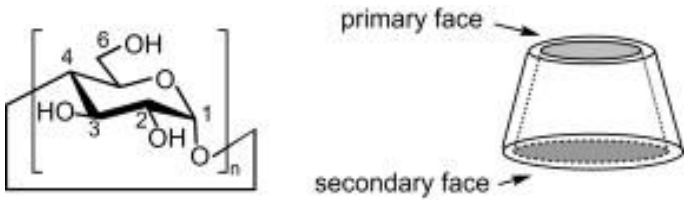

Figure 3.5. The structures of the cyclodextrin cavities, where *α*-CD *n*=6; *β*-CD *n*=7; and *γ*-CD *n*=8.[34]

Whilst cyclodextrin host-guest chemistry has been developing for the last century, the potential of CB[*n*]s has only been explored actively since the 1980s. Although arguably still in its infancy, the area is expanding rapidly and the advantages of this younger family over the CDs are being championed by researchers in the field.[35] Firstly, the cavity sizes available encompass and exceed the available cyclodextrins.[35] The CB[*n*]s all have outstanding thermal stability, exceeding 370 ºC, compared to 200 ºC with CDs.[36] In general, CB[6] has been found to bind guests with higher affinity than its cyclodextrin counterpart, α-CD.[35] The affinity of CB[*n*]s can be several orders of magnitude higher than their CD counterparts when the guest is cationic.[37]

Given these advantages, CB[*n*]s have the potential to compete with CD in the future. In particular, interest is growing in the field of drug delivery, where CB[*n*]s have been shown to alter the solubility and improve the stability of an incorporated drug.

3.2 IS CB[6] A COST EFFECTIVE MODEL FOR CB[7]?

For use as a drug delivery agent, the CB[7] homologue has received the most attention as a result of its superior aqueous solubility.[4] It has also been shown to form complexes with a range of organic and inorganic drug moieties.[2,3,38-40] The published procedures for isolating CB[7] from a mixture of homologues remain complicated and labour intensive[41] and although available commercially, CB[7] remains costly (£106.50 per 100 mg)[42] making it a precious commodity. In early formulation studies it is necessary to have a plentiful supply of the compound under investigation to allow for a variety of assays with a sufficient number of repeats for statistically valid results. It would therefore be useful to have a cheaper analogue as a model for CB[7], which could be used in early formulation studies.

First to be discovered and most widely investigated, the CB[6] homologue is simple to synthesise on the bulk scale.[43] In terms of recognition behaviour; the protonation, selectivity, and the mechanism of guest binding of CB[6] can likely be applied across

the entire CB[*n*] family.[35] This suggests that CB[6] could be a suitable model for CB[7].

Whilst chemical reactivity of CB[6] and CB[7] may be similar, CB[6] remains significantly less soluble in water than CB[7] (0.018 mM for CB[6], 20-30 mM for CB[7]).[15,44] As solubility is a controlling factor in dissolution, altering solubility can have a significant effect on bioavailability of a drug or drug complex. This means that whilst CB[6] may prove a useful model in some studies, its limitations may become apparent during, for example, moisture uptake, gelling and drug release studies.

It is noted that any formulations that are produced for comparison will have to undergo testing to examine drug homogeneity, robustness, gelling ability and bioadhesion.

3.3 POLYMORPHISM AND PSEUDOPOLYMORPHISM

3.3.1 The implications of polymorphism and pseudopolymorphism

Polymorphism is the ability of a compound to exist in multiple crystalline forms, with differing unit cells. Each unique crystal form is called a polymorph or crystalline modification.[45] Whilst different polymorphs of the same compound have identical molecular formulae, the molecules pack together in different three-dimensional configurations.[46] Pseudopolymorphs are hydrates and solvates of the same compound.[45] They are not true polymorphs, as they contain solvent molecules, so the chemical composition of the material is altered. Hydrates of drug can form and change readily by absorbing and desorbing atmospheric water.

Different polymorphs, solvates and hydrates will have different melting points, density, hardness, heat capacity, hygroscopicity, crystal morphology, optical

properties, electrical properties, crystal growth and solubility.[45] This can have massive implications for pharmaceutical applications, as solubility ultimately affects bioavailability *in vivo*. The emergence of various polymorphs of a compound can be further complicated by spontaneous transformations between forms. According to Ostwald's Rule, over time polymorphs will transform from the least stable form to the most stable form, under the influence of a thermodynamic drive.[47] Such transitions can occur during manufacture, transport and storage and are often accelerated by grinding, compaction, presence of solvents and changes in temperature. Unfortunately, as a compound transforms into a more stable crystalline form, the solubility of the compound will reduce. This was a significant issue for Abbot Laboratories in 1998 when a more stable, less soluble polymorph of their anti-human immunodeficiency virus (HIV) drug Ritonovir emerged after the drug was already on the market. This caused a reduction of the solubility and bioavailability of the drug, which had to be withdrawn and reformulated at a massive cost to the company.[48]

It is now common practice for drugs and excipients to undergo solid state screening to establish as many different polymorphs and pseudopolymorphs at the preformulation stage of the discovery pipeline. As well as establishing the most appropriate form to be carried through to testing and formulation at the earliest stage possible, intellectual property law has to be taken into account.

3.3.2 Solid state forms of CB[6]

The author has previously reported a reproducible method for producing micro-crystalline CB[6] by redissolving large CB[6] crystals in concentrated HCl and forcing rapid precipitation with the addition of water.[43] This method has produced particle sizes in the range 30-165 μm which are soluble in simulated gastric fluid to a concentration of 4.5-4.7 g/mL, with more consistent and rapid dissolution characteristics than their larger crystal counterparts.[43]

Although this gave a product with suitable particle size, it was unknown if it was a suitable polymorph or pseudopolymorph of CB[6] that was being produced, or even if it was a consistent solid form each time. Kemp *et al.* and Ripmeeister *et al.* have reported that each different sized cucurbituril, and their drug host-guest complexes, are associated with anywhere between 3-60 water molecules in the solid form.[49,50] This work suggested that formation of a specific hydrate may be influenced by acid type and concentration, crystal growth conditions and salt effects.

Given this apparent high potential for hydrate/pseudopolymorph formation, as well as the potential for any molecule to exist in multiple crystal forms, the most suitable form would have to be determined before commencing formulation investigations.

3.4 EVALUATION OF NASAL INSERTS USING NON-PHARMACEOPOEIAL METHODS

Lyophilised nasal inserts are dosage forms which have been investigated by a small number of research groups. There are currently no commercial drug products which utilise these dosage forms, and as such they are not yet governed by any standard pharmacopoeial tests. In spite of this, a number of tests have been reported in the literature which can be used to evaluate drug homogeneity, robustness, gelling ability, bioadhesion and drug release,

3.4.1 Rudimentary methods for comparing behaviour of inserts

Bertram and Bodmeier have reported methods for the testing of nasal insert formulations. For example, a method for examining moisture uptake whereby a pre-weighed insert is placed on a sponge soaked in absorption medium and weighed at regular time points.[51] The team have also reported a method adapted from Nakamura and colleagues for measuring bioadhesion using an agar and mucin plate.[52,53] Inserts

were placed on the agar surface and the plate positioned at an angle. During the experiment the linear displacement of the insert was recorded as a function of time.

As well as these rudimentary techniques, instruments which have been routinely applied in other fields have also been employed to examine nasal inserts. For example the texture analyser, an instrument developed for the food industry, has found application characterising the physicochemical properties of pharmaceutical formulations.

3.4.2 Evaluating Robustness – texture analysis

The final insert formulation must be hard enough to withstand patient handling.[52] The sponge-like form of the insert is vital for *in situ* gelling and drug release,[52] and therefore the dimensions must be recovered rapidly following any compression experienced during removal from packaging and insertion in the nose. Inserts with hardness equal to or exceeding 2 N have been found to be handled easily and without damage.[52] As mentioned previously, the texture analyser (Figure 3.6) has been used extensively in industry to characterise the textural properties of various foodstuffs and in the mechanical analysis of adhesives. The instrument finds routine application in the analysis of the mechanical characteristics of pharmaceutical formulations, including polymer swelling,[54] tablet disintegration,[55] formulation hardness[56] and adhesion on agar.[57] The texture analyser can also be used to examine mucoadhesion with excised animal tissue.[58]

Figure 3.6. The texture analyser TA XT2.[59]

3.4.3 Rheology and micro-rheology

Rheology is the study of how a material deforms and flows (from the Greek *rheos*, to flow).[60] The science considers a material's elasticity (ability to regain shape after a deformation) and its viscosity (ability to resist flow). In the pharmaceutical industry, these parameters are important in quality control, and affect the design, manufacture, transport, use and storage of liquid or semisolid formulations. Examining the rheological properties of a formulation can help understand the nature of the system under study and how it can be optimised.

Additionally, rheology can be used to study the mucoadhesive behaviour of a polymer. Although different theories of mucoadhesion exist, it is widely accepted that physical entanglement and electrostatic interactions between polymer chains and mucin are likely to produce changes in the rheological behaviour of the two species.[61]

Traditional bulk rheology, carried out on a macroscopic scale, requires sample volumes $\geq$ 1 mL. This can be difficult if the sample being studied is particularly expensive or scarce. The development of nano- and micro-technology has driven the development of techniques to study physical phenomena on the very small scale. Coupled with the increased availability of sophisticated equipment at relatively low

prices, this has led to the development of new techniques, including micro- and nano-rheology. A micro-rheological technique, such as laser-field oscillation (optical tweezers), employs the same principles as bulk rheology, but requires only a very small sample size (~ 10 µL). With optical tweezers, a micron-sized particle is trapped in a strongly focused beam of light. The motion of the bead within the beam is tracked, and its trajectory directly related to the viscoelastic properties of the surrounding fluid.[60]

3.5 AIMS

Although CB[7] is probably the most useful homologue for drug delivery applications, it is complicated to isolate and expensive to purchase. For early formulation studies, it would be useful to have a cheaper analogue as a model compound which could be used in its place. It has been suggested that lessons learned from experiments with CB[6] can be applied to the other CB[*n*] homologues. Although this may be true in terms of chemical reactivity, it may not hold true for formulation development as an important difference between CB[6] and CB[7] is their solubility in aqueous media. Solubility directly influences dissolution and bioavailability, therefore this solubility difference may make CB[6] an unsuitable model for CB[7] in pharmaceutical applications. Cucurbit[6]uril can be produced on the gram scale in the laboratory[43] and tested against commercially available CB[7].

In order to determine if CB[6] is a potential model for CB[7], aims of this work are to:

- synthesise CB[6];
- recrystallise CB[6] from a number of solvent systems/conditions before selecting the most favourable solid form to proceed with;
- formulate CB[6] and CB[7] into nasal insert dosage forms with HPMC;
- examine these formulations for moisture uptake, spreadability, hardness, and mucoadhesive potential; and determine whether or not inclusion of CB[6] in the formulation has the same effect on these properties as inclusion of CB[7];
- examine the hydrated gels with optical trapping techniques, in order to assess if CB[6] and CB[7] affect the rheological properties of the gels in the same way.

3.6 MATERIALS AND METHODS

3.6.1 Materials

Paraformaldehyde, glycoluril, hydrochloric acid, acetone, sulfuric acid, 1,4-dioxane (99%), Isoquinoline (97%) and 1,6-dibromohexane and CB[7] were obtained from Sigma-Aldrich. Additional CB[7] was obtained from Anthony Day (University of New South Wales, Australia). **It should be noted that, due to economic constraints, supply of CB[7] was limited.** All water was obtained from a MilliQ water purification system or distilled in house. 0.22 μm nylon filter paper and Grade 1 45 mm diameter filter paper were obtained from Whatman. Hydroxypropyl methylcellulose was obtained from Colorcon Ltd (Kent, UK). Ultrapure agar granules were obtained from Merck Microbiology (Merck KGaA, Darmstadt, Germany). Cyanoacrylate gel used was Bostik Superglue gel (Bostik Ltd, UK).

3.6.2 Instruments

Powder X-ray diffraction: ~50 mg of sample was placed in the well of a 28-well plate supported by kapton film (7.5 μm thickness). Data were collected on a Bruker AXS D8Advance transmission diffractometer equipped with θ/θ geometry, primary monochromatic radiation (Cu Kα1, λ= 1.54056Å), a Braun 1D position sensitive detector (PSD) and an automated multi-position *x*-*y* sample stage. Data were collected from 4-35° 2θ with a 0.015° 2θ step size and 1 s step-1 count time. Structure solution was carried out using Dash v3.2.

Infrared spectroscopy: Infrared spectra were recorded on a Thermoscientific, Nicolet iS10 smart iTR, ATR-FTIR spectrometer in the range of 550-4000 cm^{-1}.

Thermogravimetric analysis (TGA): TGA was carried out under a nitrogen atmosphere in a Mettler Toledo TGA/STDA851e, operating with a TS0801 RO Sample Robot (Mettler-Toledo, Leicester, UK). Samples of 2-6 mg were compacted in ceramic pans. Change in mass with temperature was examined by heating linearly

from 25-200 ºC at a rate of 2 ºC per minute. Data analysis was performed on Mettler STARe software.

Texture analysis (TA): TA was carried out on TA XT2 (Stable Microsystems, Godalming, UK) used with a 5 kg load cell. Data gathered were analysed using Texture Exponent software (Stable Microsystems, Godalming, UK). For measuring hardness and springiness, the instrument was used in compression mode with a 20 mm cylindrical aluminium probe. Disc formulations were evaluated using the following parameters: 1 mm/s pre-test speed, 1 mm/s test speed, 10 mm/s post-test speed, 20% strain target mode, 20 s hold time, 0.04903 N trigger force.

For instrumental specifications relating to UV-vis spectroscopy, elemental analysis and ^{1}H NMR, see section 2.4.2.

3.6.3 Methods

Synthesis of CB[6]: Micro-crystalline CB[6] was prepared as per the method published by the author in *Molecular Pharmaceutics*.[43] 10-100 g of glycoluril was stirred with 4.4-44 g of paraformaldehyde (1:2 mole ratio) in 18 M H_2SO_4 (55 mL per 10 g glycoluril) at ~70 ºC overnight, producing cream to brown coloured solutions with large amounts of off-white precipitate. The reaction was cooled to room temperature before MeOH was added (~300 mL per 55 mL H_2SO_4). The ensuing reaction was exothermic, accompanied by violent effervescence. The resulting precipitate was then collected by vacuum filtration and washed with copious amounts of warm water. The crude CB[6] was dried under vacuum and dissolved in concentrated HCl. The solution was left uncovered in the fume hood to allow crystallisation of pure CB[6] after a period of days or weeks. The crystals were then collected from the mother liquors and washed with HCl:H_2O (1:1 v/v), before being rinsed with water. To produce micro-crystalline CB[6] the crude crystals were dissolved in a minimum volume of concentrated HCl at room temperature, and water was added to precipitate micro-crystalline product. The product was collected by vacuum filtration over nylon filter paper (0.22 µm) and

washed with copious amounts of water. Each batch was dried in an oven at 110 ºC for several hours then passed through a 500 µm sieve.

Re-crystallisations: CB[6] was recrystallised from a number of solvent systems and conditions, as outlined in Table 3.2, below.

Table 3.2. Conditions used for re-crystallising CB[6].

Sample	Solvent	Antisolvent	Crystallisation Conditions	Drying Conditions
1	HCl 37% *	$H_2O^{\dagger}$	Ambient	Ambient
2	HCl 37% *	$H_2O^{\dagger}$	Ambient	110 ºC
3	HCl 37% *	$H_2O^{\dagger}$	-4 ºC	Ambient
4	HCl 37% *	$H_2O^{\dagger}$	-4 ºC	110 ºC
5	HCl 37% *	-	Ambient	Rotary evaporated then ambient
6	HCl 37% *	-	Ambient	Rotary evaporated then 110 ºC
7	HCl 37%‡	H_2O	Ambient	Rotary evaporated then ambient
8	HCl 37%‡	H_2O	Ambient	Rotary evaporated then 110 ºC
9	HCl 37% *	$MeOH^{\dagger}$	Ambient	Ambient
10	HCl 37% *	$MeOH^{\dagger}$	Ambient	110 ºC
11	HCl 37% *	$Acetone^{\dagger}$	-4 ºC	ambient
12	HCl 37% *	$Acetone^{\dagger}$	-4 ºC	110 ºC
13	H_2SO_4 *	H_2O	Ambient	Ambient
14	H_2SO_4 *	H_2O	Ambient	110 ºC
15	HNO_3 *	H_2O	Ambient	Rotary evaporated then ambient
16	HNO_3 *	H_2O	Ambient	Rotary evaporated then 110 ºC
17	Examined without further processing			

* as a minimum volume; † as an excess; ‡ 1:1 ratio

Solubility: Solubility in NaCl solution was assessed by adding 10 µL aliquots of 0.15 M NaCl solution to an accurately weighed sample of CB[6], sonicating for 2 min, and repeating until fully dissolved.

Preparation and pipetting of gels: Hydroxypropyl methylcellulose gels were prepared by stirring 1%-4% (w/w) K4MP polymer powder into water or NaCl solution. One third of the liquid volume was added at 80 ºC and stirred until homogeneous. The remaining liquid was added at room temperature and the gel

stirred for ~20 min before incubation overnight at 4 ºC to allow removal of air bubbles created by stirring. After this time, 300 µL of gel was pipetted into 0.2 mL polythene micro-centrifuge tubes and/or bespoke disc moulds. For the centrifuge tubes, a hypodermic needle was used to pierce a small hole in the bottom to allow the air within the tube to escape as the gel entered. In all cases, Gilson piston-type pipette tips were used due to the high viscosity of the polymer gels. Disc formulations were prepared for assays where the irregular shape of the insert would introduce excessive error when comparing formulations. In these instances, a more regular shape with two flat surfaces allowed for easy and reproducible positioning of the formulation on surfaces.

It should be noted that percentage weights expressed in this thesis pertain to the gel before lyophilisation. For example, 1% (w/w) means 1% (w/w) of gel before lyophilisation, not 1% (w/w) of the final lyophilised disc or insert.

Lyophilisation: Lyophilisation of nasal inserts and discs was carried out on a Christ Epsilon 1 6D freeze dryer. The freeze drying programme is described in Table 3.3, below. After lyophilisation, all inserts and discs were stored in a desiccator until needed.

Table 3.3. Freeze drying method, "Method 1" for Christ freeze dryer.

Method 1					
	Step	**Time (hours)**	**Shelf temp (ºC)**	**Vacuum (mbar)**	**Safety Pressure (mbar)**
1	Load		+ 20	-	-
2	Freeze	01:00	- 30	-	-
3	Freeze	01:00	- 40	-	-
4	Freeze	01:00	- 50	-	-
5	Freeze	02:00	- 60	-	-
6	Main Dry	10:00	+ 10	0.16	1.65
7	Main Dry	10:00	+ 15	0.055	1.65
8	Main Dry	04:00	+ 20	0.055	1.65
9	Final Dry	00:10	+ 25	0.011	1.65

Scanning electron microscopy (SEM): To analyse morphology of the samples scanning electron microscope was employed. Samples were cut in vertical and horizontal directions and mounted on aluminium stabs to observed uniformity of the structure. Samples were then gold coated using spatter coater; in addition a thin stripe of silver paint was applied from the surface of the sample to the stab to prevent accumulation of the charge which typically occurs for porous structures. Samples were viewed in scanning electron microscope (Ultra Zeiss SEM) at 5 kV. Due to high porosity of some of the samples charging effects were observed and a charge compensator was used. Several images with different magnifications were collected for each sample.

Dynamic adhesion study on agar/mucin: 6 g of ultrapure agar was heated to boiling in 200mL PBS (until it went clear) and then allowed to cool to 30-40 ºC. Meanwhile, 4 g of porcine stomach mucin was dispersed with stirring in 100 mL PBS at 30-40 ºC. This was then stirred into the warm agar and the solution made up to 400 mL. This solution of 1.5% agar 1% mucin (w/v) was poured into a 25 cm x 25 cm plate and allowed to cool. Plates were sealed with cling film and incubated at 4 ºC overnight. Before use, the plates were allowed to equilibrate to room temperature for ~30 min. Discs of lyophilised formulations were pressed gently onto the agar/mucin surface. The plate was then sealed with clingfilm to prevent drying and placed at 80 º to the horizontal. The distance the discs/gel front travelled was recorded as a function of time.

Moisture uptake: A rudimentary method for moisture uptake was adapted from Bertram and Bodmeier.[51] Household sponge (Santex Household Sponge, Santex GmbH, Wald-Michelbach, Germany) was cut to fit the wells of a six-well culture plate. The sponge was soaked in the uptake medium overnight and an excess of medium added to the wells to ensure the sponge remained saturated. Sponges were soaked in the uptake buffer and placed in a six-well plate with an excess of uptake medium to ensure that the sponges would remain saturated (Figure 3.7). 0.22 µm nylon filter paper (25 mm diameter, Whatman) was placed on top of the sponges and allowed to equilibrate for 30 min at room temperature. The saturated filter papers

were then weighed. Accurately weighed inserts were placed on top of the filter paper and moisture uptake was recorded as the weight of the insert (total weight of insert and filter paper minus weight of wet paper) recorded as a percentage of dry insert weight with time.

Figure 3.7. The set up for a moisture uptake experiment using sponges saturated in the absorption media and the inserts placed on a nylon membrane.

***Ex vivo* mucoadhesion:** Porcine heads were obtained from Ramsay's of Carluke on the morning of the assay. The heads were pre-halved, allowing for easy access to the conchae (the rolls of cartilage covered in thin respiratory mucosa, which create turbinates for inspired air, Figure 3.8).

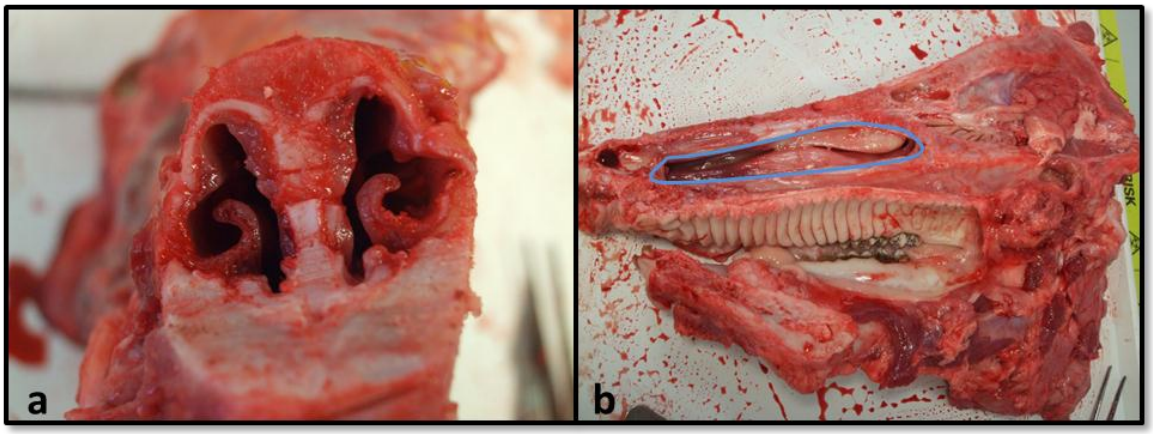

Figure 3.8. Photographs of porcine heads showing a) front on view with the snout removed. Conchae are visible at each side of the septum, these form the turbinates which inspired air passes through; and b) cross-section of the head. The blue outline shows the nasal cavity, the location of the conchae.

The superior conchae were carefully excised with a scalpel and used immediately. Once excised, the rolls of cartilage were carefully unfolded and the tissue prised off using tweezers (Figure 3.9). The section of tissue was then mounted, mucosal side up, into the TA mucoadhesion rig (Stable Microsystems, Godalming, UK, Figure 3.10). The disc formulation under investigation was attached to a 10 mm cylindrical delrin probe (Stable Microsystems, Godalming, UK) using double-sided tape and lowered onto the surface of the tissue (Figure 3.10). It was held in place with a force of 0.02 N for 60 sec before being pulled off at a rate of 10 mm/s. The parameters for the test were chosen after consulting the work of Wong,[58] Martin[62] and Khutoryanskaya.[63] Wong *et al.* found that increasing the contact time and the speed of removing the probe gave more consistent results. The paper also recommended that both peak force of detachment and the work of adhesion should be reported.[58] Khutoryanskaya *et al*. found that a higher contact force of 0.1 N gave inconsistent results and breaking during the removal of the probe[63] and Martin *et al.* used a lower contact force of 0.02 N, 60 s contact time and raised the probe 15 mm post-test.[62] In light of this data, these conditions were adopted: the TA was used in adhesive test mode with the following parameters: 1 mm/s pre-test speed, 0.5 mm/s test speed, 10 mm/s post-test speed, 0.02 N applied force, 15 mm return distance, 60 s contact time, 0.05 N trigger force. Data was analysed using a macro (Table 3.4).

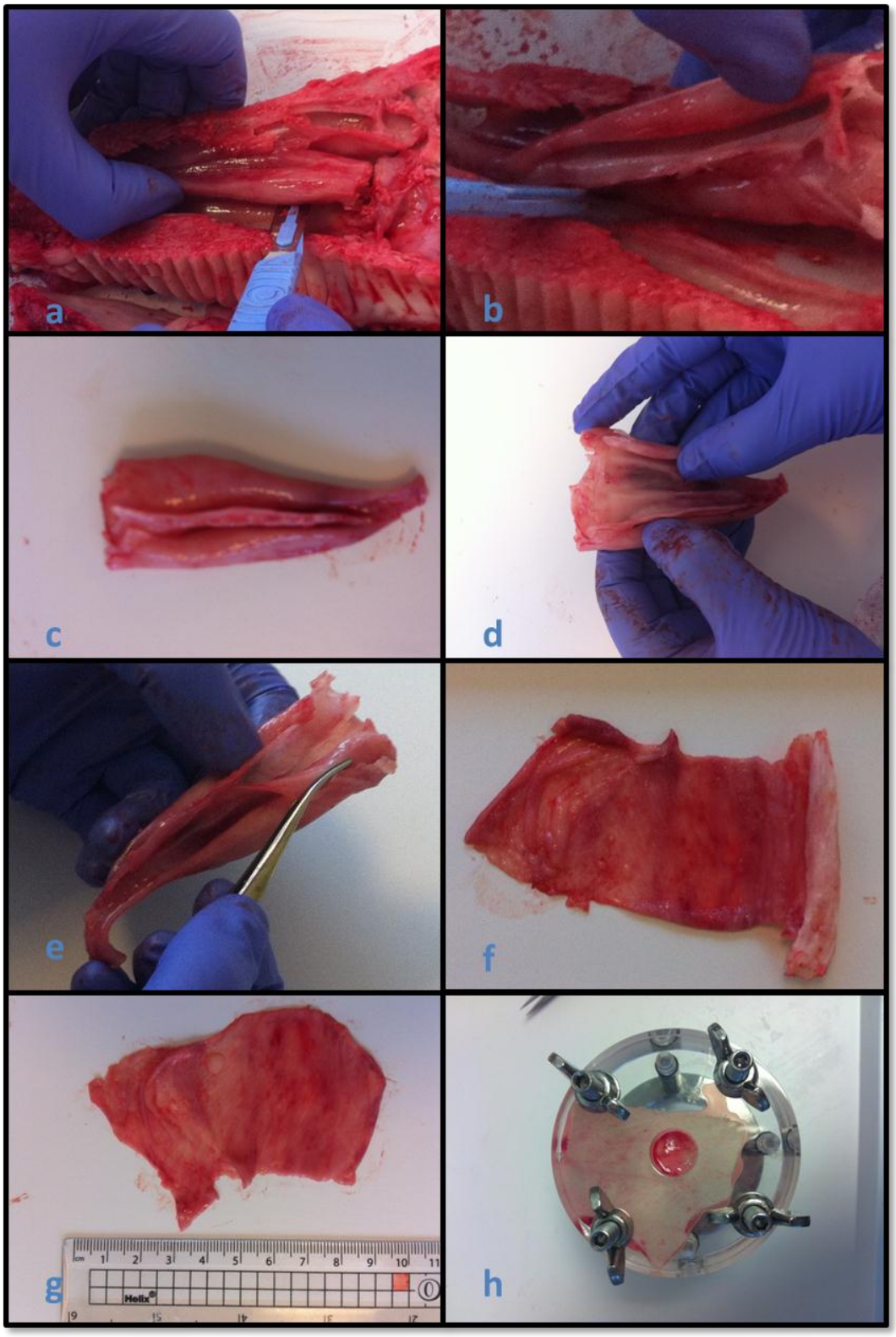

Figure 3.9. Photographs showing the extraction of mucosa: a) and b) incisions are made where the conchae meet the cavity wall; c) the conchae are removed in one piece; d) the cartilage is unrolled; e) the mucosa is peeled off the cartilage; f) a section of partially removed tissue; g) a piece of mucosa with all of the cartilage removed; and h) a piece of mucosa mounted in the mucoadhesive rig, awaiting adhesion study.

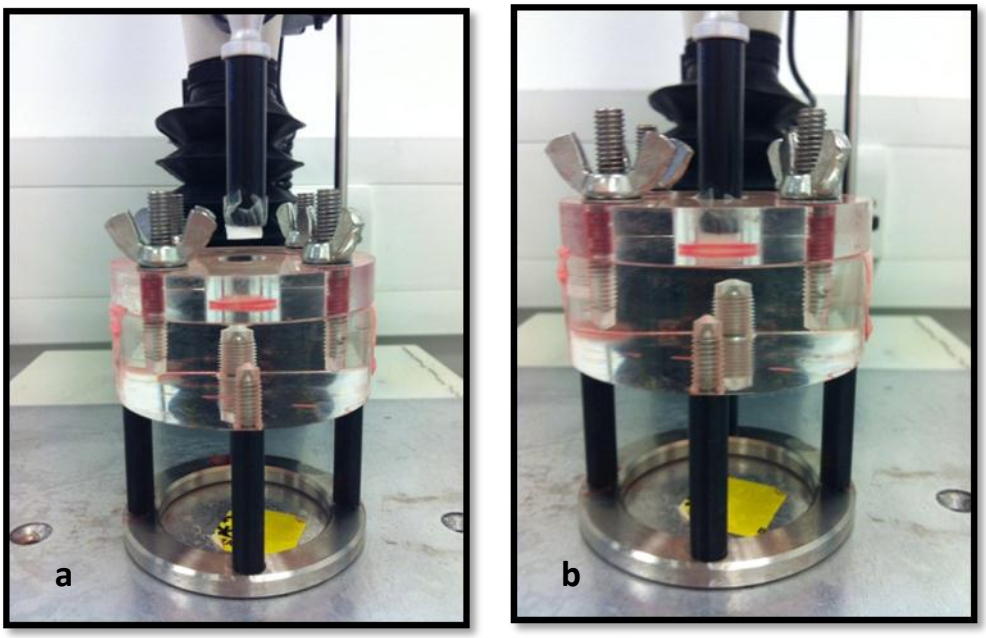

Figure 3.10. Photographs showing a) the disc lyophilisate attached to the probe pre-test; and b) the probe lowered until the disc touches the mucosa.

Table 3.4. The 60 s mucoadhesion macro used for analysing *ex vivo* mucoadhesion data.

60 s Mucoadhesion Macro	
1	Clear Graph Results
2	Redraw
3	Go to . . (Time, 50 s)
4	Search Forwards
5	Go to . . (Force, 0 N)
6	Drop Anchor
7	Search Forwards
8	Go to . . (Force, 0 N)
9	Drop Anchor
10	Area (Active vs. Active)
11	Search Forwards
12	Go to Peak +ve value . . (Force)
13	Maxima . . Force

Micro-rheology: Micro-rheology was carried out using LaserQuantum laser (1064 nm, 3 W), Nikon TE2000U microscope with a Nikon Plan Fluor objective lens (magnification: 100x, N/A:1.3, Oil Immersion), Boulder NonLinear Systems Spacial Light Modulator (XY series P512-1064) and a Dalsa Genie HM640 camera. Control

software was written in LabView. 200 µL of polystyrene 3.0 µm microspheres (Polysciences Europe GmbH, Eppelheim, Germany) were diluted to 10 mL in distilled water. Polymer gel samples were prepared for analysis by adding 10 µL microsphere solution to 200 µL of sample and vortexing for 30 sec. Samples for synergy studies were prepared by adding enough mucin to obtain 0.5% (w/w) mucin 0.5% (w/w) HPMC gel solutions of varying CB[*n*] concentration. Microspheres were added before stirring for an hour and then incubating at 4 ºC overnight.

Statistical Analysis: The collected data were analysed using one-way Analysis of Variance (ANOVA) or paired *t*-test with Minitab v15 (Minitab Inc., Coventry, UK). Tukey's test was used to determine individual significance. A *P* value below 0.05 was considered significant. Release and uptake were compared using an f_2 similarity profile (Equation 1), calculated using Microsoft Excel 2010 (Microsoft Corporation, Washington, USA). An f_2 similarity factor ≥50 denoted equivalence.

$$f_2 = 50 \times \log\left[\frac{100}{\sqrt{1 + \frac{\sum_{t=1}^{t=n}[\bar{R}(t) - \bar{T}(t)]^2}{n}}}\right]$$

Equation 1. For calculating the f_2 similarity factors where *R(t)* is the percentage of reference drug at a time, *t*, after initiation of the study; *T(t)* is the percentage of the test drug at time *t*.

3.7 RESULTS AND DISCUSSION

3.7.1 Synthesis and recrystallisation of CB[6]

Cucurbit[6]uril was synthesised by heating paraformaldehyde and glycoluril in concentrated sulfuric acid. Large product crystals were obtained by slow crystallisation from concentrated HCl. These were then dissolved in concentrated HCl and precipitation of microcrystalline CB[6] was forced upon the addition of H_2O. The product was analysed by ^{1}H-NMR, and the resultant spectrum is shown in Figure 3.11. Peak '**a**' (δ 5.60, s) represents the methine proton of the glycoluril unit which does not couple to neighbouring protons. At first glance of the molecular structure, the two methano protons would appear to be equivalent. The ^{1}H NMR spectrum however shows two distinct doublets '**b**' and '**c**' (δ 5.70-5.74 ppm and δ 4.31-4.35 ppm respectively). The peak multiplicity arises from the geminal coupling between these two protons. The difference in chemical shift values suggests that the C-$\underline{H}_b$ bond lies in the plane of the carbonyl bond and experiences a greater magnetic deshielding effect, and therefore a greater chemical shift. The C-$\underline{H}_c$ bond extends outwards, away from the macrocycle and as such H_c does not experience the same magnetic deshielding as H_b, resulting in a lower chemical shift.

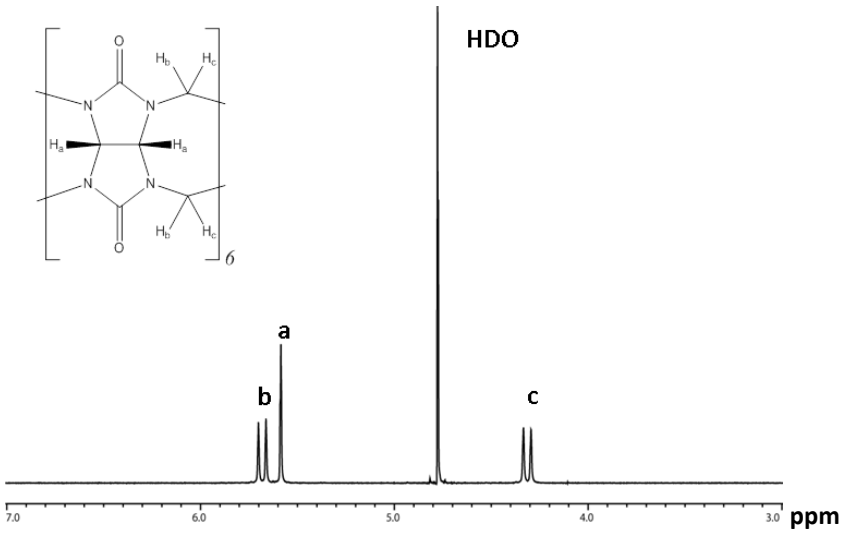

Figure 3.11. ^{1}H NMR spectrum of cucurbit[6]uril, obtained in D_2O with added NaCl.

The micro-crystalline CB[6] product was then recrystallised from a number of solvent and atmospheric conditions.

3.7.2 Examination of various forms of CB[6]

Kemp and colleagues suggested that the formation of specific CB[*n*] hydrates may be influenced by acid type and concentration, crystal growth conditions and salt effects.[49] By recrystallising CB[6] from a number of solvent and atmospheric conditions (*see section 3.6.3*), it was hoped that different crystalline forms could be produced. This would be useful as a way exploring the polymorphic potential of the homologue and obtaining the most useful solid form for development of the nasal insert formulations.

Powder X-ray diffraction data was then obtained for all of the samples. No unit cell parameters could be determined from the data, or subsequent single-crystal analysis. No unit cell data for pure CB[6] has been reported in the literature, suggesting that other researchers have been unable to elucidate this from X-ray crystallography. Samples 1, 2, 6, 7, 11, 16 and 17 were chosen for further analysis, as these produced the most dissimilar PXRD diffractograms (Figure 3.12). The solvent conditions used to obtain these samples are reviewed in Table 3.2. Samples 1, 2, 6 and 17 showed a higher degree of crystallinity than the others, evident by sharper peaks and a more defined baseline. These particular samples had all been either examined without further processing or recrystallised from aqueous HCl systems. This suggests that water and HCl may be incorporated into the crystal stoichiometrically, but the other solvents (*e.g.* HNO_3, acetone, H_2SO_4) are not. Samples 7, 11 and 16 were not chosen for further examination, as they showed a high degree of disorder and amorphous character. This may be due to non-stoichiometric quantities of solvent and/or the way in which the samples were dried.

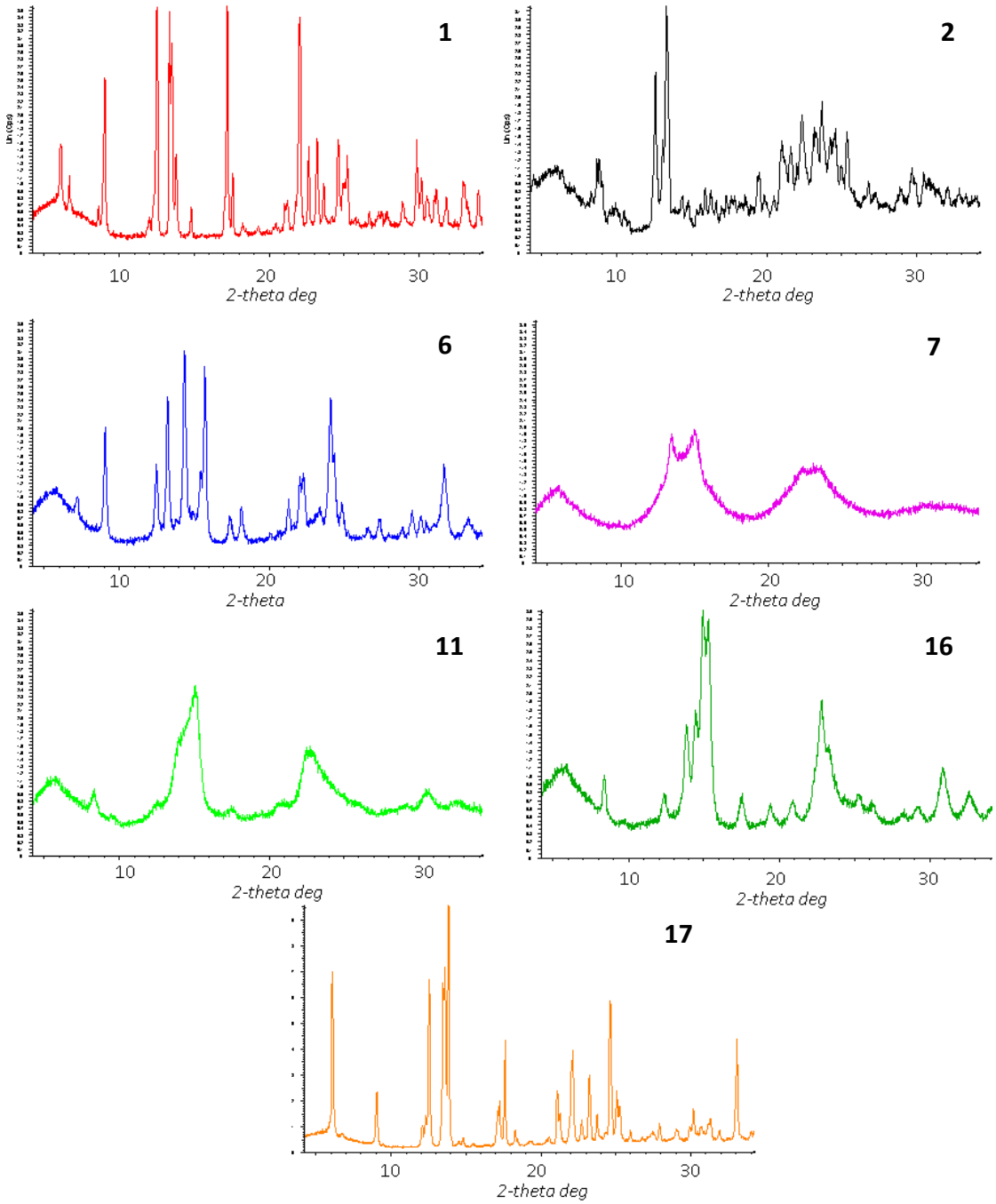

Figure 3.12. PXRD diffractograms for samples 1, 2, 6, 7, 11, 16 and 17, respectively.

Table 3.2. Recrystallisation conditions for samples chosen for further investigation following PXRD analysis. Those in bold were chosen for further investigation.

Sample	Solvent	Antisolvent	Crystallisation Conditions	Drying Conditions
1	**HCl 37% ***	**$H_2O^{\dagger}$**	**Ambient**	**Ambient**
2	**HCl 37% ***	**$H_2O^{\dagger}$**	**Ambient**	**100 ºC**
6	**HCl 37% ***	**-**	**Ambient**	**Rotary evaporated then 100 ºC**
7	HCl 37%‡	$H_2O^{\ddagger}$	Ambient	Rotary evaporated then ambient
11	HCl 37% *	Acetone†	-4 ºC	Ambient
16	HNO_3 *	H_2O	Ambient	Rotary evaporated then 100 ºC
17	**Examined without further processing**			

* as a minimum volume; † as an excess; ‡ 1:1 ratio

Thermogravimetric analysis of the samples showed that they lost varying amounts of weight upon heating (Figure 3.13 and Table 3.3). This suggests that the samples may indeed represent different hydrates and/or solvates, having incorporated varying amounts of solvent into the structure during processing. Although this was not carried out in duplicate, error due to exposure to ambient humidity was minimised by storing all of the samples in a desiccator prior to testing.

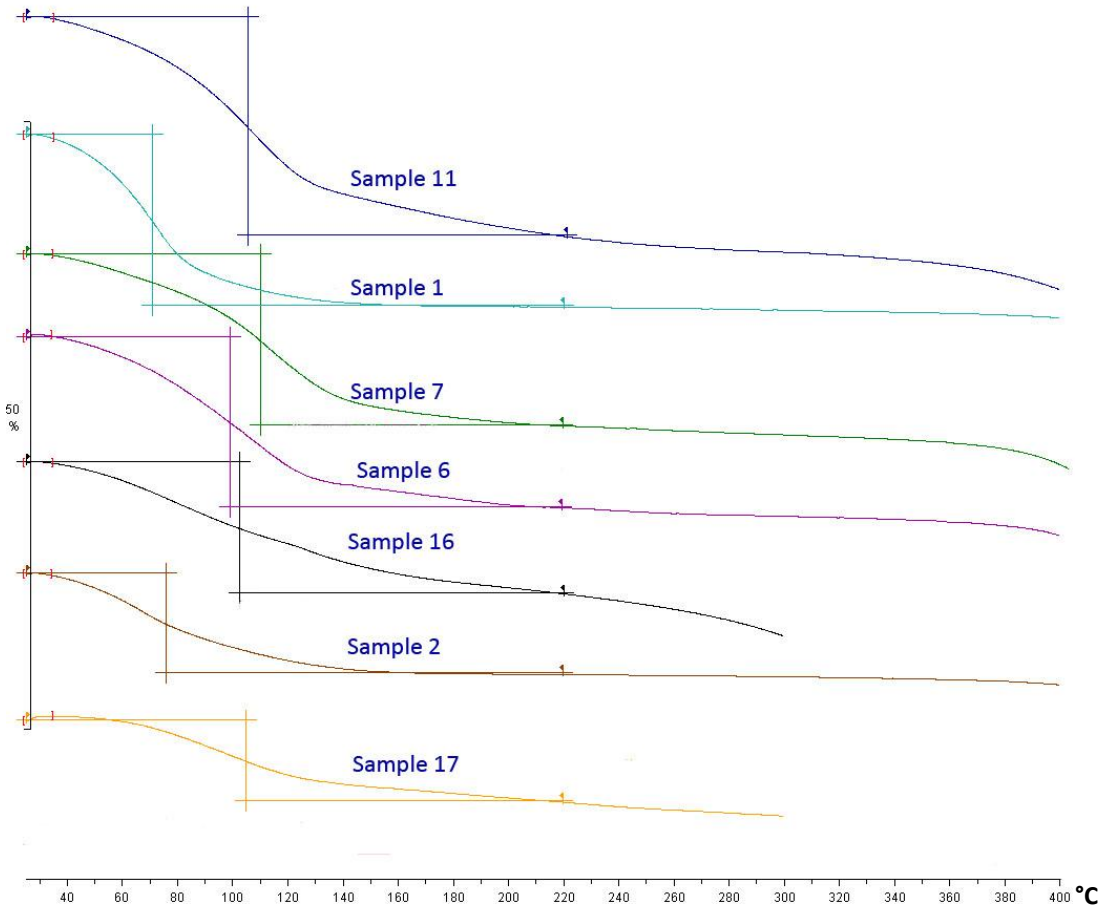

Figure 3.13. Thermogravimetric analysis results for samples 11, 1, 7, 6, 16, 2 and 17; stacked in order of % weight loss with sample 17 losing least weight between 0-220 °C.

Table 3.3. Weight loss upon heating from 0-220 °C

Sample	Weight loss (%)
11	18.01
1	14.14
7	14.06
6	14.00
16	10.79
2	8.27
17	6.67

Sample 17 was produced by the original method without further recrystallisation. Having the lost the least amount of weight upon heating, this would indicate it

contained the least amount of co-crystallised water and/or acid. As well as being more pure, this was an advantage as crystals containing less water tend to have a higher aqueous solubility. This is because a crystal containing stoichiometric amounts of water will have less of a thermodynamic gain forming new hydrogen bonds when dissolving. For these reasons, it was decided to proceed using the original method to produce CB[6], with no further recrystallisation.

Further investigation into the polymorphic potential of cucurbit[6]uril would be required before any industrial pharmaceutical application of the excipient. This would include determining the most suitable solid form (hydrate, solvate or polymorph) and would provide an insight into the solubility range which could exist with CB[6].

3.7.3 Determining the most favourable polymer grade to use

McInnes and colleagues demonstrated the use of HPMC to produce nasal inserts.[64] A number of different grades of HPMC are available commercially, and three were investigated as candidates for producing the lyophilised nasal inserts. To do this, discs of 1%, 2% and 3% (w/w) gels were prepared using three different grades of HPMC (K100LV, K15MP and K4MP), lyophilised using freeze dryer Method 1. The three polymer grades were chosen to represent a range of viscosities with K100 LV, K4MP and K15MP reported as 100; 4,000; and 15,000 mPa. s respectively when prepared at 2% in water at 20 °C.[65]

The hardness and springiness (Figure 3.14) of these discs was examined using the texture analyser. Disc formulations were used for the texture analysis experiments so that flat surfaces of a uniform size and shape were under investigation, allowing for more accurate comparison. The torpedo shape of the insert formulation would have resulted in inconsistencies related to sample positioning.

Statistical analysis of springiness of 1%, 2% and 3% K15MP were not significantly different from each other (*P*=0.857). This was also true of 1%, 2% and 3% K4MP (*P*=0.547). K100LV only showed significant difference (*P*=0.001) in springiness when going from 1% to 3%. This suggested that small changes in polymer concentration as a result of experimental error do not have a significant effect on the texture analysis results.

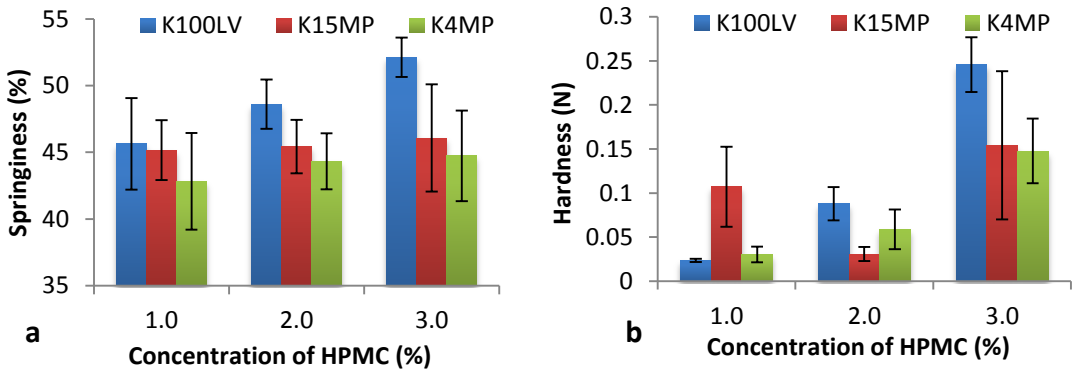

Figure 3.14. Textural analysis of HPMC discs of various grades and concentrations, showing a) springiness, and b) hardness (*n*=6).

The hardness of K100LV 1%, 2% and 3% discs were significantly different (*P*=0.000); 2% and 3% K15MP had significantly different hardness (*P*=0.005) although 1% did not differ significantly from 3%. For K4MP, the only significant difference in hardness was from 1% to 3%. This suggested that the hardness of an insert made of K4MP could be tuned using different concentrations of polymer, but that a small change in concentration (*e.g.* introduced by experimental error) would not result in significant alteration of insert hardness. This may be favourable as it would mean that experimental errors introduced by small changes in polymer concentration would be negligible.

McInnes[66] and colleagues previously reported the preparation and analysis of nasal inserts containing nicotine, prepared with 2% K4MP HPMC gel. Various 2% polymer formulations have also been used by Bertram and Bodmeier[51] to prepare *in situ* gelling nasal inserts. This prior art, coupled with a more consistent hardness and springiness profile and a lower susceptibility to changes in hardness with small

changes in concentration led to the decision to continue with a 2% (w/w) K4MP HPMC gel. Additionally, the 2% K4MP inserts were more easily removed from the centrifuge tube moulds and easier to handle without deformation.

Examination of lyophilised 1%, 2% and 3% inserts by SEM showed that pore size was not affected by concentration of polymer (Figure 3.15). McInnes however reported previously that the pore size obtained reduced with increasing HPMC concentration between 0.5-3% K4MP.[64] This suggests that there may be another contributing factor. During the lyophilisation process, the water in the gels is frozen and sublimation of the ice crystals creates the pores in the nasal insert. McInnes proposed that the higher concentration of HPMC forced the water into smaller ice crystals, producing smaller pores. Whilst this may still be in operation, the effect may be minimised in this case by the use of a newer freeze dryer with greater control over the freezing and sublimation process. The method used by McInnes also held the temperature steps for longer than the process used in this study, with the freezing stage taking 420 min *c.f.* 300 min in this case. Shortening time periods between stepwise reductions in temperatures in this study may have allowed greater consistency in the size of the ice crystals.

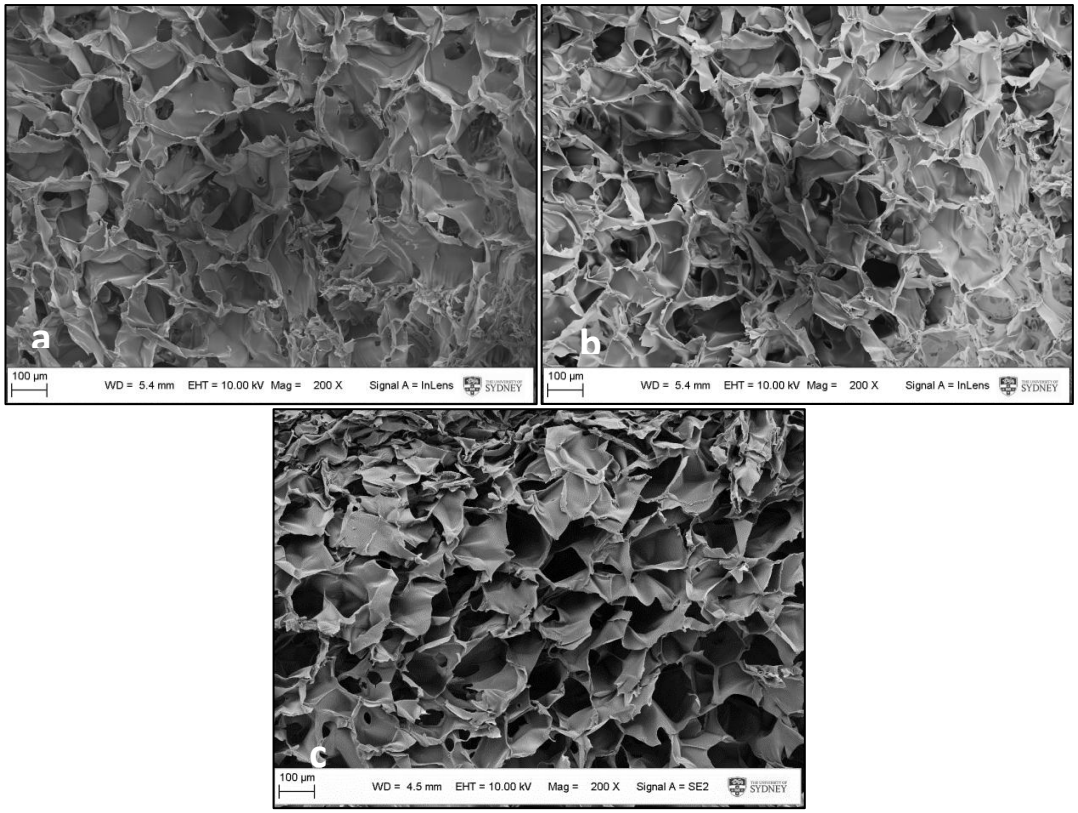

Figure 3.15. SEM micrographs of: a) 1%, b) 2% and C) 3% K4MP HPMC. At 200 × magnification, there is no apparent change in the pore size obtained.

Consequently, 2% (w/w) K4MP HPMC gels were used to make all of the inserts and discs used in subsequent work described in this thesis.

3.7.4 Preparation of lyophilised inserts and discs

In order to determine whether or not incorporation of CB[6] and CB[7] determined formulation characteristics in the same manner, inserts and discs of 2% (w/w) K4MP and 1%, 2%, 3% and 4% (w/w) CB[6] were prepared. For comparison, inserts and discs of 2% (w/w) K4MP and 1%, 2% and 3% CB[7] were also prepared. 4% CB[7] was not investigated, due to a limited supply of the homologue. Gels were prepared by dissolving the cucurbituril in 0.15 M NaCl solution (the concentration of NaCl used in SNES) at 80-90 ºC. The correct mass of polymer was then added, as a powder, to the hot solution and subjected to stirring until a homogenous gel was apparent. Cold NaCl solution was added to make the final concentrations and the gel was stirred for at least 20 min to ensure correct hydration of the polymer. NaCl

solution was used as the Na^+ ions were expected to help solubilise the CB[*n*]s, allowing homogeneous distribution in the gel for accurate dosing and consistent release.

After freeze drying, the dosage forms were examined for hardness and springiness, moisture uptake, spread on agar and *ex vivo* mucoadhesion.

3.7.5 CB[*n*]s and texture analysis

The lyophilised discs were analysed using the TA. For hardness, the CB[6] profile was non-linear, with hardness increasing from 1-2% CB[6] and then decreasing from 3% through to 4% CB[6] (Figure 3.16). Although this change is not statistically significant (P=0.259), this may suggest that increasing CB[6] content increases formulation hardness to a maximum (probably somewhere between 2-3% CB[6]) after which higher CB[6] concentration reduces formulation hardness (Figure 3.16). More data points between 2-3% would be required to find the maximum hardness achievable. Alternatively, the standard deviation associated with results for 1% and 2% could suggest that the true profile is in fact a constant decrease in hardness. Comparing this to the CB[7] profile, which increases from 1% to 2% and decreases from 2 to 3%, suggests that the former may be the case, and that increasing CB[*n*] content will increase the hardness of a formulation to a maximum, and increasing CB[*n*] content further will result in a decrease in hardness. This suggests that incorporating either CB[6] or CB[7] into a formulation of lyophilised K4MP increases its structural integrity up to a maximum concentration, upon which the structure becomes saturated and further CB[*n*] results in a decrease in structural integrity.

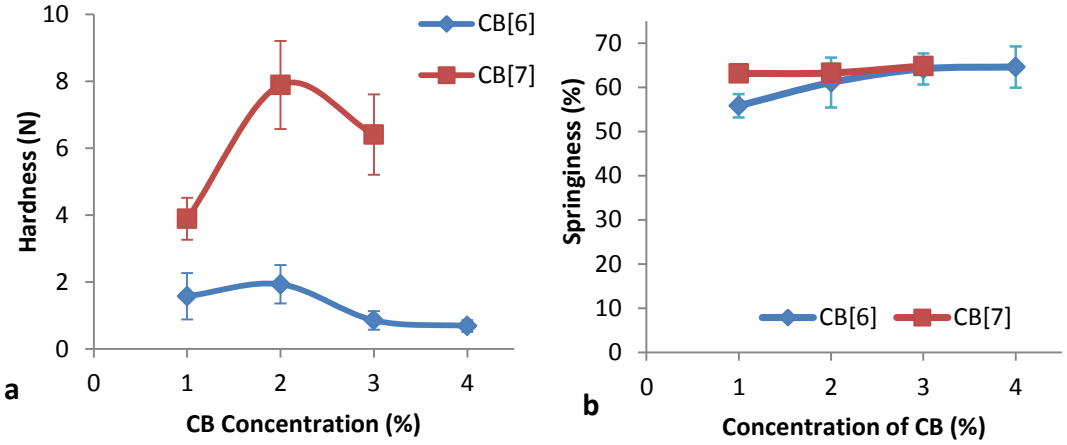

Figure 3.16. Graphs showing the a) hardness and b) springiness, of discs containing CB[6] and CB[7] (for CB[6] *n*=6, for CB[7] *n*=3). Discs containing CB[7] are significantly harder than those containing CB[6]. The springiness of discs containing 2% and 3% CB are similar. Error bars represent standard deviation.

This could be rationalised by considering the interaction of the CB[*n*] with the polymer. The carbonyl groups of the CB[*n*] are able to act as hydrogen bond acceptors to the donating groups on the polymer. In lower concentrations, they may act as points of pseudo-cross-linking, by holding H-donor groups of different polymer chains together (Figure 3.17) The research groups of Appel and Li have both recently reported the synthesis of a supramolecular gels in which CB[8] acts as a structural component.[67] In these cases, the CB[8] incorporates a moiety from two separate polymer chains into its cavity, acting as a "molecular handcuff", and a new non-covalent cross-linking device. A similar effect may be in operation, whereby the portals at either side of the CB[6]/CB[7] form non-covalent bonds with functional groups of different polymer chains, acting as a new point of cross-linking between polymer chains.

The maximum value of hardness might indicate saturation of available hydrogen bonding sites. Increasing the concentration of CB[*n*] beyond this point would mean the CB[*n*]s may only be able to hydrogen bond on one portal (Figure 3.17). Whilst this may prevent the CB[*n*] from acting as a cross-link, it may also provide steric hindrance, preventing hydrogen bonding and electrostatic interactions between

polymer chains themselves. Both of these effects would reduce the structural integrity of the system.

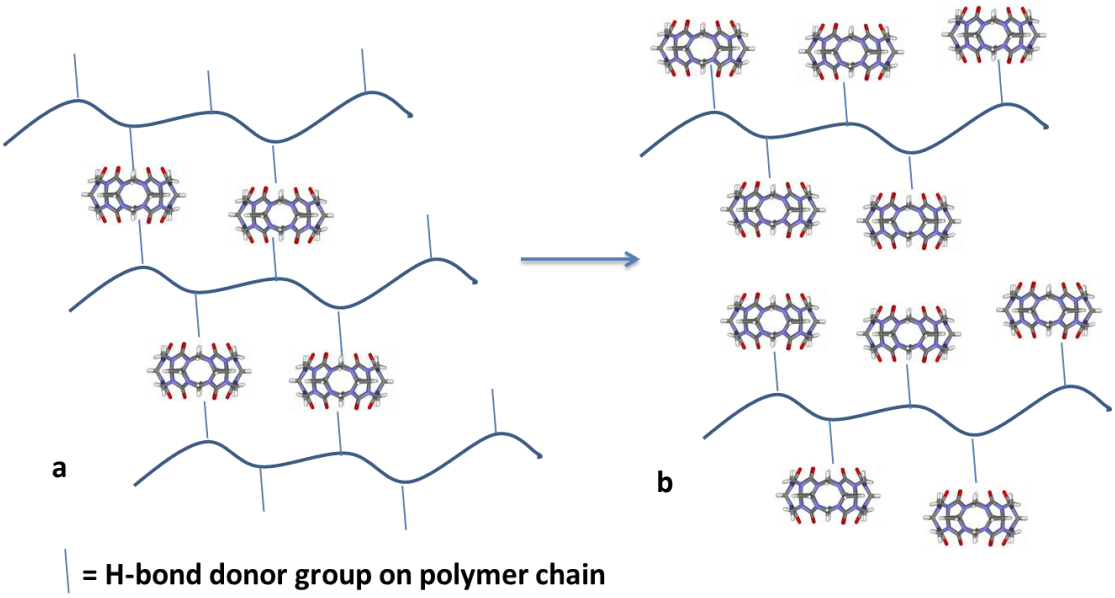

Figure 3.17. Diagram illustrating the effect of CB[*n*] on polymer structure: a) in lower concentrations, CB[*n*] may form hydrogen bonds with different chains, creating pseudo-cross-links; b) at higher concentrations, saturation of available H-donor groups on the polymer chain may not allow for pseudo-cross-linking in this way.

Although increasing CB[6] and CB[7] showed similar hardness profiles, the actual values were significantly different (P=0.00, paired t-test), with values for CB[7] being higher. This suggests that although CB[6] and CB[7] affect a formulation of lyophilised K4MP HPMC in the same way qualitatively, they do not have a quantitatively similar effect. This may be due to the two extra carbonyl groups on CB[7] *c.f.* CB[6] providing greater hydrogen bonding potential. Depending on the final formulation, this difference may be crucial. Bertram and Bodmeier suggested a minimum hardness of 2 N is required for patient handling.[52] Whilst discs containing 1-3% CB[6] did not reach this threshold, all of the 1-3% CB[7] could be considered robust enough.

The springiness of the formulations however, was more consistent between CB[6] and CB[7], with 2% and 3% formulations for each showing comparable springiness (Figure 3.16, P=0.594). This suggests that 2% or 3% CB[6] may be a suitable model

for 2% or 3% CB[7] in a lyophilised K4MP HPMC formulation when formulation springiness is a consideration. In this case, degree of hydrogen bonding may not affect springiness of the formulation. This property may only be influenced by the polymer, with the recoverability influenced by the elasticity of the polymer chains, independent of the CB[*n*] content.

Hardness and springiness are a measure of how an insert would resist and recover from mechanical deformation during handling and insertion. Once inserted, the inserts are designed to wick up water and hydrate to form a mucoadhesive gel.

3.7.6 CB[*n*]s and moisture uptake

A rudimentary method for moisture uptake was adapted from Bertram and Bodmeier.[51] Pre-weighed inserts were placed on filter paper on top of a sponge which was soaked in uptake medium. At each time point the percentage weight gain was recorded as the mass of the insert and filter paper minus the initial mass, divided by the mass of the dry insert (Equation 2).

$$\%\, weight\ gain_{t=x} = \left(\frac{(\, insert + filter)_{t=x} - (\, insert + filter)_{t=0}}{insert_{t=0}} \right) \times 100$$

Equation 2

Melia's group have reported that the presence of salts in a medium can affect the performance of an HPMC dosage form by altering their ability to gel.[68] Therefore, where Bertram and Bodmeier used PBS (pH 6) as the uptake buffer,[51] it was decided that simulated nasal electrolyte solution (SNES) may give more relevant results as it is more representative of the nasal environment.[69]

The assay was performed for inserts containing 1%-4% CB[6] using PBS (0.002 mg/mL NaCl, 0.04 µg/mL KCl, pH 7.4) and SNES (8.77 mg/mL NaCl, 2.98 mg/mL KCl, 0.59 mg/mL $CaCl_2.2H_2O$, adjusted to pH 5.5 with 1 M HCl). If the two media gave statistically different results, then SNES should be used as it is thought to be

more representative of the nasal environment. For all percentages of CB[6] content, the weight gain in PBS and SNES was similar (Figure 3.18). It was decided to use an f_2 similarity factor to determine whether or not the uptake was similar. The f_2 similarity factor was developed to determine bioequivalence in drug dissolution from an immediate release dosage form. It is a logarithmic reciprocal square root transformation of the sum of squared error[70] (*see section 3.3.6 Methods, Equation 1*), and is used by the FDA to measure the similarity in the percent of dissolution of two curves. Whilst the following data do not pertain to dissolution, and do not meet the strict requirements of the f_2, the similarity profile was used as the uptake profile was similar to a release profile and an alternative analysis was not available. Water uptake (percent) at the last timepoint was taken as 100%, and the previous data was taken as a percentage of this value.

F_2 similarity factors of **49.8** (1% CB[6]), **49.8** (2% CB[6]), **50.2** (3% CB[6]) and **50.2** (4% CB[6]) were calculated. A factor $\geq$ **50** denotes equivalence, and so rounding to the nearest significant figure, all moisture uptake in PBS is equivalent to that in SNES. It was therefore decided to move forward with PBS, as it gave similar results to SNES, but was readily available in a tablet preparation for dilution, which would be more convenient and reproducible.

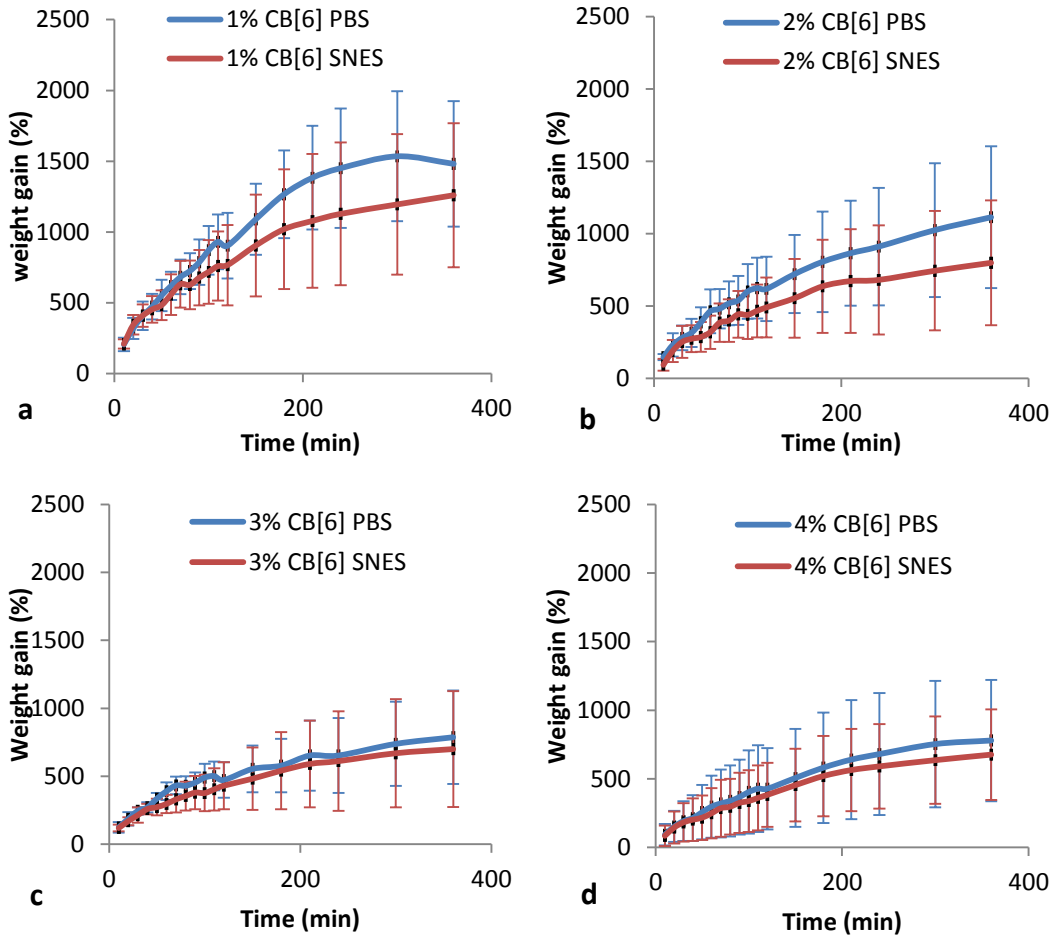

Figure 3.18. Graphs showing weight gain of inserts containing a) 1%,b) 2%, c) 3% and, d) 4% CB[6] in PBS and SNES. Error bars represent standard deviation (*n*=6).

After establishing that PBS should be used as the moisture uptake medium, the assay was repeated using inserts containing 1%-3% CB[7]. A similar trend was seen for both sets: increasing concentration of CB[*n*] acted to retard the uptake of water, observed as a reduction in weight gain (Figure 3.19). Whilst the formulations containing CB[7] took on more moisture than the inserts containing CB[6], this difference was not significant before 180 min (f_2 similarity values of 49.6, 49.5 and 49.5 for 1%, 2% and 3% CB[6] *c.f.* CB[7]).

This result suggests that in assays involving moisture uptake of lyophilised nasal inserts, increasing the amount of CB[6] in a formulation may be a suitable model for

CB[7], as both retard the uptake of moisture. This may occur because hydrogen bonds form between the CB[*n*]s and the hydroxyl groups on the HPMC, leaving fewer polar groups available for water uptake.

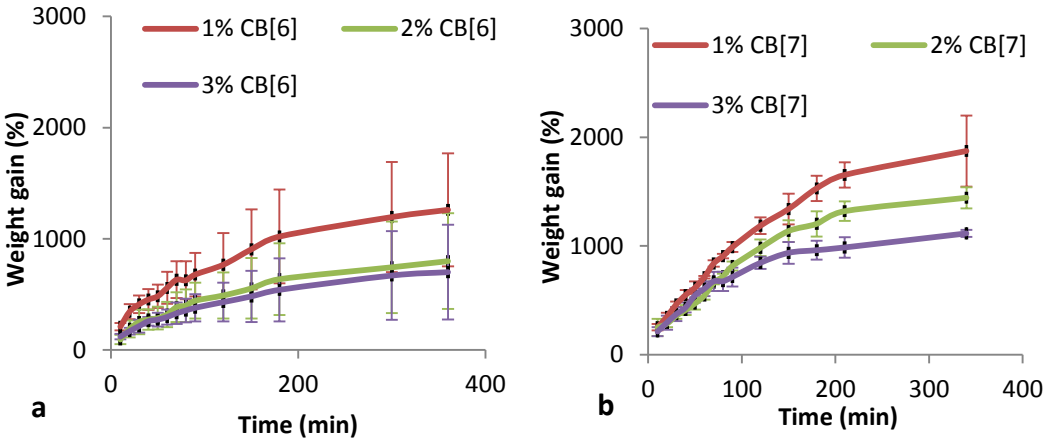

Figure 3.19. Graphs showing weight gain for 1%, 2% and 3% a) CB[6], and b) CB[7], in PBS. Error bars represent standard deviation (for CB[6], *n*=6; for CB[7], *n*=3).

Although increasing the concentration of CB[*n*] reduces the water uptake, the inserts appear to gel more rapidly (Figure 3.20). This can be observed as the inserts losing their opacity, indicating rehydration. The inserts containing 1% and 2% CB[7] only began to rehydrate at the extremities, but the 3% formulations appear to be more fully hydrated.

Figure 3.20. Photograph of a plate from the moisture uptake assay for inserts containing 1% (left), 2% (middle) and 3% CB[7], taken after 10 min. The formulations containing 3% CB[7] appears to be gelling more quickly than those containing 1% or 2%.

This increase in rate of hydration may be due to more rapid penetration of water through the insert. If the CB[*n*]s are acting as structural components of the matrix and increasing hardness, it is possible that this is also affecting the rate of water penetration. At 3% CB[7], the hardness of the formulation was reduced, potentially as a result of saturation of hydrogen bonding sites and a reduction in chain cross-linking and pseudo-cross-linking. Above this saturation point, extra CB[*n*] may crystallise in channels, as reported by Ripmeester's group (Figure 3.21).[50] If formed throughout the gel and present in the lyophilised insert, these water-filled channels may allow for more effective penetration of moisture through the insert and rapid formation of a viscous, mucoadhesive gel.

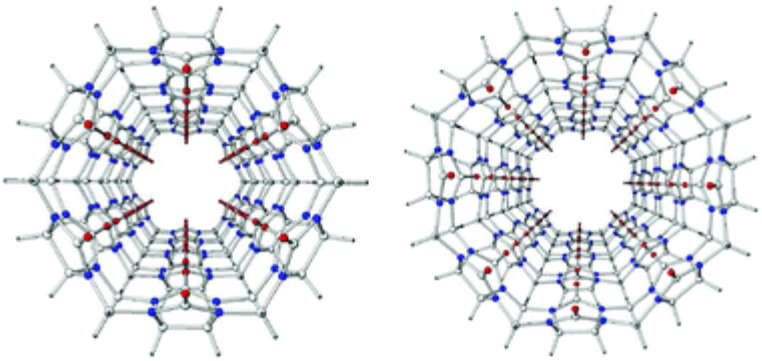

Figure 3.21. Nanotube-like architectures formed by CB[6] (left) and CB[8] (right), creating water channels.[50]

3.7.7 CB[*n*]s and formulation spread on agar

The previous assay represented the uptake of moisture by the insert once *in situ*, during which time the dry lyophilisate transforms into a viscous gel. In order to examine how this gel would spread and cover a larger surface area *in vivo*, an assay using agar plates was employed.

In this investigation, lyophilised discs of the selected formulations were pressed gently onto agar:mucin (1.5%:1%) plates (25 cm × 25 cm plates, *n*=6) The plates were then set at 80 º to the horizontal and the distance travelled by the gel front

recorded as a function of time. Bertram and Bodmeier have reported the use of PBS (pH 6) to make up the agar.[52] Since the behaviour of mucoadhesives can be affected by pH (and the pH of the nasal cavity can be as low as pH 5) as well as the presence of salts, it was decided to investigate whether or not the buffer used for making up the agar would have an effect on the assay results. The strategy was, that if the buffers gave different results then the experiments would go ahead using the SNES, which was expected to be more representative of the nasal environment.

For the assessment, two plates were made up with PBS (pH 7.4) and two plates were made up using SNES (pH 5.5). Each plate was loaded with four blank K4MP discs. There was a significant difference in the spread of the formulations between one PBS plate and one SNES plate (P=0.011), suggesting that the SNES should be used for subsequent agar plates. However, between the two SNES plates, there were significant differences in distances travelled (P=0.015), suggesting that the results were not reproducible when SNES was used. The two PBS plates, however, gave statistically similar results (P=0.971). It was therefore decided to go ahead with PBS plates for the sake of reproducibility. As a precaution, any parameter being investigated would be completed on the same plate, *i.e.* instead of running 1% on one plate and 2% on another; a sample of each would be placed on the same plate, with n = the number of plate repeats.

1% CB[6], 2% CB[6], 3% CB[6], 1% CB[7], 2% CB[7] and 3% CB[7] were tested on agar/mucin plates made up with PBS. For both CB[6] and CB[7], increasing the concentration of cucurbituril in the formulation acted to increase the speed at which the gel front travelled. This may have purely been a result of the extra weight in the gel from the increased mass of CB[n]. As shown previously, increasing the concentration of CB[n] in the formulation has been shown to reduce the weight gained from water uptake, suggesting that the increased mobility is not due to extra weight from water of hydration.

Interestingly, in each case the discs containing CB[7] gelled and spread down the plate more rapidly than the equivalent CB[6] disc (Figure 3.22). As the gels were

formulated by weight rather than by molarity, and CB[7] is heavier than CB[6]: this means that there are fewer molecules of CB[7] in a 1% (w/w) gel than molecules of CB[6] in a 1% (w/w) gel. Therefore, it may be determined from these results that CB[7] has considerably better ability to increase the rate of formulation spread on agar/mucin plates. This may be as a result of shortening the time to rehydrate (Figure 3.22). This supports the suggestion that CB[*n*]s can aid the penetration of water through the insert allowing more rapid gelling. Data were not reported after the gel front reached the edge of the plate.

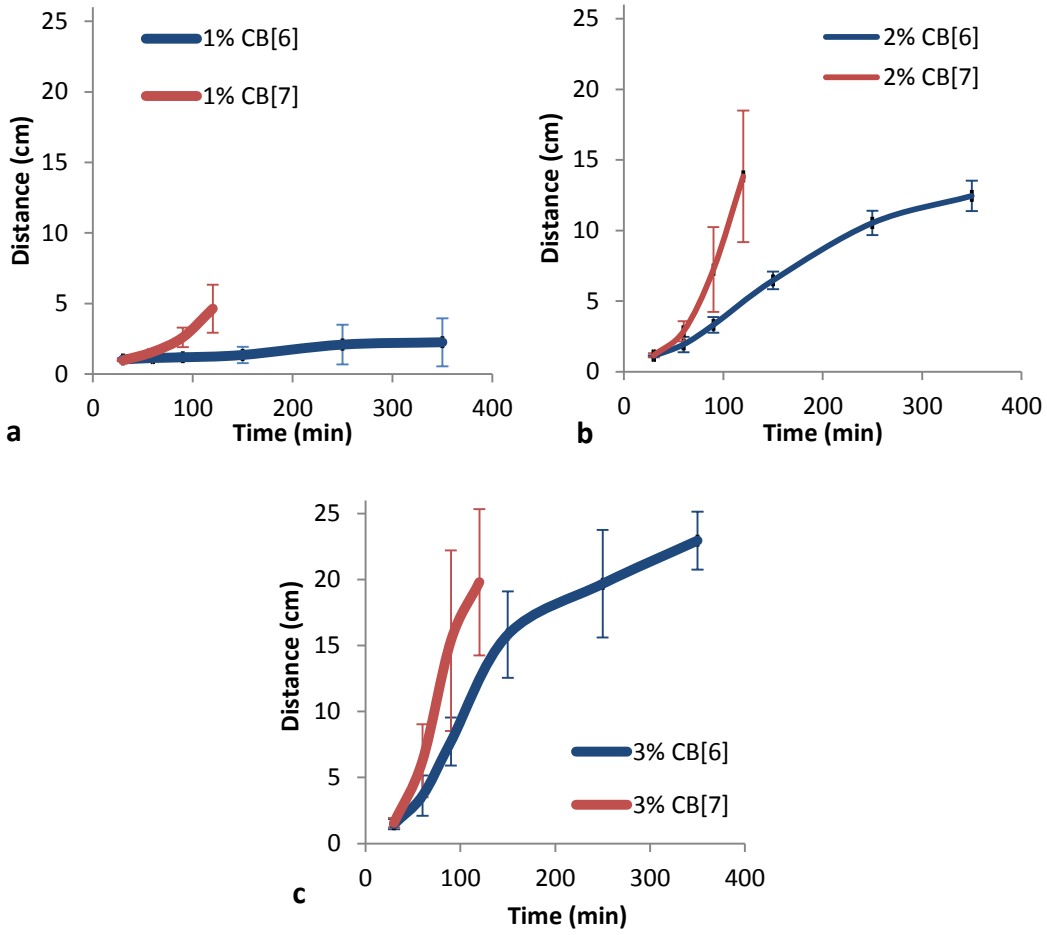

Figure 3.22. Graphs showing the distance travelled by gel front of discs containing a) 1%, b) 2%, and 3%, CB[6] and CB[7] (for CB[6], *n*=6; for CB[7], *n*=3).

Further, it is possible that polymer chain entanglement is reduced in the presence of CB[*n*] due to repositioning of the polymer chain to a more regular conformation.

This effect, reported by Hou and colleagues,[71] could result in greater polymer chain mobility and enhanced spreading ability (Figure 3.23).

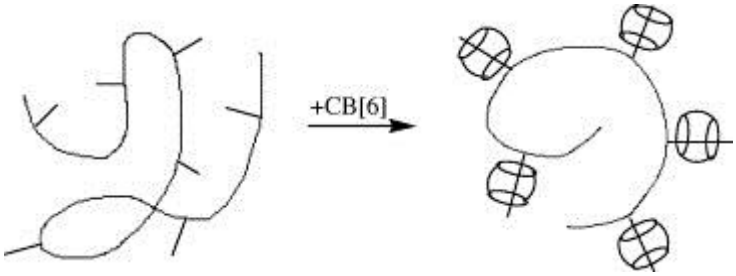

Figure 3.23. Conformational changes occurring upon encapsulation of pendant groups.[71]

This method of measuring distance travelled by the formulation on an agar/mucin plate has been described by others as a "dynamic adhesion test". During these tests, the discs did not slide down the plate as a unit, but hydrated to form a gel, which subsequently spread down the surface of the plate. As such, it was decided that this test is not a measure of adhesion of the formulation; rather it is a useful assay for observing gelling behaviour and formulation spread. A more useful method for examining adhesion is one which measures the force required to detach the formulation from the mucosa. This can be achieved using a texture analyser, in association with nasal mucosa harvested from pigs.

3.7.8 Evaluating mucoadhesion using *ex vivo* porcine mucosa

Lyophilised discs prepared from 0.1%, 0.2%, 0.3% and 0.4% CB[6] and CB[7] were analysed for mucoadhesion using the TA and freshly excised porcine nasal mucosa. The disc was lowered onto the surface of the mucosa and held for 60 s before being withdrawn. The peak force and work of adhesion (the area under the force *vs*. time curve, Figure 3.24) were recorded.

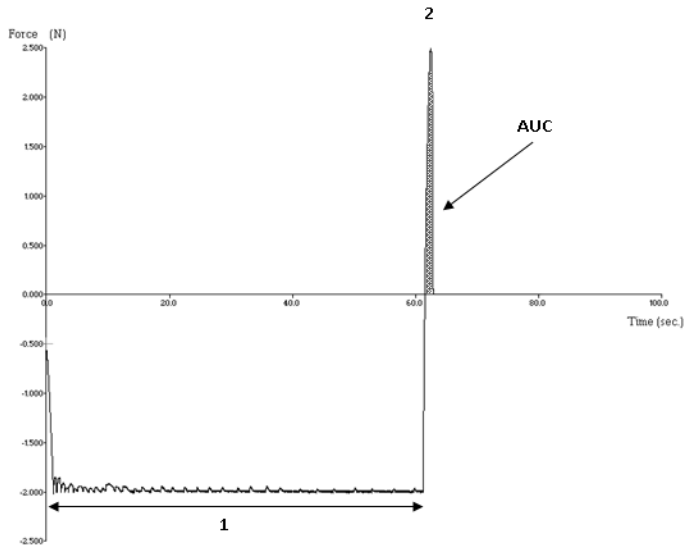

Figure 3.24. Typical plot from the TA mucoadhesion test, where 1= contact time (s) and force (N), and 2= peak force of detachment (N).

There was no significant difference in either work of adhesion or peak force of detachment between discs containing CB[6] and discs containing CB[7] in the range 0.1%-0.4% CB[*n*] (Figure 3.25). However, the average values for both of these reduced with increasing CB[7] concentration. No similar trend was observed with CB[6]. The work of adhesion and peak force of attachment for 0.3% CB[6] appears to be out of trend with the other results. This may be as a result of error in the preparation of the lyophilised discs. As both pieces of data are collected during the same test, experimental error cannot be ruled out. Lower concentrations of CB[*n*] were used in this test as supply of CB[7] was short.

In this case, CB[6] and CB[7] do not appear to affect mucoadhesion in the same manner, although results are not significant. In order to be certain of these results, the experiment should be repeated with higher concentrations of CB[*n*].

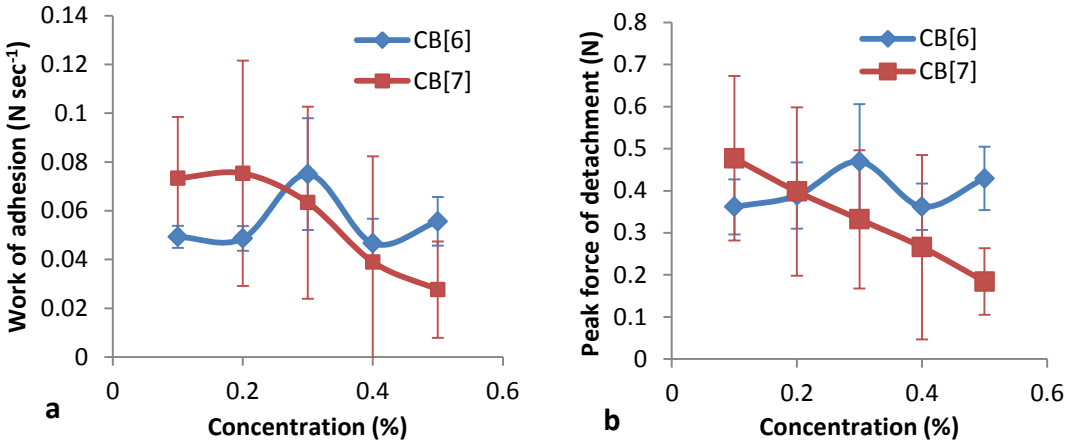

Figure 3.25. Graphs comparing a) work of adhesion, and b) peak force of detachment, for lyophilised discs containing 0.1-0.4% (*n*=3, error bars represent standard deviation).

These observations can be rationalised by considering the theories of mucoadhesion. The reduction in mucoadhesion with increased CB[7] content may be a result of increased hydrogen bonding between polymer hydoxyl groups and the carbonyl moieties on the cucurbituril which would cause a reduction in chain mobility, particularly if CB[*n*]s are indeed forming cross-links between polymer chains. As interpenetration of polymer/mucin chains is a contributing factor in mucoadhesion,[72,73] this reduction in chain mobility would be expected to be detrimental to mucoadhesion.

This probable contribution of functional groups on the CB[*n*] might result in saturation of hydrogen bonding sites within the polymer, leaving them less able to interact with mucus glycoproteins.[72,73] This is pertinent to the adsorption theory of mucoadhesion, whereby attractive forces between functional groups contribute to mucoadhesion. This trend may not be seen with the CB[6] discs because there are fewer carbonyl groups on the CB[6] than CB[7]. If this is the case, repeating the experiment with CB[8] would be expected to reduce mucoadhesion further. Repeating the experiment with a higher concentration range may also provide further insight into this phenomenon.

A limitation of this TA technique becomes apparent when considering the fracture theory of mucoadhesion. This theory supposes that the strength of the mucoadhesive bond is the force required to pull the two surfaces apart, and forms the basis of the TA technique. This assumes that the point of failure is the interface between the surface of the mucosa and the surface of the polymer disc.[72] The point of failure may, however, be a point within the disc or the mucosa. The apparent trend in mucoadhesion observed with altering CB[7] concentration suggests that the force required to separate the surfaces is a function of CB[7] concentration. This suggests that the point of failure is either the interface or a point within the disc.

Whilst some of the results and theories discussed may seem counterintuitive, it should be noted that the contribution of CBs to the physicochemical properties of the inserts is thought to vary with concentration.

3.7.9 Optical tweezers for analysing rheology on the microscopic scale

Traditional bulk rheology, carried out on a macroscopic scale, requires sample volumes ≥ 1 mL. Due to the high cost of CB[7], preparing samples of this size would not have been possible. A micro-rheology technique, such as optical tweezers, retains the same principles as bulk rheology, but requires only a very small sample size (~10 µL). Optical tweezers is a technique whereby a micron-sized particle is trapped in a strongly focused beam of light. The motion of the particle within the beam is tracked, and its trajectory directly related to the viscoelastic properties of the surrounding fluid, in this case the samples under investigation.[60]

Micro-rheology was used to examine samples of 0.5% HPMC (w/w) gel containing 0.1-0.4% CB[6] and 0.1-0.3% CB[7]. As no suitable particles for tracking existed in these samples (perfectly spherical, with a known refractive index), 3 µm diameter polystyrene beads were added to the samples before investigation. All samples tested were viscoelastic, following neither purely viscous nor purely elastic behaviour (Figure 3.26).

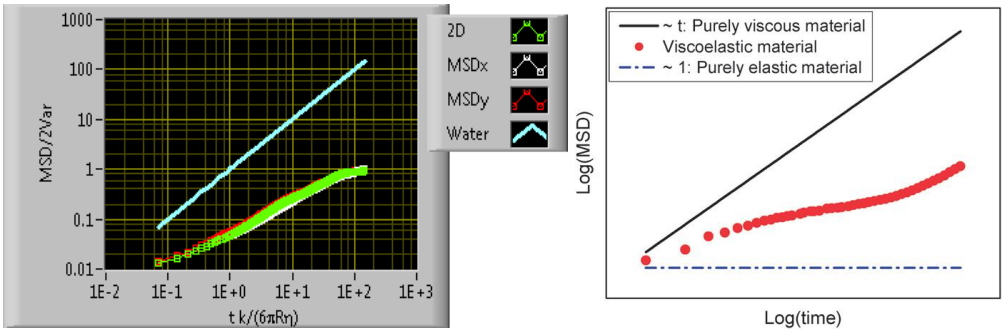

Figure 3.26. Left: typical mean square displacement (MSD) output from the micro-rheology investigation. The red line represents motion in the y-direction, white the x-direction, green the average of both directions and blue water, a purely viscous material. Right: Figure from Yao and colleagues representing the MSD behaviour of thermally excited probe particles for three different materials – purely viscous, purely elastic and viscoelastic.[60]

The technique was also used to gather data on the elastic modulus (*G'*), the loss or viscosity modulus (*G''*) and the viscosity (η, Figure 3.27). In the region where *G'* is higher, the material displays more elastic behaviour. At higher frequencies the *G''* dominates, and the materials display more viscous behaviour. For all samples, η decreased with increasing shear rate. This indicated that the materials were all shear thinning, irrespective of CB[*n*] content.

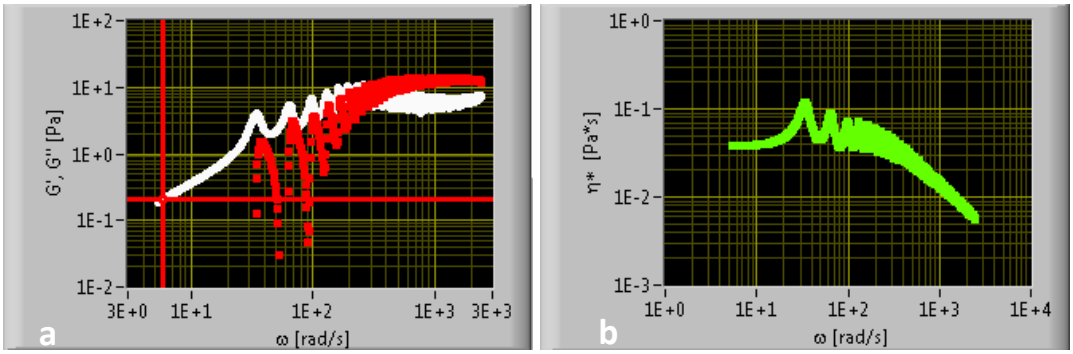

Figure 3.27. Typical output from micro-rheology experiment showing: a) G' (red) and G'' (white); and b) viscosity versus frequency.

For samples of 0.5% HPMC (w/w) gel (before lyophilisation), increasing the concentration of CB[6] from 0.1% to 0.4% acted to increase the viscosity of the gel at frequencies above 150 Hz (Figure 3.28a). However, no trend in viscosity was evident with CB[7] (Figure 3.28b).

Increased viscosity could be attractive in a mucoadhesive formulation, as it can help to overcome rapid MCC. During MCC the cilia bend backwards, and if the bend is too great due to excessive mucus viscosity, the system does not work effectively and clearance rate is reduced. Therefore a highly viscous mucoadhesive may overcome MCC in a similar fashion.[74] High viscosity has been reported as detrimental to some nasal formulations, but this is generally related to droplet size and surface area covered.[75] Increasing the viscosity of these formulations by increasing CB[6] content is not however expected to be an issue, as increasing CB[6] content was actually shown to increase the surface area covered by the formulation during the test on agar/mucin plates.

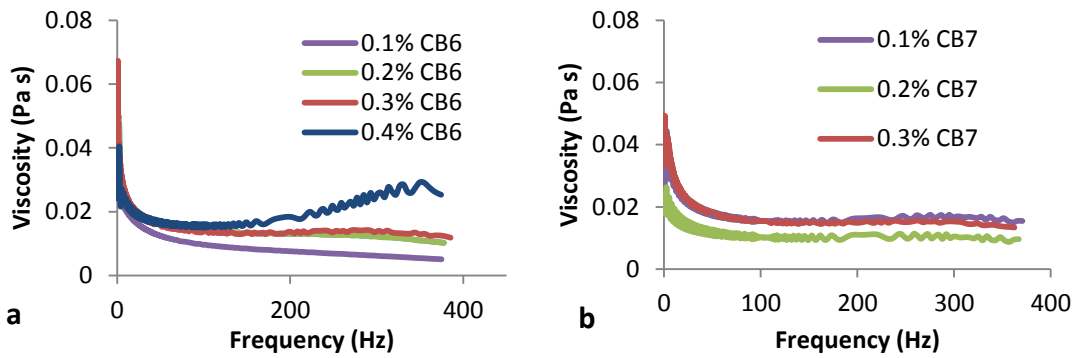

Figure 3.28. Graphs comparing the viscosities of gels containing a) 0.1%-0.4% CB[6]. Above 150 Hz, the viscosity increases with increasing CB[6] content; and b) 0.1%-0.3% CB[7]. There is no apparent trend in viscosity.

The viscosity of a mixture of mucin and a mucoadhesive polymer has been used as an indicator of the strength of mucoadhesion.[76] In cases where the viscosity of the mixture exceeds the sum viscosities of the individual components, synergism is said

to be occurring. The difference between the expected viscosity (η_{exp}) and observed viscosity of the mixture (η_{obs}) is known as the viscosity enhancement ($\eta_{enhance}$).

Optical tweezers were employed as a novel method to investigate whether CB[6] and CB[7] had the same effect on mucoadhesive synergy. The viscosities of a mixture of 0.5% mucin and 0.5% K4MP, containing varying amounts of CB[6], were measured at 302 Hz and compared with values obtained for 0.5% mucin solution and 0.5% K4MP containing varying amounts of CB[7]. The viscosity enhancement ($\eta_{enhance}$) and the relative viscosity enhancement (η_{rel}) were then calculated from the viscosities of the mucin solution alone (η_m), the polymer-CB[*n*] solution alone (η_p), the mixture (η_{obs}) and the expected viscosity (η_{exp}), using the following equations from Thirawong *et al*.[76]

$$\eta_{exp} = \eta_p + \eta_m \qquad \textbf{Equation 3}$$

$$\eta_{enhance} = \eta_{obs} - \eta_{exp} \qquad \textbf{Equation 4}$$

$$\eta_{rel} = {}^{\eta_{obs}}/_{\eta_{exp}} \qquad \textbf{Equation 5}$$

Thirawong and colleagues have previously used traditional bulk rheology to investigate synergism between mucin and pectin.[76] This is an example where synergism is occurring, with a positive relative viscosity enhancement which increases upon increasing the concentration of mucin (Figure 3.29). If synergism were occurring between the CB[*n*]s and the mucin, a similar graph would be expected.

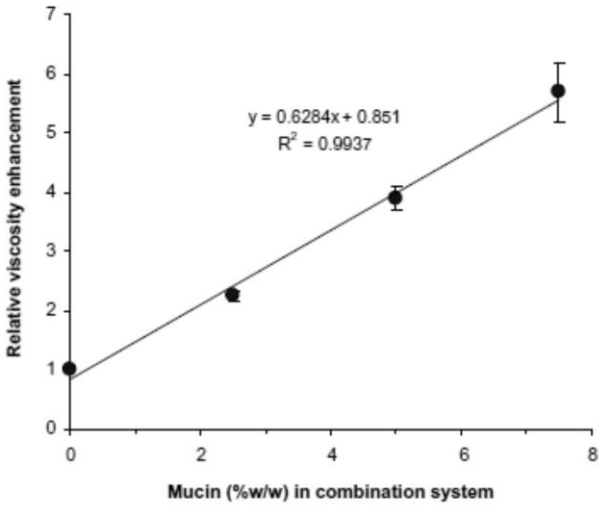

Figure 3.29. Graph from the paper by Thirawong and colleagues showing the effect of increasing mucin concentration in 1% pectin solution.[76] This represents a system where rheological synergism is in effect.

In this work, increasing the amount of CB[6] in the mixture acted to reduce $\eta_{enhance}$ and η_{rel} (Figure 3.30). Furthermore, for concentrations above 0.1% CB[6], increasing CB[6] concentration was detrimental to viscosity, which may be indicative of reduced mucoadhesion. This may be due to the hydrogen bonding of CB[*n*]s with the polymer, competing with the mucus for donor and acceptor sites. This would reduce the amount of hydrogen bonding that could be established between the polymer and mucus, reducing the forces of mucoadhesion which could be achieved. Additionally, polymer chains with CB[6]s hydrogen bonded to hydrophilic moieties may untangle. Although this may allow for greater intermingling of mucin and polymer chains, the steric bulk of associated CB[6]s may inhibit tangling, producing a negative synergy. Similarly, increasing the amount of CB[7] in the mixture acted to reduce $\eta_{enhance}$ and η_{rel} up to 0.3%, with an increase in the trend at 0.4% (Figure 3.31). Further investigation would be required to determine whether or not a positive enhancement could be reached with increasing CB[7] concentration.

In this investigation, increasing the concentration of CB[6] and CB[7] from 0.1% to 0.3% acted to reduce the viscosity of the polymer/mucin mixture, indicating a potential reduction in mucoadhesive behaviour. CB[6] and CB[7] both had a deleterious effect on viscosity at 0.3% and 0.4%. This indicates that CB[6] and

CB[7] do not enhance viscosity in the presence of mucin, and would be detrimental to any rheological synergy occurring between the HPMC and the mucin. Whilst this may be detrimental to the sum of mucoadhesion, further work would be required to determine whether or not this was a tolerable decrease.

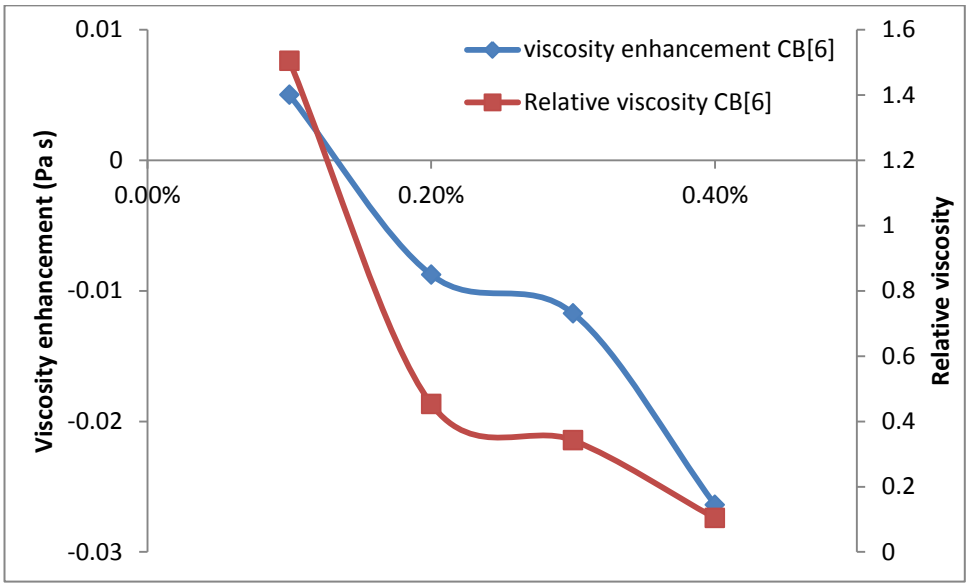

Figure 3.30. Graph showing the viscosity enhancement and relative viscosity enhancements achieved upon increasing CB[6] concentration.

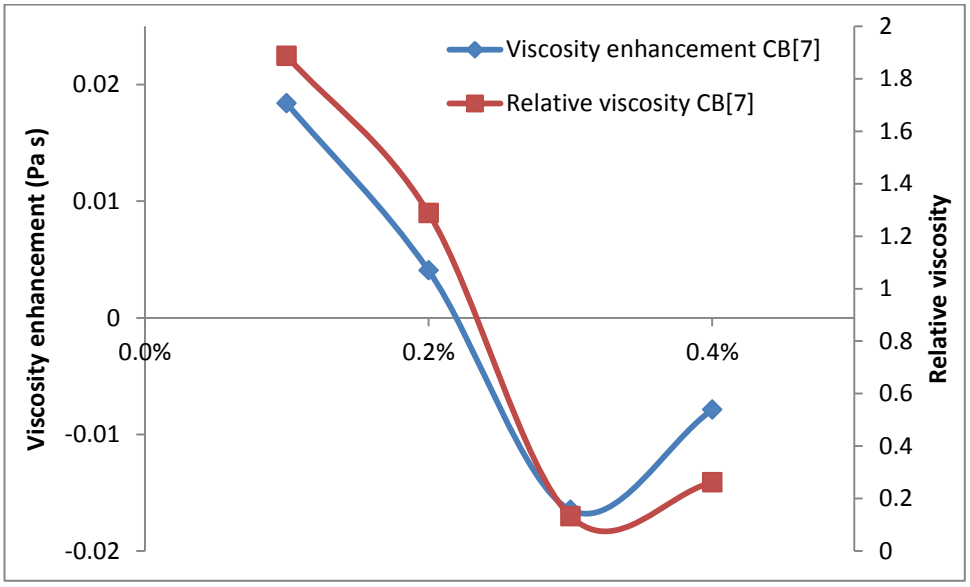

Figure 3.31. Graph showing the viscosity enhancement and relative viscosity enhancements achieved upon increasing CB[7] concentration.

Under these conditions up to 0.3%, increasing CB[6] content has a similar qualitative effect as increasing CB[7] concentration and may be a suitable model. Repeating at higher concentrations of CB[7] would indicate whether the increase at 0.4% marks a change in the system or experimental error. It should, however, be noted that these samples were of dilute, wet formulations without freeze drying and therefore not fully representative of a rehydrating nasal insert/disc, which would be too viscous to be examined by this technique.

In order to examine the rheology of the hydrated CB[*n*] nasal insert at relevant concentrations, a bulk rheometer could be utilised. This would however require a considerable quantity of CB[*n*].

3.8 CONCLUSIONS

Cucurbiturils are receiving attention as potential drug delivery vehicles in pharmaceutical formulations. Whilst CB[7] is useful in terms of size and solubility,[1] it remains relatively expensive to purchase and complicated to isolate.[41] It has been stated that lessons learned from CB[6] can be applied to the whole CB[*n*] family,[35] and so CB[6] has been investigated as a cost-effective model for CB[7], in a lyophilised nasal insert formulation.

Nasal insert and disc formulations containing 1%-4% CB[6] and 1-3% CB[7] were produced and compared in a series of tests. It was found that increasing CB[6] and CB[7] concentration both increased the formulation hardness to a maximum, after which further increase was detrimental. This suggested that at lower concentrations, CB[*n*]s were acting as structural components, contributing to structural integrity. A model where the carbonyl portals of CB[*n*]s form hydrogen bonds with hydroxyl groups on the HPMC has been proposed, with pseudo-cross-links forming when a CB[*n*] links two polymer chains. This results in reduced structural integrity. A similar effect has recently been reported by Lin and co-workers, who observed gelation of modified chitosan upon encapsulation of two side-chain modifications into CB[8].[35] Once the structure was saturated however, a further increase in concentration reduced hardness, thought to be through saturation of donor sites and steric hindrance reducing the ability of the system to form a network. Any future application of a CB[*n*]-HPMC matrix may, therefore, require careful tuning of the composition to obtain the required network strength.

Increasing the concentration of CB[6] and CB[7] reduced the amount of water taken up by the formulation, but improved the rate at which the inserts gelled and spread on agar/mucin. In these situations, CB[6] proved to be a useful model for CB[7], affecting the formulation in a similar manner. The reduction of water uptake with increased CB[*n*] concentration supported the idea that CB[*n*]s hydrogen bond to the polar groups on the polymer, saturating these sites and reducing the potential for water uptake. Improvements to gelling and subsequent spread (with less water

uptake) may be attributed to more rapid, deep penetration of water into the lyophilisate. This may be due to excess CB[*n*]s forming water channels through the polymer matrix.

For mucoadhesion, no trend was observed with increasing CB[6] concentration from 0.1% to 0.5%. The same range of CB[7] concentration however showed a reduction in mucoadhesion with increasing CB[7] content, suspected to be due to reduced polymer chain mobility with the increasing structural contribution of the CB, as well as saturation of functional groups which may have otherwise contributed to mucoadhesive interactions. This supports the model where CB[7] acts as a point of cross-linking between polymer chains, increasing structural integrity of the polymer system. The concentration range under investigation was reduced due to a lack of CB[7]. Examining a wider concentration range may produce significant results and provide further insight into this behaviour.

In the micro-rheology investigation, increasing the concentration of CB[6] from 0.1% to 0.4% acted to increase the viscosity of the gel at frequencies above 150 Hz However, no trend in viscosity was apparent with CB[7]. This experiment was limited by the quantity of CB[7] available, and increasing the concentration range examined may provide more useful results in the future.

Examining synergy in viscosity, increasing the concentration of CB[6] and CB[7] from 0.1% to 0.3% acted to reduce the viscosity of the mixture, indicating a reduction in mucoadhesive potential. Both CB[6] and CB[7] had a deleterious effect on viscosity at 0.3% and 0.4%. Under these conditions increasing CB[6] content up to 0.3%, has a similar qualitative effect as increasing CB[7] concentration and may be a suitable model.

In order to gain a better understanding of the effect of CB[*n*]s on mucoadhesion, similar variables to those of Thirawong and coworkers' could be used: keeping the concentration of the mucoadhesive (in this case HPMC, containing CB[*n*]) constant and increasing the mucin concentration.[76] This may indicate whether or not synergism is still occurring in the system between the HPMC and the mucin, or has

been cancelled out altogether by the CB[*n*]. It would also be useful to study the rheology of the hydrating insert, although this would be too viscous to study using the optical tweezers technique.

In conclusion, in lyophilised HPMC nasal inserts, CB[6] has showed promise as a model for CB[7] and lessons learned from CB[6] may be used to make predictions about CB[7]. Where the formulation is affected due to hydrogen bonding with CB[*n*], the alteration will be more pronounced with CB[7] than CB[6], therefore, if a definitive quantitative result is required, CB[7] should be used.

Although the tests described in this chapter gave an indication of how CB[6] and CB[7] may affect a lyophilised nasal insert formulation, they did not indicate how they might affect the formulation when a guest molecule was encapsulated. To address this, and in order to study the release of the CB[*n*]s from the formulation, a UV-active or fluorescent guest molecule would have to be encapsulated.

3.9 REFERENCES

(1) Walker, S., Oun, R., McInnes, F.J. and Wheate, N.J., *Isr. J. Chem.*, 2011, **51**, 616-624.

(2) McInnes, F.J., Anthony, N.G., Kennedy, A.R. and Wheate, N.J., *Org. Biomol. Chem.*, 2010, **8**, 1477-0520.

(3) Wheate, N.J., *J. Inorg. Biochem.*, 2008, **102**, 2060-2066.

(4) Macartney, D.H., *Isr. J. Chem.*, 2011, **51**, 600-615.

(5) Saleh, N.i., Meetani, M.A., Al-Kaabi, L., Ghosh, I. and Nau, W.M., *Supramol. Chem.*, 2011, **23**, 654-661.

(6) Saleh, N.i., Khaleel, A., Al-Dmour, H., al-Hindawi, B. and Yakushenko, E., *J. Therm. Anal. Calorim.*, 2013, **111**, 385-392.

(7) Behrend, R., Meyer, E. and Rusche, F., *Liebigs Ann. Chem.*, 1905, **339**, 1-37.

(8) Freeman, W.A., Mock, W.L. and Shih, N.-Y., *J. Am. Chem. Soc.*, 1981, **103**, 7367-7368.

(9) Haouaj, M.E., Luhmer, M., Ko, Y.H., Kim, K. and Bartik, K., *J. Chem. Soc., Perkin Trans. 2*, 2001, 804-807.

(10) Jeon, Y.M., Kim, H., Whang, D. and Kim, K., *J. Am. Chem. Soc.*, 1996, **118**, 9790-9791.

(11) Whang, D., Jeon, Y.-M., Heo, J. and Kim, K., *J. Am. Chem. Soc.*, 1996, **118**, 11333-11334.

(12) Kim, J., Jung, I.S., Kim, S.Y., Lee, E., Kang, J.K., Sakamoto, S., Yamaguchi, K. and Kim, K., *J. Am. Chem. Soc.*, 2000, **122**, 540-541.

(13) Hoffmann, R., Knoche, W., Fenn, C. and Buschmann, H.-J., *J. Chem. Soc, Faraday Trans.*, 1994, **90**, 1507-1511.

(14) Day, A., Arnold, A.P., Blanch, R.J. and Snushall, B., *J. Org. Chem.*, 2001, **66**, 8094-8100.

(15) Lee, J.W., Samal, S., Selvapalam, N., Kim, H.-J. and Kim, K., *Acc. Chem. Res.*, 2003, **36**, 621-630.

(16) Marquez, C., Hudgins, R.R. and Nau, W.M., *J. Am. Chem. Soc.*, 2004, **126**, 5806-5816.

(17) Day, A.I., Blanch, R.J., Arnold, A.P., Lorenzo, S., Lewis, G.R. and Dance, I., *Angew. Chem.-Int. Ed.*, 2002, **41**, 275-277.

(18) Germain, P., Létoffe, J.M., Merlin, M.P. and Buschmann, H.J., *Thermochim. Acta*, 1998, **315**, 87-92.

(19) Buschmann, H.J., Jansen, K., Meschke, C. and Schollmeyer, E., *J. Solution Chem.*, 1998, **27**, 135-140.

(20) Jansen, K., Buschmann, H.J., Wego, A., Döpp, D., Mayer, C., Drexler, H.J., Holdt, H.J. and Schollmeyer, E., *J. Inclus. Phenom. Macro.*, 2001, **39**, 357-363.

(21) Mock, W.L. and Pierpont, J., *J. Chem. Soc., Chem. Commun.*, 1990, 1509-1511.

(22) Mock, W.L., Irra, T.A., Wepsiec, J.P. and Adhya, M., *J. Org. Chem.*, 1989, **54**, 5302-5308.

(23) Mock, W.L., Irra, T.A., Wepsiec, J.P. and Manimaran, T.L., *J. Org. Chem.*, 1983, **48**, 3619-3620.

(24) Das, D. and Scherman, O.A., *Isr. J. Chem.*, 2011, **51**, 537-550.

(25) Hwang, I., Baek, K., Jung, M., Kim, Y., Park, K.M., Lee, D.-W., Selvapalam, N. and Kim, K., *J. Am. Chem. Soc.*, 2007, **129**, 4170-4171.

(26) Buschmann, H.-J., *Isr. J. Chem.*, 2011, **51**, 533-536.

(27) Meschke, C., Buschmann, H.-J. and Schollmeyer, E., *Polymer*, 1999, **40**, 945-949.

(28) Kim, K., Oh, D.H., Nagarajan, E.R., Ko, Y.H. and Samal, S., *Cucurbituril-Containing Polymer, Stationary Phase and Column Using the Same*, 2009, US7520982,

(29) Karcher, S., Kornmüller, A. and Jekel, M., *Water Sci. Technol.*, 1999, **40**, 425-433.

(30) Ghosh, I. and Nau, W.M., *Adv. Drug Deliver. Rev.*, 2012, **64**, 764-783.

(31) Davis, M.E. and Brewster, M.E., *Nat. Rev. Drug Discov.*, 2004, **3**, 1023-1035.

(32) Challa, R., Ahuja, A., Ali, J. and Khar, R., *AAPS PharmSciTech*, 2005, **6**, E329-E357.

(33) Loftsson, T. and Brewster, M.E., *J. Pharm. Pharmacol.*, 2010, **62**, 1607-1621.

(34) Guan, Z., Wang, Y., Chen, Y., Zhang, L. and Zhang, Y., *Tetrahedron*, 2009, **65**, 1125-1129.

(35) Lagona, J., Mukhopadhyay, P., Chakrabarti, S. and Isaacs, L., *Angew. Chem. Int. Ed.*, 2005, **44**, 4844-4870.

(36) http://www.anshulindia.com/pdfs/Cyclodextrins.pdf, *accessed 4th September 2012.*

(37) Mohanty, J., Bhasikuttan, A.C., Nau, W.M. and Pal, H., *J. Phys. Chem. B*, 2006, **110**, 5132-5138.

(38) Jeon, Y.J., Kim, S.-Y., Ko, Y.H., Sakamoto, S., Yamaguchi, K. and Kim, K., *Org. Biomol. Chem.*, 2005, **3**, 2122-2125.

(39) Wang, R. and Macartney, D.H., *Org. Biomol. Chem.*, 2008, **6**, 1955-1960.

(40) Wyman, I.W. and Macartney, D.H., *J. Org. Chem.*, 2009, **74**, 8031-8038.

(41) Jiao, D., Zhao, N. and Scherman, O.A., *Chem. Comm.*, 2010, **46**, 2007-2009.

(42) http://www.sigmaaldrich.com/catalog/product/aldrich/545201?lang=en&region=GB, *accessed 19th June 2012.*

(43) Walker, S., Kaur, R., McInnes, F.J. and Wheate, N.J., *Mol. Pharmaceut.*, 2010, **7**, 2166-2172.

(44) Buschmann, H.-J., Cleve, E., Jansen, K., Wego, A. and Schollmeyer, E., *Mat. Sci. Eng. C*, 2001, **14**, 35-39.

(45) Giron, D., *Thermochim. Acta*, 1995, **248**, 1-59.

(46) Haleblian, J. and McCrone, W., *J. Pharm. Sci.*, 1969, **58**, 911-929.

(47) Threlfall, T., *Org. Process Res. Dev.*, 2003, **7**, 1017-1027.

(48) Bauer, J., Spanton, S., Henry, R., Quick, J., Dziki, W., Porter, W. and Morris, J., *Pharm. Res.*, 2001, **18**, 859-866.

(49) Kemp, S., Wheate, N.J., Wang, S., Collins, J.G., Ralph, S.F., Day, A.I., Higgins, V.J. and Aldrich-Wright, J.R., *J. Biol. Inorg. Chem.*, 2007, **12**, 969-979.

(50) Bardelang, D., Udachin, K.A., Leek, D.M. and Ripmeester, J.A., *Cryst. Eng. Comm.*, 2007, **9**, 973-975.

(51) Bertram, U. and Bodmeier, R., *Eur. J . Pharm. Biopharm.*, 2006, **63**, 310-319.

(52) Bertram, U. and Bodmeier, R., *Eur. J . Pharm. Biopharm.*, 2006, **27**, 62-71.

(53) Nakamura, F., Ohta, R., Machida, Y. and Nagai, T., *Int. J. Pharm.*, 1996, **134**, 173-181.

(54) Li, H. and Gu, X., *Int. J. Pharm.*, 2007, **342**, 18-25.

(55) Abdelbary, G., Eouani, C., Prinderre, P., Joachim, J., Reynier, J. and Piccerelle, P., *Int. J. Pharm.*, 2005, **292**, 29-41.

(56) Siddiqui, A. and Nazzal, S., *Int. J. Pharm.*, 2007, **341**, 173-180.

(57) McInnes, F., Baillie, A.J. and Stevens, H.N.E., *J. Pharm. Pharmacol.*, 2007, **59**, 759-767.

(58) Wong, C.F., Yuen, K.H. and Peh, K.K., *Int. J. Pharm.*, 1999, **180**, 47-57.

(59) http://128.121.92.221/TAXT2_Texture_Analyzer.htm, *accessed 9th June 2011*.

(60) Yao, A., Tassieri, M., Padgett, M. and Cooper, J., *Lab Chip*, 2009, **9**, 2568-2575.

(61) Sriamornsak, P. and Wattanakorn, N., *Carbohyd. Polym.*, 2008, **74**, 474-481.

(62) Martin, L., Wilson, C.G., Koosha, F. and Uchegbu, I.F., *Eur. J . Pharm. Biopharm.*, 2003, **55**, 35-45.

(63) Khutoryanskaya, O.V., Potgieter, M. and Khutoryanskiy, V.V., *Soft Matter*, 2010, **6**, 551-557.

(64) McInnes, F.J., *In-Vitro and in-Vivo Properties of a Lyophilised Nasal Dosage Form*, University of Strathclyde, 2003.

(65) http://www.dow.com/PublishedLiterature/dh_0050/0901b80380050865.pdf?filepath=amerchol/pdfs/noreg/324-00180.pdf&fromPage=GetDoc, *accessed 23rd March 2013.*

(66) McInnes, F.J., Thapa, P., Baillie, A.J., Welling, P.G., Watson, D.G., Gibson, I., Nolan, A. and Stevens, H.N.E., *Int. J. Pharm.*, 2005, **304**, 72-82.

(67) Appel, E.A., Loh, X.J., Jones, S.T., Dreiss, C.A. and Scherman, O.A., *Biomaterials*, 2012, **33**, 4646-4652.

(68) Williams, H.D., Ward, R., Hardy, I.J. and Melia, C.D., *Eur. J . Pharm. Biopharm.*, 2010, **76**, 433-436.

(69) Cheng, Y.-H., Watts, P., Hinchcliffe, M., Hotchkiss, R., Nankervis, R., Faraj, N.F., Smith, A., Davis, S.S. and Illum, L., *J. Control. Rel.*, 2002, **79**, 243-254.

(70) Services, U.D.o.H.a.H. *Waiver of in Vivo Bioavailability and Bioequivalence Studies for Immediate-Release Solid Oral Dosage Forms Based on a Biopharmaceutics Classification System*, Food and Drug Administration, 2000, pp 13.

(71) Hou, Z.-S., Tan, Y.-B., Kim, K. and Zhou, Q.-F., *Polymer*, 2006, **47**, 742-750.

(72) Andrews, G.P., Laverty, T.P. and Jones, D.S., *Eur. J . Pharm. Biopharm.*, 2009, **71**, 505-518.

(73) Smart, J.D., *Adv. Drug Deliver. Rev.*, 2005, **57**, 1556-1568.

(74) Quraishi, M.S., Jones, N.S. and Mason, J., *Clin. Otolaryngolog.*, 1998, **23**, 403-413.

(75) Kublik, H. and Vidgren, M.T., *Adv. Drug Deliver. Rev.*, 1998, **29**, 157-177.

(76) Thirawong, N., Kennedy, R.A. and Sriamornsak, P., *Carbohyd. Polym.*, 2008, **71**, 170-179.

4. EFFECT OF CB[6] and CB[7] ENCAPSULATION ON A NASAL INSERT FORMULATION

4.1 IMPROVING DELIVERY OF MULTI-NUCLEAR PLATINUM ANTICANCER DRUGS

4.1.1 Multi-nuclear platinum anticancer drugs

Recent research in platinum anticancer drugs has seen the field move away from cisplatin analogues and towards multi-nuclear complexes, such as BBR 3464 (Figure 4.1). These complexes are able to overcome resistance through novel binding modes (forming long range intra- and inter-strand DNA cross-links)[1,2] and can be potent at lower concentrations than cisplatin.[3-5] Additionally, the multi-nuclear complexes have shown activity against glioblastoma, a type of tumour for which the traditional cisplatin analogues have not shown significant efficacy.[3] Despite showing promising activity *in vitro*, BBR 3464 was abandoned in clinical trials due to a narrow therapeutic window, as a result of rapid metabolic decomposition and high toxicity.[3]

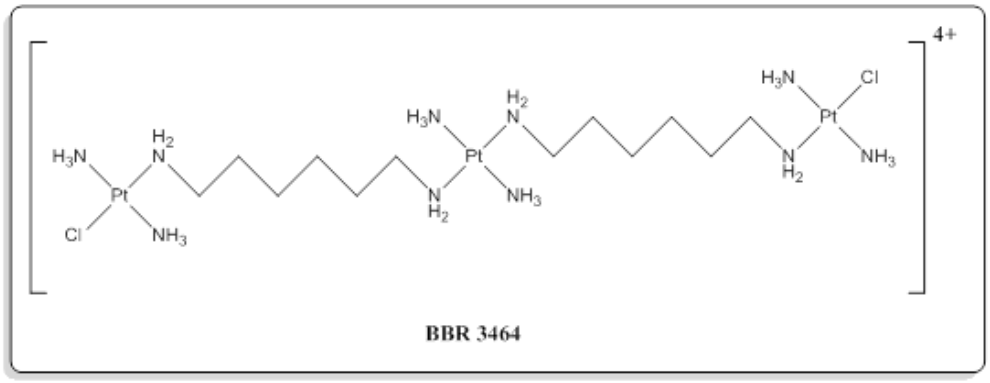

Figure 4.1. Structure of the tri-nuclear complex, BBR 3464.

The complex *trans*-[{PtCl(NH$_3$)$_2$}$_2$μ-dpzm]$^{2+}$ (di-Pt, Figure 4.2) is a water-soluble cationic species in which two transplatin moieties are joined by a *4,4*-dipyrazole methane (dpzm) linker. This complex was first reported by Wheate in 2001.[6,7] It acts by forming interstrand cross-links with DNA and has shown good activity against cisplatin-sensitive cell lines and maintains activity in resistant lines.[7,8] This success may not be realised *in vivo*, however, as Jansen and colleagues have shown that di-nuclear platinum complexes are extensively metabolised by conjugation to glutathione.[9]

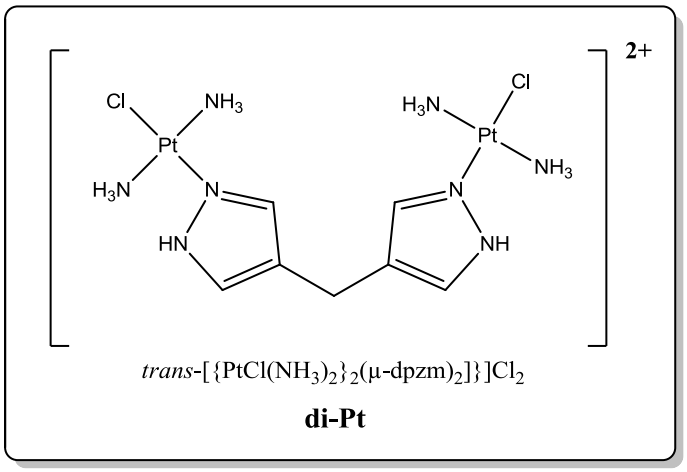

Figure 4.2. The structure of the di-nuclear species, di-Pt.

4.1.2 Protecting multi-nuclear drugs in CB[*n*]s

As toxicity and *in vivo* deactivation are major problems for the multi-nuclear platinum anticancer drugs, a number of drug delivery vehicles are emerging which employ direct drug protection strategies. One such group of delivery vehicles under investigation is the cucurbituril family (*see Chapter 3*). The substantial negative charge density created by the carbonyl portals of these macrocycles facilitates the binding of metal ions and cationic moieties,[10,11] whilst the largely non-polarisable cavity accommodates a hydrophobic moiety. In this manner, CB[7] has been shown to bind di-Pt with a binding constant of 2.1 (±0.5) × 10^5 M^{-1}, high enough to remain encapsulated *in vivo* (Figure 4.3).[12] Protecting di-Pt in CB[7] has been shown to

reduce its reactivity towards thiol-containing compounds, including glutathione, whilst not significantly altering the cytotoxicity.[13] Protecting di-Pt in CB[7] would therefore, potentially allow a greater concentration of active drug to reach the site of action. Additionally, reducing the reactivity of platinum anticancer drugs *in vivo* can reduce the toxicity of the chemotherapeutic agent, allowing a greater dose to be administered.[13]

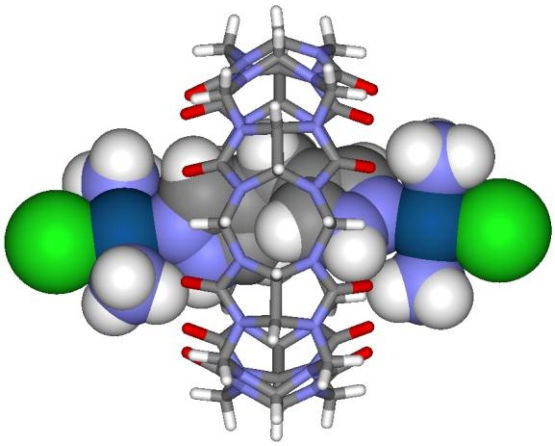

Figure 4.3. X-ray crystal structure of the di-nuclear platinum complex *trans*-[{PtCl(NH$_3$)}$_2$μ-dpzm]$^{2+}$ encapsulated within CB[7]. The dpzm ligand resides in the hydrophobic cavity, with the platinum groups positioned outside the portal.[14]

Similar success has been reported with other platinum(II)-based anticancer drugs. Oxaliplatin is susceptible to light activated degradation but oxaliplatin encapsulated in CB[7] has been shown to be stable for over one year.[15] Encapsulation in CB[7] has also improved the stability of platinum(II)-based DNA intercalators against glutathione conjugation.[16] This ability to confer stability, coupled with low toxicity[17,18] and the ability of CB[*n*] complexes to cross the cell membrane[19] make them attractive carriers for di-nuclear platinum anticancer drugs.

4.1.3 Encapsulating dyes in cucurbit[*n*]urils

As well as drugs, a number of fluorescent and UV-active dyes have been encapsulated in CB[*n*]s.[20-24] Encapsulation in CB[7] (either completely or partially) has been shown to shield against nucleophilic attack and photo-oxidation of the guest molecule, enhancing the fluorescence lifetime.[22] Inclusion of dyes has also been

used to study the kinetics of encapsulation and may allow development of photoresponsive materials, nano-scale devices and sensors.[22] Additionally, inclusion of a fluorescent or UV-active guest could allow for the study of release and distribution of a CB[*n*] complex from a pharmaceutical formulation.

4.1.4 Effect of encapsulation on nuclear magnetic resonance spectra

Nuclear magnetic resonance investigations of CB[*n*]s have revealed some interesting magnetic properties. The CB[6] cavity acts as a magnetic shield, and inclusion of small guests within the macrocycle at 1:1 molar equivalence resulted in an up-field signal shift of around 1 ppm of the guest proton resonances.[25] In addition, the portal regions exert a deshielding effect (Figure 4.4).[25]

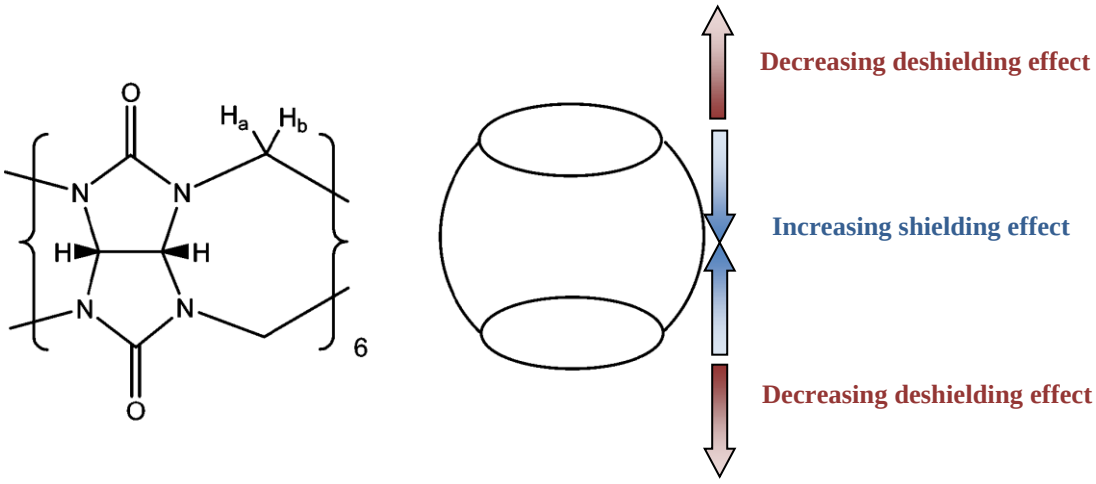

Figure 4.4. The magnetic shielding and deshielding regions of CB[6], adapted from Wheate *et al.*[25]

4.1.5 Dynamic vapour sorption

Dynamic vapour sorption (DVS) is a gravimetric technique used to examine the water uptake properties of a sample, through the production of a vapour sorption isotherm. The central component of the DVS is an ultra-sensitive microbalance housed within a precise temperature controlled incubator. Mixing dry and vapour saturated gas flows at the correct proportions alters the relative humidity (RH). Temperature and humidity probes are situated just under the sample and reference

pans to provide independent monitoring of the system (Figure 4.5).[26,27] The sample is exposed to stepwise changes in relative humidity and the change in mass is recorded. At each step the sample is allowed to reach a gravimetric equilibrium before proceeding to the next RH. The main output from the DVS data is the water sorption isotherm, which displays change in mass against RH.[26]

Pharmaceutical solids are often analysed by DVS in order to gain insight into their stability and performance as well as hydrate and solvate formation and analysis of amorphous content.[26,28-30] McInnes and colleagues have previously reported the use of DVS to examine sorption and desorption of water by nasal insert formulations. This work showed that the lyophilised formulation was capable of substantial water uptake.[31]

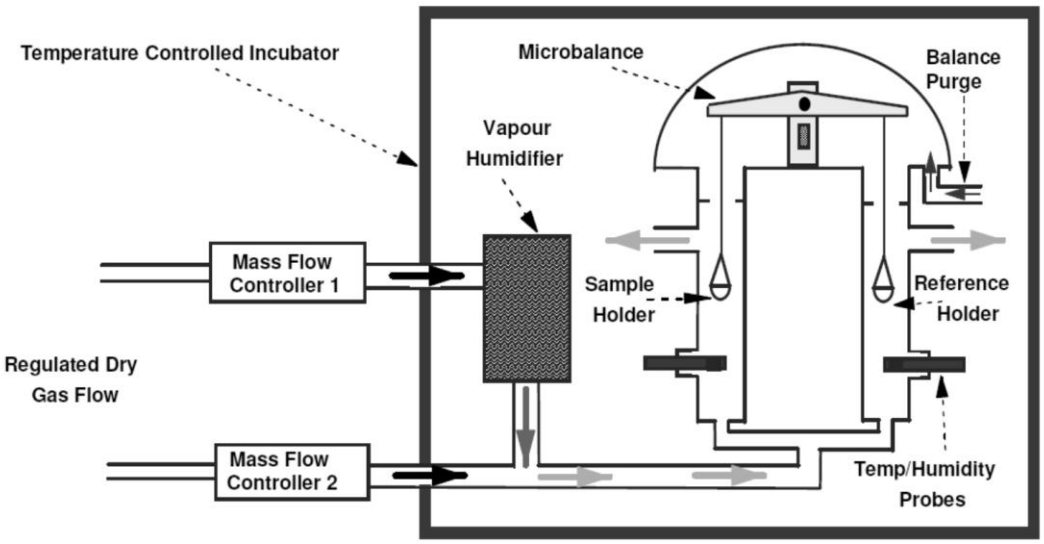

Figure 4.5. Schematic diagram of typical dynamic vapour sorption apparatus.[27]

4.2 AIMS

Multi-nuclear platinum(II) drugs such as di-Pt are able to overcome resistance through novel DNA binding modes, but have narrow therapeutic windows due to high toxicity and extensive metabolism. Protecting di-Pt in CB[7] has been shown to improve its *in vitro* stability by providing steric bulk against nucleophilic attack. Producing lyophilised nasal insert formulations containing di-Pt@CB[7] would allow for nasal delivery of this protected species. Examination of the nasal inserts would allow an insight into how the encapsulation also affects the properties of a pharmaceutical formulation. Therefore, the initial aims of this work are to:

- synthesise di-Pt;
- encapsulate di-Pt in CB[7];
- include di-Pt@CB[7] in a nasal insert formulation; and
- compare these formulations to those containing free di-Pt with a view to determining how encapsulation of the drug in CB[7] affects the formulation.

Comparing these results to those of inserts containing a CB[6] complex would allow further investigation of CB[6] as a model for CB[7]. As CB[*n*]s are not themselves UV-active or fluorescent, incorporating a dye into the cavity would allow the complex to be quantified using readily available UV-vis and/or fluorescence spectroscopy. This would allow investigation of CB[*n*]-guest distribution and ultimately the determination of whether or not CB[6] and CB[7] affect a guest molecule in a nasal insert formulation in the same way. As such, further aims are to:

- synthesise a suitable dye and encapsulate it in CB[6];
- produce nasal insert formulations containing both the dye alone and dye@CB[6] complexes; and
- examine their physiochemical properties and compare these to formulations of di-Pt and di-Pt@CB[7] with a view to determining whether or not CB[6] encapsulation is a suitable model for CB[7] encapsulation in early formulation studies.

4.3 MATERIALS AND METHODS

4.3.1 Materials

Paraformaldehyde, glycoluril, sodium chloride, phosphate buffered saline tablets (pH 7.4) hydrochloric acid, acetone, sulfuric acid, 1,4-dioxane (99%), Isoquinoline (97%) and 1,6-bibromohexane, methanol, ethanol, (*trans*-$[PtCl_2(NH_3)_2]$) (transplatin) and mucin from porcine stomach were obtained from Sigma-Aldrich. CB[7] was obtained from STREM Chemicals UK (Cambridge, UK). Dpzm was obtained from Dr Nial Wheate and used without further purification. NMR solvents were obtained from Cambridge Isotopes (Cambridge, UK). Hydroxypropyl methylcellulose was obtained from Colorcon Ltd (Kent, UK). Ultrapure agar granules were obtained from Merck Microbiology (Merck KGaA, Darmstadt, Germany). Cyanoacrylate gel used was Bostik Superglue gel (Bostik Ltd, UK). All water for syntheses was obtained from a MilliQ water purification system. Water for buffers was distilled in-house. 0.22 µm nylon filter paper and Grade 1 45 mm diameter filter paper were obtained from Whatman.

4.3.2 Synthesis and encapsulation

Prep of *trans*-$[\{PtCl(NH_3)_2\}_2\mu\text{-dpzm}]^{2+}$ (di-Pt): di-Pt is a UV-active investigational platinum drug that can be encapsulated by CB[7]. It was prepared as per the method reported previously by Wheate *et al*.[7] 300 mg transplatin (*trans*-$[PtCl_2(NH_3)_2]$) was dissolved in 250 mL water at 62 ºC with bath sonication. Dpzm (0.076 g) was added and stirred at this temperature for six hours. Heat was removed and the reaction left to stir overnight. The volume was then reduced by rotary evaporation before freeze drying. The crude product was then redissolved in a minimum volume of water at 50-56 ºC. The solution was allowed to cool before fractional precipitation was carried out using acetone. The precipitated impurity was filtered off with 0.22 µm nylon filter paper. The purified solution was evaporated to dryness. Mass was determined using electrospray mass spectroscopy and ^1H NMR obtained in D_2O.

Prep of di-Pt@CB[7]: 32 mg CB[7] was dissolved in ~40 mL water with some sonication and gentle heat (<50 ºC). 20 mg di-Pt (1:1 mole ratio) was added left to stir overnight at RT. The solution was then rotary evaporated to dryness and ^{1}H NMR in D_2O used to confirm encapsulation.

Preparation of 2,2'-(alkylene-1,6-diyl)diisoquinolium (K6) K6 is a fluorescent organic dye which can be encapsulated by CB[6]. 2.4 mL isoquinoline was heated to 85 ºC in 50 mL dioxane. 1.6 mL 1,6-dibromohexane was added and the reaction refluxed at 100-102 ºC for five hours. The heat was removed and the reaction left to stir overnight at RT. A white precipitate was collected over 0.22 µm nylon filter paper and washed with diethyl ether. A ^{1}H NMR was obtained, confirming the presence of impurities, including dioxane. Pure crystals were obtained from an EtOH solution by solvent exchange with diethyl ether. Single crystal X-ray diffraction was carried out on a product crystal.

Preparation of K6@CB[6]: The crystalline product (27.5 mg), known as K6, was stirred in 75 mL H_2O at 54 ºC with 50 mg CB[6] (1:1 mole ratio). The heat was removed after one hour and the reaction left to stir overnight. The solution was then rotary evaporated to dryness and a ^{1}H NMR obtained in D_2O.

4.3.3 Preparation of gels prior to lyophilisation

Hydroxypropyl methylcellulose gels were prepared by dissolving the required amount of di-Pt, di-Pt@CB[7], K6 or K6@CB[6] in NaCl solution at 80-90 ºC. Hydroxypropyl methylcellulose powder (Grade K4MP) was added and stirred until homogenous. Cold NaCl solution was then added to produce 2% (w/w) HPMC gels. These were stirred with an overhead stirrer for 20 min before incubation at 4 ºC overnight to allow removal of air bubbles created by stirring. The gels were then pipetted into microcentrifuge tubes or disc moulds, as described previously (*see Chapter 2*). Disc formulations were prepared for assays where the irregular shape of the insert would introduce excessive error when comparing formulations. In these

instances, a more regular shape with two flat surfaces allowed for simplified and reproducible positioning of the formulation.

4.3.4 Lyophilisation of the formulations

Lyophilisation of nasal inserts and discs was carried out on a Christ Epsilon freeze dryer. Two methods were used, which are described below (Table 4.1 and Table 4.2). Method 2 was developed to overcome issues relating to meltback which emerged during the project. After lyophilisation, inserts and discs were stored in a desiccator at room temperature until required.

Table 4.1. Freeze drying method, "Method 1" for Christ freeze dryer.

Method 1					
	Step	**Time (hours)**	**Shelf temp (ºC)**	**Vacuum (mbar)**	**Safety pressure (mbar)**
1	Load		+ 20	-	-
2	Freeze	01:00	- 30	-	-
3	Freeze	01:00	- 40	-	-
4	Freeze	01:00	- 50	-	-
5	Freeze	02:00	- 60	-	-
6	Main Dry	10:00	+ 10	0.16	1.65
7	Main Dry	10:00	+ 15	0.055	1.65
8	Main Dry	04:00	+ 20	0.055	1.65
9	Final Dry	00:10	+ 25	0.011	1.65

Table 4.2. Freeze drying method, "Method 2" for Christ freeze dryer.

Method 2					
	Step	**Time (hours)**	**Shelf temp (ºC)**	**Vacuum (mbar)**	**Safety pressure (mbar)**
1	Load		+ 20	-	-
2	Freeze	01:00	- 30	-	-
3	Freeze	01:00	- 40	-	-
4	Freeze	01:00	- 50	-	-
5	Freeze	02:00	- 60	-	-
6	Main Dry	10:00	+ 2	0.16	1.65
7	Main Dry	10:00	+ 5	0.055	1.65
8	Main Dry	04:00	+ 10	0.055	1.65
9	Final Dry	00:10	+ 25	0.011	1.65

4.3.5 Analytical techniques

Single crystal X-ray diffraction (XRD): Crystals of K6 were coated in mineral oil and mounted on glass fibres. Data were collected at 123 K on a Bruker Nonius Apex II CCD diffractometer using monochromated Mo/Kα radiation. The heavy atom positions were determined by Patterson methods and the remaining atoms located in difference electron density maps. Full matrix least-squares refinement was based on F^2, with all non-hydrogen atoms anisotropic. While hydrogen atoms were mostly observed in the difference maps, they were placed in calculated positions riding on the parent atoms and were refined isotropically. The structure solution and refinement used the programs SHELX-86,[32] SHELX-97 and the graphical interface WinGX.[33] Absorption corrections made with SADABS (Sheldrick, G.M., 2001, Version 2.03. Bruker AXS Inc.), and figures generated using Mercury 1.4.2 (Build 2).

Dynamic vapour sorption (DVS): Dynamic vapour sorption experiments were carried out on a DVS 1000 (Surface Measurement Systems, Cheshire, UK) running on DVSWin software and data analysed in DVS Data Analysis Suite running in Microsoft Excel 97. The controlled cycle of RH started with a drying phase at 0% to remove any residual moisture. Relative humidity was raised incrementally to 95% whilst maintaining an atmospheric temperature of 25 ºC. The cycle was then reversed, with RH decreasing to 0% before repeating. Progression to the next step was allowed when the sample weight remained constant (weight change over 20 min less than 0.002 mg min^{-1}) or if the maximum step time (999 min) had been reached. Due to the length of time the samples took to run (exceeding one week) only one of each was examined and a quarter of a lyophilised disc was used each time. Samples were stored in a desiccator prior to use and carefully quartered using a scalpel immediately before loading.

Differential scanning calorimetry (DSC): DSC was carried out under a nitrogen environment in a Mettler Toledo DSC822e, operating with a TS0801 RO Sample

Robot (Mettler-Toledo, Leicester, UK). Samples of 2-6 mg were examined in aluminium pans with pierced lids. Thermal transitions were examined by heating linearly from 25-400 ºC at a rate of 10 ºC per minute. Data analysis was performed using Mettler STARe software.

UV distribution analysis: UV calibration curves were obtained for both free di-Pt and di-Pt@CB[7] in PBS (pH 7.4) with added K4MP HPMC. These were then used to quantify the species in various solutions. Distribution of the di-Pt in inserts was assessed by carefully slicing the inserts (*n*=3) into three segments (tip, middle and bottom). These segments were carefully weighed before being dissolved up to 10 mL with PBS. The samples were analysed on a Varian Carey 50 Bio UV-visible spectrophotometer scanning between 200-300 nm, operating with Carey WinUV software. Absorbance readings for free di-Pt were recorded at 219 nm (λ_{max}). Absorbance for di-Pt@CB[7] were recorded at 234 nm (λ_{max}). All samples were analysed in multiple (*n*=3). Data were exported as ASCII files and processed with Microsoft Excel 2010. Concentration of di-Pt/di-Pt@CB[7] per mg of insert was then calculated for each section.

Fluorescence distribution analysis: Fluorescence calibration curves were obtained for both free K6 and K6@CB[6] in PBS (pH 7.4) following addition of K4MP HPMC. Samples were analysed with $\lambda_{excitation}$=252 nm and $\lambda_{emission}$=378 nm (K6) or $\lambda_{emission}$=364 nm (K6@CB[6]) was recorded.

Franz cell release: Release of drug or dye from the inserts was assessed using borosilicate glass Franz cells with flat ground joints, stirred using a V6A stirring unit (Figure 4.6 and Figure 4.7; PermeGear Inc., Hellertown, PA, USA). Connected to a pump, this system maintained a constant temperature water jacket around the release medium and stirred each of the cells independently. The release medium was equilibrated to 33 ºC for 30 min, and cellulose filter paper (45 mm diameter, Grade 1, Whatman) clamped between the donor and receiver chambers. The system was sealed with paraffin film and allowed to equilibrate for a further 10 min. A nasal insert was then placed in each donor chamber on top of the filter paper (*n*=3) and the

chambers re-sealed to maintain the moist atmosphere. Samples of 0.8 mL were extracted from the receiver chambers at timed intervals and the volume replaced immediately with fresh medium. Samples were analysed by UV-vis spectroscopy, fluorescence spectroscopy or inductively coupled plasma mass spectrometry.

For *ex vivo* studies the filter paper was replaced with a section of freshly excised porcine nasal mucosa, removed within four hours of slaughter. Immediately after excision, the tissue was fixed to the flat ground joint of the donor chamber with cyanoacrylate gel to create a sealed donor chamber with the mucosa side in contact with to dosage form. Once in place, the joint was sealed with parafilm and clamped.

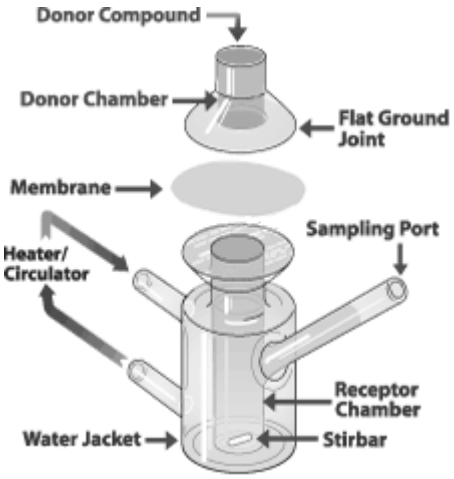

Figure 4.6. Diagram of a Franz cell. The donor chamber is separated from the receptor chamber by a synthetic or *ex vivo* membrane. Samples are removed from the receptor chamber *via* the sampling port.[34]

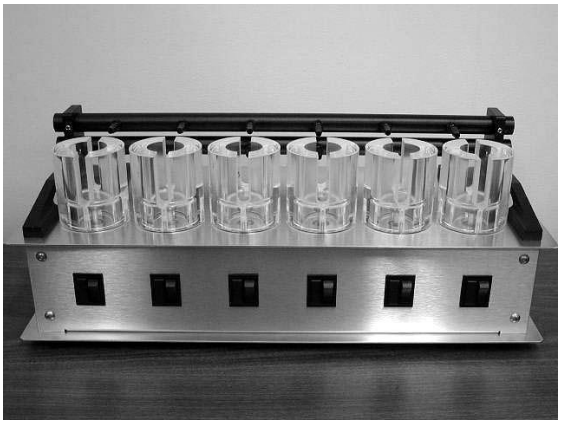

Figure 4.7. The PermeGear V6A stirrer. Each of the six acrylic holders houses a Franz cell.[34]

Inductively coupled plasma mass spectrometry (ICP-MS): Quantification of platinum was carried out using an Agilent 7700x Inductively Coupled Plasma-Mass Spectrometer. The instrument was optimised to yield maximum sensitivity for platinum, which was measured at *m/z* 195. Samples were prepared for analysis in 2% HCl.

For instrumental specifications and methods relating to scanning electron microscopy, thermogravimetric analysis, dynamic adhesion study on agar/mucin (formulation spread), moisture uptake, ex vivo mucoadhesion and statistical analysis, see section 3.6. For nuclear magnetic resonance, see section 2.4.

4.4 RESULTS AND DISCUSSION

4.4.1 Synthesis and encapsulation of *trans*-[{PtCl(NH_3)$_2$}$_2$μ-dpzm]$^{2+}$

Trans-[{PtCl(NH_3)$_2$}$_2$μ-dpzm]$^{2+}$ (di-Pt) was synthesised from transplatin and dpzm linker as per a method published by Wheate (Figure 4.8).[7] Purification of the product by fractional precipitation from water with acetone furnished di-Pt (*m*/*z*=677 by electrospray mass spectroscopy) with a 24% yield. This yield may be improved by more careful and selective precipitation and removal of impurities, although this may result in reduced purity of the product. Analysis by ^{1}H NMR in D_2O showed resonances at 7.69 ppm (s, pyrazole H3), 7.74 ppm (s, pyrazole H5) and 3.82 ppm (s, -CH_2-), consistent with the di-Pt product reported by Wheate.[7]

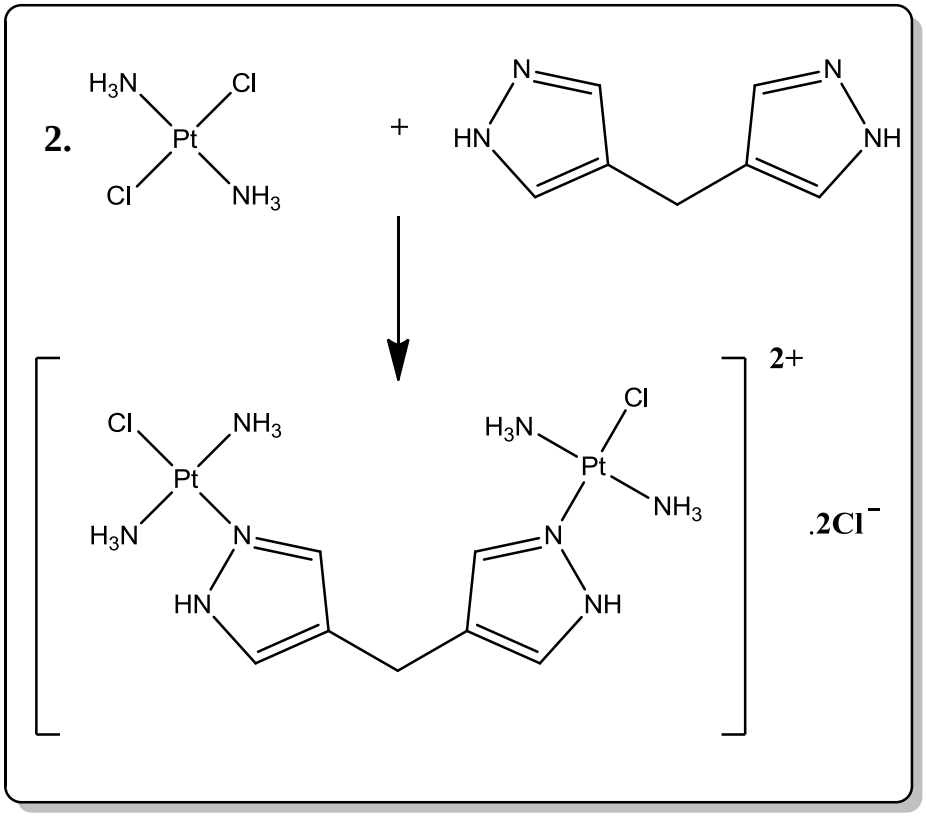

Figure 4.8. Di-Pt is synthesised from transplatin and dpzm (2:1 ratio).

The isolated di-Pt was encapsulated within CB[7] and the product analysed by ^{1}H-NMR in D_2O (Figure 4.9). The NMR spectrum for di-Pt shows the aromatic H3 and

H5 protons of the dpzm linker to be nearly equivalent, at around 7.7 ppm. The NMR spectrum of the di-Pt@CB[7] product retained the peaks for CB[7], and showed a non-equivalent shift in the H3 and H5 protons of the dpzm linker (7.34 and 6.26 ppm). Additionally, the resonance for the -CH_2- protons shifts from 3.82 ppm to 2.91 ppm. These shifts are consistent with a 1:1 host:guest complex, where the dpzm moiety nests inside the cavity of CB[7] with the platinum nuclei sitting just outside the portals. In this conformation, the H3 and H5 protons are experiencing different magnetic environments and the shifts on the NMR spectrum become non-equivalent. This inclusion is driven by the hydrophobic effect and stabilised by six hydrogen bonds.[35]

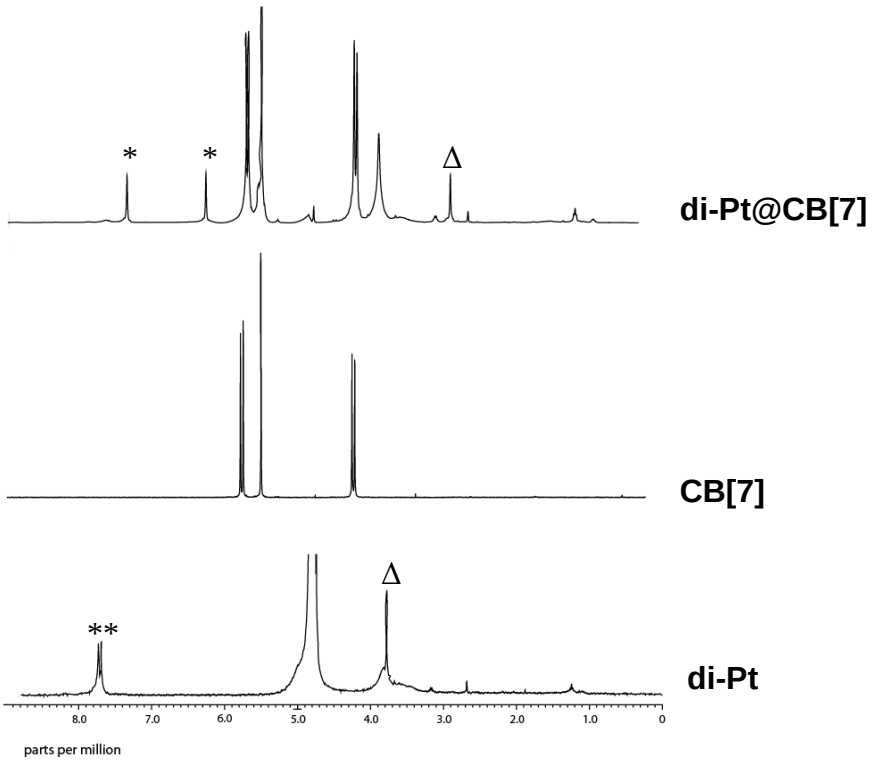

Figure 4.9. ^{1}H NMR spectra of di-Pt, CB[7] and di-Pt@CB[7]. The H3 and H5 protons (*) of the dpzm ligand experience different magnetic environments due to the encapsulation and experience non-equivalent upfield shifts. The -CH_2- protons (Δ) are inside the CB[7] cavity and also experience shielding, evident from the upfield shift.

4.4.2 Synthesis and encapsulation of K6

2,2'-(alkylene-1,6-diyl)diisoquinolium (K6) is an organic fluorescent dye which fits inside CB[6].[36] K6 was synthesised from isoquinoline and 1,6-dibromohexane in dioxane (Figure 4.10) and the crude product was washed with diethyl ether.

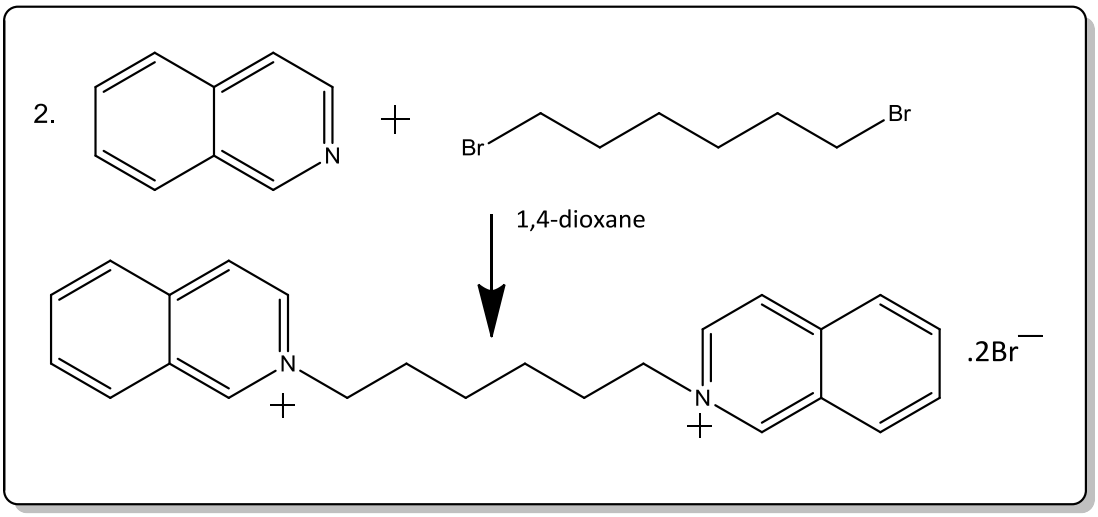

Figure 4.10. Reaction scheme for the synthesis of K6.

To remove residual dioxane, the product was purified by recrystallisation from EtOH using solvent exchange with diethyl ether. ^{1}H NMR of K6 (see Figure 4.11) δ: 9.46 ppm (s, -CH**g**); 8.27 ppm (d, -CH**a**); overlapping multiplets at ~8.16, ~8.03 and ~7.43 ppm (-CH**f**, -CH**b** and –CH**c**, -CH**e** and -CH**d**); 4.52 ppm (t, -CH_2**h**), 1.90 ppm (m, -CH_2**i**) and 1.22 ppm (m, **j**). The structure of the product was confirmed using X-ray diffraction of a single crystal (Figure 4.12).

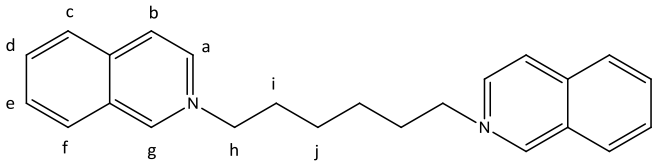

Figure 4.11. The structure of K6, with protons numbered for ^{1}H NMR data. Charges are omitted for clarity.

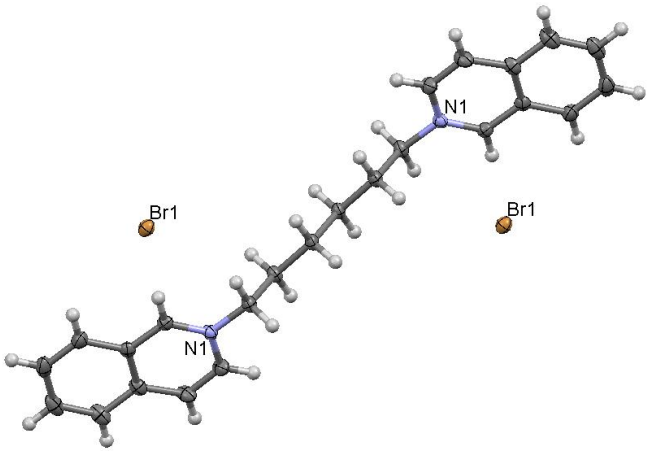

Figure 4.12. The structure of K6, elucidated from X-ray diffraction of a single crystal, shown as the bromide (as synthesised).

Subsequent encapsulation of K6 in CB[6] was confirmed by ^{1}H NMR (Figure 4.13). The proton resonances for the alkyl moieties (resonances labelled **h**, **i** and **j**) experience an upfield shift, consistent with increased shielding resulting from encapsulation inside the CB[6] cavity. The resonances for the aromatic isoquinoline protons which neighbour the nitrogen experience a downfield shift, this is consistent with being outside of the cavity, near to the portals and therefore experiencing a deshielding effect.[25]

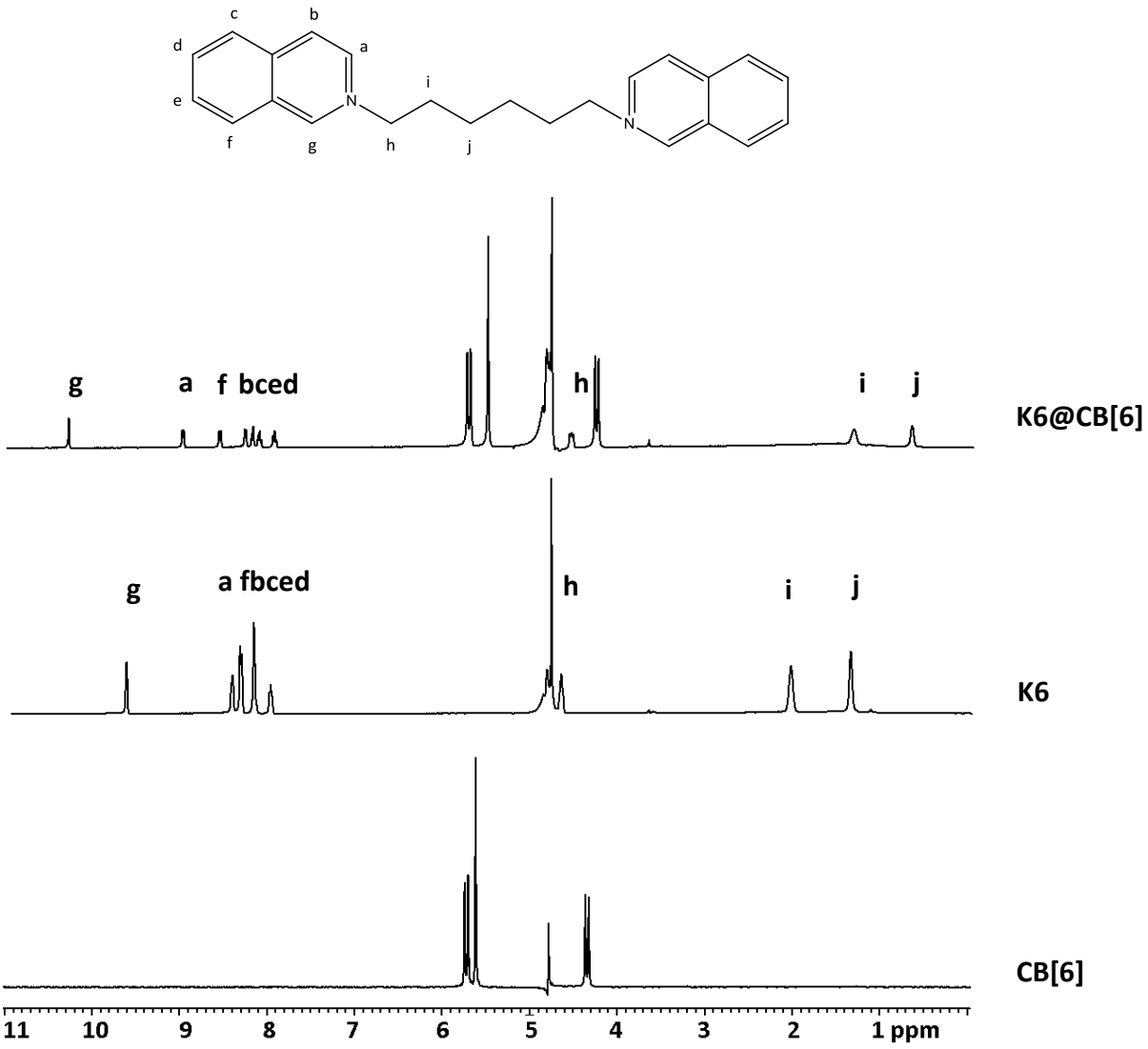

Figure 4.13. NMR spectra of CB[6], K6 and K6@CB[6]. After encapsulation, the alkyl resonances i and j experience an upfield shift and the aromatic resonances nearest the portals experience a downfield shift.

4.4.3 Thermal analysis of host-guest complexes

Differential scanning calorimetry is used routinely to analyse product stability in the pharmaceutical industry.[37] It can detect melting, crystallisation, sublimation, dehydration, desolvation, glass transitions and polymorphic transitions. Melting is an endothermic process whereby the sample being tested takes in heat. This is recorded as an endotherm (downward pointing peak) on the DSC trace. Crystallisation is an exothermic event which would be recorded as an upward

pointing peak. The peak melting temperatures (T_m) were measured for di-Pt, di-Pt@CB[7], K6, K6@CB[6], CB[6] and CB[7].

The CB[6] and CB[7] showed no thermal events (apart from some water loss) from 25 ºC until the cucurbiturils begin to decompose at around 370 ºC. For di-Pt alone, there were no major thermal events in this temperature range (Figure 4.14), but there was a shift from the baseline around 180-360 ºC, which indicates a shift in heat capacity, possibly as a result of a glass transition. When encapsulated in CB[7], however, there are no deviations from the baseline after the water loss, until the CB[7] itself begins to decompose at around 370 ºC. This data indicates that encapsulation of di-Pt in the CB[7] has improved the thermal stability of di-Pt.

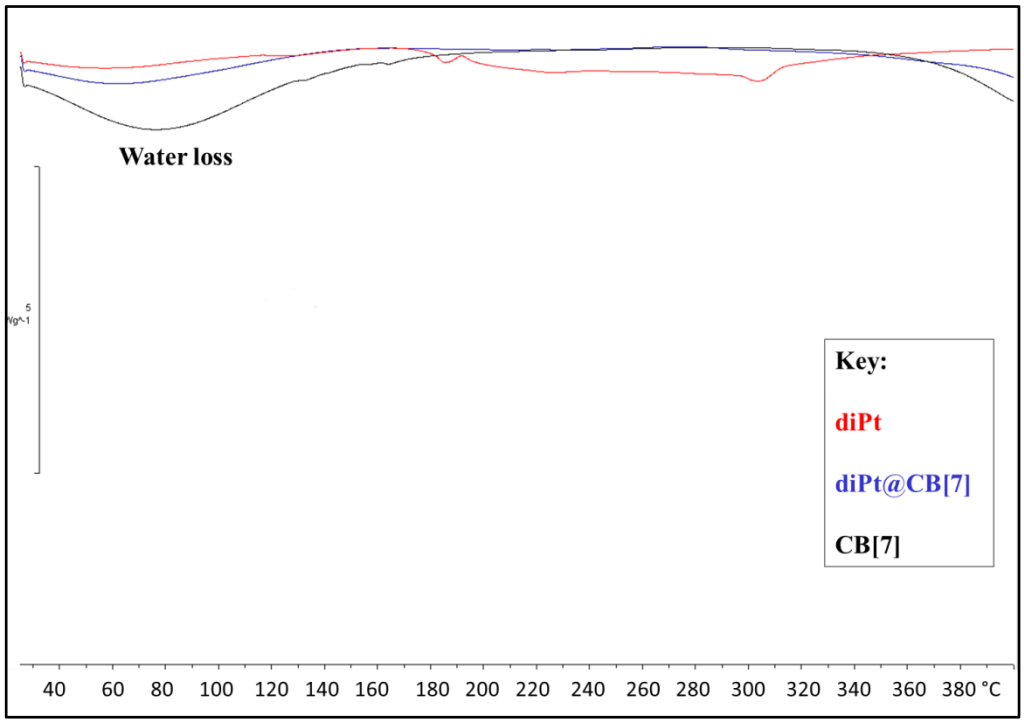

Figure 4.14. DSC trace for di-Pt, di-Pt@CB[7] and CB[7], showing that encapsulation of di-Pt in CB[7] has improved its thermal stability.

The result for K6 was more apparent. The K6 produced an endotherm upon heating with an onset around 40 °C, this was probably desolvation of residual dioxane (Figure 4.15). After this, it showed a melt with T_m=234 °C, immediately followed by a second endotherm, possibly indicating a reduction of the dye (Figure 4.15). Once

encapsulated in CB[6] however, after desolvation/water loss, there are no thermal events until the CB[6] itself starts to decompose. This indicates that encapsulating K6 inside CB[6] improves its thermal stability.

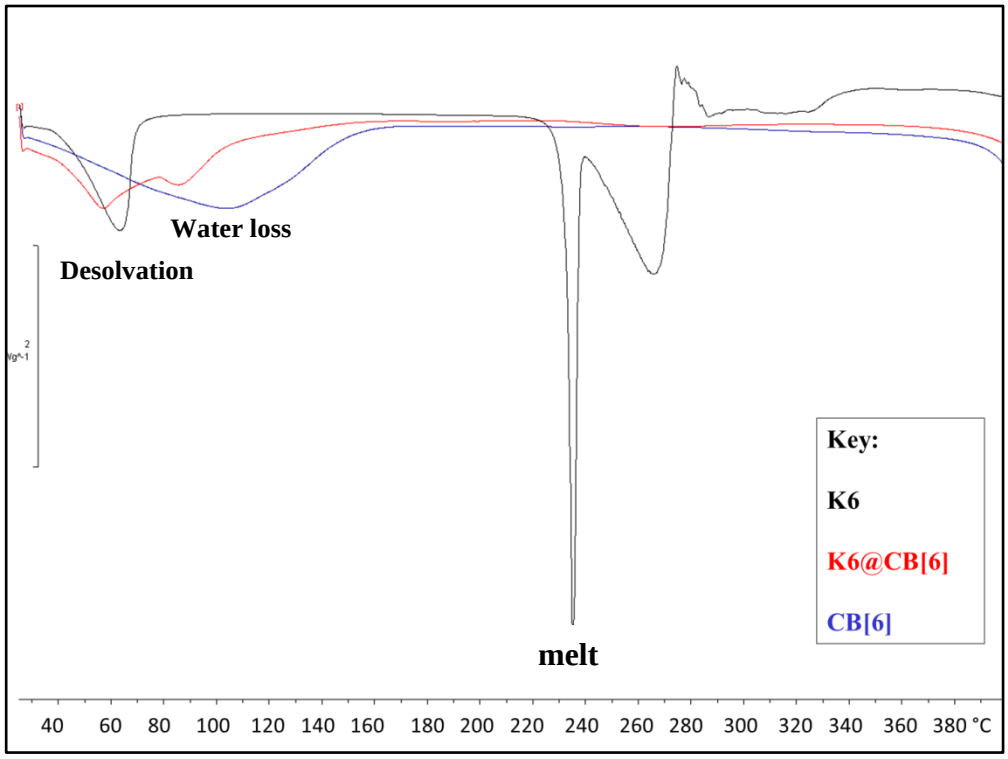

Figure 4.15. DSC trace for K6, K6@CB[6] and CB[6]. The free K6 had a peak melt temperature at 234 °C. Once encapsulated in CB[6], the baseline remains constant until the CB[6] begins to decompose.

Both CB[6] and CB[7] have improved the thermal stability of a guest molecule, showing that they both act as protecting agents for the guest. Similar enhanced thermal stability of ranitidine in CB[7] has been reported by others.[38] The K6@CB[6] and di-Pt@CB[7] complexes were subsequently formulated into lyophilised nasal inserts and discs and subject to a number of assays to determine whether or not CB[6] and CB[7] affected the distribution and/or release of the guest molecules from the formulation.

4.4.4 Thermal analysis of nasal insert formulations

When the nasal insert formulations containing K6 and K6@CB[6] were analysed by TGA, no useful data could be obtained as the HPMC began to degrade before any peaks could be observed. However, it was interesting to note that once heated to 200 ºC, the insert containing only K6 showed a colour change from white to pink, where the insert containing K6@CB[6] showed no colour change (Figure 4.16). This indicated that even in the lyophilised insert formulation, the K6 is more stable when encapsulated in CB[6]. Increased thermal stability of drugs encapsulated in CB[*n*]s has also been reported by Wang and McCartney who reported increased thermal stability of ranitidine in CB[7].[38] The formulations containing di-Pt and di-Pt@CB[7] were not examined.

Figure 4.16. Photographs of the samples after TGA analysis. The formulation containing K6 (left) had turned pink. The insert containing K6@CB[6] remained white (right).

Inserts were also tested to see if the encapsulation affected the drug distribution, moisture uptake, spread, and/or mucoadhesion of the formulation, as well as release of the drug/dye molecule from the formulation.

4.4.5 Determining whether or not encapsulation affects drug distribution

In order to have consistent dosing and drug release from a pharmaceutical formulation, the drug must be evenly distributed throughout the dosage form.

Spectroscopic methods were applied in order to determine whether or not encapsulation in CB[6] and/or CB[7] affected the distribution of their guest molecule. Inserts containing one of the following: di-Pt, di-Pt@CB[7], K6 or K6@CB[6]; were carefully sliced into three sections: tip, middle and bottom (n=6). These segments were accurately weighed before being dissolved in PBS and made up to 5 mL in volumetric flasks. Samples containing di-Pt were analysed by UV-vis spectroscopy. Samples containing K6 were analysed by fluorescence spectroscopy.

The data were analysed by dividing the emission or absorption reading by the weight of the original insert section. This normalised absorption/emission was then taken as a percentage of the total emission/absorption (per mg) for the whole insert (Figure 4.17). For di-Pt, the average distribution of the dose was: **34.1% tip**, **33.3% middle** and **32.6% bottom**. As the inserts are freeze dried vertically and upside-down with the tip pointing downwards, the slight increase from bottom to tip suggests that there may be some settling of the drug before the gel is frozen. When encapsulated in CB[7], the average distribution improves: **33.3% tip**, **33.2% middle** and **33.5% bottom**, although this improvement is not significant.

This effect was more pronounced between K6 and K6@CB[6] (Figure 4.17). Free K6 showed the following average distribution: **73.1% tip**, **18.1% middle** and **8.8% bottom**; displaying a much more pronounced accumulation towards the tip. The complex K6@CB[6] showed the following, improved distribution: **45.4% tip**, **29.4% middle** and **25.2% bottom**. This showed that encapsulation in CB[6] significantly improved the distribution profile of K6 in the inserts (P_{tip}=0.002, P_{middle}=0.000 and P_{bottom}=0.000, paired t-test).

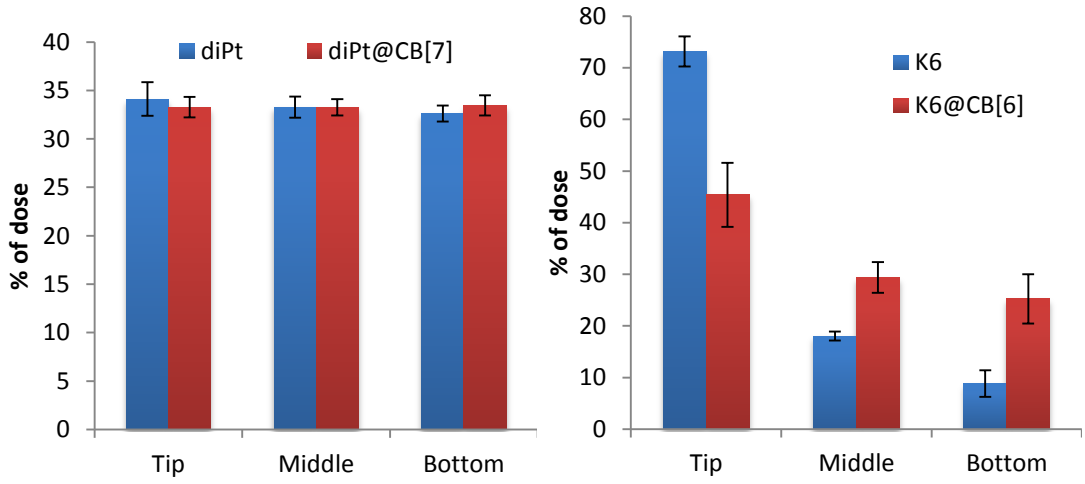

Figure 4.17. Graphs showing the distribution of a) di-Pt, and b) K6, in lyophilised inserts. Encapsulation in CB[6] improves the average distribution profile (*n*=6). Error bars represent standard deviation.

In these cases, both CB[6] and CB[7] have stabilised the dispersion of their guest molecules. Although CB[6] has improved the dispersion of K6 to a greater degree than CB[7] has di-Pt, this is influenced by the fact that free di-Pt shows a more even distribution than free K6 in the first place. The distribution of the compounds in the lyophilisate is likely related to their solubility in the HPMC gel. The less soluble they are, the more likely they are to precipitate and sediment towards the tip.

The tests that followed were carried out to ascertain how encapsulation of K6 and di-Pt affected the physical properties of the final lyophilised dosage form.

4.4.6 Determination of the effect of encapsulation on moisture uptake

Lyophilised inserts containing either di-Pt or di-Pt@CB[7] were examined for moisture uptake in SNES (*n*=6). For the first 220 min the weight gain, representing moisture uptake, was similar (Figure 4.18). This indicated that encapsulating di-Pt in CB[7] did not affect the behaviour of the insert in terms of moisture uptake in this buffer. This would suggest that *in vivo*, the two formulations would wick up moisture and gel at a similar rate.

The experiment was repeated for inserts containing either K6 or K6@CB[6] in order to determine if the encapsulation of K6 in CB[6] affected the inserts' moisture uptake behaviour. In this case, the K6@CB[6] displayed reduced moisture uptake capacity, with significantly less moisture uptake over the duration of the study (f_2=-38.596, Figure 4.18). This indicated that encapsulation of K6 in CB[6] acted to reduce the moisture uptake capacity of the lyophilised inserts. This would suggest that *in vivo*, the formulation will not gel as rapidly, potentially affecting mucoadhesion. Whilst this may be detrimental, it may also prevent overhydration which would be detrimental to overall residence time. If CB[6] encapsulation resulted in insufficient moisture uptake, another hydrophilic excipient, such as microcrystalline cellulose, could be included. Alternatively, using a different grade of HPMC with more rapid water uptake characteristics could be explored.

In these examples, CB[6] and CB[7] encapsulation do not affect the formulations in a similar manner. Therefore K6@CB[6] is not a suitable model for di-Pt@CB[7] when considering moisture uptake.

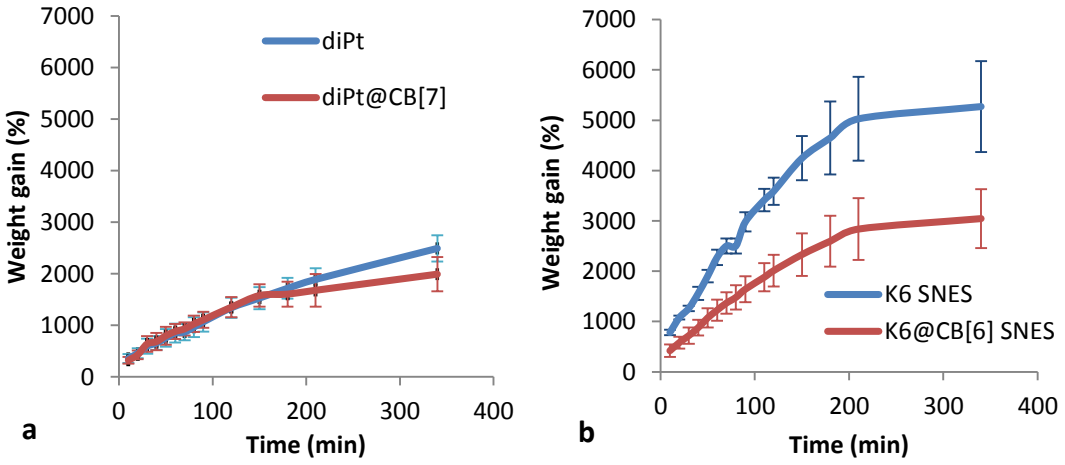

Figure 4.18. Graphs showing the moisture uptake (SNES) of inserts containing: a) di-Pt and di-Pt@CB[7]. For the first 200 min, the uptake is similar; and b) K6 and K6@CB[6]. The inserts containing K6@CB[6] take up less moisture across the entire timescale (*n*=6).

4.4.7 Determining whether or not encapsulation affects formulation spread

If the uptake of moisture is reduced, the hydration of the insert may be compromised. This would reduce the mobility of the HPMC chains and subsequent surface area covered by the gelled formulation, ultimately reducing the bioavailability of the drug dose. In order to examine the gelling and subsequent spread of the inserts, and determine if this is affected by encapsulation in CB[*n*], an agar/mucin spread study was carried out.

Whilst encapsulation of K6 in CB[6] acted to reduce the moisture uptake capacity of the formulation, the agar/mucin experiment indicated previously that encapsulation of K6 in CB[6] produced no significant effect on the spread of the formulations (Figure 4.19). This suggests that this reduction in moisture uptake does not ultimately affect formulation spread.

In the case of di-Pt and di-Pt@CB[7], encapsulation was shown to have no effect on moisture uptake in the previous sponge test (Figure 4.18). However, encapsulation of di-Pt in CB[7] acted to increase the distance travelled by the fully-gelled formulation (Figure 4.19). Whilst the K6@CB[6] inserts took on less moisture than the K6 inserts, the fact that the spread of the formulation was not significantly affected (f_2=51.9, equivalent) suggests that any extra moisture in the K6 formulations may have been redundant in the gelation process, possibly acting counter-productively as a diluent. In the case of di-Pt and di-Pt@CB[7], there was no significant difference in the moisture uptake upon encapsulation but the di-Pt@CB[7] formulation spread further. This suggests that the formulations containing CB[*n*] may have been able to gel more efficiently than the non-encapsulated di-Pt/K6 formulations. This suggests that the formulation was able to use the absorbed moisture more effectively, creating a more efficient gel, and is in agreement with the theory discussed in Chapter 3, whereby CB[*n*]s can aid the penetration of water through the insert allowing more rapid gelling. This theory was however rationalised by the formation of CB[*n*] stacks forming channels through which water could ingress, as well as hydrogen bonding between the CB[*n*] and the

absorbed water. The presence of a guest molecule within the cavity of the CB[*n*]s may make water channels unlikely in this situation. Instead, it is possible that the carbonyl-rimmed portals of the CB[*n*]s remain sterically unencumbered enough to permit hydrogen bonding to water molecules, effectively pulling it through the formulation and improving hydration and gel formation. Others, including Yi and colleagues, have previously reported crystal structures wherein CB[*n*]s hydrogen bond to multiple water molecules whilst encapsulating a guest molecule.[39] Additionally, it is possible that if the CB[*n*] is still able to hydrogen-bond with a guest molecule encapsulated, they can still hydrogen bond to hydrophilic groups on the polymer, producing conformational changes[40] in the chain (untangling) during and following hydration. This would allow for greater chain mobility and enhanced spreading.

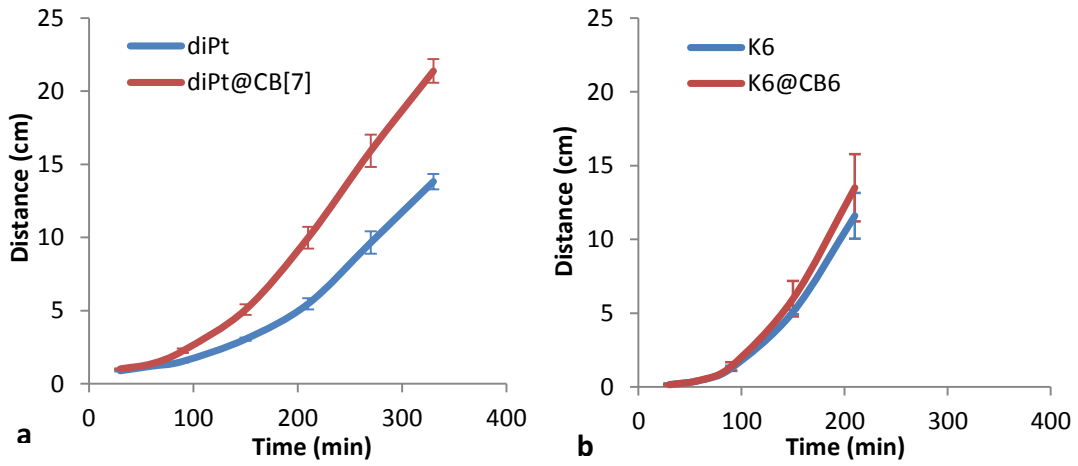

Figure 4.19. Graph comparing the spread of formulations containing: a) di-Pt with di-Pt@CB[7] on agar/mucin plates (*n*=6). The encapsulated form spreads further on the plate; and b) K6 with K6@CB[6] on agar/mucin plates (*n*=6). Data were not recorded after the gel front reached the end of the plate.

The inserts were then examined using the TA to determine whether or not encapsulating K6 and/or di-Pt had an effect on mucoadhesion.

4.4.8 Determining whether or not encapsulation affects mucoadhesion

Disc formulations of K6, K6@CB[6], di-Pt and di-Pt@CB[7] were examined using the mucoadhesive rig on the TA, with excised porcine nasal mucosa. Peak force of

detachment (the maximum force required to break the connection between the disc and the mucosa) and work of adhesion (the area under the force *vs*. time curve) were recorded.

For K6 and K6@CB[6], encapsulation of the dye resulted in an increase in the average, but no significant change, in peak force of detachment (Figure 4.20) and work of adhesion (Figure 4.20). This may have been as a result of large errors resulting from the sample size (*n*=3). In this instance, sample size was limited by the amount of starting materials and porcine tissue available.

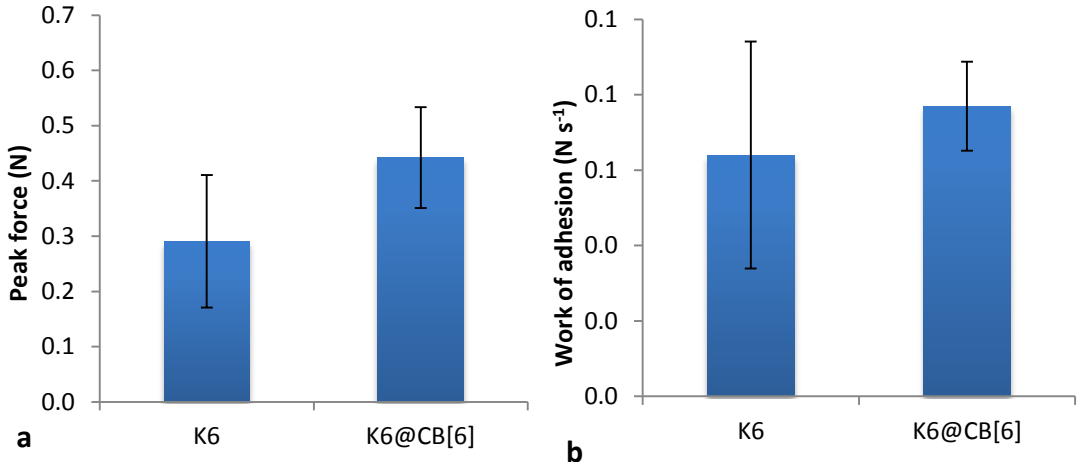

Figure 4.20. Graph comparing the a) peak force of detachment, and b) work of adhesion, for disc formulations containing K6 and K6@CB[6] (*n*=3) from porcine nasal mucosa. There is no significant difference.

In the case of di-Pt and di-Pt@CB[7], the formulations containing the encapsulated form produced an increase in mucoadhesion (Figure 4.21). This was recorded as an increase in both average peak force of detachment and average work of adhesion (*P*=0.003 and *P*=0.014, respectively). This suggests that the inclusion of CB[7] in the formulation may increase the mucoadhesive potential of the formulation. This may be a result of improving the gelling efficiency of the formulation, or through the CB[7] itself acting as a structural component in the gel.

The wettability theory of mucoadhesion considers the physical contact of the polymer with the mucosa as it spreads across the surface penetrating the irregularities

and anchoring itself. Therefore, the increase in mucoadhesion may result from the increased spread of the di-Pt@CB[7] formulation compared to the di-Pt formulation.

Considering the contribution of functional groups, the availability of hydrogen bonding groups in a mucoadhesive polymer has been shown to contribute to mucoadhesion by increasing the total number of non-covalent bonds in the system.[41] The presence of CB[*n*] in the inserts adds hydrogen bonding acceptors to the system, allowing a greater overall sum of non-covalent interactions. This is in line with the adsorption theory of mucoadhesion. When considering these results alongside the water uptake study, the contribution of polymer hydration to mucoadhesion can also be rationalised. Formulations of K6@CB[6] and di-Pt@CB[7] absorbed less water than the K6 and di-Pt counterparts, yet were more mucoadhesive. This indicates that the K6 and di-Pt formulations may have hydrated excessively and mucoadhesion is reduced due to the formation of a slippery mucilage.[42] Additionally, considering the theory that the presence of CB[*n*] in the insert results in detangling of the polymer chain during and following swelling and/or hydration, this may allow more rapid interpenetration of mucin and polymer chains during the contact stage of the mucoadhesion study. This would in turn allow greater entanglement (consistent with the interpenetration theory of mucoadhesion) and non-covalent interaction between the polymer and mucin, enhancing mucoadhesion.

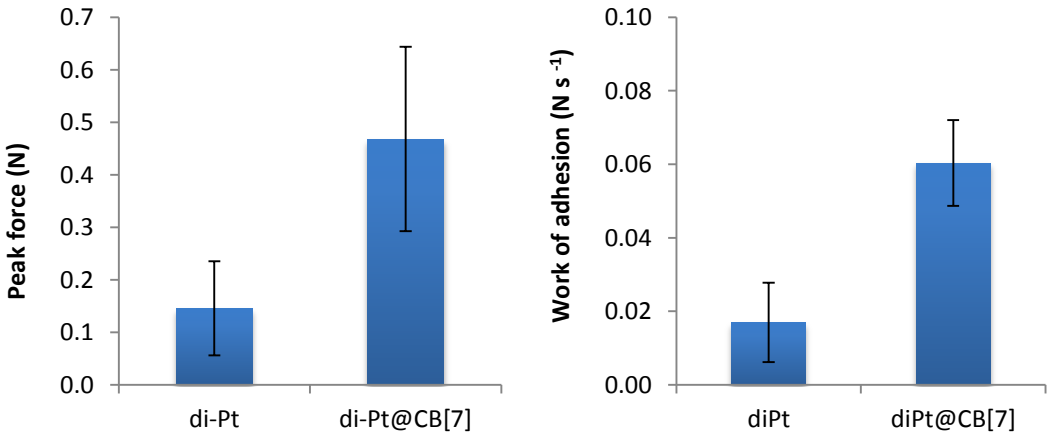

Figure 4.21. Graphs comparing the a) peak force of detachment, and b) work of adhesion, for disc formulations containing di-Pt and di-Pt@CB[7] (*n*=3). The formulation containing the encapsulated form was harder to remove from the mucosa.

Both encapsulation of K6 in CB[6] and di-Pt in CB[7] increased mucoadhesion (although this was not a statistically significant difference with K6). This supports the use of CB[6] as a model for CB[7]. The next step was to determine whether or not the release of K6 or di-Pt from the formulation was affected by encapsulation in a CB[*n*].

4.4.9 Determining whether or not encapsulation affects release

In vitro release of K6 and di-Pt from their respective inserts was modelled using Franz cells containing release medium at 33 ºC. This temperature was chosen to reflect the lower temperature of the nose, compared to an internal body temperature of 37 °C.[43] The donor chamber was separated from the receiving chamber by Grade 1 cellulose filter paper. This paper, with large pore size, was chosen as it would allow the greatest freedom of diffusion between the chambers. 0.8 mL aliquots were removed from the stirring release medium at measured time points and replaced with fresh medium.

The initial release experiment was carried out in PBS and analysed by UV-vis spectroscopy. In this case, release of di-Pt and di-Pt@CB[7] from nasal inserts was equivalent (Figure 4.22, f_2 similarity factor of 51.26).

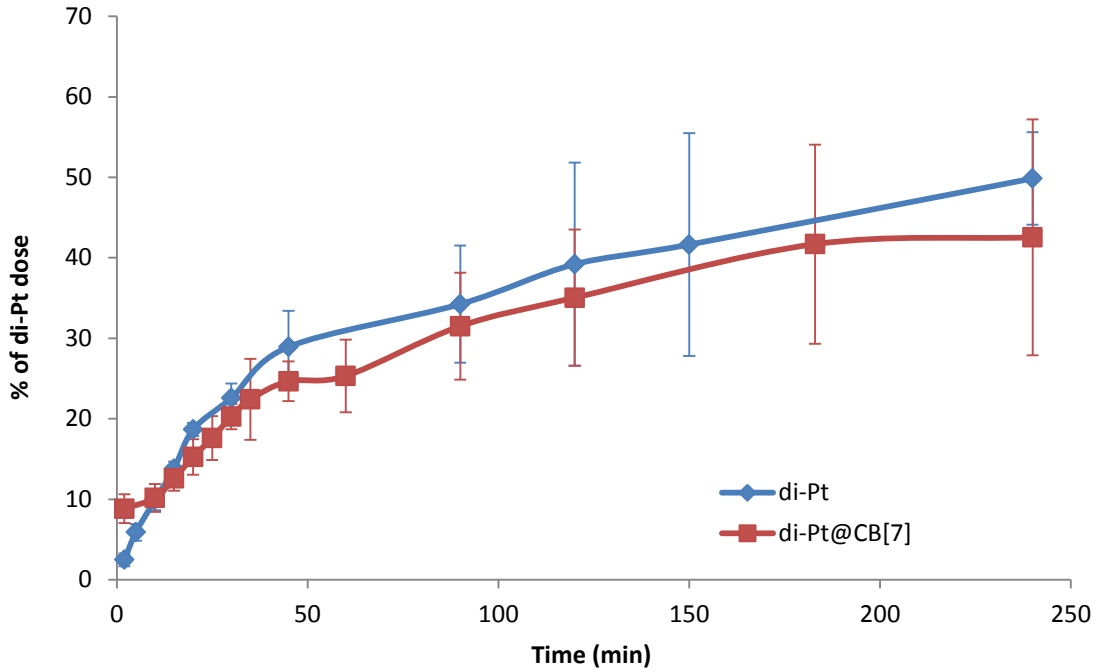

Figure 4.22. Graph comparing the release of di-Pt from inserts containing di-Pt and di-Pt@CB[7], as measured by UV-vis spectroscopy (*n* = 3). Release is equivalent.

Whilst others have carried out similar release studies using PBS as the release medium, it was decided that SNES should also be investigated, as it was presumed that it, along with lowered temperature, would contribute to a more accurate model for nasal drug release.[31]

Three nasal inserts containing K6 and three containing K6@CB[6] were examined. The samples were analysed by fluorescence spectroscopy and concentration of K6 released was calculated using calibration curves obtained for K6 and K6 as a component of K6@CB[6]. Samples were excited at 252 nm and emission was monitored at 378 nm for K6 and 364 nm for K6@CB[6]. Release was plotted as equivalent K6 released (Figure 4.23). From this, it can be seen that encapsulation of K6 in CB[6] is detrimental to the release of K6@CB[6] from the inserts (f_2=5.707, not equivalent). It is possible that this apparent lowered release of K6@CB[6] is due to K6 being freed from the K6@CB[6] complex. As release was only monitored at the wavelength pertaining to the encapsulated form, the total K6 released (free and encapsulated) remains unknown.

The release studies may have benefited from running a sample of the drug/dye without HPMC, a blank HPMC insert, and a blank release cell in parallel to the insert under investigation, as well as accurately measuring the full dose by fluorescence spectroscopy and presenting the release data as %.

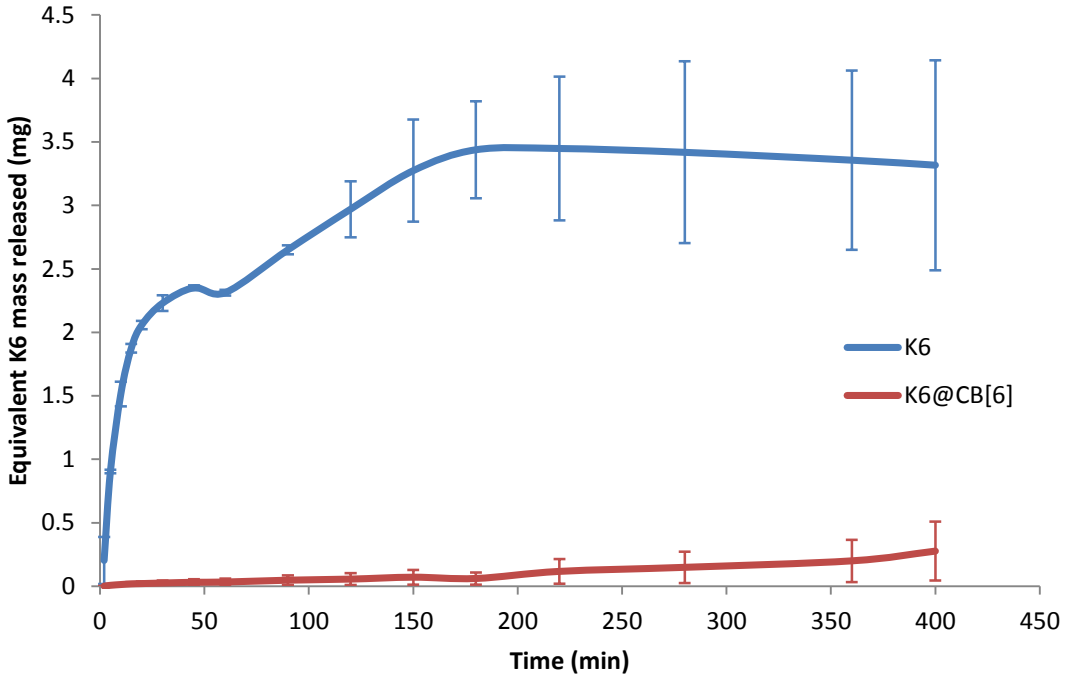

Figure 4.23. Graph comparing the release of K6 from nasal insert formulations (*n*=3). The blue line represents release from inserts containing free K6. The red line represents the mass of K6 released in the encapsulated form.

The release of di-Pt and di-Pt@CB[7] was then modelled, with the same experimental parameters. In an effort to overcome analytical problems associated with the free and encapsulated forms of di-Pt, along with any aquation products, ICP-MS was used to analyse the samples. This technique has proven useful for the detection and quantification of heavy metals in pharmaceuticals, and allows for direct measurement of the amount of platinum in the samples, rather than one particular species of platinate.[44]

Samples were prepared for analysis by diluting 500 µL of the sample with 2,500 µL of 4% HCl and making up to 5 mL with water. This produced a 10× dilution in 2% HCl, bringing the samples within the detection limits of the instrument, and providing adequate sample volume for automatic sampling. Three full inserts were also analysed in order to obtain a reading for 100% dose. Data obtained after 60 min were unreliable due to analyst error, and have been excluded from discussion.

Release of di-Pt@CB[7] from the nasal inserts was significantly lower than di-Pt (Figure 4.24, f_2=39.593). This suggests that encapsulation in CB[7] is detrimental to the release of di-Pt from nasal inserts. This is similar to the effect of CB[6] encapsulation on K6, and may be as a result of the increased hydrogen bonding network in the polymer providing resistance against diffusion of the drug or dye through the gel and into the release medium. It is known that changes to mucus structure can affect the diffusivity of a drug and subsequent bioavailability and so this may also be the case for the mucoadhesive polymer itself.[45]

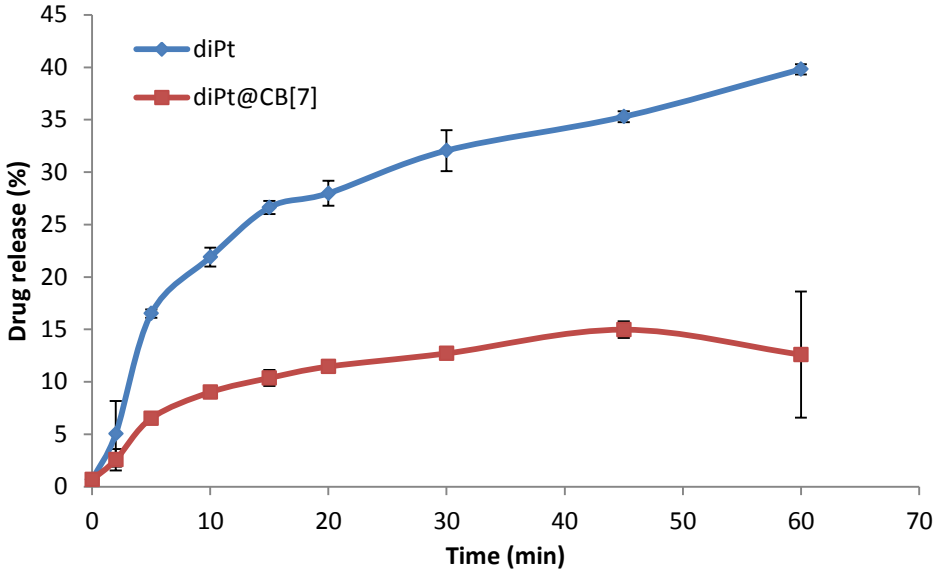

Figure 4.24. Graph comparing the release of di-Pt and di-Pt@CB[7] from nasal inserts (*n*=3). Data obtained after 60 min are not shown.

Whilst these encapsulations have been apparently detrimental to drug release from the nasal insert, studies by others have shown that formulations which release fastest

can give lowest tissue levels. For example, Charrois and colleagues found that liposomal formulations of doxorubicin with slowest rates of release produced the highest drug concentrations in tumours, and best therapeutic activity of the formulations tested.[46] Whilst extending drug release from a nasal dosage form may not be preferable due to MCC, these results suggest that CB[*n*]s may be useful in extended release formulations. Further investigation of this possibility is warranted.

Additionally, it has been shown that the release medium affects the release rate from the nasal insert formulations. Lapidus and Lordi have shown that salts reduce the activity of water, retarding hydration of the matrix and resulting in decreased drug release.[47] However, when salt concentration is increased beyond a certain point, the massive reduction in water activity prevents uniform hydration of the matrix resulting in irregular gel structure. This can lead to dose dumping.[47] Release media should therefore be chosen to reflect the physiological conditions as closely as possible.

Furthermore, the disparity between the results of the di-Pt/di-Pt@CB[7] release in SNES and PBS could be further rationalised by giving consideration to the pH of the release medium (assuming the analytical method was not an influence). The release in PBS (pH 7.4, *see Figure 4.22*) was not affected by the presence of CB[7] but the release in SNES (pH 5.5, *see Figure 4.24*) was significantly reduced. This can be rationalised by considering the electrostatic association of H^+ to the carbonyl portals of CB[7] in the acidic SNES environment, acting to improve structural integrity of the system and therefore slowing the release. In the higher pH environment of PBS, there is higher concentration of OH^- ions which repel the carbonyl portals, introducing structural weakening. This could then lead to breakdown of the HPMC-CB[7] matrix, increasing the rate of drug release. A similar phenomenon has recently been reported by Lin and colleagues, who have developed a supramolecular gel based on chitosan derivatives with CB[8] acting as a non-covalent cross-linker. Release from this gel has been shown to be pH responsive.[48] In order to confirm, this would need to be repeated in buffers with different pH but similar electrolyte composition.

4.4.10 Determining whether or not encapsulation affects release through tissue

Modifying the Franz cell release apparatus by replacing the filter paper with a section of porcine nasal tissue allowed for the examination of release through nasal tissue. In these experiments, the release medium was PBS pH 7.4, chosen to mimic the bloodstream. Porcine tissue was fixed to the ground glass joint of the donor chamber using cyanoacrylate glue (Figure 4.25). Once the glue was dried, excess tissue was cut away. The donor chamber was placed onto the receiving chamber and the joint sealed with parafilm before being clamped in place. 0.5 mL of medium was placed in the donor chamber to keep it moist and the chamber sealed with parafilm and wrapped in aluminium foil.

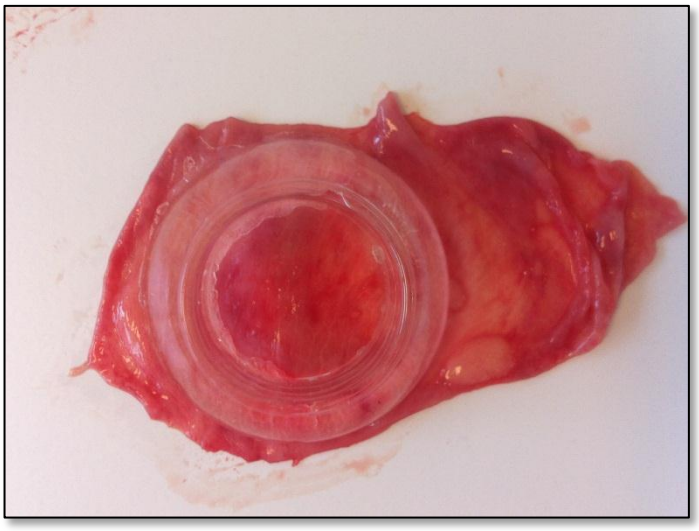

Figure 4.25. Photograph showing a donor chamber being fixed to the porcine nasal tissue with cyanoacrylate glue. Excess tissue was then cut away.

The cells were allowed to equilibrate for 30 min before the inserts under investigation were placed in the donor chamber on top of the mucosa and the cells re-covered. Aliquots of 0.8 mL were removed at time intervals and passed through 0.2 µm syringe filters to sterilise. Three each of inserts containing K6, K6@CB[6], di-Pt and di-Pt@CB[6] were examined.

For samples containing K6 and K6@CB[6], analysis by fluorescence spectroscopy proved impossible due to the presence of one or more fluorescent species producing strong signals overlapping with the wavelength of interest.

The release samples containing di-Pt and di-Pt@CB[7] were prepared as discussed previously, and analysed for platinum content by ICP-MS. Whilst neither type reached 100% release through porcine mucosa, the inserts containing di-Pt@CB[7] showed reduced release rate compared to di-Pt alone (Figure 4.26). This reduction, however was not significant prior to 280 min, but does suggest that encapsulation of di-Pt in CB[7] may act to reduce the drug's ability to be absorbed across the nasal mucosa. This may be a result of reduced diffusivity of the di-Pt@CB[7] complex through the HPMC matrix due to increased hydrogen bonding. Alternatively, it may mean that the complex is sequestered into the tissue and retained there, rather than passing into the release medium. This analysis could have been improved by homogenising the tissue after the experiment and quantifying any platinum which had been sequestered.

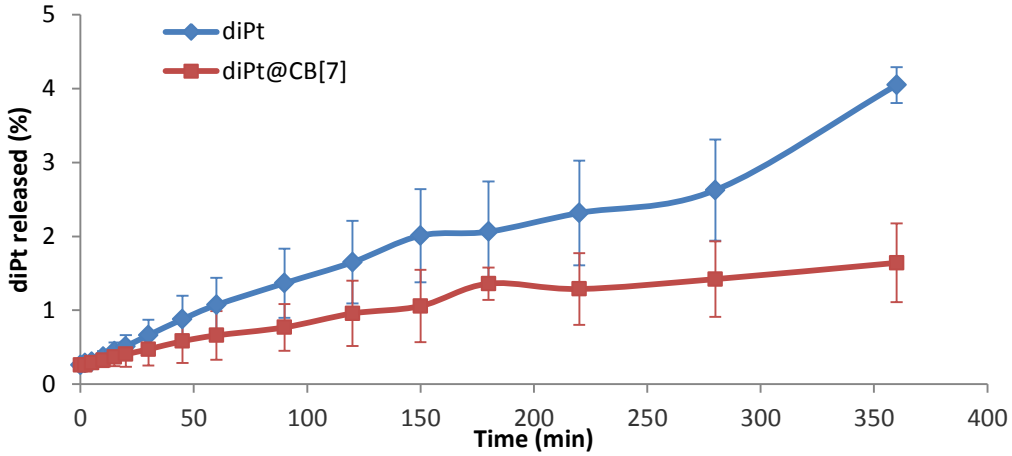

Figure 4.26. Graph comparing the release of platinum from inserts containing di-Pt and di-Pt@CB[7]. Data are plotted as mg of di-Pt released, regardless of encapsulation state. Error bars represent standard deviation (*n*=3).

4.4.11 Scanning electron microscopy of insert internal structure

The inserts were examined using SEM, in order to examine any influence the CB[*n*]s may have on the polymer structure. At 1,000 × magnification, di-Pt can clearly be seen as rough substance on the smooth surface of the polymer (Figure 4.27a). At the same magnification, there is no evidence of di-Pt@CB[7] on the polymer surface (Figure 4.27b), suggesting that the complex may have been incorporated into the polymer structure. This may render the di-Pt@CB[7] locked within the formulation explaining reduced release of di-Pt@CB[7], which would be dependent on erosion of the polymer matrix – a relatively slow process compared to release of di-Pt which would be dependent only on dissolution of the di-Pt in absorbed release medium.

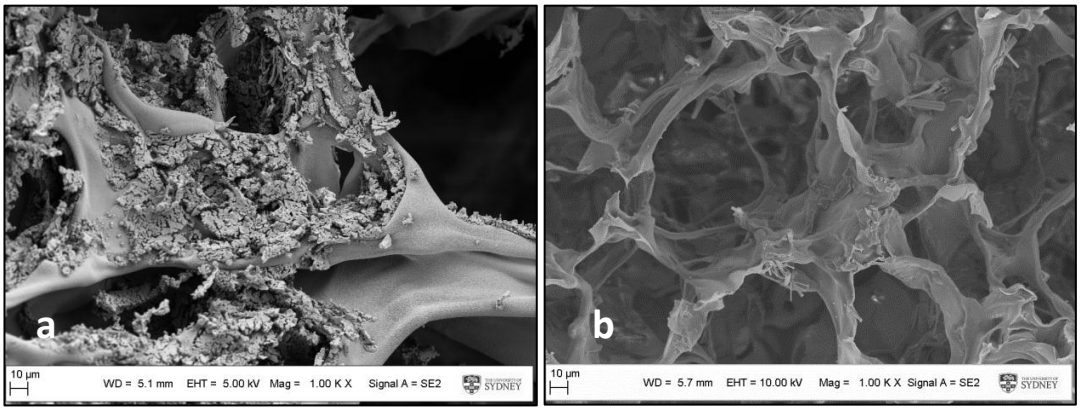

Figure 4.27. SEM micrographs (1,000 × magnification) of inserts containing a) di-Pt and b) di-Pt@CB[7].

A similar study of inserts containing K6 and K6@CB[6] appeared to show the opposite. Whilst the micrograph of the insert containing K6 showed smooth leaves of polymer with no apparent K6 on the surface; the K6@CB[6] was apparent as crystals on the polymer surface (Figure 4.28). This suggests that the K6 dye was incorporated into the polymer structure but encapsulation in CB[6] prevents this from happening. This may be a result of reduced solubility of K6@CB[6] in the wet polymer matrix.

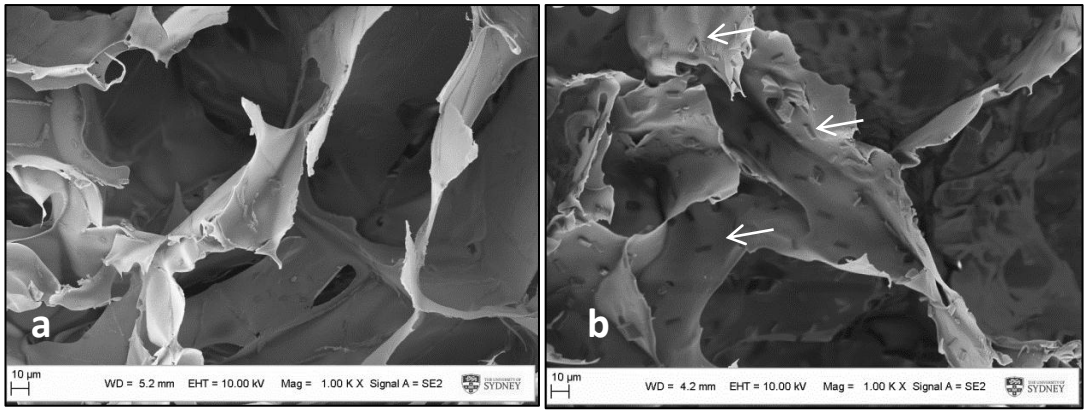

Figure 4.28. SEM micrographs (1,000 × magnification) of inserts containing a) K6 and b) K6@CB[6] (indicated with arrows).

4.4.12 Dynamic vapour sorption

During the DVS investigations, inserts were subjected to two cycles of RH steps ranging from 0% to 95% (absorption) followed by 95% to 0% (desorption), whilst recording the change in mass at each step. A typical DVS trace is shown (Figure 4.29).

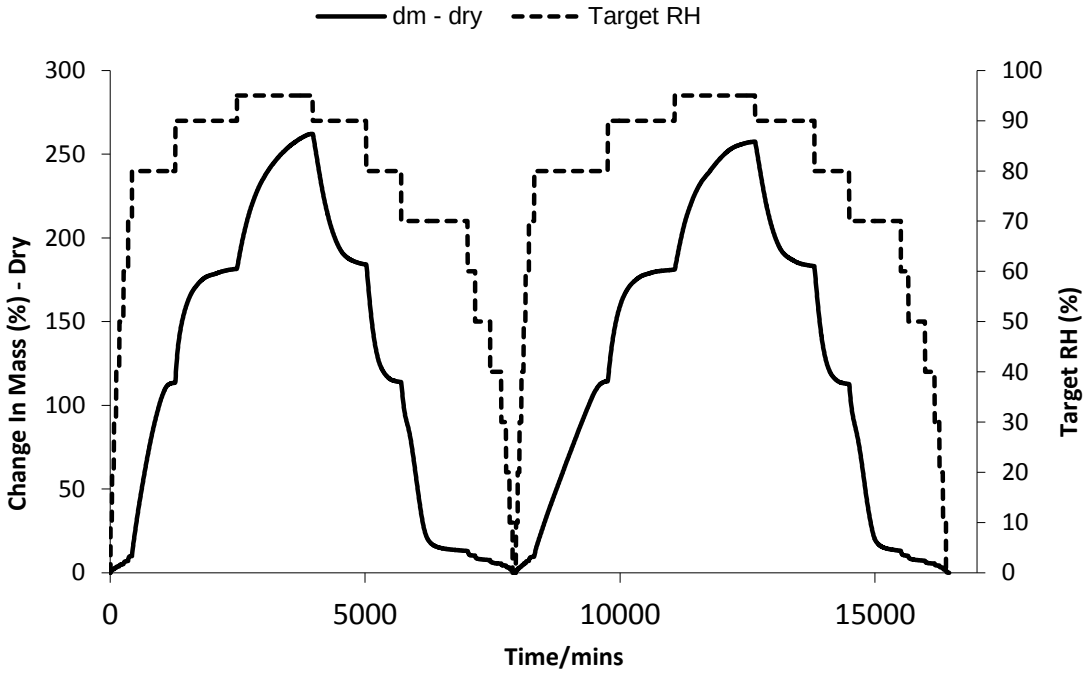

Figure 4.29. Typical DVS trace of a nasal insert exposed to two cycles of relative humidities from 0% to 95% (sorption) and then 95% to 0% (desorption).

Dynamic vapour sorption of all the inserts demonstrated substantial weight gain due to absorption of water (Table 4.3). This was consistent with the results from McInnes and colleagues, who suggested that the inserts would be capable of absorbing water rapidly in the nasal cavity.[31]

For K6, encapsulation in CB[6] acted to slightly increase the water absorption potential in the first cycle, and then decrease it in the second. This change in behaviour suggests an irregularity in the structure, consistent with SEM images showing randomly crystallised K6@CB[6] on the polymer surface. Additionally, polymer chain conformational changes induced by CB[6] associating to the hydrophilic regions of the polymer chain may account for this difference. Although similar behaviour was seen in the blank insert, the blank contained more water at the beginning of the assay, which may have reduced water uptake potential in the first cycle. For di-Pt, encapsulation in CB[7] acted to reduce water uptake on both cycles. This is consistent with the hypothesis that CB[7] saturates the hydrogen bonding groups of the HPMC, retarding incorporation of water into the polymer matrix. Additionally, the fact that there was reduced uptake on both cycles suggests that the inclusion of CB[7] has conferred a regularity in the system. Both of these observations are consistent with the SEM images, which suggested that CB[7] encapsulation allows the di-Pt to be incorporated into the polymer matrix, in a regular fashion.

Table 4.3. Dynamic vapour sorption data for inserts.

Insert type	Total H_2O absorbed (% of dry weight)	
	Cycle 1	Cycle 2
Blank	289.1	318.5
K6	324.5	323.2
K6@CB[6]	325.7	317.5
di-Pt	262.2	257.5
di-Pt@CB[7]	223.9	228.6

4.4.13 Effect of freeze-drying method on nasal inserts

When the first inserts containing di-Pt@CB[7] were produced, they were of an unfavourable morphology. The tips of the inserts appeared shrivelled, with uneven surfaces. Two reasons were proposed: firstly, that the di-Pt@CB[7] had settled into the tips prior to lyophilisation. The UV-vis study of insert sections described previously showed that distribution of di-Pt@CB[7] throughout the inserts was homogenous. The second theory was that during the freeze-drying process, the sample tips of the frozen inserts began to defrost before the water could be sublimed from that area. This phenomenon is known as meltback and is summarised in Figure 4.30. When this occurs, the sponge-like network formed by the polymer around the pockets of water is broken down, and the shape and texture is lost. It was decided that reducing the temperature of the major drying process might help keep the water from melting, whilst still allowing its sublimation.

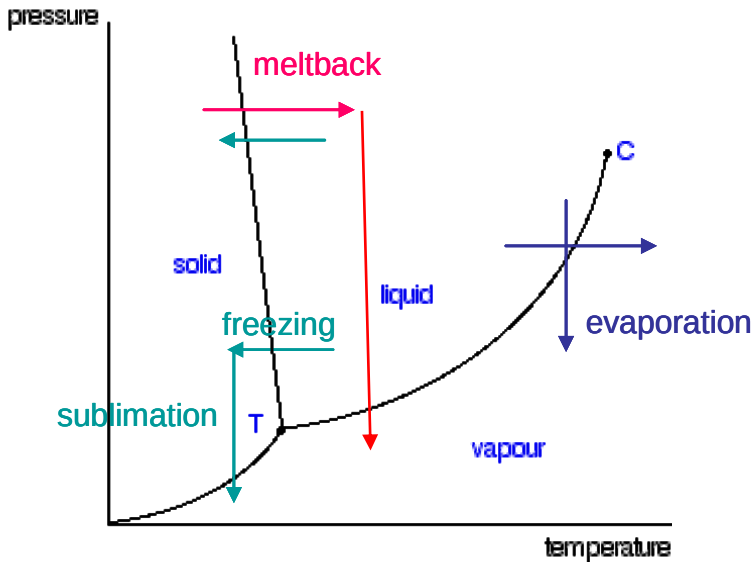

Figure 4.30. Phase diagram for water showing the processes of evaporation by reducing pressure and/or increasing temperature; lyophilisation, which entails freezing followed by sublimation without passing back through the liquid phase; and meltback, whereby the frozen water melts. This water is then partially or fully evaporated off, rather than sublimed.

The freeze dryer was reprogrammed (Method 2) to reach and maintain a lower temperature during the main drying phase. This approach was successful in

overcoming the meltback problem (Figure 4.31). It is clear from the emergence of this problem however that the freeze-drying conditions may have to be re-optimised each time the formulation is altered.

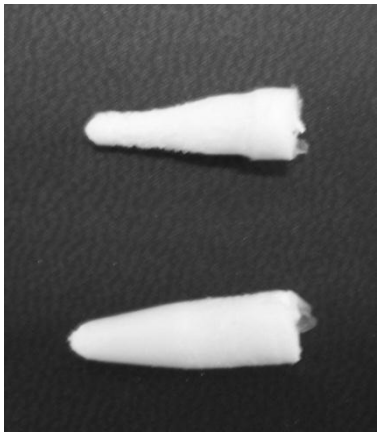

Figure 4.31. An image of a nasal inserts containing di-Pt@CB[7]. One insert shows inconsistent shape due to meltback (top). The other was lyophilised using modified conditions.

Scanning electron microscopy examination of inserts containing di-Pt@CB[7] freeze dried using Method 1 and Method 2 was carried out. The micrographs show increased pore size when lyophilised on Method 2 (Figure 4.32), indicating that altering the freeze drying cycle will affect the final form of the lyophilisate and potentially its physiochemical properties.

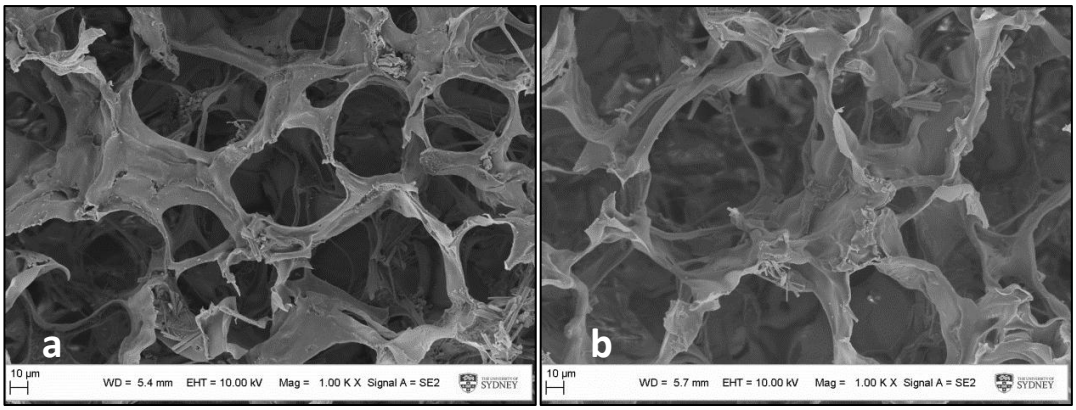

Figure 4.32. SEM micrographs (1,000 × magnification) of lyophilised inserts containing di-Pt@CB[7], freeze dried using a) method 1, and b) method 2. The insert lyophilised on method 2 has larger pore size.

In order to evaluate this, a release study was carried out using Franz cells. Release of di-Pt@CB[7] from inserts lyophilised on Method 1 was analysed by UV spectroscopy and compared to those lyophilised on Method 2. Whilst release from the inserts was equivalent, release from the Method 2 inserts was associated with much narrower errors, suggesting release more consistent and repeatable (Figure 4.33). This supported the argument that Method 2 produced inserts with a more consistent structure and, therefore, drug release.

The initial burst release followed by a lag may be a result of the hydration kinetics of the insert, with drug near the surface released quickly due to adsorption of water at the surface of the insert, and solubilisation of the drug in this area.[49] This would be followed by a lag during which water is absorbed and penetrates the bulk of the insert. Drug release from oral HPMC dosage forms has been shown to be complex because the structure of HPMC exposed to water is strongly time-dependant.[50] Additionally, the initial capillary uptake of water results in swelling of the HPMC, blocking the porous channels. The newly formed gel-layer at the interface also acts as a barrier to water diffusion.[51]

Colombo and colleagues have shown that drug release rate from HPMC dosage forms is linearly related to the surface area exposed to the dissolution medium.[52] The nasal insert formulation already has irregular 3-dimensional shape, and the exact positioning of the insert on the mucosal surface would influence the contact surface area. If the structure of the insert is even less regular due to meltback in freeze-drying, then more error is introduced in contact surface area and, therefore, release kinetics.

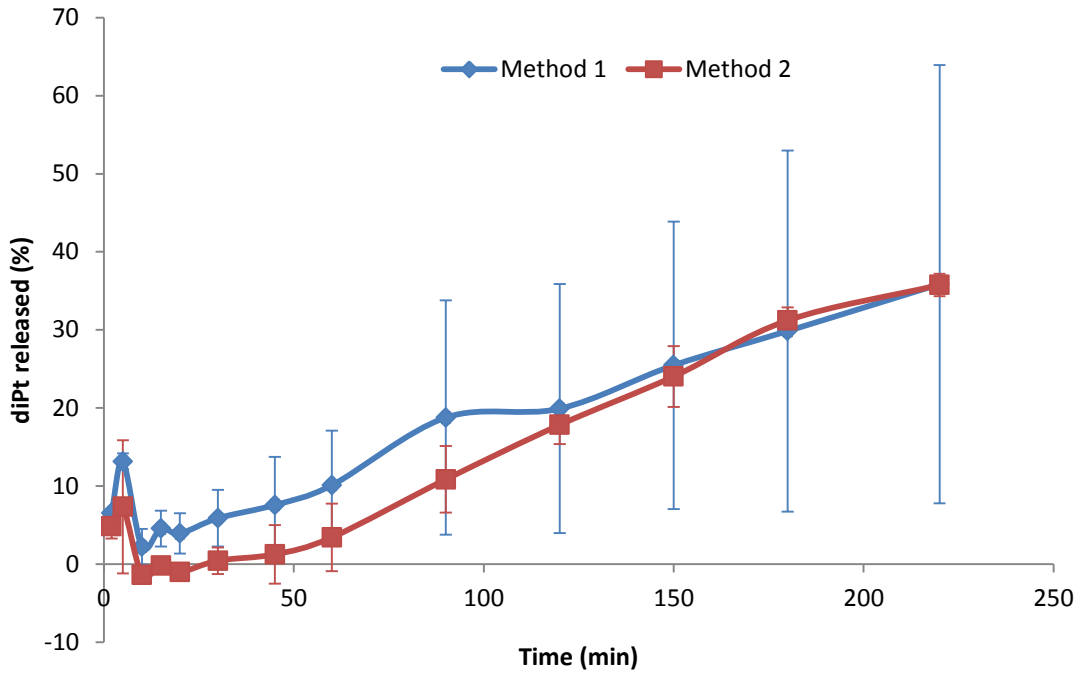

Figure 4.33. Graph comparing the release of di-Pt, as di-Pt@CB[7], from inserts freeze dried on Method 1 and Method 2. Although release was equivalent, release from Method 2 inserts was more consistent.

4.5 CONCLUSIONS

Di-Pt has been synthesised and encapsulated in CB[7], which has been shown previously to reduce the reactivity of the drug. In order to determine whether CB[6] encapsulation affects a molecule in the same manner as CB[7] encapsulation, K6 fluorescent dye was synthesised, encapsulated in CB[6]. It was found that encapsulating these model compounds in CB[*n*]s has improved their thermal stability, as determined by DSC. This not only means that the drugs have improved stability for storage and transport, but could infer reduced reactivity and enhanced stability *in vivo*. This is in agreement with the work of Wheate and colleagues who observed reduced reactivity of di-Pt@CB[7] compared to native di-Pt.[7]

These protected species have been incorporated into lyophilised nasal insert formulations, produced from 2% (w/w) K4MP HPMC gel containing NaCl. These formulations were compared to those containing free di-Pt or K6 in a number of non-pharmacopoeial tests. When examined for drug distribution, both K6@CB[6] and di-Pt@CB[7] showed improved distribution compared to inserts containing the free compounds.

Examinations of spread on agar/mucin and mucoadhesion suggested that CB[6] and CB[7] encapsulation affected the inserts in the same manner. These results can all be rationalised by considering the hydrogen bonding potential of the systems under investigation. Hydrogen bonding can occur between hydrophilic polymer chain residues and the carbonyl portals of the CB[*n*]s, shown in Chapter 3 to increase the hardness of the inserts. Additionally, hydrogen bonding between the CB[*n*]s and waters of hydration has also resulted in more efficient gelling, spreading and mucoadhesion. The hydrogen bonding system and/or hydrophobic interactions are also thought to bring about an "untangling" of the polymer chains, allowing increased interpenetration of polymer and mucin chains.

Hydrogen bonding may also be a crucial factor affecting the macroscopic behaviour of these inserts. The encapsulation of the drug/dye in CB[6] or CB[7] appears to

provide additional structural integrity to the insert as a result of increased inter-chain pseudo-cross-linking. The increased size and number of carbonyl groups of the CB[7], compared to the CB[6],[11] provides more hydrogen bonding potential and a greater number of non-covalent cross links in the matrix. Additionally, the delta negative moieties may contribute to other electrostatic interactions such as van der Waals interactions[53] between the HPMC/CB[*n*] network and mucus.

Encapsulating the drug/dye in CB[*n*] has reduced the rate of release in SNES. This is thought to be a result of reduced diffusivity of the drug through the polymer and/or polymer-mucin matrix when CB[6] or CB[7] is present. The pH of the environment has also been shown to influence the drug release. In this manner, CB[*n*]s may be a useful tool for deliberately extending release of a drug from an HPMC matrix and as such, the benefits of CB[*n*]s as excipients in drug formulations merits further investigation. It should be noted that the pH and/or ion concentration of the release medium is very important for release studies, and the most representative medium should always be sought in order to build a reliable model for release.

CB[6] and CB[7] have both proven to enhance both the encapsulated compound and, in some cases, the performance of the final formulation. It most of these investigations, encapsulating di-Pt in CB[7] has a similar qualitative effect on the molecule as incorporating K6 in CB[6]. The extent of these effects however was often different. The difference between a non-encapsulated drug formulation and an encapsulated one will likely depend on the physiochemical properties of the drug/dye in question. As such, if reliable predictions are required it would be more appropriate to use the actual drug/CB[*n*] combination, rather than a model.

As well as satisfying the aims set out at the beginning of this chapter, this work may represent the formulation of a pH-responsive supramolecular delivery system for di-Pt. Further development of this technology in another field of study could see a CB[*n*]-HPMC delivery system capable of enhanced drug targeting; for example, to the lower digestive tract following oral delivery.

Pham and Lee have reported that the rate of polymer swelling, dissolution and subsequent drug release from oral HPMC formulations increased with either higher drug loading or lower viscosity grades of HPMC.[54] Both of these strategies could be employed to increase the rate of drug release from the inserts if this was required.

Another useful investigation may be to use a drug which can be encapsulated by both CB[6] and CB[7], so that results are not skewed by the inherent differences in the model drugs and their formulations (*e.g.* free K6 was more poorly distributed in inserts than free di-Pt, altering the magnitude of the improvement upon encapsulation).

Colombo and colleagues have shown that drug release rate from HPMC dosage forms is linearly related to the surface area exposed to the dissolution medium.[52] The torpedo shape of the nasal insert and error introduced with exact positioning of the insert on the mucosa means that a consistent and reproducible release profile may be difficult to achieve in practise. The use of a cylindrical shaped insert along with a suitable applicator may alleviate this source of error.

Whilst di-Pt has potential as an anticancer drug, it has not entered clinical trials and remains unapproved for clinical use. The chapter that follows describes the encapsulation of the clinically relevant drug cisplatin in CB[7], and its subsequent formulation into nasal inserts, and the effect this encapsulation has on the performance of the inserts.

4.6 REFERENCES

(1) Zou, Y., Vanhouten, B. and Farrell, N., *Biochemistry*, 1994, **33**, 5404-5410.

(2) Wu, P.K., Kharatishvili, M., Qu, Y. and Farrell, N., *J. Inorg.Biochem.*, 1996, **63**, 9-18.

(3) Billecke, C., Finniss, S., Tahash, L., Miller, C., Mikkelsen, T., Farrell, N.P. and Bogler, O., *Neuro-Oncology*, 2006, **8**, 215-226.

(4) Riccardi, A., Meco, D., Ferlini, C., Servidei, T., Carelli, G., Segni, G., Manzotti, C. and Riccardi, R., *Cancer Chemother. Pharmacol.*, 2001, **47**, 498-504.

(5) Servidei, T., Ferlini, C., Riccardi, A., Meco, D., Scambia, G., Segni, G., Manzotti, C. and Riccardi, R., *Eur. J. Cancer*, 2001, **37**, 930-938.

(6) Wheate, N.J. and Collins, J.G., *J. Inorg. Biochem.*, 2001, **86**, 478-478.

(7) Wheate, N.J., Cullinane, C., Webster, L.K. and Collins, J.G., *Anti-Cancer Drug Des.*, 2001, **16**, 91-98.

(8) Wheate, N.J., Evison, B.J., Herlt, A.J., Phillips, D.R. and Collins, J.G., *Dalton T.*, 2003, 3486-3492.

(9) Jansen, B.A.J., Brouwer, J. and Reedijk, J., *J. Inorg.Biochem.*, 2002, **89**, 197-202.

(10) Lee, J.W., Samal, S., Selvapalam, N., Kim, H.-J. and Kim, K., *Acc. Chem. Res.*, 2003, **36**, 621-630.

(11) Lagona, J., Mukhopadhyay, P., Chakrabarti, S. and Isaacs, L., *Angew. Chem. Int. Ed.*, 2005, **44**, 4844-4870.

(12) Wheate, N.J., *J. Inorg. Biochem.*, 2008, **102**, 2060-2066.

(13) Wheate, N.J., Day, A.I., Blanch, R.J., Arnold, A.P., Cullinane, C. and Collins, J.G., *Chem. Commun.*, 2004, 1424-1425.

(14) Kennedy, A.R., Florence, A.J., McInnes, F.J. and Wheate, N.J., *Dalton T.*, 2009, 7695-7700.

(15) Jeon, Y.J., Kim, S.-Y., Ko, Y.H., Sakamoto, S., Yamaguchi, K. and Kim, K., *Org. Biomol. Chem.*, 2005, **3**, 2122-2125.

(16) Kemp, S., Wheate, N.J., Pisani, M.P. and Aldrich-Wright, J.R., *J. Med. Chem.*, 2008, **51**, 2787-2794.

(17) Hettiarachchi, G., Nguyen, D., Wu, J., Lucas, D., Ma, D., Isaacs, L. and Briken, V., *PLoS ONE*, 2010, **5**, e10514.

(18) Uzunova, V.D., Cullinane, C., Brix, K., Nau, W.M. and Day, A.I., *Org. Biomol. Chem.*, 2010, **8**, 2037-2042.

(19) Montes-Navajas, P., Gonzalez-Bejar, M., Scaiano, J.C. and Garcia, H., *Photochem. Photobio. S.*, 2009, **8**, 1743-1747.

(20) Urbach, A.R. and Ramalingam, V., *Isr. J. Chem.*, 2011, **51**, 664-678.

(21) Parvari, G., Reany, O. and Keinan, E., *Isr. J. Chem.*, 2011, **51**, 646-663.

(22) Biczók, L., Wintgens, V., Miskolczy, Z. and Megyesi, M., *Isr. J. Chem.*, 2011, **51**, 625-633.

(23) Bhasikuttan, A.C., Dutta Choudhury, S., Pal, H. and Mohanty, J., *Isr. J. Chem.*, 2011, **51**, 634-645.

(24) Koner, A.L. and Nau, W.M., *Supramol. Chem.*, 2007, **19**, 55-66.

(25) Wheate, N.J., Taleb, R.I., Krause-Heuer, A.M., Cook, R.L., Wang, S., Higgins, V.J. and Aldrich-Wright, J.R., *Dalton T.*, 2007, 5055-5064.

(26) Buckton, G., *Thermochim. Acta*, 2000, **347**, 63-71.

(27) *Surface Measurement Systems Dvs User Guide*, 9.2 ed., Middlesex.

(28) York, P., *Int. J. Pharm.*, 1983, **14**, 1-28.

(29) Vogt, F.G., Brum, J., Katrincic, L.M., Flach, A., Socha, J.M., Goodman, R.M. and Haltiwanger, R.C., *Cryst. Growth Des.*, 2006, **6**, 2333-2354.

(30) Burnett, D., Thielmann, F. and Sokoloski, T., *J. Therm. Anal. Calorim.*, 2007, **89**, 693-698.

(31) McInnes, F.J., Thapa, P., Baillie, A.J., Welling, P.G., Watson, D.G., Gibson, I., Nolan, A. and Stevens, H.N.E., *Int. J. Pharm.*, 2005, **304**, 72-82.

(32) Sheldrick, G.M., *Acta Crystall. A-crys.*, 2008, **64**, 112-122.

(33) Farrugia, L., *J. App. Crystallogr.*, 1999, **32**, 837-838.

(34) http://www.permegear.com/v6stirrers.htm, *accessed 15th September 2012.*

(35) Kennedy, A.R., Florence, A.F., McInnes, F.J. and Wheate, N.J., *Dalton T.*, 2009,

(36) Fan, Z.-F., Xiao, X., Zhang, Y.-Q., Xue, S.-F., Zhu, Q.-J., Tao, Z. and Wei, G., Unpublished work.

(37) Clas, S.-D., Dalton, C.R. and Hancock, B.C., *Pharm. Sci. Technol. To.*, 1999, **2**, 311-320.

(38) Wang, R. and Macartney, D.H., *Org. Biomol. Chem.*, 2008, **6**, 1955-1960.

(39) Yi, J.-M., Zhang, Y.-Q., Cong, H., Xue, S.-F. and Tao, Z., *J. Mol. Struct.*, 2009, **933**, 112-117.

(40) Hou, Z.-S., Tan, Y.-B., Kim, K. and Zhou, Q.-F., *Polymer*, 2006, **47**, 742-750.

(41) Madsen, F., Eberth, K. and Smart, J.D., *Biomaterials*, 1998, **19**, 1083-1092.

(42) Andrews, G.P., Laverty, T.P. and Jones, D.S., *Eur. J . Pharm. Biopharm.*, 2009, **71**, 505-518.

(43) Mygind, N. and Dahl, R., *Adv. Drug Deliver. Rev.*, 1998, **29**, 3-12.

(44) Nageswara Rao, R. and Kumar Talluri, M.V.N., *J. Pharm. Biomed. Anal.*, 2007, **43**, 1-13.

(45) Ugwoke, M.I., Agu, R.U., Verbeke, N. and Kinget, R., *Adv. Drug Deliver. Rev.*, 2005, **57**, 1640-1665.

(46) Charrois, G.J.R. and Allen, T.M., *BBA - Biomembranes*, 2004, **1663**, 167-177.

(47) Lapidus, H. and Lordi, N.G., *J. Pharm. Sci.*, 1966, **55**, 840-843.

(48) Lin, Y., Li, L. and Li, G., *Carbohyd. Polym.*, 2013, **92**, 429-434.

(49) Newman, A.W., Reutzel-Edens, S.M. and Zografi, G., *J. Pharm. Sci.*, 2008, **97**, 1047-1059.

(50) Siepmann, J., Kranz, H., Bodmeier, R. and Peppas, N.A., *Pharm. Res.*, 1999, **16**, 1748-1756.

(51) Bajwa, G.S., Hoebler, K., Sammon, C., Timmins, P. and Melia, C.D., *J. Pharm. Sci.*, 2006, **95**, 2145-2157.

(52) Colombo, P., Catellani, P.L., Peppas, N.A., Maggi, L. and Conte, U., *Int. J. Pharm.*, 1992, **88**, 99-109.

(53) Dodou, D., Breedveld, P. and Wieringa, P.A., *Eur. J. Pharm. Biopharm.*, 2005, **60**, 1-16.

(54) Pham, A.T. and Lee, P.I., *Pharm. Res.*, 1994, **11**, 1379-1384.

5. NASAL INSERTS FOR THE DELIVERY OF CISPLATIN@CB[7]

5.1 CISPLATIN - THE GOLD STANDARD 30 YEARS ON

5.1.1 The slow acceptance of new platinum anticancer drugs

Since the approval of cisplatin, 23 platinum-based drugs have entered clinical trials. Of these, only carboplatin and oxaliplatin have achieved worldwide approval.[1]

Whilst encapsulating di-Pt in CB[7] has been shown to improve activity, di-Pt remains an experimental drug complex which has not entered the clinic. As yet, BBR 3464 is the only multi-nuclear platinum drug to reach clinical trials and no clinical advances have been reported since 2006. There are currently no new small molecule platinum-based drugs entering clinical trial, a situation which has persisted since 1999.[1,2] Despite problems with toxicity and resistance, cisplatin remains clinically relevant.

5.1.2 Cisplatin remains a clinically important chemotherapeutic

Thirty years after its approval, cisplatin remains one of the best-selling anti-cancer drugs in the world and is included in 32 out of 78 cancer chemotherapy regimens listed in Martindale.[3] In combination therapies, cisplatin has achieved an 83% cure rate against non-metastasised testicular cancer,[4] is one of the most effective treatments against melanoma and non-small-cell lung cancer, and has considerable activity against ovarian cancer.[5] In addition to these approved uses, cisplatin has shown effectiveness in a number of off-label indications.

5.1.3 Off-label use of cisplatin for nasal cancers

A medicine is said to be prescribed "off-label" when it is used outside the terms of its licensed indication.[6] The practise is not uncommon; for example, a survey in Strasbourg University Hospital in 2002 found that as many as 58% of medications for hormone-refractory prostate cancer patients were prescribed off-label.[7] Off-label prescribing occurs frequently in paediatrics, rare diseases and oncology where the range of effective licensed drugs is limited or the approved indications for use are very specific. Prescribing an anticancer drug off-label involves: for example, prescribing for an age group, dose, regime, delivery route or type of cancer for which approval has not been gained.[6]

Although cisplatin is only approved in the UK for testicular, lung, cervical, bladder, head and neck, and ovarian cancers[8] (and in the USA for metastatic testicular, ovarian and bladder cancer), it has been used off-label for treatment of cancers pertaining to the nose and nasal cavity, including but not limited to: esthesioneuroblastoma,[9,10] tumours of the paranasal sinuses,[11] malignant melanoma of the nasal cavity,[12] nasopharyngeal tumours[13-15] and other cancers originating in the mucous membranes of the head and neck.[16] Cisplatin has also been dosed locally to tumours of the nasal cavity.[17] Carcinoma of the nasal cavity and paranasal sinuses accounts for up to 0.8% of reported human malignancies. Whilst rare, these types of tumours are currently associated with poor prognosis, as the disease is usually diagnosed at an advanced stage.[18]

5.1.4 Local delivery for reduced systemic side-effects

Cisplatin-induced toxicities include nephrotoxicity, neurotoxicity, and ototoxicity and are associated with the systemic dose required to reach effective levels at the target site. Local delivery of chemotherapeutics has been shown to increase the amount of drug delivered to the target organ/site of action.[19] Local delivery can also reduce the dose required to be administered, and in turn reduce associated systemic

toxicities.[20] Neurotoxicity associated with cisplatin administration has been linked to accumulation of platinum in the peripheral central nervous system, with higher accumulation leading to more severe side-effects.[21] Cisplatin is a small polar drug with a log *P* of -2.53 ± 0.28.[22] Other low MW hydrophilic compounds have shown low systemic bioavailability from the nose without the use of absorption enhancers. For example, systemic bioavailability of nasal morphine in the order of 10% of the equivalent IV dose.[23] This suggests that a majority of cisplatin delivered to the nose would remain local, reducing systemic side-effects.

As cisplatin has shown usefulness in treatment of nasal cancers, a formulation for local delivery of the drug to the nasal cavity would be of potential benefit, and so it was decided to move away from systemic delivery towards a local delivery formulation for this drug. Whilst this may increase the drug levels that can be achieved in the target site and reduce systemic toxicities, cisplatin resistance remains an issue.

5.1.5 Cisplatin resistance remains problematic

Cisplatin resistance can be an intrinsic property of the tumour (as seen with colorectal, lung and prostate cancer) or can be acquired through treatment (as often reported with ovarian cancer).[24] Acquired cisplatin resistance can result from 1) alterations in drug transport, leading to reduced intracellular accumulation; 2) elevated levels of metallothioneins and/or glutathione resulting in increased drug metabolism; 3) changes in DNA repair and tolerance mechanisms; and 4) changes in the apoptotic programmed cell death pathway.[24] Overcoming cisplatin resistance could enable the drug to be used to treat more tumour types, and allow treatment to remain effective for longer. Clinical trial data for platinum anticancer drugs shows that efforts to reduce side effects and improve efficacy have seen a shift in focus away from developing new drugs, towards improving the delivery of already approved ones.[25]

5.1.6 Overcoming cisplatin side effects and resistance with drug delivery vehicles

One strategy to improve the delivery of platinum chemotherapeutics involves utilising drug delivery vehicles to improve drug stability, tumour targeting and tumour uptake. Systems involving carbon nanotubes, metal nanoparticles,[26] nanocapsules,[27] dendrimers,[28] macrocycles and liposomes have all been investigated. Kirkpatrick and colleagues have shown that cisplatin delivered using polyamidoamine (PAMAM) dendrimers has a higher maximum tolerated dose and is more effective against a tumour xenograph than native cisplatin.[28]

SPI-077 was a liposomal formulations of cisplatin which reached Phase II clinical trials. SPI-077 failed due to a lack of bioavailability *in vivo*.[1] Although this formulation ultimately failed in trial, another liposomal formulation, Lipoplatin™ (Regulon Inc., Mountain View, California), is currently in Phase III clinical trials. This formulation utilises a polyethylene glycol coating and has enhanced plasma half-life. As well as showing improved anticancer activity, Lipoplatin-based regimes have shown reduced haematological toxicity, ototoxicity, nephrotoxicity, vomiting/nausea and asthenia compared to native cisplatin-based controls (Figure 5.1).[29-36]

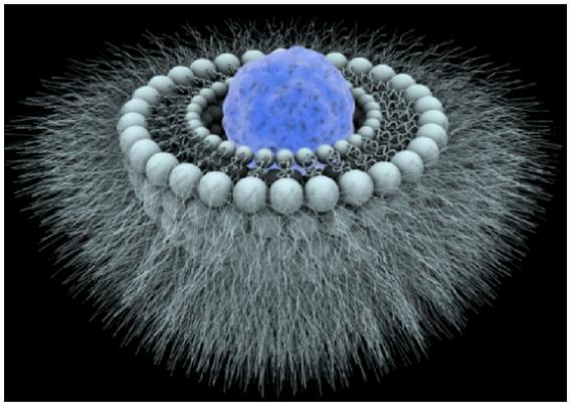

Figure 5.1. Representation of Lipoplatin. A cisplatin molecule (blue) is shown inside a liposome. A coating of polyethylene glycol helps avoid detection by macrophages and increases plasma half-life.[37]

The progression of Lipoplatin™ to Phase III clinical trials is encouraging progress in the use of drug delivery vehicles for platinum anticancer drugs.

5.1.7 Overcoming cisplatin resistance with cucurbit[7]uril

Another class of drug delivery vehicle being investigated for platinum chemotherapeutics is the cucurbituril family. Plumb and colleagues have demonstrated recently that cisplatin encapsulated in CB[7] (cisplatin@CB[7], Figure 5.2) was no more active than free cisplatin in cisplatin sensitive and resistant ovarian carcinoma cell lines (A2780 and A2780/cp70 respectively).[38] However, when an *in vivo* study was carried out in mice, xenographs of A2780/cp70 were sensitive to cisplatin@CB[7]. Examining whole body pharmacokinetics, it was found that cisplatin persists in the circulation for longer when administered as cisplatin@CB[7].[38] This suggests that although no difference was seen in cell activity, the encapsulation protects the drug from degradation, allowing increased cytotoxicity *in vivo*.[38] The CB[7] formulation could be of benefit, where cisplatin has shown to be clinically relevant, with prolonged activity achieved using this encapsulation.

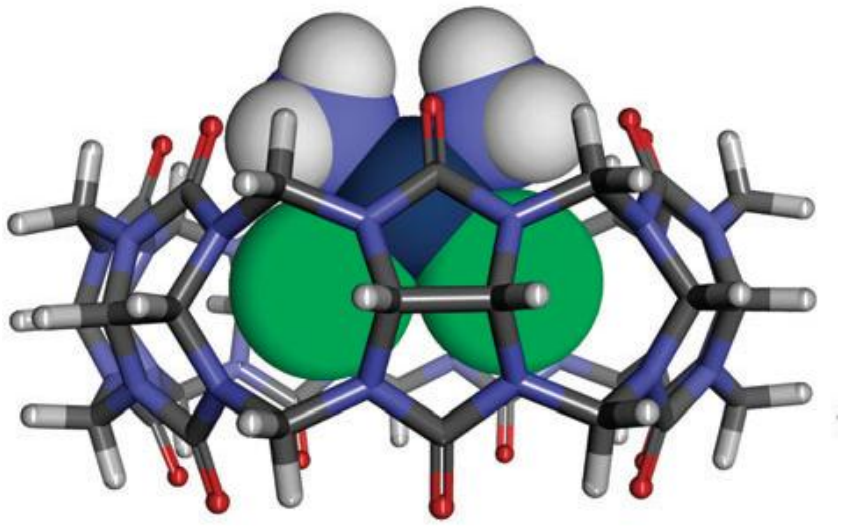

Figure 5.2. Molecular model of the preferred mode of binding of cisplatin in CB[7]. The chlorido ligands (green) are pointing into the cavity, shielding them from attack.[38]

5.1.8 Binding mode

Molecular modelling has shown that the preferred binding mode of cisplatin inside CB[7] orients the chlorido ligands inside the macrocycle cavity. In this manner, four hydrogen bonds can operate between the ammine hydrogens of the drug and the oxygens of the carbonyl groups (Figure 5.3). These hydrogen bonds have lengths of 2.15, 2.22, 2.38 and 2.44 Å and stabilise the encapsulation.[38]

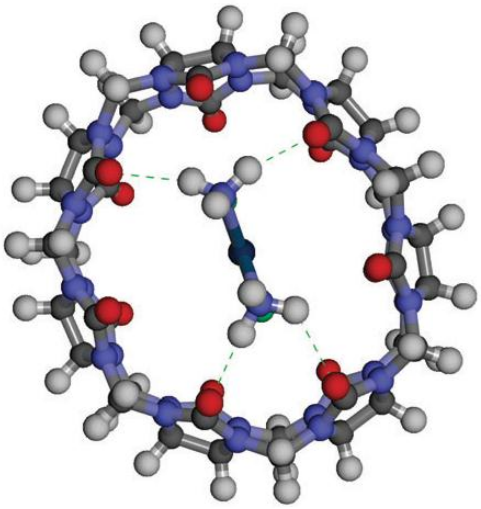

Figure 5.3. A molecular model of the binding of cisplatin within CB[7], showing the four hydrogen bonds (dashed green lines) from the drug's ammine hydrogen atoms to the host carbonyl oxygen atoms.[38]

5.2 AIMS

Cancers of the nasal cavity are rare, but associated with poor prognosis, in part due to late diagnosis. Improving the treatment of these cancers could extend the survival rate of patients. The activity of cisplatin (shown to be useful against nasal cancers) has been improved by encapsulating in CB[7]. Formulating this complex into a dosage form for local delivery to the nose is expected to provide increased drug levels at the target site. The use of a lyophilised nasal insert formulation could overcome rapid MCC and allow for extended residence time in the nasal cavity (*see Chapter 1*) Such a drug formulation, if successful, may help improve the prognosis for oncology patients presenting with nasal cancers.

The aims of this project are, therefore, to:

- encapsulate cisplatin inside CB[7];
- examine the stability of cisplatin@CB[7];
- formulate cisplatin@CB[7] into lyophilised nasal inserts; and to
- examine these inserts for handleability, drug distribution, moisture uptake, mucoadhesion and drug release to examine how the encapsulation affects the formulation.

5.3 MATERIALS AND METHODS

5.3.1 Materials

Cisplatin, phosphate buffered saline tablets (pH 7.4), hydrochloric acid, sodium chloride, potassium chloride, calcium chloride, acetone and mucin from porcine stomach were obtained from Sigma-Aldrich. Cucurbit[7]uril was obtained from STREM Chemicals UK (Cambridge, UK). NMR solvents were obtained from Cambridge Isotopes. Hydroxypropyl methylcellulose was obtained from Colorcon Ltd (Kent, UK). Ultrapure agar granules were obtained from Merck Microbiology (Merck KGaA, Darmstadt, Germany). Cyanoacrylate gel used was Bostik Superglue gel (Bostik Ltd, UK). All water was obtained from a MilliQ water purification system. 0.22 µm nylon filter paper and Grade 1 45 mm diameter filter paper were obtained from Whatman. NMR solvents were obtained from Cambridge Isotopes (Cambridge, UK).

5.3.2 Preparation of cisplatin@CB[7]

40 mg of CB[7] was dissolved in 75 mL H_2O. 10 mg cisplatin was added and the reaction stirred at room temperature overnight. The solution was rotary evaporated to reduce volume before being freeze dried. A ^1H NMR obtained in D_2O confirmed encapsulation.

5.3.3 Preparation of gels prior to lyophilisation

Gels were prepared by dissolving the required amount of cisplatin/cisplatin@CB[7] (1:1 M) in NaCl solution at 80-90 ºC. Hydroxypropyl methylcellulose powder (Grade K4MP) was added and stirred until homogenous. Cold NaCl solution was then added to produce 2% (w/w) HPMC gels. These were stirred with an overhead stirrer for 20 min before incubation at 4 ºC overnight. The gels were then pipetted into microcentrifuge tubes or disc moulds, as described previously (*see Chapter 3*).

In order to assess the effect of NaCl on the inserts, blank gels containing no cisplatin or cisplatin@CB[7] were also prepared using either NaCl solution or water.

5.3.4 Lyophilisation of the formulations

Lyophilisation of nasal inserts and discs was carried out on a Christ Epsilon freeze dryer. Two methods were used, detailed in Table 5.1 and Table 5.2, below. After lyophilisation, inserts and discs were stored in a desiccator until needed.

Table 5.1. Freeze drying programme, Method 2, for the lyophilisation of nasal inserts.

Method 2					
	Step	**Time (hours)**	**Shelf temp (ºC)**	**Vacuum (mbar)**	**Safety Pressure (mbar)**
1	Load		+ 20	-	-
2	Freeze	01:00	- 30	-	-
3	Freeze	01:00	- 40	-	-
4	Freeze	01:00	- 50	-	-
5	Freeze	02:00	- 60	-	-
6	Main Dry	10:00	+ 2	0.16	1.65
7	Main Dry	10:00	+ 5	0.055	1.65
8	Main Dry	04:00	+ 10	0.055	1.65
9	Final Dry	00:10	+ 25	0.011	1.65

Table 5.4. Freeze drying programme, Method 3 for lyophilisation of nasal inserts.

Method 3					
	Step	**Time (h:min)**	**Shelf temp (ºC)**	**Vacuum (mbar)**	**Safety Pressure (mbar)**
1	Load		+ 20	-	-
2	Freeze	01:00	- 30	-	-
3	Freeze	01:00	- 40	-	-
4	Freeze	01:00	- 50	-	-
5	Freeze	02:00	- 60	-	-
6	Main Dry	10:00	- 60	0.16	1.65
7	Main Dry	04:00	- 50	0.055	1.65
8	Main Dry	02:00	- 40	0.055	1.65
9	Main Dry	02:00	- 30	0.055	1.65
10	Main Dry	02:00	- 20	0.055	1.65
11	Final Dry	04:00	+ 10	0.055	1.65
12	Final Dry	00:30	+ 25	0.055	1.65

5.3.5 Analytical techniques

Inductively coupled plasma mass spectrometry: Quantification of platinum was carried out with an Agilent Inductively Coupled Plasma-Mass Spectrometer. The instrument was optimised to yield maximum sensitivity for platinum, which was measured at *m/z* 195. For release studies, samples were prepared for analysis in 2% HCl. For distribution studies, inserts were carefully sliced into three sections which were weighed. Segments were then dissolved to produce 5 mL samples in 2% HCl for analysis. Concentration of platinum was normalised to the mass of the segment being analysed, and the average % of dose recorded (n=3).

For instrumentation and techniques related to formulation spread on agar and moisture uptake, see Chapter 2. For ^{1}H NMR, TGA, DVS, TA and mucoadhesion, see Chapter 3. For DSC and Franz cell release, see Chapter 4.

5.4 RESULTS AND DISCUSSION

5.4.1 Encapsulating cisplatin in CB[7]

The white product obtained from stirring cisplatin and CB[7] in water overnight was analysed by ^{1}H NMR, which confirmed encapsulation. The CB[7]-CH resonance at 5.58 ppm splits, with one peak shifted marginally upfield (5.63 ppm), and one downfield (5.55 ppm) (Figure 5.4). This is consistent with the bound form (or forms) being in exchange with free CB[7].[39] Additionally, the CB[7] doublet at 4.2 ppm splits in a similar manner, indicating a system of exchange, rather than a permanently bound form.

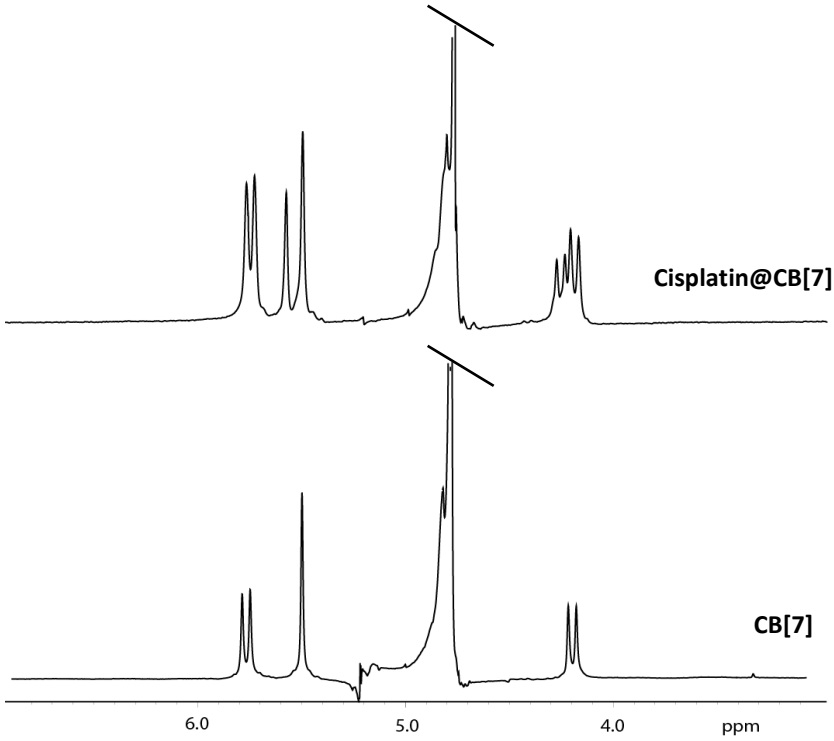

Figure 5.4. ^{1}H NMR stack showing CB[7] (bottom) and cisplatin@CB[7] (top).

5.4.2 Thermal stability of cisplatin and cisplatin@CB[7]

In order to understand how encapsulation in the CB[7] affected the cisplatin, thermal analysis of the free and encapsulated forms was carried out. Samples of cisplatin, CB[7] and cisplatin@CB[7] were analysed by DSC (Figure 5.5). Upon heating from 25-300 ºC, both CB[7] and cisplatin@CB[7] showed water loss at the start of the cycle. The DSC trace for cisplatin showed an endotherm with a peak at 332 ºC, consistent with a melt.[40] The melt temperature quoted in the literature is 270 ºC, consistent with the peak onset. Cisplatin@CB[7] showed no such endotherm in this temperature range, with no deviation from the baseline until the point where the CB[7] began to degrade. This shows that encapsulation in CB[7] has inferred thermal stability on the cisplatin, and may have implications in preventing drug degradation during processing, storage and the production of HPMC gels, which require elevated temperatures.[41] Unfortunately, useful thermal data from TGA of the final polymeric formulation could not be obtained as the polymer began to degrade below 200 ºC, before any cisplatin thermal events could take place.

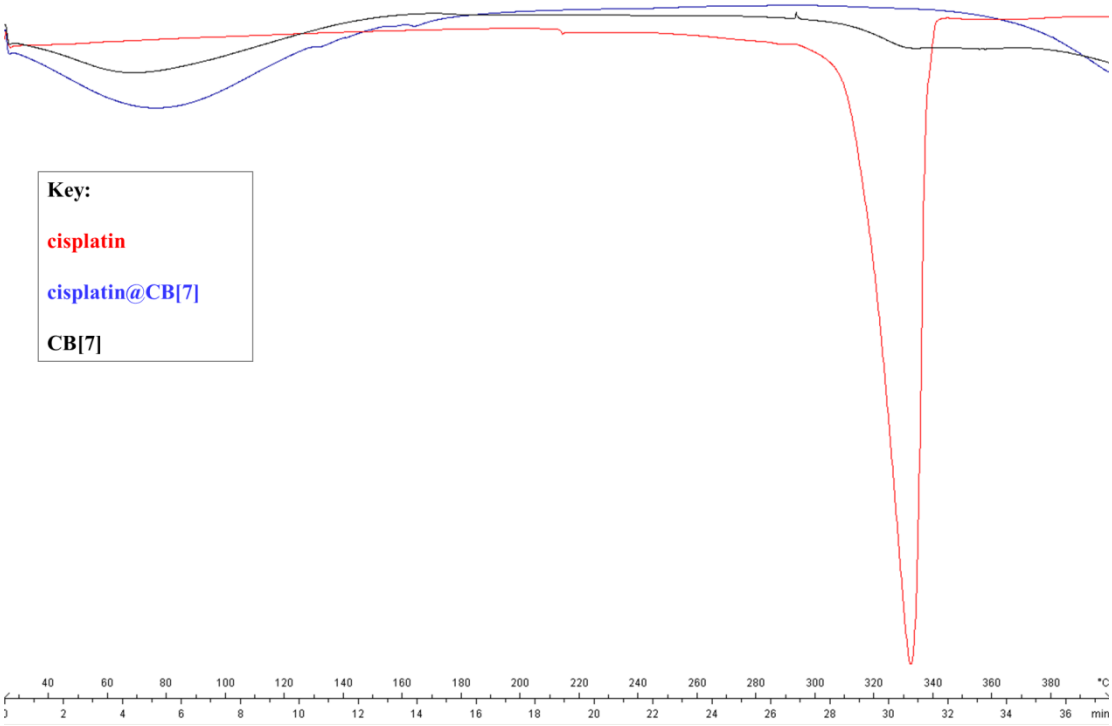

Figure 5.5. DSC trace for cisplatin, cisplatin@CB[7] and CB[7] alone.

5.4.3 Preparation of lyophilised nasal inserts

Following successful encapsulation of cisplatin into CB[7], the complex was then incorporated into HPMC nasal inserts. In order to determine how the encapsulation of cisplatin affected the performance of the formulation, lyophilised nasal inserts and discs were produced containing either native cisplatin or cisplatin@CB[7], with equal concentration of cisplatin. NaCl solution was used as the Na^+ ions associate to the CB[*n*] portals, allowing the CB[*n*]s to dissolve more readily.[42,43] This was favourable for improving distribution of cisplatin in the insert and bioavailability.

Inserts and discs were lyophilised using two different cycles. The first cycle, Method 2, produced good discs, but the nasal inserts containing cisplatin@CB[7] were subject to meltback (Figure 5.6). As both morphologies were freeze dried from 300 µL of gel, the difference was thought to be a result of the shape of the moulds. A similar problem has been reported by Thapa[44] who found that lyophilisates freeze dried in long moulds with a small area open to the atmosphere were prone to

meltback. Although the same overall volume, the inserts were longer and thinner than the discs, with a smaller surface area open to the environment of the freeze dryer. The nature of this shape meant that the water from the tip of the insert (oriented downwards in the freeze dryer) had to sublime and pass through the entire length of the insert in order to exit through the open mouth of the microcentrifuge tube. The length of the insert means that there is more resistance to vapour flow and so the water in the tip is not completely removed from the system before the temperature is raised. The remaining water then melts, causing structural collapse.[44]

Method 3 was developed to overcome this problem. In this new method, the temperature was lowered to -60 ºC as previously, but instead of increasing the temperature as soon as the vacuum was applied, the temperature was held at -60 ºC for ten hours before proceeding, and the remainder of the main drying section carried out at sub-zero temperatures. Maintaining lower temperatures for longer in this manner eliminated meltback by preventing frozen water from melting, thus preventing structural collapse. This was effective at producing nasal insert formulations with a consistent, spongy texture and no obvious evidence of meltback. As starting materials were scarce, the method was developed to ensure that the water was kept well below the freezing point and eliminate the need for trial and error. Should the formulation be developed further, the method should be fine-tuned to produce optimum results with minimum time and energy cost.

Figure 5.6. Image of lyophilised nasal inserts containing cisplatin, lyophilised using Method 2 (top) and Method 3 (bottom). The top insert shows shrivelled morphology, indicating meltback.

5.4.4 Effect of NaCl on nasal insert formulations

The inclusion of NaCl in the formulation was expected to increase the solubility of the CB[*n*], both in the gel during production and *in situ*. Polymer gels were produced using 0.15 M NaCl solution, the concentration found in simulated nasal electrolyte solution. The rehydrated insert would be expected to have a higher NaCl concentration *in situ*. Although this may alter nasal homeostasis, it has been found that nasal absorption can be increased by the inclusion of NaCl, due to shrinkage of the nasal epithelial mucosa.[45,46] As a further advantage, increasing the content of Cl^- in the polymer gel may help the cisplatin remain chlorinated, through a common ion effect. This is similar to the effect observed when cisplatin is injected into the bloodstream. The high concentration of chloride ions in the bloodstream (0.1 M) keeps the cisplatin from aquating until it has been taken up into cells.[47] In the same manner, it was expected that the concentration of Cl^- ions in the nasal secretions and hydrated insert would prevent hydration and deactivation of cisplatin.

In order to investigate the effect of salt on the *in vitro* properties of lyophilised nasal inserts, blank HPMC inserts made with NaCl solution and inserts made with MilliQ water were compared directly. The hardness and springiness of lyophilised discs with and without NaCl was measured using the texture analyser (Figure 5.7). It was found that inclusion of NaCl in the formulation led to a statistically significant reduction in hardness (P=0.003) and springiness (P=0.000). This may be because the HPMC is non-ionic and as such, will not form significant electrostatic interactions with added Na^+ or Cl^- ions, and so their presence may reduce the structural integrity of the system. The presence of NaCl in HPMC hydrogels has been shown to weaken intermolecular hydrogen bonding, allowing it to be more easily disrupted.[48]

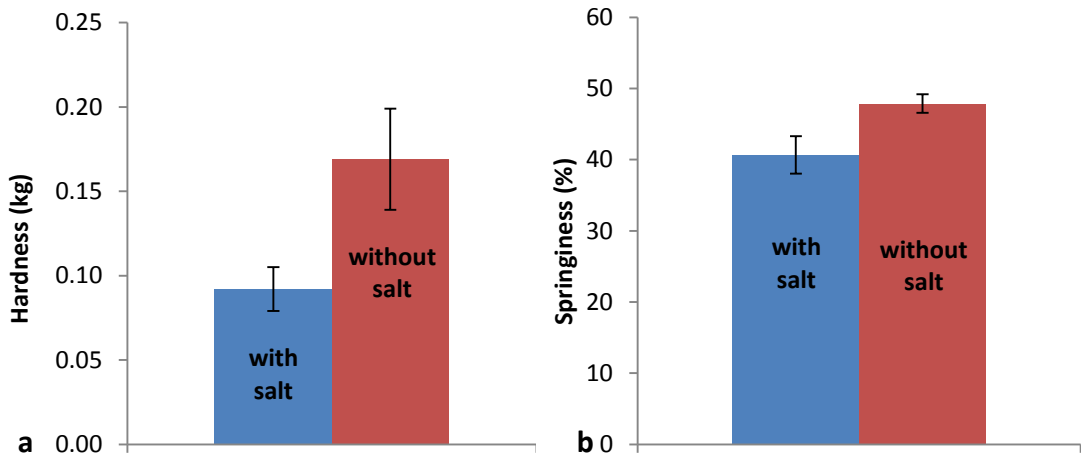

Figure 5.7. Graphs comparing the a) hardness, and b) springiness, of lyophilised HPMC discs with and without salt (n=3, error bars represent standard deviation).

The agar/mucin spread test was performed with the NaCl-containing and NaCl-free discs to determine whether or not the presence of salt had an effect on the distance travelled down a plate of agar/mucin positioned at 80 º to the horizontal (Figure 5.8). After 12 min it was observed that discs containing NaCl appeared to be hydrating more rapidly than those without NaCl. This behaviour is expected, as salt ions attract more hydration water molecules, promoting water uptake into the inserts.[48] Although the distances travelled by the hydrated gels were similar for the first 150 min, the discs containing NaCl subsequently spread further than those without. Kajiyama and colleagues have reported that HPMC tablets containing NaCl show a reduced disintegration time in water, related to a positive enthalpy of dissolution.[49] Liu and co-workers have found that NaCl weakens intermolecular hydrogen bonding in HPMC hydrogels by attracting water molecules, making hydrogen bonding easily disrupted.[48] This will reduce the force holding the gel together, allowing greater spread. Additionally, Mitchell and co-workers have shown that dehydrating HPMC gel results in greater interaction between hydrophobic methoxy groups, increasing viscosity.[50] This suggests that if NaCl attracts more water into the polymer, then hydrophobic interactions and therefore viscosity could be reduced. Therefore, a reduction in both hydrogen bonding strength and hydrophobic interaction may reduce the force holding the gel together, subsequently increasing the surface area covered by the gel *in situ*. This may act to make the active ingredients more rapidly bioavailable, although it may be detrimental to mucoadhesion.

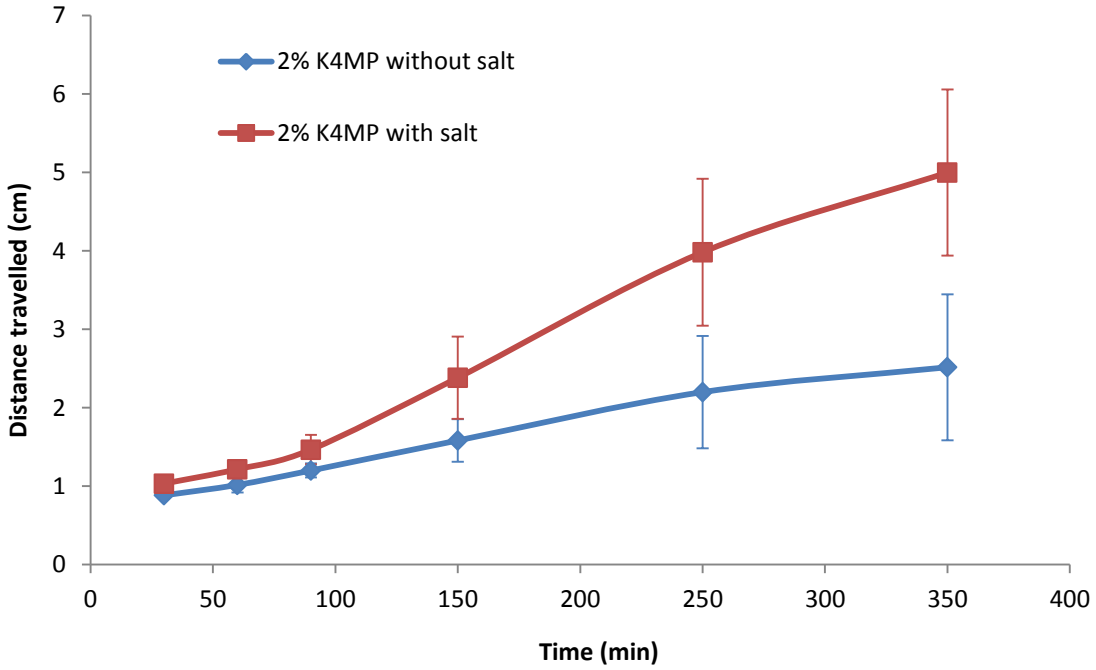

Figure 5.8. Graph showing the distance spread on agar/mucin plate, as a function of time, for HPMC discs with and without NaCl.

In order to determine if the presence of NaCl had any influence on the bioadhesive potential of the formulations, the texture analyser *ex vivo* mucoadhesion test was carried out using porcine nasal tissue (n=3). Neither peak force of detachment or work of adhesion was significantly different (P=0.195 and P=0.187, respectfully, paired t-test) between inserts with and without NaCl (Figure 5.9). The average peak force of detachment and work of adhesion were lower, suggesting that the inclusion of NaCl may act to reduce bioadhesion. The NaCl may have attracted more water molecules into the system allowing more rapid hydration, as was eluded to when the discs containing NaCl appeared to hydrate more rapidly. This may have caused reduced viscosity of the polymer, resulting in the lower average peak force of detachment and work of adhesion.

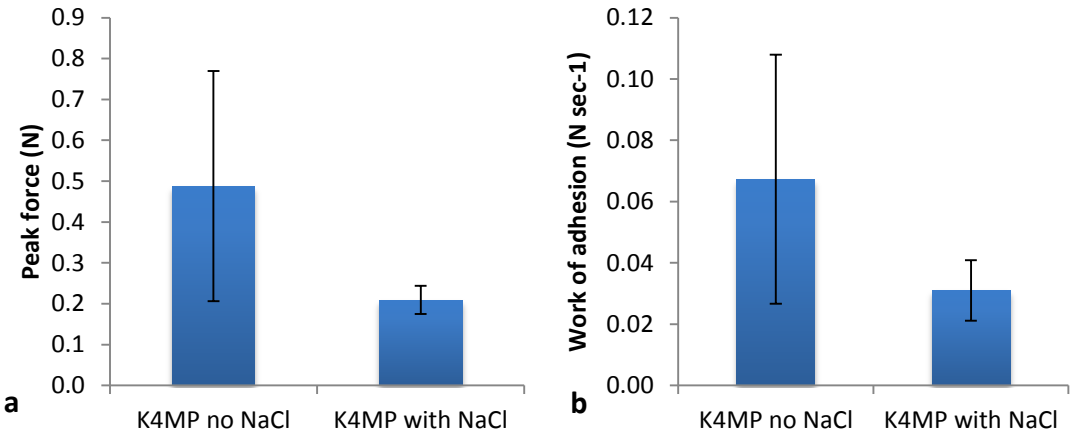

Figure 5.9. Graphs comparing the a) peak force of detachment and b) work of adhesion, for adhesion of lyophilised K4MP discs on porcine nasal mucosa (*n*=3, error bars represent standard deviation).

This study would have benefited from water uptake experiments. These were not carried out due to availability of the DVS instrument, and time cobstraints.

Inserts containing 4% (w/w) CB[6] with and without NaCl were examined by SEM to investigate structure of the polymer and drug complex (note that CB[6] was used instead of CB[7] due to cost). The micrographs revealed that without NaCl the regular porous structure was no longer present. With NaCl, the structure became more ordered, with more defined pores visible (Figure 5.10). In this case, as CB[6] is also present, the observation may be because the NaCl in the wet gel has dissolved the CB[6], allowing it to become incorporated into the polymer matrix. Excess salt is seen on the surface of the polymer (Figure 5.10). The presence of NaCl may have affected the structure of HPMC in solution, prior to freeze drying. The NaCl may have attracted water molecules towards itself, away from the HPMC. This may have had an effect similar to salting-out, whereby to minimise free energy the hydrophobic methoxy substitutions orient themselves towards each other, and water molecules group together. This could mean that pockets of water in the gel were larger, resulting in larger ice crystals and larger, more defined pores in the final lyophilisate. These larger pores would also allow for more rapid and deep penetration of moisture during hydration, which would also help explain why the inserts containing NaCl hydrated and spread more effectively. In light of these results, inserts containing cisplatin or cisplatin@CB[7] were prepared using NaCl solution, rather than water.

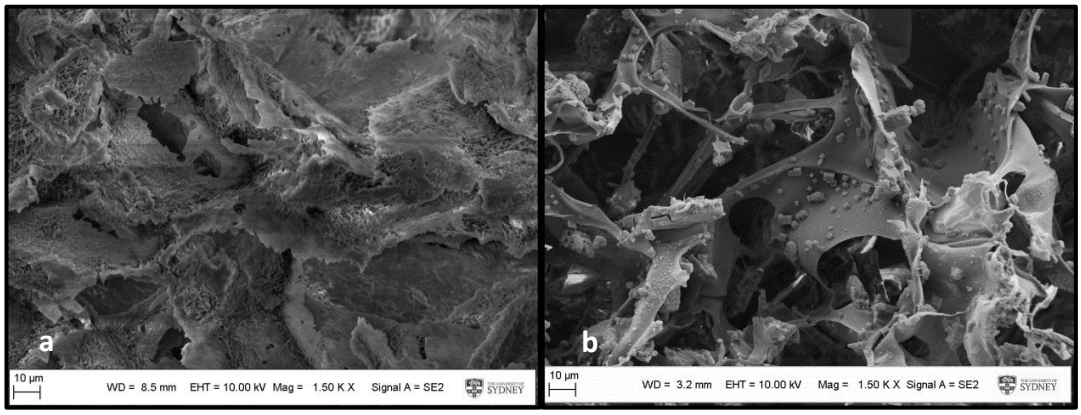

Figure 5.10. SEM micrographs of lyophilised nasal inserts containing 4% CB[6] a) without and b) with NaCl. Both images recorded at 1,500 × magnification.

5.4.5 Distribution of cisplatin in lyophilised nasal inserts

Distribution of cisplatin throughout the lyophilised nasal inserts was examined by ICP-MS. Results showed that the average platinum distribution was improved with encapsulation in CB[7] (Figure 5.11). The difference however was not statistically significant (P_{tip}=0.451, P_{middle}=0.788 and P_{bottom}=0.585, paired *t*-test). The error associated with the cisplatin@CB[7] samples (standard deviation, *n*=3) was smaller, indicating that the distribution may be more reproducible with cisplatin@CB[7], over native cisplatin. This may be due to an increase in aqueous solubility upon encapsulation in CB[7]. Cucurbituril has not been shown previously in the literature to improve drug distribution in a solid dosage form. Note that the "tip" of the insert is named to reflect the direction of insertion, and is in fact oriented downwards in the freeze dryer.

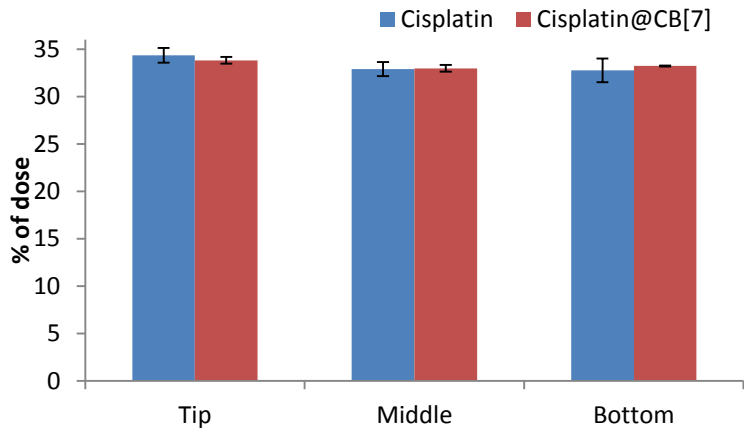

Figure 5.11. Graph comparing the distribution of cisplatin through lyophilised inserts containing cisplatin and cisplatin@CB[7] (*n*=3, error bars represent standard deviation).

5.4.6 Texture analysis of lyophilised disc formulations

Disc formulations of cisplatin and cisplatin@CB[7] were examined for hardness and springiness, in order to provide information about ease of handling prior to insertion. Hardness indicates the force of compression which can be withstood by the insert, and springiness indicated how the insert could recover back to its spongy shape after compression. Whilst the inserts containing cisplatin@CB[7] had reduced average values for hardness and springiness, the difference in hardness compared to cisplatin inserts was not significant ($P_{hardness}$=0.527, $P_{springiness}$=0.291, paired *t*-test, Figure 5.12). Importantly, the average measurement of hardness did not fall below 2 N, the minimum required to withstand normal patient handling.[51]

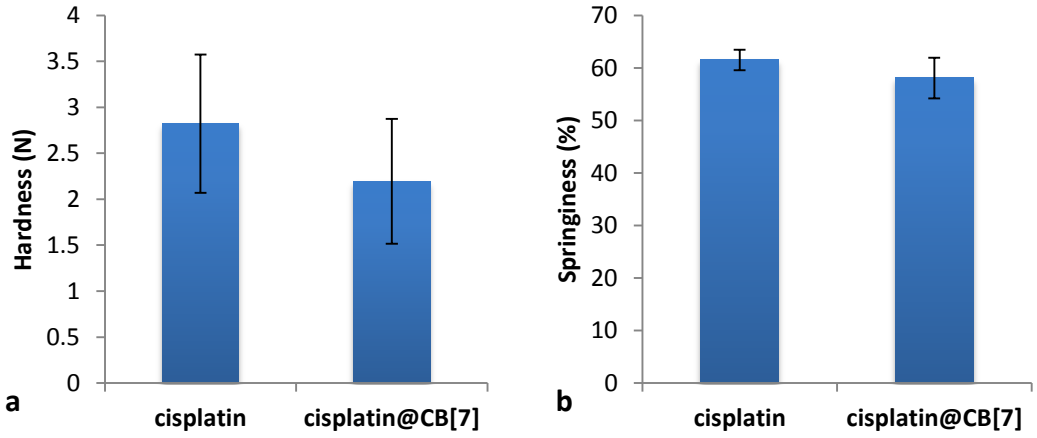

Figure 5.12. Graphs comparing the a) hardness and b) springiness, of lyophilised HPMC discs containing cisplatin with those containing cisplatin@CB[7] (*n*=3, error bars represent standard deviation).

5.4.7 Moisture uptake of formulations

Lyophilised inserts containing either cisplatin or cisplatin@CB[7] were examined for moisture uptake in SNES (*n*=3). For the first 150 min the weight gain, representing moisture uptake was higher for the encapsulated form (Figure 5.13). This indicated that encapsulating cisplatin in CB[7] helps to increase moisture uptake in the time immediately after insertion, which may assist gelling, and therefore bioadhesion and subsequent drug release. This difference in moisture uptake behaviour may be due to the carbonyl groups on the CB[7] acting as hydrogen bond acceptors for waters of hydration. In Chapter 2 it was observed that increasing the percentage of CB[6] or CB[7] in the formulation acted to reduce the moisture uptake. In Chapter 3, encapsulation of K6 in CB[6] also acted to reduce the moisture uptake of nasal inserts. The difference in these findings may be related to the aqueous solubility of these species. K6 appears to be less water soluble when encapsulated in CB[6], whereas the aqueous solubility of cisplatin appears to increase when encapsulated in CB[7]. This increased hydrophilicity may be the driving force for enhanced moisture uptake in the system in the early stages.

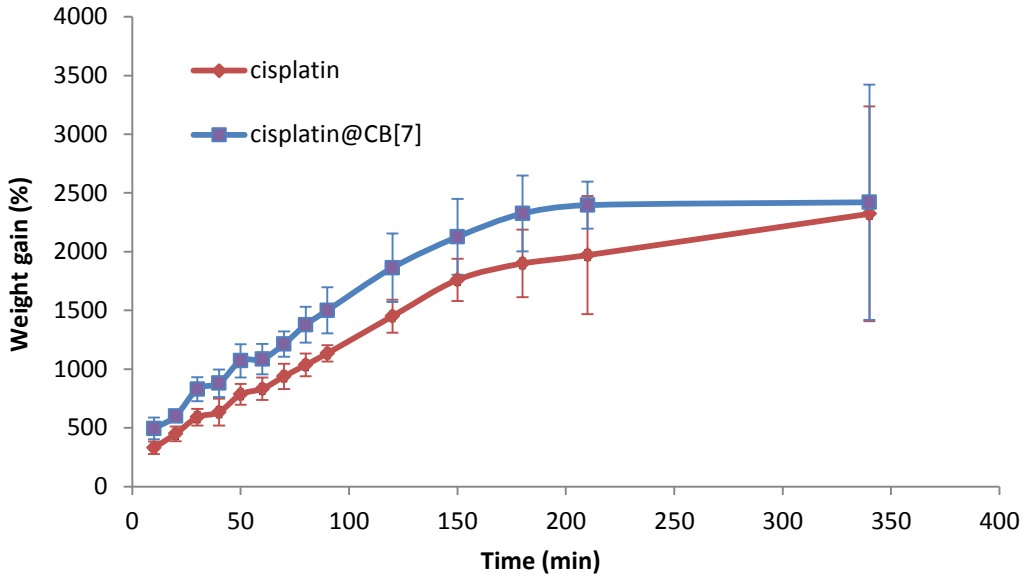

Figure 5.13. Graphs comparing the water uptake of lyophilised inserts containing cisplatin with those containing cisplatin@CB[7].

The moisture uptake potential of the inserts was also examined by DVS. Instead of SNES, the instrument uses distilled water. Quartered disc-shaped lyophilisates were used for this experiment in order to minimise sample size but maintain a repeatable shape. These results showed that the cisplatin@CB[7] inserts absorbed less water than both native cisplatin and blank discs (Table 5.3). This suggests that encapsulating the cisplatin in CB[7] is detrimental to the lyophilisate's ability to absorb water and hydrate to form a bioadhesive gel. This means it may be more rapidly cleared through MCC and the drug would ultimately be less bioavailable. This data is contradictory to the results of the moisture uptake experiment. This may be a result of experimental error – the length of time taken to run the samples on the DVS (> 1 week), meant that it was only possible to carry out one repeat. Additionally, the influence of the electrolytes in the SNES may result in these differences. However, it could also be argued that these differences are negligible when pertaining to such large percentage water gains.

It should also be noted that DVS data represents water uptake from the vapour form, which is not necessarily representative of liquid water uptake from the mucosal surface in vivo. This data may be more useful for predicting the behaviour of the side(s) of the insert that are not in contact with the mucosa, and absorbing water vapour from the inhaled/exhaled air.

Table 5.3. DVS data for lyophilised HPMC discs.

Insert type	Initial water content (%)	Total H_2O absorbed (% of dry weight)	
		Cycle 1	Cycle 2
Blank	0.1	289.1	318.5
Cisplatin	0.0	324.9	315.0
Cisplatin@CB[7]	0.0	215.8	216.8

Examining the sorption/desorption isotherms can provide further insight in to the process of the insert absorbing water. For both cisplatin and cisplatin@CB[7] containing inserts, the sorption curves followed an almost exponential profile, whereby the more water the insert absorbed, the greater its potential to absorb water (Figure 5.14). This happens because as the insert absorbs water and hydrates, the mobility of the polymer chains increases, exposing more hydroxyl groups.[52] The carbonyl groups on CB[*n*]s act as hydrogen bond acceptors. If the presence of CB[7] in the insert increases the network of electrostatic bonds in the system, the mobility of the chains will be reduced, and a reduced number of hydroxyl groups will be exposed for further hydration. Additionally, if the hydroxyl groups of the polymer are hydrogen bonded to the carbonyls of the CB[7], the system will be more saturated and less water may be incorporated into the gel. The moisture uptake in SNES may be different because the Na^{+} Ca^{2+} and K^{+} ions from the SNES can associate to the δ^{-ve} carbonyl portals *via* electrostatic interactions. This means that the hydrogen bonds between the carbonyl portals and the polymer hydroxyl groups cannot form. The hydroxyl groups of the polymer are then free to hydrogen bond to the absorbed water, as they are in the formulations with no cucurbituril. This may explain the discrepancy between the DVS and moisture uptake data.

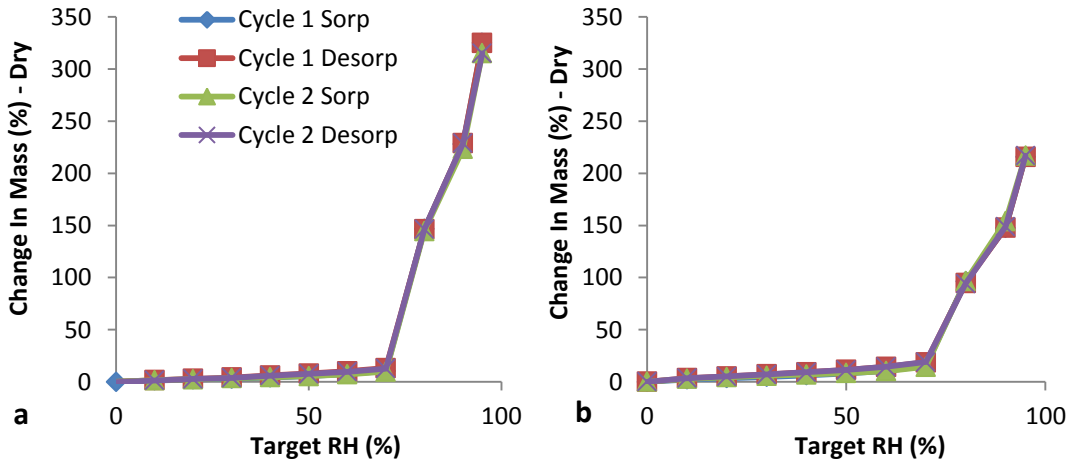

Figure 5.14. Isotherms for lyophilised HPMC formulations containing a) cisplatin and b) cisplatin@CB[7].

5.4.8 Formulation spread on mucin/agar

In order to further examine the gelling and spreading properties of the formulations, their spread on mucin/agar plates was observed. The distance travelled by the gel front of HPMC discs containing cisplatin was compared to those containing cisplatin@CB[7] (*n*=3, Figure 5.15). This test is intended to model the gelling and spreading of the lyophilised inserts once *in situ*, and is important as the greater surface area that is covered, the more drug can permeate through the mucosa.[53] The spread distance was equivalent for these formulations over 350 minutes (f_2=99.09, equivalent). This suggests that encapsulating cisplatin in CB[7] has not affected how the formulation spreads. This result was unexpected, as in Chapter 3 it was shown that increasing the amount of CB[6] or CB[7] in the formulation acted to increase spread. In Chapter 4, K6@CB[6] and di-Pt@CB[7] formulations spread further than their non-encapsulated counterparts. This suggests that the change induced by encapsulation in a CB[*n*] is dependent on the properties of the native drug in the first instance.

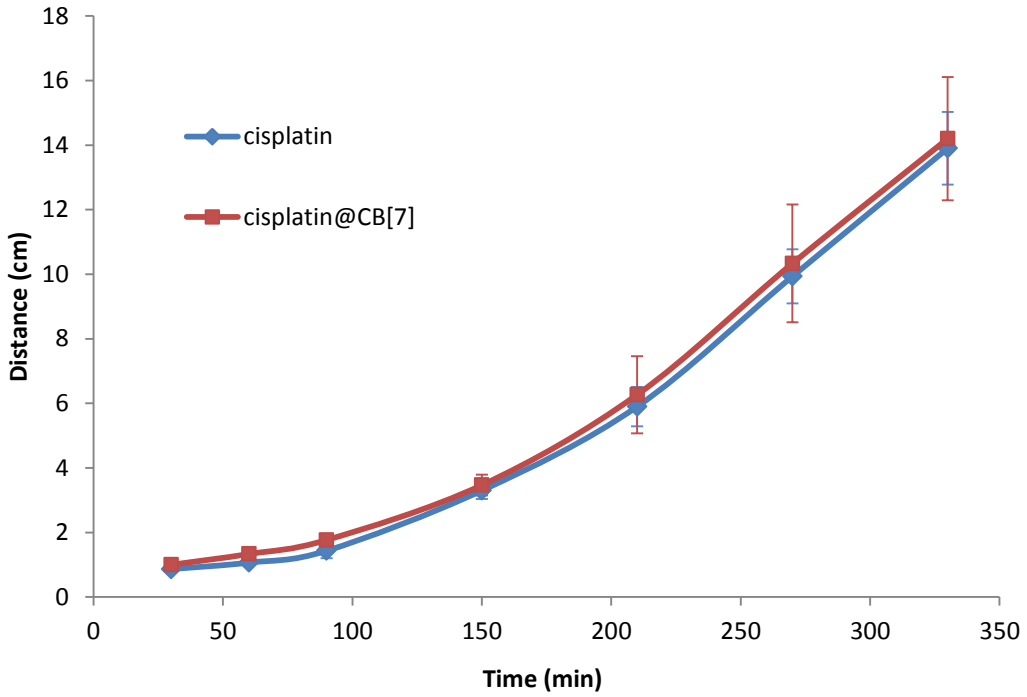

Figure 5.15. Graph comparing the spread of HPMC discs containing cisplatin with those containing cisplatin@CB[7].

5.4.9 *Ex vivo* mucoadhesion

The test produced no significant difference in mucoadhesion between cisplatin and cisplatin@CB[7] inserts, with large errors (Figure 5.16). This may be attributed to natural variances in tissue. Additionally, the limited availability of starting material meant that only three repeats could be carried out. Increasing the number of repeats may produce statistically significant results.

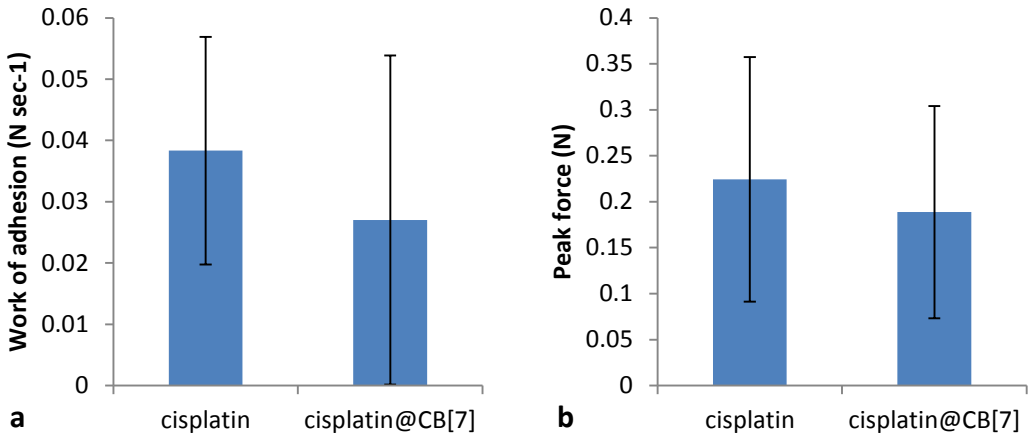

Figure 5.16. Graphs comparing the a) work of adhesion, and b) peak force of detachment; for lyophilised HPMC disc formulations containing cisplatin and cisplatin@CB[7] (*n*=3, error bars represent standard deviation).

5.4.10 *In vitro* drug release using Franz cells

Release of cisplatin and cisplatin@CB[7] from the inserts was modelled *in vitro*, using Franz cells and SNES at 33 ºC as the release medium. Samples were removed at predetermined time points and analysed by ICP-MS (*n*=3, Figure 5.17 and Figure 5.18). There was no significant difference between the amount of cisplatin released from lyophilised inserts containing cisplatin or cisplatin@CB[7] (f_2=99.99, equivalent), suggesting that CB[7] encapsulation does not affect the release of cisplatin from the inserts (Figure 5.18). The release from inserts containing cisplatin@CB[7] had smaller average standard deviation (±0.007, *c.f.* ±6.629) suggesting that the release is more consistent and repeatable. This may be related to

the more even distribution of cisplatin@CB[7] in the nasal inserts compared to native cisplatin.

Repeating the release in deionised water rather than SNES may provide more insight into the role of electrolytes in the release medium. If the release of cisplatin@CB[7] is reduced *c.f.* cisplatin in pure water, it could suggest that the K^+, Na^+ and Ca^{2+} ions in the SNES play an important role in the hydration of the polymer system. By associating themselves to the CB[7] portal, they may block hydrogen bonding between the CB[7] and polymer, allowing increased chain mobility and subsequent drug release. If this is the case, without these ions in the release medium, the CB[*n*]s would remain hydrogen bonded to the polymer, reducing chain mobility and drug release in deionised water.

The early peak in drug release in the inserts has also been observed with di-Pt and di-Pt@CB[7], suggesting that it is not an analytical error. This supports the theory that the initial burst is related the complex hydration kinetics of the insert, whereby the drug near the surface is quickly dissolved and released in a burst before the insert could properly gel and control release.[54] The following lag, while water is absorbed and penetrates the insert, results in a reduction in concentration when the sample is removed and replaced with fresh medium. Additionally, the initial capillary uptake of water results in swelling of the HPMC, blocking the porous channels. The newly formed gel-layer at the interface also acts as a barrier to water diffusion.[55]

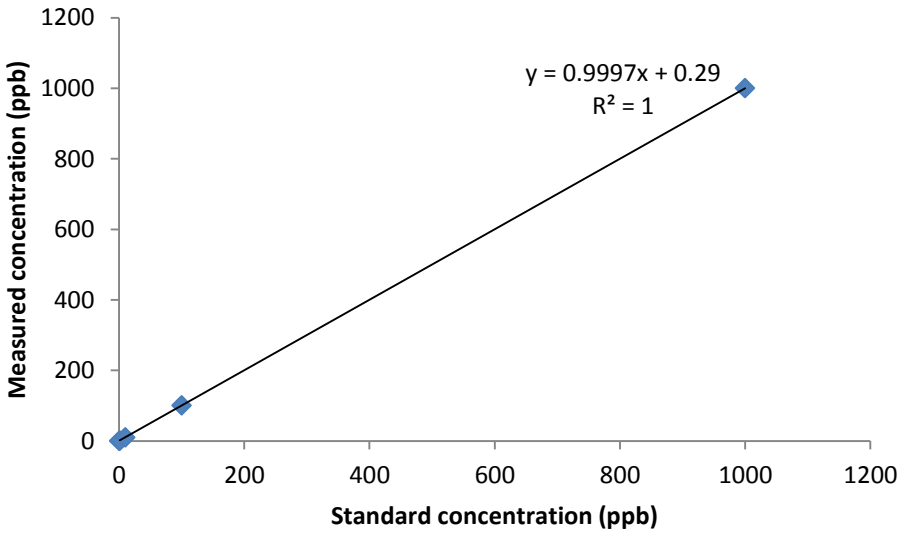

Figure 5.17. Calibration data for ICP MS analysis of cisplatin release *in vitro*.

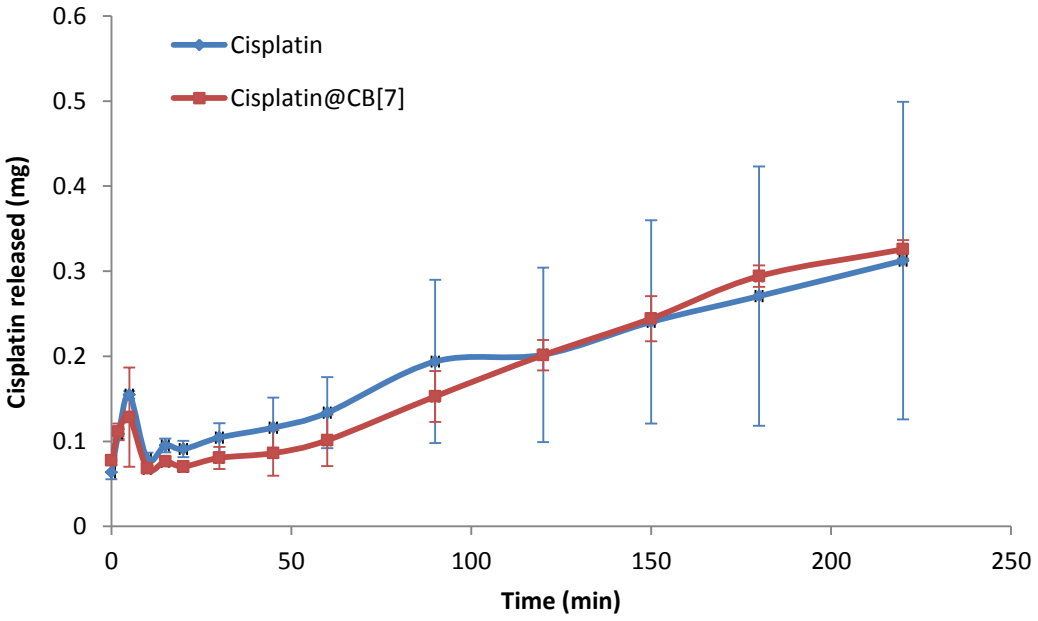

Figure 5.18. Graph comparing the release of cisplatin from inserts containing cisplatin with those containing cisplatin@CB[7]. Error bars represent standard deviation (*n*=3).

As CB[7] encapsulation of cisplatin did not significantly affect the *in vitro* release from lyophilised nasal inserts, the *ex vivo* release was examined to determine if the encapsulation affected drug absorption.

5.4.11 *Ex vivo* release through porcine nasal tissue

In order to model the effect of CB[7] encapsulation of cisplatin on absorption through the nasal mucosa, the Franz cell release was repeated with freshly excised porcine nasal tissue. The SNES release medium was replaced with PBS, pH 7.4 to model the bloodstream. ICP MS analysis of the samples revealed that although the average amount of cisplatin released from cisplatin@CB[7] inserts was less than that of the cisplatin inserts, the difference was not significant (f_2=99.89, equivalent. Figure 5.19 and Figure 5.20). This suggests that encapsulating cisplatin in CB[7] is not detrimental to the uptake of the drug from nasal insert formulations.

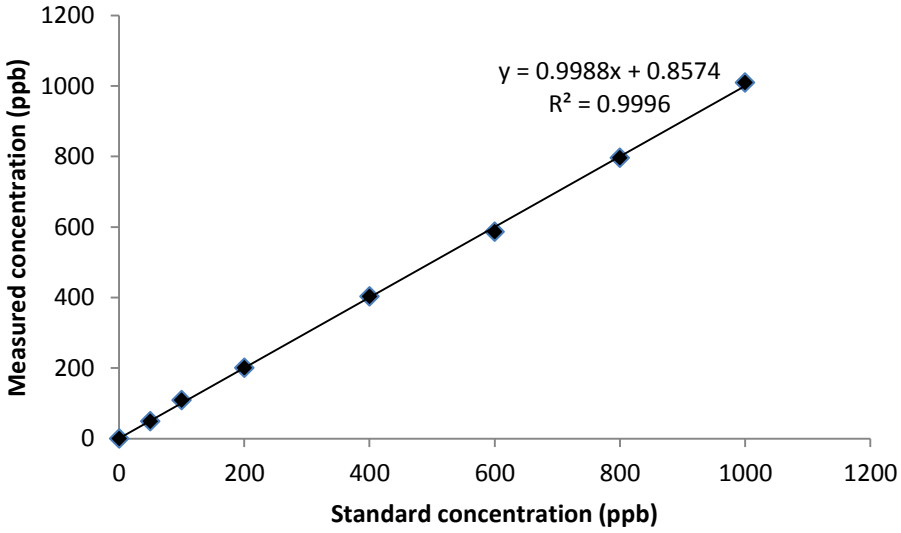

Figure 5.19. Calibration data for ICP MS analysis of *ex vivo* cisplatin release.

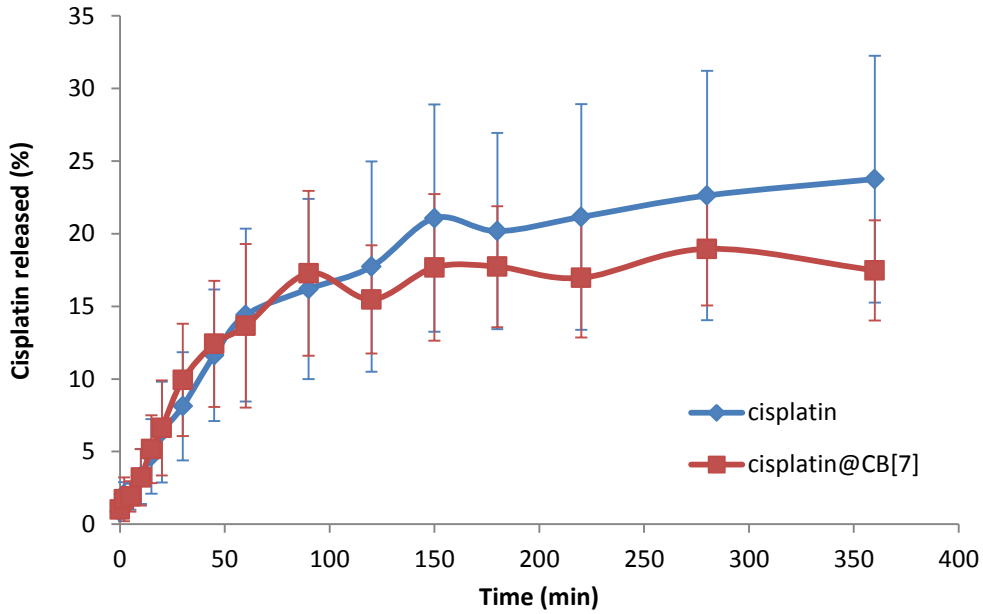

Figure 5.20. Graph comparing the release of cisplatin and cisplatin@CB[7] from lyophilised nasal inserts, through porcine nasal tissue. Error bars represent standard deviation (*n*=3).

The higher concentrations of cisplatin released (around double) compared to the *in vitro* release may be a result of the change in release medium. Since the release of cisplatin and cisplatin@CB[7] were similar in the earlier SNES *in vitro* release, and also in this PBS *ex vivo* release, this suggests that it is not due to the presence of CB[7], rather it is an effect of the release medium on the polymer. Therefore, as the *in vitro* and *ex vitro* experiments were not carried out in parallel, the results should not be compared directly. The lack of a "burst release" in the early stages suggests that diffusion through the tissue is the limiting factor here, rather than release from the insert itself. Additionally, sequestering of the platinum into the tissue may be masking the burst release.

The reliability of this result however is dependent upon the mechanism(s) by which cisplatin and cisplatin@CB[7] are taken up into cells. Although a passive mechanism for cisplatin uptake is generally accepted, there is evidence that an active transport mechanism is in operation.[56] Whilst CB[7] and CB[8] have been shown to cross the cell membrane with a guest molecule contained,[57] the mechanism by which this occurs remains unreported in the literature. If absorption of one or both of these cisplatin species involves an active transport mechanism, it may be possible that

these are not functioning in the excised tissue. An *in vivo* test may be required to fully understand how CB[7] encapsulation affects the uptake of the native and encapsulated cisplatin.

5.4.12 Considerations for a nasal insert applicator device

There are currently no drugs on the market which utilise a lyophilised nasal insert formulation. If the dosage form was to make it to clinical trial, some other practical aspects would have to be considered. During transport and storage, the lyophilised insert would need to be kept in an airtight container in a dry atmosphere to prevent any moisture uptake. Additionally, the inserts would have to be protected from any mechanical compression which may result in a loss of the absorptive sponge-like form. A practical consideration of a nasal insert formulation is the ease of use for the patient. Nasal drug delivery is associated with a higher degree of patient acceptability than parenteral or, in some cases, oral delivery. However, nasal medications are often administered incorrectly by patients,[58] which may result in reduced bioavailability and efficacy.

The use of a medical device, similar to a device for vaginal drug delivery (*e.g.* pessary applicator) would allow for easier application into the nasal cavity (Figure 5.21). Housed in such a device, the insert would have partial protection from compression. The applicator, with a pre-loaded insert, could then be sealed individually in a foil packet, keeping the device and the insert clean and dry.

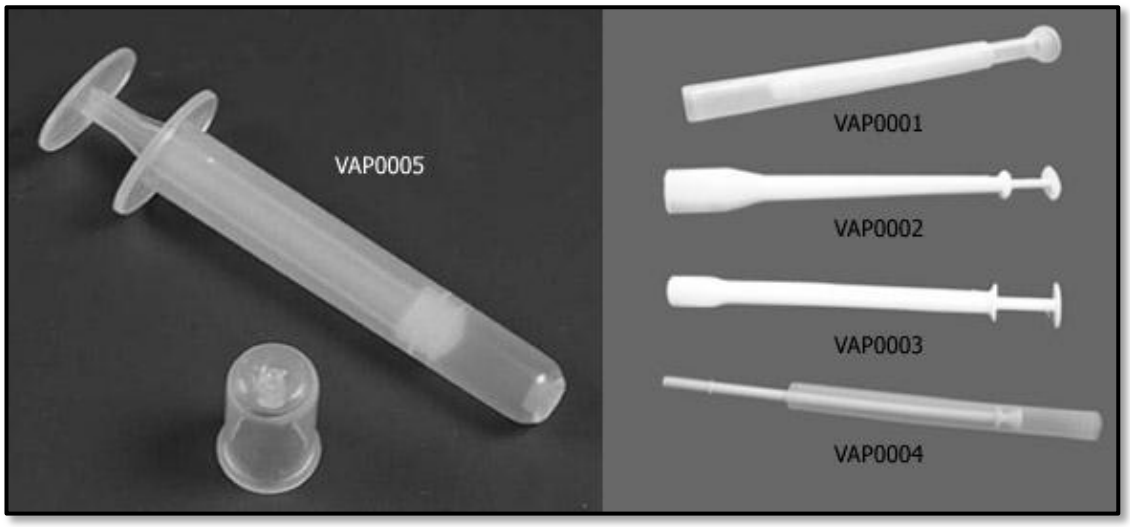

Figure 5.21. Image showing examples of medical devices for vaginal drug delivery.[59]

5.5 CONCLUSIONS

Cisplatin has been successfully encapsulated in CB[7], as demonstrated by ^{1}H NMR. The encapsulation has been shown to improve the thermal stability of the native drug, as demonstrated by differential scanning calorimetry. Cisplatin@CB[7] has then been formulated with HPMC (Grade K4MP) into lyophilised nasal inserts. Control inserts containing equimolar quantities of native cisplatin have also been produced for comparison. The freeze drying program, Method 3, has been developed to eliminate meltback. Given more time and more starting material, the programme could be further optimised for this formulation.

The inserts containing either cisplatin or cisplatin@CB[7] were then examined with a view to establish how encapsulation of the drug affected the formulation. Neither hardness or spreadability of the inserts were significantly altered with encapsulation of cisplatin in CB[7]. Inserts containing cisplatin and those containing cisplatin@CB[7] both showed average hardness > 2 N, and are therefore expected to withstand normal patient handling. The mucoadhesion of disc formulations on *ex vivo* porcine nasal mucosa was also not significantly affected by encapsulation. Discs being compared were tested on different areas of the same piece of tissue in an attempt to minimise error, however a large standard deviation still occurred in the results. Increasing the sample size may produce more significant results. Additionally, modifying the test parameters to reduce the contact force, increase the contact time and increase the speed at which the probe is removed[60-62] have been shown to improve consistency in results and should be considered. Khutoryanskiy's research group have developed a synthetic hydrogel capable of mimicking the bioadhesive properties.[62,63] The use of these hydrogels could potentially improve the precision of mucoadhesion results, allowing comparisons between formulations to be more easily made. Additionally, such a synthetic polymer would negate the need for animal tissue in these experiments.

Where there were differences observed between cisplatin and cisplatin@CB[7] inserts, these were thought to be related to a change in aqueous solubility and hydrogen bonding potential. Distribution of cisplatin and cisplatin@CB[7] were not

significantly different, but the small improvement recorded upon encapsulation may allow for more accurate and precise dosing and drug release. This was confirmed with the *in vitro* release from the inserts whereby the standard deviation associated with cisplatin@CB[7] was smaller than that of native cisplatin inserts.

Contradictory results from SNES moisture uptake and instrument controlled DVS highlighted that the electrolytic composition of the uptake medium was an important parameter in the test. It is hypothesised that the +ve ions in the SNES can associate to the CB[7] portals aiding solubility and increasing chain mobility exposing more polymer hydroxyl groups and aiding water uptake. Additionally, the association of these ions at the CB[7] portals may act as a steric barrier to hydrogen bonding between the CB[7] and the polymer, providing increased polymer chain mobility. As these high ion concentrations are not present in the distilled water, the CB[7] in the formulation acts as a hydrogen bond acceptor for the polymer hydroxyl groups. This increases the number of hydrogen bonds in the system, reducing polymer chain mobility and slowing the ingress of water.

The inclusion of NaCl in the formulation was favourable as the presence of Na^+ ions has been shown to aid the dissolution of CB[*n*]s in aqueous solutions. Additionally, increasing the Cl^- concentration of the gels would help keep the cisplatin from degrading *via* aquation. The addition of an ionic component to a non-ionic polymer resulted in a reduction of structural integrity. Subsequent reduction in hydrogen bond strength made the hydrated formulation more spreadable. Additionally, the changes to the structure of water in the gels brought about by the presence of NaCl produced larger, more defined pores in the lyophilised nasal insert.

A medical device, based on a pessary applicator, has been considered to improve the transport, storage and administration of the nasal insert formulation.

The lyophilised nasal insert formulation is still in its infancy, having been investigated by only a small number of research groups. As such, there is a lack of standardised tests for the dosage forms. Additionally, a limited availability of *in vivo*

data means that whilst physical properties of the inserts can be investigated, the clinical relevance of the results can only be eluded to. The limited availability of CB[7] for the project has meant that the number of repeats has been low (n=3). Increasing the number of repeats would improve the reliability of the data and may produce more significant findings. Additionally, the solubility of cisplatin@CB[7] could not be determined due to limited supply of CB[7] and the complex behaviour of cisplatin in solution making instrumental analytical measurements difficult.

Other types of nasal delivery system which enhance drug permeability without the use of absorption promoters are emerging. Matsuyama and colleagues have reported that drug absorption in the nose can be improved using insoluble powdered fillers. The drug is thought to adhere to the surface of the filler particles, and dissolves rapidly once deposited in the nose. The high drug concentration produced drives the enhanced diffusion into the epithelial membrane.[64]

5.6 REFERENCES

(1) Wheate, N.J., Walker, S., Craig, G.E. and Oun, R., *Dalton T.*, 2010, **39**, 8113-8127.

(2) Hensing, T.A., Hanna, N.H., Gillenwater, H.H., Camboni, M.G., Allievi, C. and Socinski, M.A., *Anti-Cancer Drug.*, 2006, **17**, 697-704.

(3) *Martindale: The Complete Drug Reference*, 35th ed., Pharmaceutical Press, London, 2007.

(4) Einhorn, L.H., *P. Natl. Acad. Sci. USA*, 2002, **99**, 4592-4595.

(5) Kelland, L., *Nat. Rev. Cancer*, 2007, **7**, 573-584.

(6) Levêque, D., *Lancet Oncol.*, 2008, **9**, 1102-1107.

(7) Levêque, D., Michallat, A., Schaller, C. and Ranc, M., *Bull. Cancer* 2005, **92**, 498-500.

(8) British National Formulary, http://www.medicinescomplete.com/mc/bnf/current/PHP5487-platinum-compounds.htm#PHP5489, *accessed 12th January 2013.*

(9) Mishima, Y., Nagasaki, E., Terui, Y., Irie, T., Takahashi, S., Ito, Y., Oguchi, M., Kawabata, K., Kamata, S. and Hatake, K., *Cancer*, 2004, **101**, 1437-1444.

(10) Kim, D.W., Jo, Y.H., Kim, J.H., Wu, H.G., Rhee, C.S., Lee, C.H., Kim, T.Y., Heo, D.S., Bang, Y.J. and Kim, N.K., *Cancer*, 2004, **101**, 2257-2260.

(11) Samant, S., Robbins, K.T., Vang, M., Wan, J. and Robertson, J., *Arch. Otolaryngol. Head Neck Surg.*, 2004, **130**, 948-955.

(12) Albertsson, M., Tennvall, J., Andersson, T., Biorklund, A., Elner, A. and Johansson, L., *Melanoma Res.*, 1992, **2**, 101-104.

(13) Palazzi, M., Guzzo, M., Bossi, P., Tomatis, S., Cerrotta, A., Cantu, G., Locati, L.D. and Licitra, L., *Tumori*, 2004, **90**, 60-65.

(14) Chan, A.T., Ma, B.B., Lo, Y.M., Leung, S.F., Kwan, W.H., Hui, E.P., Mok, T.S., Kam, M., Chan, L.S., Chiu, S.K., Yu, K.H., Cheung, K.Y., Lai, K., Lai, M., Mo, F., Yeo, W., King, A., Johnson, P.J., Teo, P.M. and Zee, B., *J. Clin. Oncol.*, 2004, **22**, 3053-3060.

(15) Chua, D.T., Sham, J.S. and Au, G.K., *Head Neck*, 2004, **26**, 118-126.

(16) http://www.off-label.com/Drug/resultsDrugUS.cfm?drug=cisplatin, *13th August 2012*.

(17) Paiva, M.B., Bublik, M., Castro, D.J., Udewitz, M., Wang, M.B., Kowalski, L.P. and Sercarz, J., *Photomed. Laser Surg.*, 2005, **23**, 531-535.

(18) Dubey, S.P., Murthy, D.P., Kaleh, L.K. and Vele, D.D., *Auris Nasus Larynx*, 1999, **26**, 57-64.

(19) Xie, Y., Aillon, K.L., Cai, S., Christian, J.M., Davies, N.M., Berkland, C.J. and Forrest, M.L., *Int. J. Pharm.*, 2010, **392**, 156-163.

(20) Keskar, V., Mohanty, P.S., Gemeinhart, E.J. and Gemeinhart, R.A., *J. Control. Release*, 2006, **115**, 280-288.

(21) Gregg, R.W., Molepo, J.M., Monpetit, V.J., Mikael, N.Z., Redmond, D., Gadia, M. and Stewart, D.J., *J. Clin. Oncol.*, 1992, **10**, 795-803.

(22) Screnci, D., McKeage, M.J., Galettis, P., Hambley, T.W., Palmer, B.D. and Baguley, B.C., *Br. J. Cancer*, 2000, **82**, 966-972.

(23) Illum, L., Watts, P., Fisher, A.N., Hinchcliffe, M., Norbury, H., Jabbal-Gill, I., Nankervis, R. and Davis, S.S., *J. Pharmacol. Exp. Ther.*, 2002, **301**, 391-400.

(24) Köberle, B., Tomicic, M.T., Usanova, S. and Kaina, B., *Biochim. Biophys. Acta*, 2010, **1806**, 172-182.

(25) Wheate, N.J., *Nanomedicine*, 2012, **7**, 1285-1287.

(26) Wagstaff, A.J., Brown, S.D., Holden, M.R., Craig, G.E., Plumb, J.A., Brown, R.E., Schreiter, N., Chrzanowski, W. and Wheate, N.J., *Inorg. Chim. Acta*,

(27) Chupin, V., de Kroon, A.I.P.M. and de Kruijff, B., *J. Am. Chem. Soc*, 2004, **126**, 13816-13821.

(28) Kirkpatrick, G.J., Plumb, J.A., Sutcliffe, O.B., Flint, D.J. and Wheate, N.J., *J. Inorg. Biochem.*, 2011, **105**, 1115-1122.

(29) Boulikas, T., *Oncol. Rep.*, 2004, **12**, 3-12.

(30) Boulikas, T., *Cancer Therapy*, 2007, **5**, 351-376.

(31) Boulikas, T., Stathopoulos, G.P., Volakakis, N. and Vougiouka, M., *Anticancer Res.*, 2005, **25**, 3031-3030.

(32) Jehn, C.F., Boulikas, T., Kourvetaris, A., Possinger, K. and Luftner, D., *Anticancer Res.*, 2007, **27**, 471-475.

(33) Stathopoulos, G.P., Boulikas, T., Vougiouka, M., Deliconstantinos, G., Rigatos, S., Darli, E., Villotou, V. and Stathopoulos, J.G., *Oncol. Rep.*, 2005, **13**, 589-595.

(34) Stathopoulos, G.P., Boulikas, T., Vougiouka, M., Rigatos, S.K. and Stathopoulos, J.G., *Oncol. Rep.*, 2006, **15**, 1201-1204.

(35) Stathopoulos, G.P., Rigatos, S., Stathopoulos, J. and Batzious, S., *J. Drug Del.Therap.*, 2012, **2**, 106-109.

(36) Koukourakis, M.I., Giatromanolaki, A., Pitiakoudis, M., Kouklakis, G., Tsoutsou, P., Abatzoglou, I., Panteliadou, M., Sismanidou, K., Sivridis, E. and Boulikas, T., *Int. J. Radiat. Oncol.*, 2010, **78**, 150-155.

(37) http://www.hindawi.com/journals/jdd/2012/581363/fig1/, *14th August 2012.*

(38) Plumb, J.A., Venugopal, B., Oun, R., Gomez-Roman, N., Kawazoe, Y., Venkataramanan, N.S. and Wheate, N.J., *Metallomics*, 2012, **4**, 561-567.

(39) Wheate, N.J., Buck, D.P., Day, A.I. and Collins, J.G., *Dalton T.*, 2006, **3**, 451-458.

(40) Differential Scanning Calorimetry (Dsc) a Beginner's Guide, http://www.perkinelmer.com/CMSResources/Images/44-74542GDE_DSCBeginnersGuide.pdf, *accessed 12th August 2012.*

(41) McInnes, F.J., Anthony, N.G., Kennedy, A.R. and Wheate, N.J., *Org. Biomol. Chem.*, 2010, **8**, 1477-0520.

(42) Hoffmann, R., Knoche, W., Fenn, C. and Buschmann, H.-J., *J. Chem. Soc, Faraday Trans.*, 1994, **90**, 1507-1511.

(43) Wheate, N.J., Kumar, P.G.A., Torres, A.M., Aldrich-Wright, J.R. and Price, W.S., *J. Phys. Chem. B*, 2008, **112**, 2311-2314.

(44) Thapa, P., *Studies of a Lyophilised Nasal Delivery System*, University of Strathclyde, 2000.

(45) Ohwaki, T., Ando, H., Watanabe, S. and Miyake, Y., *J. Pharm. Sci.*, 1985, **74**, 550-552.

(46) Ohwaki, T., Ando, H., Kakimoto, F., Uesugi, K., Watanabe, S., Miyake, Y. and Kayano, M., *J. Pharm. Sci.*, 1987, **76**, 695-698.

(47) Kartalou, M. and Essigmann, J.M., *Mutat. Res.-Fund. Mol. M.*, 2001, **478**, 23-43.

(48) Liu, S.Q., Joshi, S.C. and Lam, Y.C., *J. App. Polym. Sci.*, 2008, **109**, 363-372.

(49) Kajiyama, A., Takagi, H., Moribe, K. and Yamamoto, K., *Chem. Pharm. Bull.*, 2008, **56**, 598-601.

(50) Mitchell, K., Ford, J.L., Armstrong, D.J., Elliott, P.N.C., Rostron, C. and Hogan, J.E., *Int. J. Pharm.*, 1990, **66**, 233-242.

(51) Bertram, U. and Bodmeier, R., *Eur. J . Pharm. Biopharm.*, 2006, **27**, 62-71.

(52) Perdomo, J., Cova, A., Sandoval, A.J., García, L., Laredo, E. and Müller, A.J., *Carbohydr. Polym.*, 2009, **76**, 305-313.

(53) Arora, P., Sharma, S. and Garg, S., *Drug Discov. Today*, 2002, **7**, 967-975.

(54) Newman, A.W., Reutzel-Edens, S.M. and Zografi, G., *J. Pharm. Sci.*, 2008, **97**, 1047-1059.

(55) Bajwa, G.S., Hoebler, K., Sammon, C., Timmins, P. and Melia, C.D., *J. Pharm. Sci.*, 2006, **95**, 2145-2157.

(56) Gately, D.P. and Howell, S.B., *Br. J. Cancer*, 1993, **67**, 1171-1176.

(57) Montes-Navajas, P., Gonzalez-Bejar, M., Scaiano, J.C. and Garcia, H., *Photochem. Photobio. S.*, 2009, **8**, 1743-1747.

(58) McInnes, F.J., O'Mahony, B., Lindsay, B., Band, J., Wilson, C.G., Hodges, L.A. and Stevens, H.N.E., *Eur. J. Pharm. Sci.*, 2007, **31**, 25-31.

(59) http://www.china-vials.com/product/vaginal-applicators-vaginal-syringes.htm, *Accessed 19th August 2012.*

(60) Martin, L., Wilson, C.G., Koosha, F. and Uchegbu, I.F., *Eur. J . Pharm. Biopharm.*, 2003, **55**, 35-45.

(61) Wong, C.F., Yuen, K.H. and Peh, K.K., *Int. J. Pharm.*, 1999, **180**, 47-57.

(62) Khutoryanskaya, O.V., Potgieter, M. and Khutoryanskiy, V.V., *Soft Matter*, 2010, **6**, 551-557.

(63) Hall, D.J., Khutoryanskaya, O.V. and Khutoryanskiy, V.V., *Soft Matter*, 2011, **7**, 9620-9623.

(64) Matsuyama, T., Morita, T., Horikiri, Y., Yamahara, H. and Yoshino, H., *J. Cont. Rel.*, 2007, **120**, 88-94.

6. CONCLUSIONS AND OUTLOOK

Cisplatin is one of the most widely prescribed and effective anti-cancer chemotherapeutics in clinical use. Unfortunately, this use is limited by resistance and dose limiting toxicity. In an effort to improve platinum-based chemotherapy, some of the focus has shifted away from developing new drugs, towards improving the delivery of those which already exist. This includes the use of drug delivery vehicles and exploration of new delivery routes.

Nasal drug delivery offers the advantages of a large surface area for drug absorption, no need for parenteral administration, avoidance of hepatic first pass metabolism and high patient acceptability. Additionally, it may be useful for local delivery of chemotherapeutics to cancers of the nasal cavity. Nasal drug delivery is, however, hampered by rapid clearance and metabolism. Lyophilised nasal inserts provide a robust single-unit dosage form for drug delivery to the nose and hydrate *in situ* to form a mucoadhesive polymer gel which resists MCC, allowing longer time for drug absorption in the nose.

This work investigated the use of single-walled CNTs and CB[*n*]s as potential vehicles to improve the delivery of platinum drugs, as a component of nasal insert formulations.

6.1 CARBON NANOTUBES

The delivery of cisplatin conjugated to carboxylic acid functionalised CNTs was investigated, as it was expected that the increased size would allow greater accumulation in tumours through the EPR effect. Whilst the rate of attachment of aquated cisplatin per functional group was low, this represented up to 91.6% of the starting material. This suggests there is potential to improve the extent of platinum loading by repeating with higher concentrations of aquated cisplatin. The Pt-CNTs were successfully dispersed in water using Pluronic F-127. Following lyophilisation,

this product was suspended in simulated GI fluid, suggesting potential bioavailability following oral administration. A similar investigation in simulated nasal electrolyte solution will be required to provide evidence for nasal bioavailability. The use of CNTs was halted due to safety concerns.

Should this work resume, the next steps would be increasing the extent of conjugation, followed by *in vitro* biological testing. Careful consideration would need to be given to the assay(s) and controls used, so that any interference from the CNTs themselves could be accounted for. If successful at improving the efficacy of the cisplatin, the Pt-CNTs in Pluronic F-127 could then be included in nasal insert formulations and investigated for nasal drug delivery. Other strategies which may be utilised include the use of a tumour targeting group such as folate, and the use of US-CNTs which have shown enhanced uptake in cisplatin resistant cell lines.

6.2 CUCURBIT[*n*]URILS

The cucurbiturils are a family of macrocycles which have been shown to improve the stability and efficacy of platinum(II) chemotherapeutics. Whilst CB[7] is the most useful in terms of size and solubility, it is expensive to buy and complicated to isolate. In this investigation, CB[6] has been shown to be a suitable low-cost model for CB[7] in HPMC nasal inserts, so far as they both affect formulation hardness, reduce moisture uptake and improved the spread of the hydrated inserts.

A theory to explain this behaviour has been proposed whereby, at lower concentrations, the CB[*n*]s form hydrogen bonds with the hydroxyl groups on the polymer chains, acting as points of pseudo-cross-linking and contributing to structural integrity. At higher concentrations, the hydrogen bonding sites on the polymer become saturated, reducing the potential for water uptake in the system. After this saturation point, excess CB[*n*]s may stack to form channels through the network. These channels may assist the rapid penetration of water, resulting in improved hydration and spreading. The cross-linking behaviour and subsequent

reduction in chain mobility is thought to be responsible for reduced mucoadhesion which was observed with increasing CB[6] and CB[7] concentration.

In these investigations, CB[6] has shown promise as a model for CB[7] and lessons learned from CB[6] may be used to make predictions about CB[7]. Whilst CB[6] and CB[7] may have a similar effect on formulation, where this effect is due to hydrogen bonding, it will be more pronounced with CB[7]. Repeating these assays with wider concentration ranges may give more insight into the nature of the interactions between the HPMC and CB[*n*]s. Any future application of a CB[*n*]-HPMC matrix may require careful tuning of the composition to obtain the required network strength, gelling ability and mucoadhesive potential.

CB[6] and CB[7] have been shown to increase the thermal stability of the di-nuclear platinum(II) drug di-Pt, and the fluorescent dye, K6. Additionally, the encapsulated forms have also shown improved distribution throughout a lyophilised nasal insert. Again, increased structural integrity of the lyophilised nasal insert through hydrogen bonding is also thought to occur. The pH of the environment has been shown to influence the drug release. This work may represent the formulation of a pH-responsive supramolecular delivery system for di-Pt. Whilst this has resulted in the reduced release of di-Pt@CB[7] compared to free di-Pt in SNES, further development of this technology in another field could result in, for example a CB[*n*]-HPMC delivery system capable of enhanced drug targeting to the lower digestive tract following oral delivery. Alternatively, CB[*n*]s may be a useful tool for deliberately extending release of a drug from an HPMC matrix.

CB[*n*]s have, therefore, been shown to be useful as pharmaceutical excipients which may be exploited to: thermally and physically protect an encapsulated drug; act as a structural component of an HPMC matrix, providing structural integrity; extend the release of a drug from an HPMC matrix; and/or form a pH (or ion) responsive matrix with HPMC, capable of releasing a drug load upon entering a more alkaline environment. CB[*n*]s have, therefore, been shown to warrant further investigation as pharmaceutical excipients for controlled release.

Encapsulating cisplatin in CB[7] has been shown by others to improve activity in cisplatin resistant xenographs. In this thesis, the encapsulation has also been shown to improve the thermal stability of the drug. Cisplatin@CB[7] has been included in lyophilised nasal inserts with hardness capable of withstanding patient handling. The encapsulation has not significantly affected the hardness, spreadability or mucoadhesion of the formulation. Additionally, the release of cisplatin@CB[7] was more repeatable than its cisplatin counterpart. *In vivo* testing would be required to determine if this nasal insert formulation is effective for the delivery of CB[7]-protected cisplatin to the nasal cavity. If successful, this may represent a new delivery route for cisplatin and improved local delivery of cisplatin to resistant cancers of the nasal cavity.

In this investigation, the presence of salts both in the formulation and in the release and or uptake medium has been shown to be important. It is hypothesised that by associating to the CB[*n*] portals, positive ions not only increase the aqueous solubility of the CB[*n*], but also act as a steric barrier to hydrogen bonding between the CB[*n*] and the polymer, providing increased chain mobility in the hydrating polymer.

With more time and funding, further work would include examining release over a range of pH and ion concentrations to further understand release kinetics. This could be further understood by measuring the aqueous solubility and log *P* of the free and encapsulated drugs. An *in vivo* study would give better insight into bioavailability of the cisplatin from the CB[7]-HPMC formulation, particularly if active transport mechanisms are in operation. Also, further testing of CB[*n*]s would be required to ensure their safety, for example, a metabolism study. Additionally, determining the maximum concentration within which CB[*n*]s contribute to structural integrity through cross-linking polymer chains would be of use to future applications.

It should be noted that the low availability of CB[7] for the project has been a limiting factor, and meant that the number of repeats has been low (*n*=3 in some

cases). Increasing this number would improve the reliability of the data and may produce more significant findings.

Although this work utilised CB[6] and CB[7], which are commercially available, a number of modified cucurbiturils now exist which could prove more useful for drug delivery. For example, Lyle Isaacs' research group have recently developed two acyclic cucurbituril derivatives capable of drug encapsulation.[1] The open-ended form of these new molecules allows them to encapsulate a wider number of guests than the rigid CB[*n*]s (Figure 6.1). These new molecular containers can increase the solubility and bioavailability of anticancer drugs such as paclitaxel, and show low cytotoxicity. Whilst this thesis demonstrates the usefulness of CB[*n*]s in a pharmaceutical formulations of platinum(II) anticancer drugs, it is true that any industrial application will probably use modified cucurbiturils. It is expected that more types of formulations will be investigated as these modified-CB compounds become readily and commercially available.

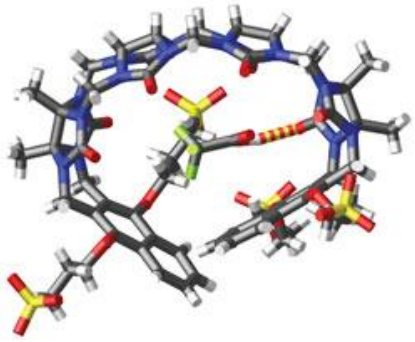

Figure 6.1. Molecular model of an acyclic cucurbituril derivative interacting with CF_3CO_2H (C, grey; H, white; N, blue; O, red; F, green; hydrogen bond, red and yellow stripe). The open-ended shape allows the molecule to wrap around its guest.[1]

(1) Ma, D., Hettiarachchi, G., Nguyen, D., Zhang, B., Wittenberg, J.B., Zavalij, P.Y., Briken, V. and Isaacs, L., *Nat Chem*, 2012, **4**, 503-510.

7. APPENDICES

Appendix 1: List of abbreviations

AFM	Atomic force microscopy
ATP	Adenosine triphosphate
BBB	Blood brain barrier
BP	British Pharmacopoeia
C_{60}	Buckminsterfullerene
CB[*n*]	Cucurbit[*n*]uril, where *n*=5, 6, 7, 8 or 10
CD	Cyclodextrin
CNS	Central nervous system
CNT	Carbon nanotube
CTR-1	Copper transporter-1
DCS	Differential centrifugal sedimentation
DIPEA	*N*,*N*-Diisopropylethylamine
di-Pt	*trans*-[{PtCl(NH_3)$_2$}$_2$μ-dpzm]$^{2+}$
DNA	Deoxyribonucleic acid
dpzm	4,4-dipyrazole methane
DSC	Differential scanning calorimetry
DVS	Dynamic vapour sorption
EPR	Enhanced permeability and retention
EtOH	Ethanol
F-AAS	Flame atomic absorption spectroscopy
***f*-CNT**	Functionalised carbon nanotube
FDA	Food and Drug Administration (USA)
GI	Gastrointestinal
GRAS	Generally regarded as safe
GSH	Glutathione
HEPA	High-efficiency particulate air

HIV	Human immunodeficiency virus
HPMC	Hydroxypropyl methylcellulose
ICP-MS	Inductively coupled plasma mass spectroscopy
IN	Intranasal
IR	Infrared
IV	intravenous
K6	2,2'-(alkylene-1,6-diyl)diisoquinolium
MCC	Mucociliary clearance
MeOH	Methanol
MTT	2-(4,5-dimethyl-2-thiazolyl)-3,5-diphenyl-2H-tetrazolium bromide
MW	Molecular weight
MWCO	Molecular weight cut-off
MWNT	Multi-walled carbon nanotube
NDD	Nasal drug delivery
NMR	Nuclear magnetic resonance
PAMAM	Polyamidoamine
PBS	Phosphate buffered saline
Pt-CNT	Cisplatin conjugated carbon nanotube
PXRD	Powder X-ray diffraction
RH	Relative humidity
RNA	Ribonucleic acid
RT	Room temperature
SDS	Sodium dodecyl sulfate
SEM	Scanning electron microscopy
SNES	Simulated nasal electrolyte solution
SWNT	Single-walled carbon nanotube
TA	Texture analyser/texture analysis
TAF	Tumour angiogenesis factor
TEM	Transmission electron microscopy
TGA	Thermogravimetric analysis
US	Ultra-short
UV	Ultraviolet

UV-vis	Ultraviolet-visible
VEGF	Vascular endothelial growth factor
VPF	Vascular permeability factor
WHO	World Health Organisation
X@CB[*n*]	Compound “X” encapsulated in CB[*n*]
XRD	X-ray diffraction

Appendix 2: Publications and presentations

Wheate, N.J, **Walker, S.**, Craig, G.E and Oun, R., The status of platinum drugs in the clinic and clinical trials, *Dalton T*., 2010, **39**(35), 8113-8127.

Walker, S., Kaur, R., McInnes, F.J. and Wheate, N.J., Synthesis, processing and solid state excipient interactions of cucurbit[6]uril and its formulation into tablets for oral delivery, *Mol. Pharmaceut*., 2010, **7**(6), 2166-2172.

Walker, S., McInnes, F.J. and Wheate, Chemical processing and oral tablet formulation of the macrocycle cucurbit[6]uril, *UK Symposium on Physical Organic Chemistry*, 2010, Bristol, UK.

Walker, S., McInnes, F.J. and Wheate, N.J., Development of pharmaceutical formulations containing cucurbit[*n*]urils, *2nd International Conference on Cucurbiturils*, 2011, Cambridge, UK.

Walker, S., McInnes, F.J. and Wheate, N.J., Cucurbit[*n*]urils for nasal delivery of multinuclear platinum anticancer drugs, *15th International Conference on Biological Inorganic Chemistry*, 2011, Vancouver, Canada.

Walker, S., Oun, R., McInnes, F.J. and Wheate, N.J., The potential of cucurbit[*n*]urils in drug delivery, *Isr. J. Chem*., 2011, **51**(5-6), 616-624.

Appendix 3: K6 single crystal X-ray diffraction data

Table 1. Crystal data and structure refinement for K6.

Identification code	K6	
Empirical formula	C24 H26 Br2 N2	
Formula weight	502.29	
Temperature	123(2) K	
Wavelength	0.71073 Å	
Crystal system	Monoclinic	
Space group	P 21/n	
Unit cell dimensions	a = 9.0503(5) Å	α= 90°
	b = 7.8606(2) Å	β= 97.367(6)°
	c = 15.5772(13) Å	γ = 90°
Volume	1099.03(11) $Å^3$	
Z	2	
Density (calculated)	1.518 Mg/m^3	
Absorption coefficient	3.700 mm^{-1}	
F(000)	508	
Crystal size	0.20 x 0.20 x 0.10 mm^3	
Theta range for data collection	3.45 to 28.00°.	
Index ranges	-11<=h<=11, -10<=k<=10, -20<=l<=20	
Reflections collected	13372	
Independent reflections	2643 [R(int) = 0.0420]	
Completeness to theta = 27.00°	99.8 %	
Absorption correction	Semi-empirical from equivalents	
Max. and min. transmission	0.690 and 0.481	
Refinement method	Full-matrix least-squares on F^2	
Data / restraints / parameters	2643 / 0 / 127	
Goodness-of-fit on F^2	1.045	
Final R indices [I>2sigma(I)]	R1 = 0.0304, wR2 = 0.0685	
R indices (all data)	R1 = 0.0400, wR2 = 0.0727	
Largest diff. peak and hole	0.632 and -0.357 $e.Å^{-3}$	

Table 2. Atomic co-ordinates ($\times 10^4$) and equivalent isotropic displacement parameters ($Å^2 \times 10^3$) for K6. U(eq) is defined as one third of the trace of the orthogonalized U^{ij} tensor.

	x	y	z	U(eq)
C(1)	6901(3)	-185(3)	8126(2)	26(1)
C(2)	7507(3)	436(3)	8902(2)	29(1)
C(3)	6619(3)	1308(3)	9448(2)	24(1)
C(4)	7159(3)	1917(3)	10282(2)	31(1)
C(5)	6224(3)	2757(3)	10761(2)	33(1)
C(6)	4725(3)	3042(3)	10440(2)	33(1)
C(7)	4158(3)	2425(3)	9644(2)	28(1)
C(8)	5096(2)	1539(3)	9136(1)	21(1)
C(9)	4536(2)	873(3)	8322(2)	20(1)
C(10)	4786(3)	-685(3)	6994(2)	22(1)
C(11)	5448(3)	198(3)	6258(2)	22(1)
C(12)	4694(3)	-431(3)	5383(1)	21(1)
N(1)	5404(2)	25(2)	7849(1)	20(1)
Br(1)	4356(1)	4574(1)	7311(1)	24(1)

Table 3. Bond lengths and angles of K6.

C(1)-C(2)	1.353(4)
C(1)-N(1)	1.378(3)
C(1)-H(1)	0.9500
C(2)-C(3)	1.419(3)
C(2)-H(2)	0.9500
C(3)-C(4)	1.412(3)
C(3)-C(8)	1.414(3)
C(4)-C(5)	1.368(4)
C(4)-H(4)	0.9500
C(5)-C(6)	1.402(4)
C(5)-H(5)	0.9500
C(6)-C(7)	1.369(4)
C(6)-H(6)	0.9500
C(7)-C(8)	1.416(3)
C(7)-H(7)	0.9500
C(8)-C(9)	1.404(3)
C(9)-N(1)	1.324(3)
C(9)-H(9)	0.9500
C(10)-N(1)	1.485(3)
C(10)-C(11)	1.528(3)
C(10)-H(10A)	0.9900
C(10)-H(10B)	0.9900
C(11)-C(12)	1.526(3)
C(11)-H(11A)	0.9900
C(11)-H(11B)	0.9900
C(12)-C(12)#1	1.535(4)
C(12)-H(12A)	0.9900
C(12)-H(12B)	0.9900
C(2)-C(1)-N(1)	120.5(2)
C(2)-C(1)-H(1)	119.8
N(1)-C(1)-H(1)	119.8
C(1)-C(2)-C(3)	120.9(2)
C(1)-C(2)-H(2)	119.6

C(3)-C(2)-H(2)	119.6
C(4)-C(3)-C(8)	118.7(2)
C(4)-C(3)-C(2)	124.0(2)
C(8)-C(3)-C(2)	117.3(2)
C(5)-C(4)-C(3)	120.0(2)
C(5)-C(4)-H(4)	120.0
C(3)-C(4)-H(4)	120.0
C(4)-C(5)-C(6)	121.4(2)
C(4)-C(5)-H(5)	119.3
C(6)-C(5)-H(5)	119.3
C(7)-C(6)-C(5)	120.0(2)
C(7)-C(6)-H(6)	120.0
C(5)-C(6)-H(6)	120.0
C(6)-C(7)-C(8)	119.9(2)
C(6)-C(7)-H(7)	120.1
C(8)-C(7)-H(7)	120.1
C(9)-C(8)-C(3)	119.0(2)
C(9)-C(8)-C(7)	121.0(2)
C(3)-C(8)-C(7)	119.9(2)
N(1)-C(9)-C(8)	121.3(2)
N(1)-C(9)-H(9)	119.4
C(8)-C(9)-H(9)	119.4
N(1)-C(10)-C(11)	111.31(18)
N(1)-C(10)-H(10A)	109.4
C(11)-C(10)-H(10A)	109.4
N(1)-C(10)-H(10B)	109.4
C(11)-C(10)-H(10B)	109.4
H(10A)-C(10)-H(10B)	108.0
C(12)-C(11)-C(10)	110.49(18)
C(12)-C(11)-H(11A)	109.6
C(10)-C(11)-H(11A)	109.6
C(12)-C(11)-H(11B)	109.6
C(10)-C(11)-H(11B)	109.6
H(11A)-C(11)-H(11B)	108.1
C(11)-C(12)-C(12)#1	112.7(2)
C(11)-C(12)-H(12A)	109.0

C(12)#1-C(12)-H(12A)	109.0
C(11)-C(12)-H(12B)	109.0
C(12)#1-C(12)-H(12B)	109.0
H(12A)-C(12)-H(12B)	107.8
C(9)-N(1)-C(1)	121.0(2)
C(9)-N(1)-C(10)	120.39(19)
C(1)-N(1)-C(10)	118.57(19)

Symmetry transformations used to generate equivalent atoms: #1 -x+1,-y,-z+1

Table 4. Anisotropic displacement parameters ($\text{Å}^2 \times 10^3$) for K6. The anisotropic displacement factor exponent takes the form: $-2\pi^2[h^2 a^{*2} U^{11} + ... + 2 h k a^* b^* U^{12}]$

U^{11}	U^{22}	U^{33}	U^{23}	U^{13}	U^{12}	
C(1)	20(1)	36(1)	24(1)	2(1)	6(1)	4(1)
C(2)	19(1)	44(1)	24(1)	4(1)	2(1)	0(1)
C(3)	27(1)	25(1)	22(1)	2(1)	5(1)	-6(1)
C(4)	32(1)	37(1)	24(1)	0(1)	2(1)	-13(1)
C(5)	52(2)	26(1)	22(1)	-2(1)	5(1)	-15(1)
C(6)	54(2)	21(1)	28(1)	-1(1)	15(1)	2(1)
C(7)	34(1)	24(1)	28(1)	0(1)	7(1)	5(1)
C(8)	26(1)	17(1)	21(1)	3(1)	6(1)	-2(1)
C(9)	19(1)	19(1)	22(1)	4(1)	6(1)	0(1)
C(10)	26(1)	22(1)	18(1)	-2(1)	4(1)	-3(1)
C(11)	26(1)	23(1)	17(1)	-1(1)	4(1)	-3(1)
C(12)	26(1)	20(1)	17(1)	-2(1)	6(1)	-2(1)
N(1)	20(1)	23(1)	16(1)	1(1)	4(1)	0(1)
Br(1)	22(1)	22(1)	28(1)	0(1)	6(1)	1(1)

Table 5. Hydrogen coordinates ($\times 10^4$) and isotropic displacement parameters ($\text{Å}^2 \times 10^3$) for K6.

	x	y	z	U(eq)
H(1)	7511	-769	7770	32
H(2)	8542	286	9084	35
H(4)	8172	1743	10511	37
H(5)	6598	3157	11323	40
H(6)	4104	3662	10775	40
H(7)	3136	2591	9433	34
H(9)	3515	1034	8107	24
H(10A)	3690	-542	6910	27
H(10B)	5006	-1918	6982	27
H(11A)	5312	1443	6300	26
H(11B)	6531	-38	6308	26
H(12A)	3611	-211	5342	25
H(12B)	4839	-1676	5345	25

Table 6. Torsion angles for K6.

N(1)-C(1)-C(2)-C(3)	0.2(4)
C(1)-C(2)-C(3)-C(4)	176.8(2)
C(1)-C(2)-C(3)-C(8)	-1.8(3)
C(8)-C(3)-C(4)-C(5)	-2.0(3)
C(2)-C(3)-C(4)-C(5)	179.5(2)
C(3)-C(4)-C(5)-C(6)	-0.3(4)
C(4)-C(5)-C(6)-C(7)	2.2(4)
C(5)-C(6)-C(7)-C(8)	-1.7(3)
C(4)-C(3)-C(8)-C(9)	-177.3(2)
C(2)-C(3)-C(8)-C(9)	1.4(3)
C(4)-C(3)-C(8)-C(7)	2.4(3)
C(2)-C(3)-C(8)-C(7)	-178.9(2)
C(6)-C(7)-C(8)-C(9)	179.1(2)
C(6)-C(7)-C(8)-C(3)	-0.6(3)
C(3)-C(8)-C(9)-N(1)	0.5(3)
C(7)-C(8)-C(9)-N(1)	-179.1(2)
N(1)-C(10)-C(11)-C(12)	-174.68(18)
C(10)-C(11)-C(12)-C(12)#1	179.4(2)
C(8)-C(9)-N(1)-C(1)	-2.2(3)
C(8)-C(9)-N(1)-C(10)	179.35(19)
C(2)-C(1)-N(1)-C(9)	1.8(3)
C(2)-C(1)-N(1)-C(10)	-179.7(2)
C(11)-C(10)-N(1)-C(9)	113.7(2)
C(11)-C(10)-N(1)-C(1)	-64.8(3)

Symmetry transformations used to generate equivalent atoms: #1 -x+1,-y,-z+1